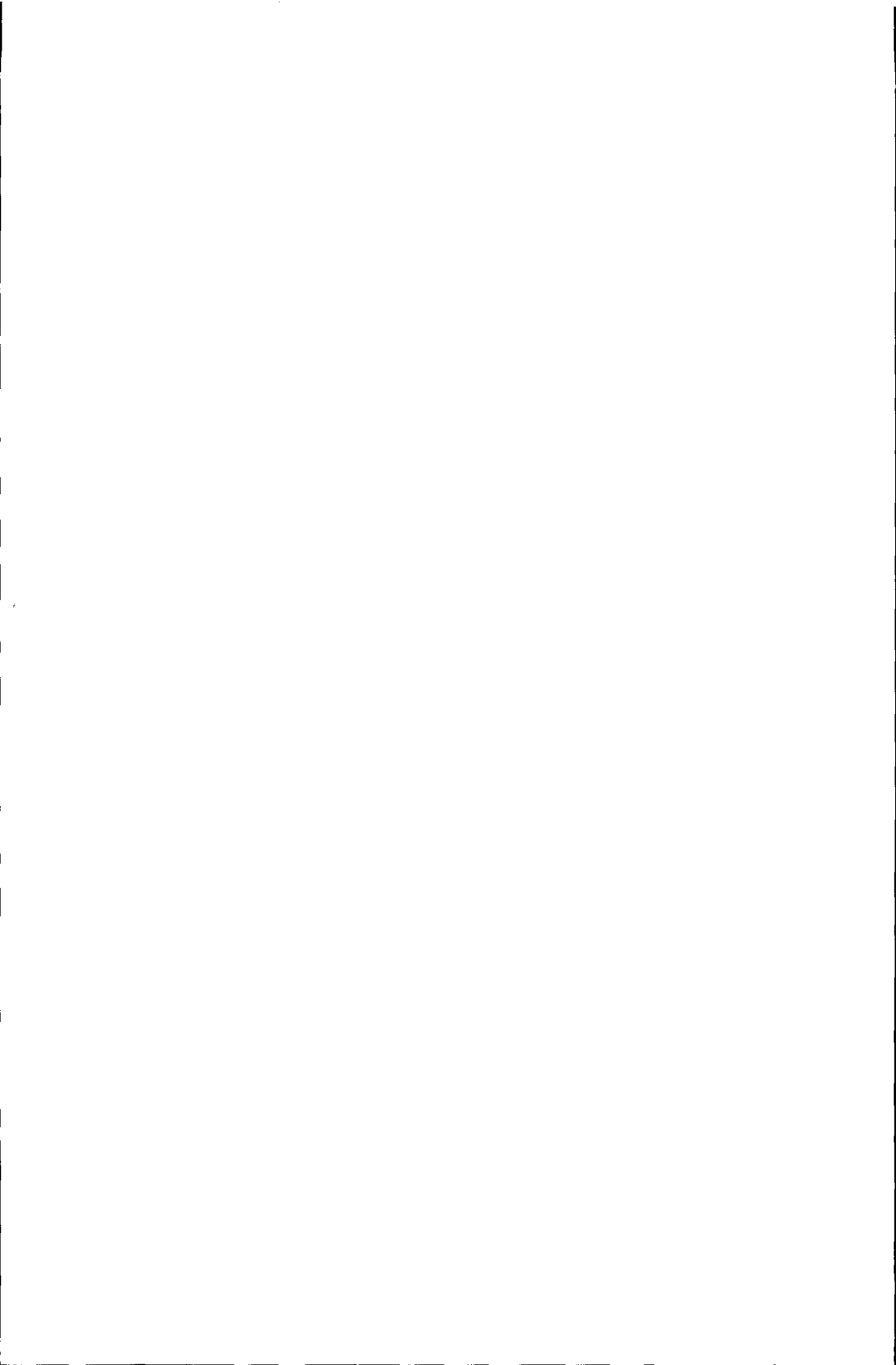


STELLINGEN  
behorende bij het proefschrift

Hydrodynamics and Mass Transfer in Packed Columns and their  
Applications for Supercritical Separations

Geert F. Woerlee

1. Slechts het parallelle gedeelte van de frictiekrachten op een vloeistoffilm hebben effect op de filmdikte in gas-vloeistofcontactors. (Hoofdstuk 3).
2. Zolang het fenomeen "flooding" niet in verband wordt gebracht met "deflooding", zullen er niet-consistente resultaten worden blijven gevonden.
3. Massatransport in gepakte kolommen kan direct gekoppeld worden aan de drukval over de pakking. (Hoofdstuk 5).
4. Door naast de gravitatie- en frictiekracht ook de rotatiekracht in de trajectbeschrijving van een druppeltje in gas-vloeistofcontactors te gebruiken, kan het moment van "flooding" beter worden voorspeld. (Hoofdstuk 4).
5. De kosten van een superkritische scheiding worden in hoofdzaak bepaald door randapparatuur (dit proefschrift).
6. De stelling "goedkoop is duurkoop" is zeker niet algemeen geldig voor pakking. (Hoofdstuk 6).
7. Dat multicomponent-massatransportmodellen tot negatieve HETP's leiden, is beduidend minder verontrustend dan dat dergelijke modellen tot hoge HETP's leiden.
8. De duidelijkste exergie-analyse is een kostenanalyse.
9. Dat promovendi niet met beide benen op de grond staan, blijkt uit het feit dat zij maar al te vaak een boekenlegger bij een proefschrift sluiten.
10. De door natuurkundigen gebruikte gemeenplaats "zeker weten door zuiver meten" toont het verschil in mentaliteit (zeker) en methode (zuiver) ten opzichte van andere wetenschappers die zich meestal beperken tot "weten is meten" of zelfs "meten is weten".
11. Dat er bij bedrijven behoefte is aan producten die de jaloezie bij de concurrent moet opwekken, blijkt uit het succes van de ISO9000-certificaten.
12. Een beter milieu begint bij een verdubbeling van de kerosineprijs.
13. Babyboom: (1945-1955)  
zich tot verzetshelden geblowd,  
een pensioen  
van kinderen geroofd.
14. Een stelling heeft een uiterste houdbaarheidsdatum.
15. Een mens heeft slechts macht over zijn mening. Slechts één weg leidt tot vrijheid: gering te achten wat niet in zijn macht ligt (Epicticus).



TR2991

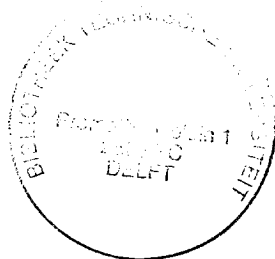
HYDRODYNAMICS AND MASS TRANSFER  
IN PACKED COLUMNS  
AND THEIR  
APPLICATIONS FOR  
SUPERCRITICAL SEPARATIONS

PROEFSCHRIFT

ter verkrijging van de graad van doctor  
aan de Technische Universiteit Delft,  
op gezag van de Rector Magnificus Prof. dr ir J. Blaauwendraad,  
in het openbaar te verdedigen ten overstaan van een commissie,  
door het College van Dekanen aangewezen,  
op maandag 15 september 1997 te 16.00 uur  
door

Geert Feye WOERLEE  
natuurkundig ingenieur

geboren te Utrecht.



Dit proefschrift is goedgekeurd door de promotor.  
Prof. dr ir J. de Graauw

Samenstelling promotiecommissie:

Rector Magnificus, voorzitter  
Prof. dr ir J. de Graauw, TU Delft, promotor  
Dr Z. Olujic, TU Delft, toegevoegd promotor  
Prof. dr ir P.J.A.M. Kerkhof, TU Eindhoven  
Prof. dr ir J. de Swaan Arons, TU Delft  
Prof. ir C.M. van den Bleek, TU Delft  
Prof. dr R.V.A. Oliemans, TU Delft  
Dr ir A.B. de Haan, DSM

CIP-DATA KONINKLIJKE BIBLIOTHEEK DEN HAAG

Woerlee, Geert Feye

Hydrodynamics and mass transfer in packed columns  
and their applications for supercritical separations / Geert F. Woerlee -Delft:  
Delft University Press  
Thesis Technische Universiteit Delft - With ref. -With summary in Dutch.  
ISBN 90-407-1497-5  
NUGI 841  
Subject headings: packed columns / supercritical extraction / mass transport

Copyright © 1997, by Geert F. Woerlee  
Wijtenbachstraat 42-III  
1093 JD Amsterdam  
The Netherlands  
TEL: 31 20 692 9263  
31 65 496 0586  
FAX: 31 20 692 9263

All rights reserved.  
No part of this publication may be reproduced, stored in a retrieval system or transmitted in any  
form or by any means, electronic, mechanical, photocopying, recording or otherwise, without  
the prior written permission from the publisher:  
Delft University Press  
Stevinweg 1  
2628 CN Delft  
The Netherlands.

Printed in the Netherlands.



Voor mijn ouders  
en  
kinda natuurlijk!



# Preface

This thesis is a result of over four years of work carried out in the framework of the Supercritical Extraction II project at the Laboratory of Process Equipment at the Delft University of Technology. The results, models and ideas contained within this thesis could not have been achieved without the assistance of a large number of people.

Firstly, I would like to thank my supervisors Jan de Graauw and Zarco Olujic for the stimulating discussions, guidance and freedom they gave me while working towards my thesis.

The many enjoyable hours spent with undergraduate students wrestling with their part of the project on supercritical separations are highlights in the years of work. I wish Peter-Jan Bosch, Ivo Hoogerwerf, Bas de Lange, Just Walter, Jeffrey de Waard, Jaap Wijnands, Arnt Aalbers, Arjan de Ruyter, Floortje Driessen, Irene Cusell, Remco Spits, Ernst-Jan Siewers, Guido Wieringa, Sander Molkenboer, Frode Bauge, Maarten Verhaar, Arnold Reijnders, Frederik Feddes, and Arjan Gerrits every success in the future with their chosen careers.

My roommates and colleagues Edwin Berends, Jaap Feddes, Jessica Reinkingh, Concha Domingo, and Frank Wubbolts, thanks for your friendship, all the help and making my task easier.

Further, I would like to acknowledge, Theo de Loos, Cor Peters, Gerard Kuiken and Chris Kleijn for their contributions on thermodynamics, physical properties and heat transfer, which topics I have not been able to close yet. However, their suggestions can be found throughout this thesis.

My special thank is for Joop Berends who enabled me to finish the chapters on hydrodynamics and mass transfer by recalculating and correcting my ideas. His contributions have been of major importance.

It would have been impossible to finish this thesis without the continuing support of all personnel of the laboratory for process equipment. I could not have completed this work and many other "smaller" jobs without their help. Many thanks everybody.

There are several individuals from the participating industry who I would like to thank personally for their contributions and suggestions. However, the list would be so extensive that it would go beyond the scope of this preface. I therefore would like to thank the companies; DSM, Shell, Unilever, Cosun (Senses), Gist-Brocades, Hoekloos, NIZO, Tastemakers, Philips, Sastech, Stork Ketels, Suiker Unie, and Zeton, for their financial and moral support via their employees.

## Preface

---

After version hundred plus, I personally got a bit exhausted evaluating in detail the grammar and spelling of the text. I therefore acknowledge Robert Endert who read and corrected the concept version of this thesis.

Finally I would like to thank Linda. It is very unlikely that I would have finished this thesis without her moral support, encouragement and care.

# Contents

CHAPTER 1	
<b>Introduction</b> .....	1
A SUPERCRITICAL FLUID .....	1
A SUPERCRITICAL SEPARATION PROCESS .....	3
INDUSTRIAL SUPERCRITICAL APPLICATIONS .....	4
THE BACKBONE OF SEPARATION DESIGN .....	5
SCOPE AND STRUCTURE .....	7
REFERENCES .....	7
CHAPTER 2	
<b>Experimental Set-Up</b> .....	9
Packed Extraction Column .....	9
The Carbon Dioxide Cycle .....	10
The Product Cycle .....	13
The Data Collection .....	13
Experimental Procedure .....	13
EXPERIMENTAL VERIFICATION .....	14
Column Stability .....	16
REFERENCES .....	16
CHAPTER 3	
<b>A Comprehensive Model for the Pressure Drop in Packed Columns</b> .....	17
MACROSCOPIC DESCRIPTION OF THE FLOWS .....	18
Solution of the Equation of Motion for Liquid Flow .....	18
The Pressure Drop Contributions .....	20
<i>frictional pressure drop</i> .....	20
<i>geometrical pressure drop</i> .....	21
The Effective Inclination Angle .....	22
The Influence of the Column Diameter on the Pressure Drop .....	24
Gas-Liquid Interaction .....	26
Calculation Procedure .....	27
RESULTS AND DISCUSSION .....	27
The Structured Packing Liquid Hold-Up .....	27
Specific Area and Column Diameter .....	29
Random Packing Pressure Drop .....	30
Structured Packing Pressure Drop .....	31
Vertical Pipe Pressure Drop .....	32
CONCLUDING REMARKS .....	33
APPENDIX 3.A .....	34
NOTATION .....	34
REFERENCES .....	36
CHAPTER 4	
<b>A Capacity Model for Packed Columns Based on Entrainment</b> .....	37
GENERAL FLOODING CONSIDERATIONS .....	38
THE FORCES ON THE DROPLETS .....	39
THE DROPLET SIZE .....	42
RESULTS .....	44
Geometrical Influences on the Flood Point .....	46

---

Influence of Physical Properties on the Flood Point.....	48
<i>the surface tension</i> .....	49
<i>the liquid viscosity</i> .....	50
<i>the gas density</i> .....	51
<i>the gas/bulk viscosity</i> .....	52
CONCLUDING REMARKS .....	52
NOTATION .....	53
REFERENCES .....	55
CHAPTER 5	
<b>Mass Transfer in Packed Columns</b> .....	<b>57</b>
MASS TRANSFER COEFFICIENTS.....	58
The Gas Phase Mass Transfer Coefficients.....	59
Review of the Liquid Phase Mass Transfer Coefficients.....	61
A COMBINED THEORY AND MODEL FOR LIQUID PHASE MASS TRANSFER.....	67
Waves on the Gas-Liquid Interface.....	67
The Characteristic Geometrical Length for Structured Packing.....	71
The Characteristic Geometrical Length for Random Packing.....	73
COMPARISON OF STRUCTURED PACKINGS .....	74
CONCLUDING REMARKS .....	76
APPENDIX 5.A (The Kelvin-Hemholtz relation) .....	77
APPENDIX 5.B (Energy Dissipation in Waves).....	80
APPENDIX 5.C (Height Equivalent to a Theoretical Plate).....	81
NOTATION .....	84
REFERENCES .....	87
CHAPTER 6	
<b>Packing Design for Specific Applications</b> .....	<b>89</b>
MODEL EXTENSION AND VALIDATION .....	89
The surface area influence.....	90
The effective inclination angle influence.....	91
The wetting of the packing.....	93
Evaluation of Performance on Basis of Column and Packing Dimensions .....	94
THE SPECIFIC DESIGN OF A PACKED COLUMN.....	95
The specific area and effective inclination angle influence .....	96
The Capacity of the Application .....	99
SUGGESTIONS TO IMPROVE THE PACKING GEOMETRY.....	100
CONCLUDING REMARKS .....	104
NOTATION .....	104
REFERENCES .....	106
CHAPTER 7	
<b>Hydrodynamics and Mass Transfer in Packed Columns using Supercritical Fluids</b> .....	<b>107</b>
FLOODING AND PRESSURE DROPS IN SUPERCRITICAL SYSTEMS ..	108
MASS TRANSFER AT SUPERCRITICAL CONDITIONS .....	112
THE DESIGN OF A PACKED SUPERCRITICAL SEPARATION COLUMN .....	115
CONCLUDING REMARKS .....	118
APPENDIX 7.A .....	119
APPENDIX 7.B (Determination of the Experimental Number of Stage) .....	120
APPENDIX 7.C (IPA - ethylene glycol - carbon dioxide) .....	121
APPENDIX 7.D (2-methyl naphthalene-hexadecane-carbon dioxide) .....	123
NOTATION .....	126
REFERENCES .....	128

---

**CHAPTER 8**  
**Overall Supercritical Process Design Considerations.....129**  
 GENERAL SOLVENT CYCLE CONSIDERATIONS..... 130  
 THE ISOBARIC PROCESS ..... 132  
     Other Plant Lay-outs..... 133  
 ISOBARIC PROCESS EXAMPLES ..... 134  
 CONCLUDING REMARKS ..... 141  
 NOTATION ..... 141  
 REFERENCES ..... 142

**CHAPTER 9**  
**The Removal of Undesirable Components from Edible Oils Using SFE 143**  
 PROCESS THERMODYNAMICS..... 143  
 PROCESS DESIGN ..... 145  
     The solvent flow ..... 146  
     Column design ..... 147  
     Flash vessels..... 148  
     The solvent extract separator..... 149  
 OVERALL PROCESS COSTS ..... 150  
 CONCLUDING REMARKS ..... 151  
 ACKNOWLEDGEMENT ..... 151  
 NOTATION ..... 151  
 REFERENCES ..... 152  
 APPENDIX 9.A (Flowsheet)..... 153  
 APPENDIX 9.B (Equipment list) ..... 154

**CHAPTER 10**  
**Process for the Removal of Aromatic Compounds from Off-Shore**  
**Production Water using Supercritical Methane .....155**  
 EXPERIMENTAL SET-UP AND PROCEDURE ..... 155  
     Thermodynamic Description..... 156  
     Process Models..... 157  
         *flash vessel*..... 157  
         *stripping vessel*..... 158  
         *continuous stripping* ..... 158  
         *batch stripping*..... 159  
 EXPERIMENTAL RESULTS ..... 160  
     The Solubility of Methane in Water..... 160  
     Distribution Factors..... 160  
     Mass Transfer Coefficients ..... 161  
 PROCESS DESIGN ..... 162  
     Process Costs..... 165  
 CONCLUDING REMARKS ..... 165  
 APPENDIX 10.A (Batch Stripping) ..... 165  
 APPENDIX 10.B (Mass Transfer Relations)..... 167  
 NOTATION ..... 167  
 REFERENCES ..... 168

**CHAPTER 11**  
**Process for the Fractionation of Citrus Oils using Supercritical Carbon**  
**Dioxide.....169**  
 EXPERIMENTAL PROCEDURE AND RESULTS..... 169  
 PROCESS DESIGN ..... 174  
     Separation Conditions ..... 174  
     Isobaric Separation..... 178  
     Separation by throttling..... 179

---

PROCESS EVALUATION.....	180
Technical Evaluation.....	180
Economical Evaluation.....	181
CONCLUDING REMARKS.....	182
NOTATION	
REFERENCES	
APPENDIX 11.A (Throttling SFE Process for citrus oils).....	186
APPENDIX 11.B (Isobaric SFE Process for citrus oils).....	187
CHAPTER 12	
<b>The Future of Supercritical Separations.....</b>	<b>189</b>
RECOMMENDATIONS.....	190
REFERENCES.....	191
Samenvatting.....	193
Summary.....	195
Curriculum Vitae.....	197



## Introduction

Although one might think otherwise, some of the peculiar properties of supercritical fluids have been known already for over hundred years. In 1879 Hannay and Hogarth discovered that when a gas was pressurised over its critical pressure it could dissolve solids. Studies involving supercritical fluids are therefore not new, but also not ancient. The technique using supercritical fluids, however, is rather recent as the first industrial applications started only two decades ago with the extraction of caffeine from coffee. It is from that time that supercritical fluids have drawn a renewed attention.

### A SUPERCRITICAL FLUID

The name supercritical fluid suggests more than it effectively means and it is as such a bit misleading. In contrast to, for instance, super-conductivity and super-fluidity it does not include a certain unique quantum state with unforeseen consequences. Firstly, a supercritical fluid is a compound above its critical temperature ( $T_c$ ). This means that, regardless the distance between the molecules, the individual molecules have on average a kinetic energy larger than the potential or attractive energy. Below the critical temperature the distance between the molecules can be decreased so that the potential energy exceeds the kinetic energy and the material condenses. The required pressure to decrease the distance of the molecules for condensation, increases with increasing temperature up to critical pressure ( $p_c$ ) and temperature. The critical temperature is the first temperature where the specific volume can be changed continuously, indicating the end of the gas liquid coexistence line as shown in figure 1.1A.

A separation process implies a mixture of two or more components. Figure 1.1B shows the phase transitions of two pure compounds (i and j) projected in one diagram. In this diagram the possible physical separation techniques can be distinguished. Basically one can identify a solid-fluid process and a fluid-fluid process. Normally one component will prefer to be in one phase above the other so that a separation can be accomplished. The fluid-solid transition or crystallisation involves a near total systematic reorganisation of the fluid structure, which in combination with a mechanical separation of the crystals could lead to a near complete separation. A total separation in a single equilibrium step is not possible in a fluid-fluid process, since the compounds will be distributed over each phase. In case the solid-liquid coexistence line of a component (j) lies at a higher temperature than the critical temperature of component (i) one could have a solid-fluid process that uses a supercritical solvent. Because the molecules of a supercritical fluid have a larger kinetic energy than a potential energy, a separation process using a supercritical fluid as extraction agent can best be compared with a gas-liquid separation.

However, figure 1.1B shows that the transitions between the fluid-fluid operations are smooth. Therefore it can be expected that theories applied to either distillation, gas stripping and liquid-liquid extraction concerning thermodynamics, physical properties, hydrodynamics and mass transfer should in general be applicable to supercritical separations. It is fair to say that the only "odd" phenomenon that takes place with supercritical fluids is that the density can be changed continuously from liquid like to gaseous like with relative small changes of temperature or pressure.

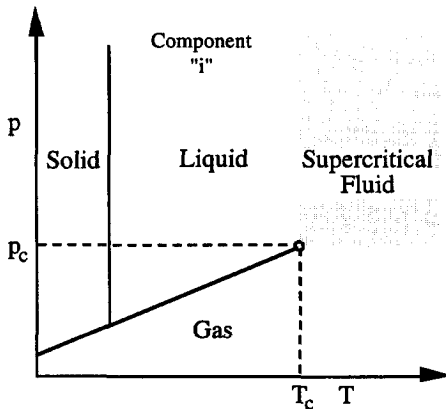


FIGURE 1.1A: Schematic temperature and pressure diagram of a pure component (i). Indicated are the different possible phases.

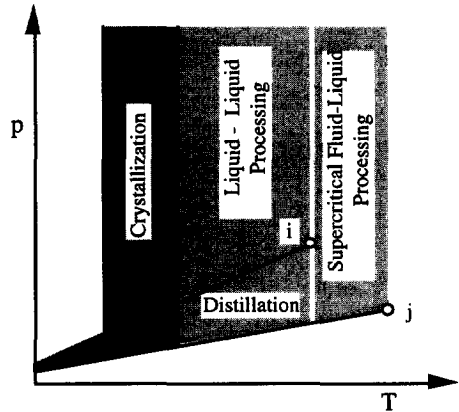


FIGURE 1.1B: Schematic temperature and pressure diagram of two components (i & j). Indicated are the resulting areas where a certain separation technique can be applied.

The solubility of a compound in a supercritical solvent is strongly dependent on the solvent density. The density as function of the temperature at various pressures of carbon dioxide, an often applied solvent, is shown in figure 1.2. Clearly figure 1.2 shows the steep changes of the density around the critical point ( $T_c = 31^\circ\text{C}$ ,  $p_c = 73.8\text{bar}$ ). Other properties as viscosity, diffusivity and solubility power can be related directly with these density changes. The diffusivity and viscosity vary inversely proportionally with density, whereas solubility power changes exponentially with density. Most engineering aspects of supercritical processes are related to the use and description of the to solvent density related changes of properties. By changing the density of the extract phase, an additional degree of freedom in the separation process can be created, by which for instance the extracted material can be recovered from the extract phase.

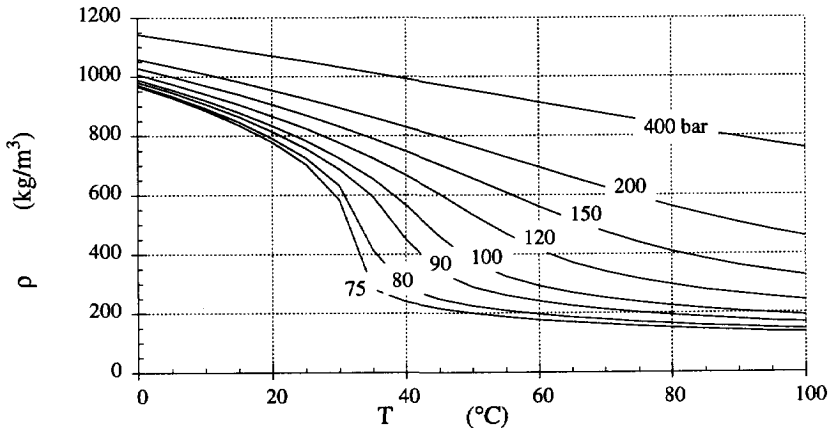


FIGURE 1.2: Carbon dioxide density as function of temperature for various pressures. The densities are calculated using the Peng-Robinson equation of state for pure carbon dioxide.

#### A SUPERCRITICAL SEPARATION PROCESS

Like distillation and liquid-liquid extraction, a supercritical fluid separation can most effectively be carried out using a counter-current process. This is done by using a column in which one phase flows down by gravity, while the other phase flows upwards because of a pressure difference over the column. Figure 1.3 shows a separation process for two components ( $j$  and  $k$ ) using a solvent ( $i$ ). In the distribution graph for component ( $j$ ) the fractions over liquid phase  $x_j$  and solvent phase  $y_j$  are plotted on a solvent free basis. A feed ( $F$ ) with a certain amount of the component that needs to be extracted enters the column on a certain level of the column and is contacted with the solvent flow. The solvent phase relatively enriched with the component ( $j$ ) flows upwards where it is contacted with the reflux stream. Depending on the size of the applied reflux ratio ( $R$ ) and the number of available equilibrium steps above the feed the extract phase can be enriched further. The liquid flowing down is at the bottom of the column contacted with "fresh" solvent, so that it is partly dissolved. The concentration of component ( $j$ ) in the fresh solvent  $y_j^0$  depends on the efficiency of the applied extract recovery method. This concentration, not only determines the purity of the bottom stream, but also the required solvent flow through the column. Both the composition of the extract ( $D$ ) and residue ( $B$ ) stream are a function of the feed to solvent ratio, the applied reflux ratio and the number of equilibrium steps in the column. The whole process is again similar to distillation and liquid-liquid extraction and is undoubtedly of the same separation family.

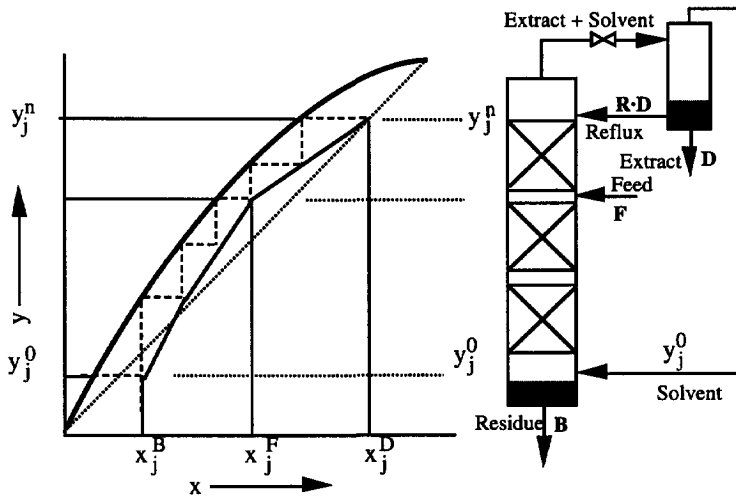


FIGURE 1.3: Counter-current (supercritical) separation process, with projected solvent free distribution graph showing the enrichment of the component in the solvent as it flows upwards.

#### INDUSTRIAL SUPERCRITICAL APPLICATIONS

Two decades ago supercritical fluids again draw attention when it was found that caffeine could be extracted using supercritical carbon dioxide. This resulted into the first commercial application of supercritical fluid extraction. It was later on followed by the extraction of hop and the production of light cigarettes both using carbon dioxide, while supercritical propane is used to extract large molecular weight compounds from oil residue in the Rose process (see e.g., McHugh and Krukoni, 1986).

After the successful start the number of new application stagnated in the eighties. Several reasons for this can be pointed out. One is undoubtedly the magical sound of the term supercritical processes, which caused too high expectations. When supercritical processes are compared with conventional techniques, the supercritical process should have clear advantages. When it hasn't, or at least not clearly, the conventional technique is obviously more appealing to any chemical manufacturer. Unfortunately, in the case where supercritical processes offer new prospects, as the creation of new products, the process suffers from substantial initial investment costs. This causes a major drawback if one first wants to probe the market prospects. The revival or maybe survival of supercritical extraction will depend on industrial feasible projects, which will lead to clear and unambiguous benefits in the end products. One of these benefits is offered by the traditionally used solvent carbon dioxide. Carbon dioxide belongs to the rapidly decreasing group of non toxic and environmental friendly chemicals, of which water and nitrogen appear to be the only other surviving members. This becomes an advantage, as rapid as the decrease of this group. It is likely that supercritical techniques will in fact replace standard techniques that use conventional solvents at this moment. An other

potential of the supercritical separation process that hardly has been explored so far, is the possibility of low energy use in a supercritical extraction process. This potential will be investigated in this thesis.

### THE BACKBONE OF SEPARATION DESIGN

The whole design of a supercritical extraction process is an interaction of several disciplines. These disciplines are playing together as the players of a football team. There only can be eleven winners or eleven losers. The heart of the process is the actual separation of the components. In the following it will be assumed that the separation is carried out in a column. The line-up of the disciplines is given in figure 1.4, where a flow diagram shows the construction of a separation process for a certain product. The top row represents the economical activity, which will be considered as a boundary condition specifying on the left hand side the products and on the right hand side the achieved benefits. The technical part of diagram, represented by the white and slightly shaded boxes, is governed by this top row and the final justification of a process is indicated by the benefits of a product. This box represents the "separation process referee" and is fed by the process costs of and the market revenues.

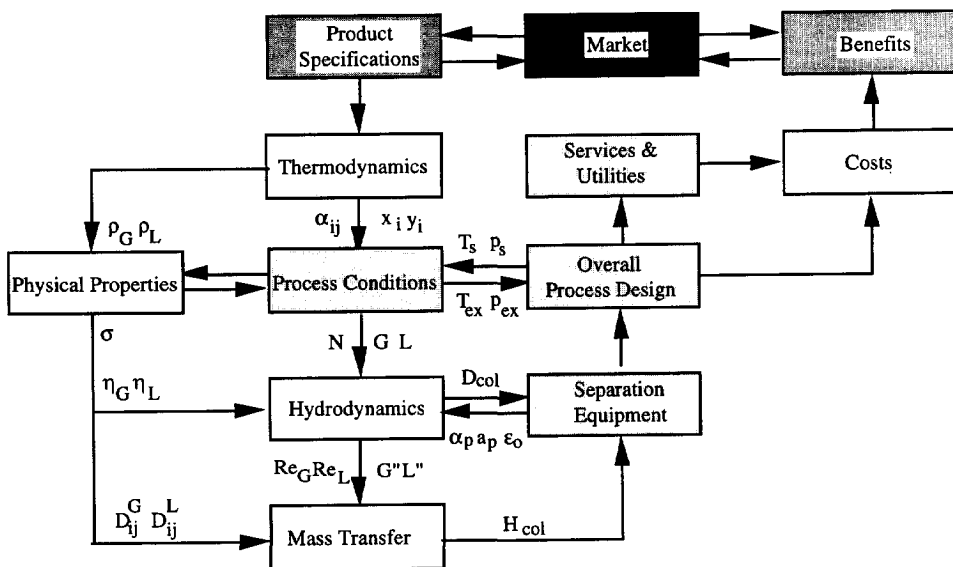


FIGURE 1.4: Flow diagram of the interacting technical and economical disciplines for the design of a separation process. The symbols representing process parameters are explained in the text.

The fundamental part of the process design is covered by the four disciplines indicated with white boxes. The whole process design is in fact close to a one way street of activities, in which a next activity is fed by the previous one. A process design has to start with establishing

the thermodynamics of the system. The thermodynamics of the specified separation will disclose the relative distribution of the components ( $x_i, y_i, \alpha_{ij}$ ) over the phases. Next to this it determines the density of the phases ( $\rho_G, \rho_L$ ) between the phases. The technical feasibility of a process is often determined on basis of thermodynamic behaviour. The next step is the selection of the process conditions, which will determine the required number of equilibrium steps ( $N$ ) and the flow rates of the phases ( $G, L$ ). Following the diagram on the left side a parallel action in the process design is the determination of the physical properties of the phases, being the viscosities ( $\eta_G, \eta_L$ ) and the diffusion coefficients ( $D_{ij}$ ) of each component with respect to every other component and the surface tension ( $\sigma$ ) between the phases. Together with the densities, the viscosities and the surface tension, are used in the calculations concerning the hydrodynamics of the system. This will lead to the technical feasible throughputs per cross section equipment area ( $G'', L''$ ) and consequently the column diameter ( $D_{col}$ ). The hydrodynamics will influence the effective mass transfer resistance, which is characterised by the Reynolds numbers ( $Re_G, Re_L$ ) of the flows for known specific interface area of the separation equipment. The fundamental part is crowned by the calculation of the required mass transfer area. This will determine the height ( $H_{col}$ ) of the separation column. Clearly, the discipline with the least accurate results will become the bottle-neck of the process design and it will be useless to carry out the other disciplines much more precise.

The engineering part of the diagram, indicated with slightly shaded boxes, is fed by the information obtained from the fundamental disciplines and the determination of the process conditions. However, the engineering disciplines also influence the fundamental part of the process design. The hydrodynamics of the system is influenced by the choice of separation equipment. In case of a packed column the internals determine the capacity of the column via the void fraction or the relative available space for the flow ( $\epsilon_0$ ), the effective inclination angle ( $\alpha$ ) of the flow and the available interface area per unit equipment volume ( $a_p$ ). By calculating the loop connecting the hydrodynamics, mass transfer and separation equipment several times, these equipment parameters can be optimised so that the most cost effective separation is created. The overall process design determines the extraction conditions ( $T_{ex}, p_{ex}$ ) and the conditions ( $T_s, p_s$ ) for the solvent recycling. These design parameters will influence the capital investments and the running costs of a process more than the design of the column itself. A supercritical process is no exception to the rule that the economic feasibility of the process, which condenses in the benefits, is determined mainly by the overall process design and not by the main equipment item; the column. In the case of supercritical extraction, both capital and running costs are strongly influenced by the choice of product recovery and solvent recycling method. For each process condition one needs to calculate both the capital and the operating costs for the always required minimisation of the total production costs.

## SCOPE AND STRUCTURE

This PhD thesis is the continuation of a study previously carried out by the de Haan (1991) on supercritical separation of liquids. It intends to investigate the influence of the fundamental disciplines and their consequences on the design of a supercritical separation plant. This has been done in the framework of a the supercritical extraction process. The supercritical extraction turns out to present an excellent process to generalise some aspects of fluid-fluid operations. Given the limitations of the pilot plant used by de Haan, a new pilot plant was designed and constructed to enable the study of several hydraulic aspects of packed columns at supercritical conditions.

The outline of this thesis will follow the subsequent steps shown in figure 1.4, since it simply forms the base structure for a separation process. After the description of the new experimental pilot plant, the first chapters focus on hydrodynamic aspects and mass transfer in packed columns. The developed models for pressure drop and mass transfer, subsequently will be used to design packed columns for specific application at conventional conditions. Experimental data at supercritical conditions on pressure drop, flooding and mass transfer, will be used to verify the models at high pressure conditions. After this some general engineering aspects of supercritical processes will be discussed, especially focusing on the potential of an isobaric supercritical separation. In the last part of this thesis three potential supercritical extraction processes will be worked out.

Rather than to end this thesis with a series of conclusions, it is tried to point out the potentials and bottle-necks concerning supercritical separations. Suggestions are made for possible future research projects to increase and improve the knowledge of supercritical separation technology.

## REFERENCES:

- [1] Haan, de A.B. (1991). *Supercritical fluid extraction of liquid hydrocarbon mixtures*. PhD Thesis, Delft: Delft University Press.
- [2] Hanney, J.B., and Hogarth, J., (1879), Proc. R. Soc. London **29** pp. 324-326.
- [3] McHugh, M.A., and Krukoni, V.J., (1986), *Supercritical Fluid Extraction: Principles and Practice*, Butterworths, Stoneham.





# Experimental Set-Up

The supercritical extraction facilities at the Laboratory of process equipment of Delft University of Technology consist of two experimental installations. The first rig, described by de Haan (1991), is a skid mounted explosion proved rig built by SITEC in 1989, which is constructed around a one meter packed bed stripping column with 35mm inside diameter and a one litre batch extraction vessel. A new experimental facility has been constructed for liquid systems using carbon dioxide as a solvent at the Delft University of Technology. Its purpose was twofold. It was built to obtain a better understanding of fundamental principles within the supercritical separation processes and it should be able to produce enough material (>5kg) to evaluate new commercial products extract with sufficient purity in a limited production time (<12h). The high purity requirement made a construction of a reflux system necessary. This has been accomplished with the installation of a double coil in the top section of the column, so that the solvent flow can be heated to decrease its solubility power. The design of the rig was completed in September 1992 and the construction took one year. The commissioning of the equipment started early January 1994 and the whole rig operated on mechanical and electrical design specification three months later. A process flowsheet is shown in figure 2.1 and a flowsheet of the utilities is shown in figure 2.2. In both flowsheets the specifications of the main plant items are indicated.

### Packed Extraction Column

The extraction column **C-1** has an internal diameter of 36mm and an overall length of 3.1 meter. The column is divided into segments of 0.40m. Between each segment, connectors are mounted which can be used for insertion of sensors of various instruments.

To enable a stable operation, the residue is removed from the bottom of the column continuously. This is done by measuring the residue level in the bottom of the column using a differential pressure transmitter (PIC-9). This liquid level signal is used to adjust proportionally a pneumatic needle valve in the bottom outlet stream. The carbon dioxide inlet is placed above the low pressure leg of the bottom level control. Above the carbon dioxide inlet the column is filled with structured packing elements, constructed of corrugated metal gauze sheets. The height of a packing element is 0.16m. The total packing height is 2.03m with a specific packing area of  $740\text{m}^2/\text{m}^3$ . An element is placed on top of a previous element with the horizontal

direction of the sheets turned over 90°. The liquid is distributed over the top of an element and flows down wetting the packing surface. The gas flows upwards through the channels formed by the sheets.

If the desired operation is a stripping column the liquid feed will be located at the connector above the packing. When the feed is placed at one of the other connectors, the column is divided into a rectifying section and a stripping section.

The pressure drop over a section of 0.86m of packing is measured using a differential pressure transmitter (PI-8). The temperature is measured at the middle of the column (TIC-5) and is controlled by adjusting the hot water flow to the column jacket. The internal diameter of the top section of the column is increased to 39mm, to enable the insertion of a double heating coil used to produce the reflux. Both the double coil and the jacket of the top section are provided with a separate oil service flow. The total heating area of the coil and jacket is equal to 0.18m<sup>2</sup>. Above the coil, a demister is placed and the temperature is measured (TI-7). The total heat input to the extract stream is determined by measuring flow and the inlet (TI-13) and outlet (TI-12) temperature of the hot oil supply. The pressure of the column is measured 2 meters above the bottom of the column (PC-6) and its reading adjusts a pneumatic needle valve controlling the operating pressure continuously. The column is protected with a burst disc of 320bar. Sapphire windows with a view diameter of 8mm are installed at all for the operation important locations.

### The Carbon Dioxide Cycle

The carbon dioxide for the extraction is contained in the supply tank **V-3**, which is maintained at a pressure of approximately 50bar. The vessel is filled with liquid carbon dioxide from the recycle stream and fresh carbon dioxide from the storage. The carbon dioxide is pressurised using pump **P-1** after which it flows through heat exchanger **E-1**. The temperature (TIC-3) and mass flow (MI-4) of the solvent entering the column are measured. After the extraction the pressure of the laden carbon dioxide flow is reduced to approximately 50bar and the phase separation occurs in separation vessel **V-4**. The expanded carbon dioxide is evaporated from the product by controlling the temperature (TIC-14) of the separation vessel by supplying hot water to the jacket of the vessel. Instead of controlling the temperature of the vessel it is also possible to maintain a certain level in the separator using the differential pressure transmitter ( $\Delta$ PC-15). The gaseous carbon dioxide is condensed in a heat exchanger **E-2** and returned to the carbon dioxide storage vessel **V-3**. The cooler **E-2** uses a water-glycol mixture as cooling medium, which is recirculated through a freon-22 refrigerator.

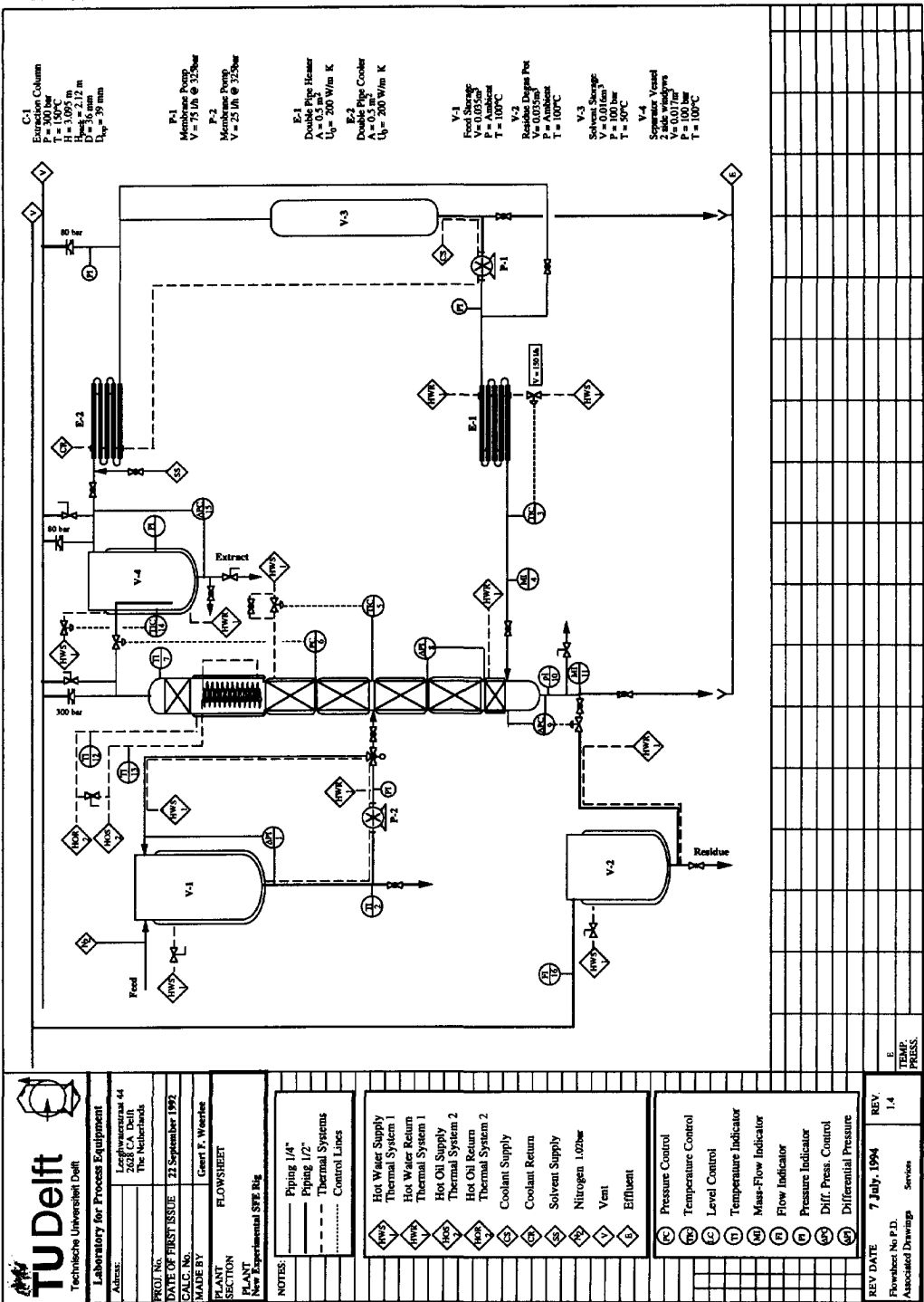


FIGURE 2.1: Process flowsheet of the main equipment for the new experimental supercritical separation set-up at Delft University of Technology.

Utilities

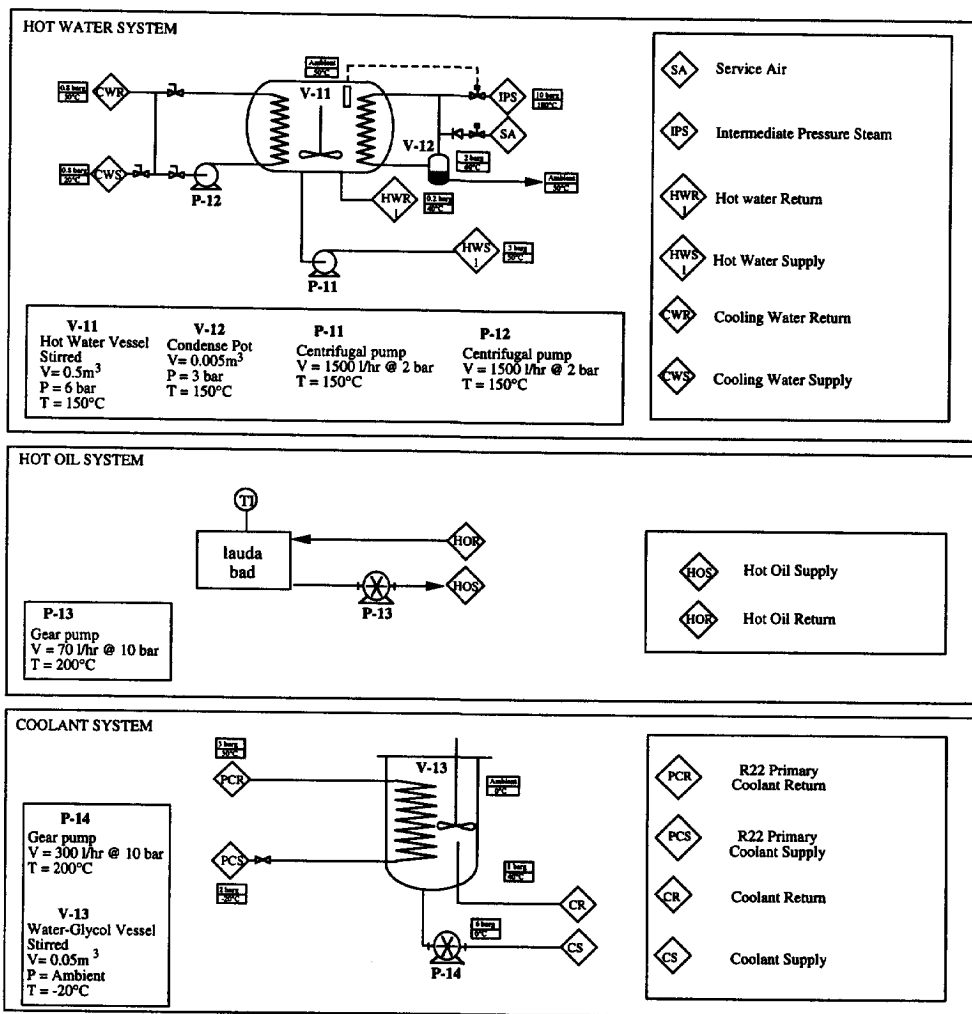


FIGURE 2.2: Flowsheet of the utilities for the new experimental supercritical separation set-up at Delft University of Technology.

### The Product Cycle

Before extraction, the original product is stored in vessel **V-1**. The level of this vessel is continuously monitored using a differential pressure cell ( $\Delta$ PI-1). The temperature of the product is also continuously measured (TI-2) and can be adjusted by using a manually operated needle valve in the hot water supply for the jacket of the vessel. The vessel can be blanketed with nitrogen if required. When the carbon dioxide cycle is established, the product can be fed by pump **P-2** into the column. The product partly dissolves in the carbon dioxide and flows as the solvent rich phase to the top of the column. The finally extracted product is expanded with the solvent to 50bar at which it is separated from the solvent by evaporating the carbon dioxide. The extract can be removed from separator vessel **V-4** after or during the experiment using the needle valve located at the bottom of the vessel.

The not extracted part of the product flows down by gravity to the bottom of the column. Before it is expanded over the needle valve, the mass (MI-11) and density ( $\rho$ I-10) are measured using a coriolis mass flow meter. The vessel **V-2** is used to store the residue of the product and operates at a near ambient pressure. The closed vessel has an outlet to purge the carbon dioxide dissolved in the residue stream. The flowrate of this purge stream is recorded automatically (FI-16). The temperature of the vessel can be adjusted manually by using the needle valve in the hot water supply line to the jacket of the vessel.

### The Data Collection.

The control of the equipment is carried out via programmable controllers and indicators. A Fischer & Porter data acquisition system takes care that the signals collected and passed on to a computer every ten seconds. This enables a dynamic analysis of the experiment using the historical trending facilities on the control computer. Cross-checks of the obtained data are made by local manometers, thermometers and flow meters, while the set values of the pump indicate the feed flows. The rig was designed in such way that no parameter was obtained without an independent second reading or check. In this way simple operating errors can be found in minutes, while mechanical or electrical difficulties are normally traced within an hour. The readings of the computer were also stored on floppy disk for external evaluation.

### Experimental Procedure

The extraction column has an operating range of 50-300 bar and 15-90°C. An experiment was started by filling the system with carbon dioxide and lining up the solvent cycle to the column. Hereafter pump **P-1** is started to pressurise the column further. When the column is on its operating pressure and temperature the product can be fed into the column using pump **P-2**. After a few minutes the product residue reaches the bottom of the column and a liquid level is established. To enable a smooth bottom flow control it was needed to trace electrically the legs

connecting the pressure difference cell and the column to ensure a constant density in the legs. In the bottom section of the column a sapphire window was placed. When the flows were stabilised it was relatively simple to find a set point that keeps the residue level in the middle of the sapphire window.

Depending on the applied flows and the solubility of the products in the solvent, a typical time required to obtain stable operation for an experiment with the column operated as stripper is ten minutes, while for the column operated in rectifying mode it typically takes one hour to reach stable operation.

Rectifying experiments showed that the reflux system operated according to its specification. This indicated that, for the product systems applied, the demister path installed in the top section of the column functions adequately.

### EXPERIMENTAL VERIFICATION

Figure 2.3 illustrates the benefits of a continuous monitoring of the solubility of the components using the bottom flows of the column. The degassed product residue stream can be calculated by subtracting the carbon dioxide flow from the total residue flow, so that the total extracted material also can be calculated on basis of the product feed and the degassed bottom flow.

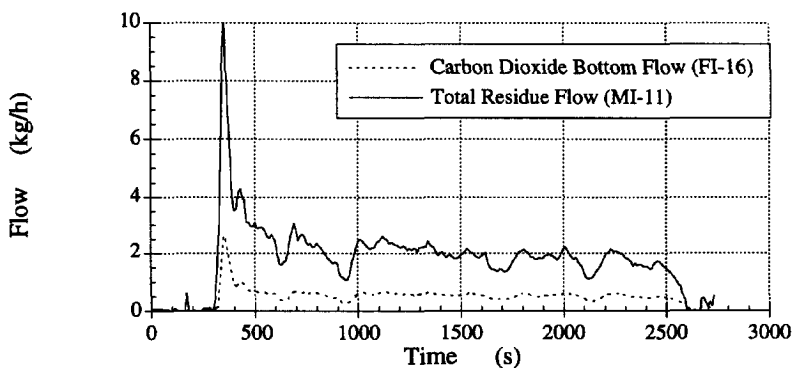


FIGURE 2.3: Measured bottom flows during an extraction experiment.

The figure also shows the start-up of the bottom level control (peak at start). Because of the sensitivity of the level indicator to small disturbances in temperature, concentration, etc., and because its settings depend on operating conditions and bottom stream properties, the response is set at a low value. This enables the adjustment of the level set-point during the experiments without causing severe disturbances, but it causes as a side effect a flow overshoot in the start-up period.

An additional benefit of the density measurement of the residue stream is that it also enables a dynamic evaluation of the experiment. According to the curve shown in figure 2.4 the first opening of the bottom valve is at 150s, and it takes about 350s for the residue density to become stable.

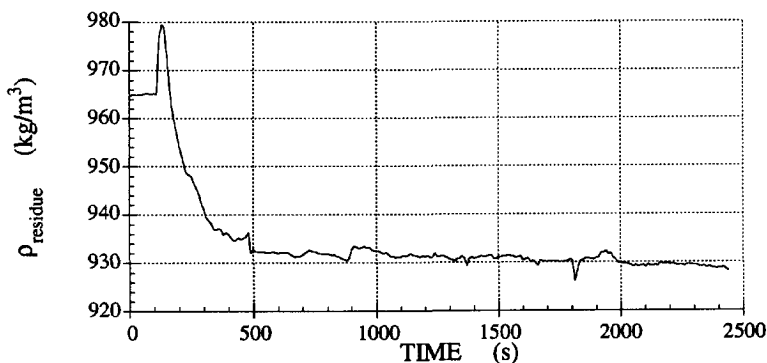


FIGURE 2.4: Measured residue density during a stripping experiment.

Varying the operating conditions and product systems we were confronted with some unexpected results, which ultimately helped to recognise some problems, which are important for the design of industrial scale installations. An example is given in figure 2.5, showing the temperatures during a stripping experiment. In this experiment an entrainer was added in the product feed. When the experiment was started, the temperatures of the carbon dioxide feed and the top and the middle of the column were within a two degree difference. However, almost directly after the start of the product feed into the column, the temperature in the top of the column rose rapidly. This seems to be caused by the instant evaporation of the low volatile entrainer into the solvent stream. The mixture of solvent-entrainer has a smaller molar volume than the pure solvent, which causes a heat release. This "condensation" heat is substantially larger than the heat required to evaporate the entrainer from the product.

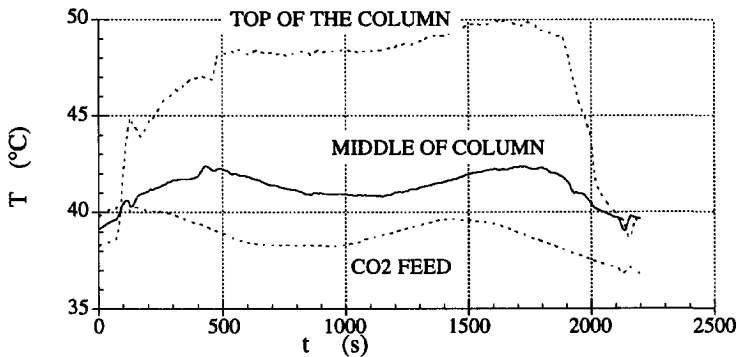


FIGURE 2.5: Measured temperatures during a stripping experiment.

#### Column Stability

Figure 2.5 contains an implicit warning for the engineer designing a supercritical separation. A supercritical solvent will carry the more soluble component, so that the largest solvent densities in an isothermally operated column are consequently found in the top of the column. This means that the operation can become unstable. A demonstration of this phenomenon can be found in the paper of Tiegs and Peter, (1985). The reported decrease of the selectivities for smaller throughputs can be explained by the hydraulic instability of the column.

The column should be designed so that no back mixing of the solvent rich phase can occur. A reflux system using a temperature increase has the advantages of stabilising the density profile of a supercritical separation column. However, the total stability of the column should be evaluated and if required the superficial solvent velocity or the pressure drop over the column should be adjusted. This can for instance be achieved by decreasing the local (top) column diameter or by applying a packing with a larger pressure drop.

#### REFERENCES:

- [1] Haan, de A.B. (1991). *Supercritical fluid extraction of liquid hydrocarbon mixtures*. PhD Thesis, Delft: Delft University Press.
- [2] Tiegs, C. and Peter, S., (1985), *Zur Trennung von Öl-/Stearinsäure-Gemischen durch Extractions mit einem überkritischen Lösungsmittel.*, *Fette-Seifen-Anstrichm.*, **87**, pp231-235.



## A Comprehensive Model for the Pressure Drop in Packed Columns

Due to the complicated nature of the counter-current gas liquid flow, earlier studies on packed column hydraulics have been mostly limited to correlating the experimental data. Newest correlations for the prediction of pressure drop, liquid hold-up, and flooding in packed columns are surveyed in Kister's book on the design of distillation columns (Kister, 1992). Although some of the described methods do incorporate sound physical basis there exists little generality among them.

The interaction between a falling film and a counter-current gas stream, appearing in equipment as wetted wall columns, falling film evaporators and reflux condensers, have been the subject of many thorough studies (Feind, 1960; Wallis, 1969; Imura et al., 1977). Zabarás and Dukler (1986) reported that the models proposed in literature for flooding have been not so successful, because of the lack of reliable local measurements needed for the evaluation of the physical mechanisms that control the process. Their experimental effort, which included measurements of the liquid distribution at up flow and down flow along with the time-depending measurements of local film thickness and pressure gradient, gave a somewhat different picture than drawn previously (Hetsroni, 1982). Anyhow, new questions arose and other speculations concerning the gas liquid interaction appeared requiring further investigations.

Recently, Kaiser (1993), who considered the liquid flow in a packed bed as a free surface gravity flow influenced by the upward flowing gas, has demonstrated that a more phenomenological approach to correlate experimental data could be rewarding if fully explored. In response to this we try to investigate the limits of a macroscopic approach to the description of the hydrodynamics of two-phase counter-current flow in a packed bed consisting of a number of inclined flow channels. In these channels annular flow is assumed and interface friction and form drag are taken into account. Closing the relations with the necessary boundary conditions a set of four equations is obtained that permits prediction of liquid hold-up and pressure drop in packed columns containing random or structured packing. Special attention is paid to the determination of the gas-liquid friction factor, since this has turned out to be the key to a successful description of the two phase flow behaviour and the description of the mass transfer in a packed bed.

### MACROSCOPIC DESCRIPTION OF THE FLOWS

It is assumed that flooding in counter-current operations is caused by the interaction at the interface of the flows. Hutton et al., (1974), postulated that at least two types of liquid-flow instability can occur to initiate flooding, depending on the effective voidage of the packed bed. The first type, observed in conventional random packing, is due to interaction between the liquid hold-up and pressure gradient. The second is a wave type instability as encountered in wetted wall columns, which can be considered as a boundary case of the inclined flow channel embodied in corrugated sheet structured packing. High performance random packing, with porosities over 90%, and shapes that promote droplets forming, represent an intermediate case. In chapter 4 of this thesis we will analyse the second type of flooding mechanism extensively. In this chapter we will examine whether pressure gradients and hold-up of all types of random and structured packing can be described in a uniform way assuming a characteristic inclined flow channel.

The geometry of a packed bed with a given porosity can be considered as a multiplicity of flow ducts consisting of a number, serially connected tubes. To keep the analysis simple, it is assumed that the steady state is maintained and that the liquid is residing in a laminar film of uniform thickness at the channel walls, separated from the gas flow by a macroscopically stable interface.

#### *Solution of the Equation of Motion for Liquid Flow*

The flow model taken here as basis for the further development is essentially that proposed by, e.g.: Brauer (1960), Hikita and Ishimi (1976), for wetted wall columns, with laminar annular liquid flow and a central gas flow. The average velocity profile of a counter-current flow in a tube with radius  $r_0$  is shown in figure 3.1.

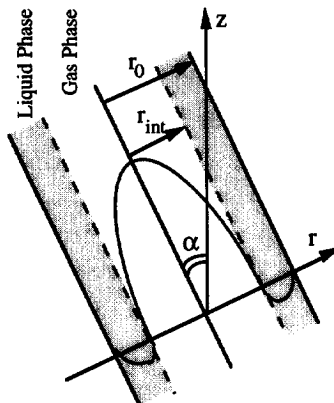


FIGURE 3.1: Velocity profile of a counter-current liquid and gas flow in a tube.

The interface is located at a distance  $r_{\text{int}}$ , which is the actual radius of the gas flow channel. Since the flow has axial symmetry, the velocity vector is dependent on the radial component  $r$  only. Then, the Navier Stokes momentum equation for a Newtonian incompressible liquid with viscosity  $\eta_L$  and density  $\rho_L$  moving in the gravitational direction enclosed by a gas with density  $\rho_G$  reduces to:

$$0 = -\left(\Delta\rho g + \frac{\partial p}{\partial z}\right) \cos \alpha + \eta_L \left[ \frac{1}{r} \frac{\partial}{\partial r} \left( r \frac{\partial u_L}{\partial r} \right) \right], \quad (3.1)$$

where  $u_L$  is the velocity,  $\Delta\rho$  is the density difference between the two phases and  $\alpha$  represents the angle of the flow with the direction of gravity. In this study  $g$  is the absolute gravitational acceleration and its direction will be taken into account by a negative sign. The pressure drop in the axial direction  $\partial p/\partial z$  over an arbitrary structure, comprises frictional resistance and geometric resistance or form drag;

$$\frac{\partial p}{\partial z} = \frac{\partial p_f}{\partial z} + \frac{\partial p_g}{\partial z}, \quad (3.2)$$

and will in general be negative as well. The geometrical resistance is equal to zero when only straight tubes are considered. However, it contributes substantially when there are obstructions or bends in the gas flow as in a packed bed. The boundary conditions for equation (3.1) are:

$$\text{for } r = r_0 : u_L = 0 \quad (3.3a)$$

$$\text{for } r = r_{\text{int}} : u_G = u_L = u_{\text{int}} \quad \text{and} \quad \eta_G \frac{\partial u_G}{\partial r} = \eta_L \frac{\partial u_L}{\partial r} \quad (3.3b)$$

where  $u_{\text{int}}$  represents the interfacial velocity. The core and annular flows are distinguished by the subscripts G and L. It is convenient to generalise the calculations by introducing a dimensionless interface radius as:

$$\theta = \frac{r_{\text{int}}}{r_0}. \quad (3.4)$$

Using the boundary conditions (3.3a) in the differential equation (3.1) the liquid velocity is found;

$$u_L(r) = \frac{(r^2 - r_0^2)}{4\eta_L} \left( \Delta\rho g + \frac{\partial p}{\partial z} \right) \cos \alpha + \left[ \frac{(1 - \theta^2) r_0^2}{4\eta_L} \left( \Delta\rho g + \frac{\partial p}{\partial z} \right) \cos \alpha + u_{\text{int}} \right] \left( \frac{\ln \left( \frac{r}{r_0} \right)}{\ln(\theta)} \right). \quad (3.5)$$

After integration and dividing by the total area ( $\pi r_0^2$ ), this yields the following expression for the superficial liquid velocity  $u_{\text{SL}}$ :

$$u_{\text{SL}} = -\frac{(1 - \theta^2)^2}{8\eta_L} \left( \Delta\rho g + \frac{\partial p}{\partial z} \right) \cos \alpha r_0^2 - \left[ \frac{(1 - \theta^2) r_0^2}{4\eta_L} \left( \Delta\rho g + \frac{\partial p}{\partial z} \right) \cos \alpha + u_{\text{int}} \right] \left( \theta^2 + \frac{1 - \theta^2}{2 \ln(\theta)} \right). \quad (3.6)$$

The superficial liquid velocity, which normally is negative, will be used as an input condition. To solve the boundary condition at the interface one uses a force balance over the core gas flow at the interface. This allows us to write the shear stress at the interface as:

$$\frac{1}{\cos \alpha} \eta_G \frac{\partial u_G}{\partial r} \Big|_{r=r_{\text{int}}} = \frac{\partial p_f}{\partial z} \frac{\theta r_0}{2}. \quad (3.7)$$

Here the frictional pressure drop is taken along the flow direction. This choice increases the distance and therefore the frictional pressure drop in the gravitational direction by a factor of one over the  $\cos \alpha$ . Using equation (3.7) for the gas flow shear stress and the derivative of the liquid velocity at the interface (equation (3.5)), the shear stress interface condition (3.3b) can be solved and the interfacial velocity can be isolated as:

$$u_{\text{int}} = - \left[ \theta^2 \ln(\theta) \left( \Delta \rho g + \frac{\partial p_g}{\partial z} \right) \cos \alpha + \frac{(1 - \theta^2)}{2} \left( \Delta \rho g + \frac{\partial p}{\partial z} \right) \cos \alpha \right] \frac{r_0^2}{2\eta_L} \quad (3.8)$$

Here relation (3.2) between friction pressure drop, geometrical and total pressure drop has been used to eliminate the frictional pressure. It is at this point that use has been made of the clear distinction between the frictional pressure drop and the geometrical pressure drop, which is an essential step in the mathematical derivations.

### The Pressure Drop Contributions

Before describing the pressure drops the approach based on pipe flow needs to be adapted for an arbitrary structure; a packed bed. Therefore the specific surface area  $a_p$  and the porosity of the packing  $\epsilon_0$  are related to the hydraulic radius as:

$$r_0 = \frac{2\epsilon_0}{a_p} \quad (3.9)$$

The effective porosity of the irrigated bed,

$$\epsilon_{\text{irr}} = \epsilon_0 - h_L = \epsilon_0 - (1 - \theta^2)\epsilon_0 = \epsilon_0\theta^2, \quad (3.10)$$

is then a simple function of the dimensionless radius, where  $h_L$  represents the operating liquid hold-up.

### Frictional Pressure Drop

As already mentioned, in a packed bed the pressure drop is generally caused by a combination of frictional resistance and the geometric resistance. The frictional pressure drop can be expressed as function of a friction factor  $f$  in a tube and the velocity differences as:

$$\frac{\partial p_f}{\partial z} = - \frac{f}{\cos \alpha} \frac{\rho_G \left( \frac{u_{SG}}{\epsilon_0 \theta^2 \cos \alpha} - u_{\text{int}} \right) \left| \frac{u_{SG}}{\epsilon_0 \theta^2 \cos \alpha} - u_{\text{int}} \right|}{\theta r_0} \quad (3.11)$$

where  $u_{SG}$  represents the superficial gas velocity, which is also used as input condition. Here, as well as in the case of the liquid phase, the superficial velocity is related to the cross section area of the column. In the column the actual gas velocity in the channels is obtained by dividing the superficial gas velocity by the irrigated bed porosity ( $\epsilon_0\theta^2$ ) and  $\cos\alpha$ . For a smooth interface the Blasius equation can be applied to estimate the friction factor of a turbulent flow,

$$4f = 0.3168 \text{Re}_G^{-0.25} \quad (3.12)$$

Here the gas flow Reynolds number is defined as:

$$\text{Re}_G = \frac{\rho_G \left| \frac{u_{SG}}{\epsilon_0 \theta^2 \cos \alpha} - u_{\text{int}} \right| 2\theta r_0}{\eta_G} \quad (3.13)$$

Both the gas load and the liquid load will influence the state of the interface, which will result in a wavy rather than a smooth interface. The consequence of this wavy interface is an increase of the radially directed shear stresses (see figure 3.2), which are directed perpendicular to the flow. Since the interface has to remain unbroken, every force on the interface has to be compensated with a reaction force. Therefore the average of the radially directed shear stresses are, when integrated over time or when integrated over the total surface area, necessarily equal to zero. As a consequence there is no other force directed parallel with the liquid flow than the force described by smooth pipe flow. However, since the energy losses are related to the square of the actual velocities, the wavy interface will cause an additional pressure drop in the gas phase. This pressure drop will be analysed in the section describing the gas-liquid interaction.

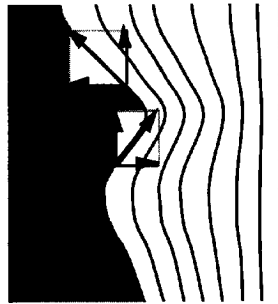


FIGURE 3.2: The friction on the interface, illustrating that the area averaged forces on the flow must equal zero.

*Geometrical Pressure Drop*

This component of the pressure drop does not affect the liquid film directly and is largely a term that expresses the amount of work done by the gas to overcome all changes in flow directions and other kinds of form drag. The Ergun equation relates the friction factor of a packed bed to its Reynolds number  $Re_p$ . The relation can be formulated as:

$$4f_p = 4(f+f_g) = 4 \left| \frac{\partial p}{\partial z} \right| \frac{\theta r_0}{\rho_G \left( \frac{u_{SG}}{\epsilon_0 \theta^2} - u_{int} \cos \alpha \right)^2} = \frac{600}{9} \frac{\eta_G}{\rho_G \left( \frac{u_{SG}}{\epsilon_0 \theta^2} - u_{int} \cos \alpha \right) \theta r_0} + \frac{28}{12} = \frac{133}{Re_p} + 2.33 \quad (3.14)$$

where both the frictional and the geometrical term is included. The relation takes into account all possible pressure drops contributions, it is therefore likely that its general form can be used to describe other types of packed beds. The only difference in the Reynolds number for the tube and for the packing is the cosine term. They are simply related as:  $Re_p = Re_G \cos \alpha$ .

Zogg (1972) measured the pressure drops of corrugated sheets with smooth unperforated surfaces and different inclinations of the flow channels and extrapolated his results for limited geometries to an infinitely wide geometry to eliminate wall effects. Figure 3.3 shows these extrapolated results as friction factors, together with the Ergun relation and the friction factor of

a smooth pipe. The characteristic coefficients were obtained by fitting the experimental data using a Ergun type relation,

$$4f_p = \frac{4f_l}{Re_p} + 4f_\infty \tag{3.15}$$

where  $f_\infty$  represents the friction coefficient at infinite Reynolds number and  $f_l$  represents the laminar part of the friction coefficient. Figure 3.3 shows that the friction factor of a packed bed can in general be represented by equation (3.15).

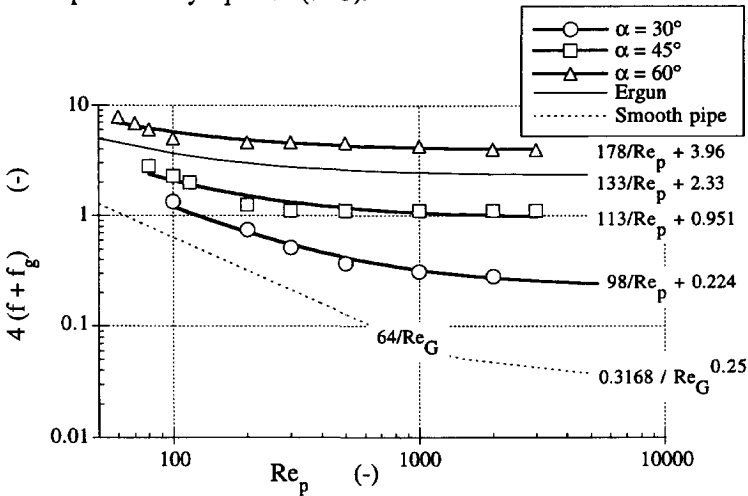


FIGURE 3.3: The packing friction factor as function of the Reynolds number for structured packing with different angles, for the Ergun relation and for a smooth vertical pipe. The structured packing data are fitted with a relation similar to the Ergun relation.

The Effective Inclination Angle

To generalise the results on the inclination angle of the flow, it is necessary to interpret the obtained coefficients shown in figure 3.3. Therefore, we have illustrated the macroscopic gas flows within corrugated sheets in figure 3.4.

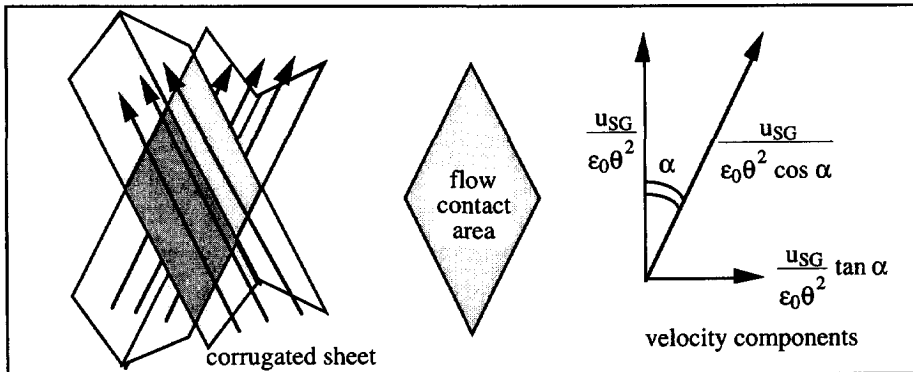


Figure 3.4: Schematic view of the gas flow in corrugated sheets. Indicated are the contact area of the flow and the velocity components.

If first the friction losses in a laminar flow are considered, it is noticed that they are fully caused by the shear stress with the walls. This means that the angle influence in the laminar part is caused by the increase of the distance that the fluid travels through the packing. By multiplying this term by  $\cos(\alpha)$  a channel friction factor should result, which is independent of the inclination angle. This is indeed the case as is shown in figure 3.5A.

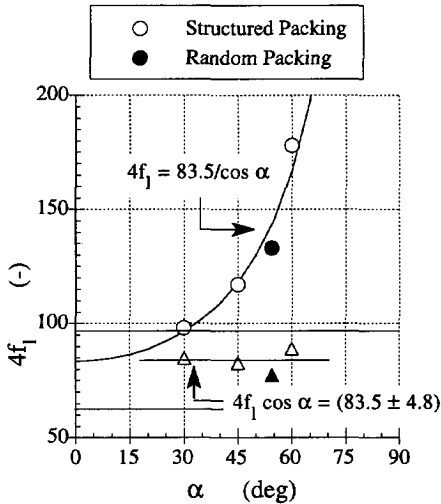


FIGURE 3.5A: The laminar part of the packing structure as function of the effective packing angle, with its natural boundaries for a cylindrical (64/Re) and parallel plate (96/Re) geometry.

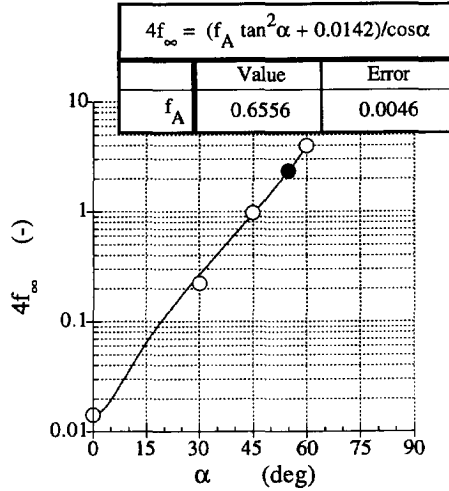


FIGURE 3.5B: The graph shows the friction factor at infinite Reynolds number as function of the effective packing angle. The random packing parameters are obtained from the Ergun relation.

The laminar friction coefficient has two natural boundaries given by the possible extreme values for a closed geometry, which are the cylindrical geometry, corresponding with a value of 64, and a rectangular or parallel plate geometry, corresponding with a value of 96. Figure 3.5A shows that an average value of 83.5 is found for this coefficient and that the data points are all within the given boundaries.

The infinite friction coefficient  $f_{\infty}$  covers the fully turbulent flow region, and is strongly effected by the open contact area of the gas flows within the packing structure. In this area the radial component of the meeting flows is opposite, causing a rotation in the flow with a subsequent increase of the turbulence. Since the friction is related to the square of the velocity component the friction factor should be proportional to the square of the tangent of the inclination angle (see figure 3.4). It is again noticed that the flow path for the gas in the corrugated sheets, and so the friction, is still increased by the increased path length as one over  $\cos \alpha$ . Finally the infinite friction factor for a single phase flow can be expressed as:

$$4f_{\infty} = \frac{0.6556 \tan^2 \alpha + 0.0142}{\cos \alpha} \quad (3.16)$$

Here the constant 0.0142 represents the infinite friction factor for a smooth pipe geometry, which value is derived by fitting the total smooth friction factor for a pipe with relation (3.15). The constant 0.6556 is fitted with the data points. Figure 3.5B shows that the behaviour of the infinite friction factor is described well by relation (3.16). The pressure drop over a non irrigated packed bed therefore can be written as:

$$\frac{\partial p}{\partial z} = - f_p \frac{\rho_G \left( \frac{u_{SG}}{\epsilon_0} \right) \left| \frac{u_{SG}}{\epsilon_0} \right|}{\theta r_0} \quad (3.17a)$$

where the packed bed friction factor is expressed as:

$$4f_p = \left( \frac{83.5}{Re_p \cos \alpha} + \frac{0.6556 \tan^2 \alpha + 0.0142}{\cos \alpha} \right) \quad (3.17b)$$

This equation can be used to determine the effective inclination angle for a packing geometry, using available dry pressure drop data. When equation (3.16) is applied using the value of 2.33 as given by the original type Ergun coefficient, a characteristic effective inclination angle of 54.9° is found for random packing. When the laminar part of the friction factor is used, an effective inclination angle of 51.1° is found. Since the friction factor at large Reynolds numbers is much more sensitive to the inclination angle the best procedure to determine the effective inclination angle is by measuring the infinite friction factor.

#### The Influence of the Column Diameter on the Pressure Drop

It has been observed that pressure drop varies with column diameter (Kister, 1992). In randomly packed columns it increases and in regularly packed columns it decreases with increasing diameter. Since the diameter can have a large influence on the pressure drop and therefore on the determined effective inclination angle, it is necessary to address this effect and adjust the main equations.

The pressure drop decrease with increasing diameter in structured packing is due to the channel endings at the wall. When the gas flow reaches the wall it has to change its direction by an angle of  $2\alpha$ . This effect can be compared with a bend or elbow in the gas flow and it can therefore be expressed as an apparent increase of the channel length. This increase depends on the shape and angle of the turn and on the Reynolds number of the flow and is generally expressed in equivalent pipe diameters. By analysing the standard tables on the pressure drop increase of bends and turns (see, e.g.: Perry and Green, 1984), it is found that the apparent pipe length increase, caused by a smooth turn in the flow direction can be approximated as: 0.4  $r_0$  times the angle of flow direction change. In a column with given diameter  $D_{col}$  and height  $H_{col}$ , a total channel length  $l_t$  for the fluid can then be calculated as (see figure 3.6):

$$l_t = \left( \frac{2}{\pi} \frac{D_{col}}{\sin \alpha} + 0.4 r_0 2\alpha \right) \left( \frac{H_{col} \tan \alpha}{\frac{2}{\pi} D_{col}} \right) \quad (3.18)$$

Here the inclination angle is expressed in degrees, which varies from 0° to 90°. The diameter of the column is multiplied by the factor  $2/\pi$ , representing the average channel length within the



column. This factor takes into account that the channels that are not going through the centre of the column are shorter. The first right hand side term of equation (3.18) represents the unit length of a channel to the wall and the additional apparent length caused by the bend at the wall of the column. The second right hand side term represents the number of such channels over the height of the column. The apparent flow path length for the gas phase within the column per unit height can be expressed as:

$$\frac{l_t}{H_{col}} = \frac{1}{\cos \alpha} \left( 1 + \frac{2.5 \epsilon_0 \alpha \sin \alpha}{a_p D_{col}} \right) \Rightarrow f_p^* = f_p \left( 1 + \frac{2.5 \epsilon_0 \alpha \sin \alpha}{a_p D_{col}} \right), \quad (3.19)$$

so that the packing friction factor can be corrected for the column diameter effects.

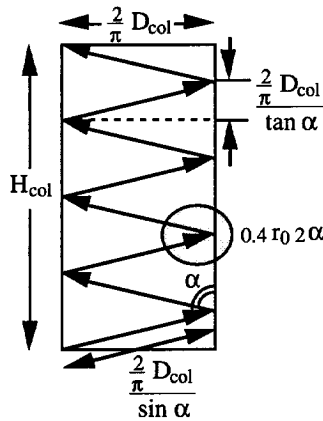


FIGURE 3.6: The flow path in a with structured packing filled column. The average sizes used to calculate the column diameter influences on pressure drop are indicated.

The cosine term is the increase in length for the gas phase, which has been taken into account in equation (3.7) for the frictional pressure drop and in the relation (3.17) for the geometrical pressure drop. The right-hand factor therefore remains as correction for the effect of the column diameter.

Since in random packing there is no well defined flow channel, the flow is not exclusively forced to turn direction at the end of the wall, but it will consider the wall as just another, in this case vertical, packing element. In smaller diameter columns the presence of the wall is felt more, causing a more vertical directed flow and therefore a smaller effective inclination angle for the packing. The effective angle of the column will become the ratio of available packing area and the total area, including the wall of the column. Adding the two area weighted angles leads to,

$$\frac{\alpha}{\alpha_0} = \frac{a_p \frac{\pi}{4} D_{col}^2}{a_p \frac{\pi}{4} D_{col}^2 + \pi D_{col}} = \frac{1}{1 + \frac{4}{a_p D_{col}}}, \quad (3.20)$$

where  $\alpha_0$  is the effective inclination angle at infinite column diameter. With equations (3.19) and (3.20) the effect of the column diameter can be estimated.

## Gas-Liquid Interaction

As stated above it can be assumed that the increasing velocity difference of the two phases, leads to a number of effects on the liquid film. The interface will first become increasingly wavy after which the gas can entrain droplets and finally force the liquid film upwards. These effects will lead to an increase of the pressure drop, which is due to extra energy dissipation in the gas phase. Therefore the pressure drop of the packed bed is written as a non disturbed pressure drop multiplied with a correction for the gas-liquid interaction;

$$\frac{\partial p}{\partial z} = -f_p (1 + \Psi_{G-L}) \frac{\rho_G \left( \frac{u_{SG}}{\theta^2 \epsilon_0} - u_{int} \cos \alpha \right) \left| \frac{u_{SG}}{\theta^2 \epsilon_0} - u_{int} \cos \alpha \right|}{\theta r_0} \quad (3.21)$$

Here  $\Psi_{G-L}$  represents the change of the friction factor due to the interaction of the gas and liquid phase. The liquid hold-up will have an important influence on the gas-liquid interaction. To describe the hold-up behaviour it is compared with the the undisturbed situation for the liquid flow. When a free falling film with a thickness ( $h_0$ ) is multiplied with the specific surface area, two characterise dimensionless numbers are found, expressing the undisturbed liquid hold-up;

$$a_p h_0 = a_p \left( \frac{3\eta_L}{\rho_L \Delta \rho g \cos \alpha} \frac{\rho_L |u_{SL}|}{a_p} \right)^{0.33} = \left( \frac{3\eta_L^2 a_p^3}{4\rho_L \Delta \rho g \cos \alpha} \frac{4\rho_L |u_{SL}|}{a_p \eta_L} \right)^{0.33} = (Ga_p^{-1} Re_L)^{0.33} \quad (3.22)$$

Here  $Re_L$  is the liquid Reynolds number and  $Ga_p$  represents the Galileo number for the packing. Equation (3.22) has the advantages that the film thickness is represented by a dimensionless number depending on the liquid flow and a dimensionless number that is depending only on the geometry and physical properties of the system.

The interaction of the gas and the liquid phase, is described using flow related dimensionless groups ( $Re_L$ ,  $Re_G$ ,  $\theta$ ) and dimensionless groups that are related to physical properties of the system ( $Ga_p$ ,  $\rho_L/\rho_G$ ,  $\eta_L/\eta_G$ ). By analysing literature data (Krehenwinkel and Knapp, 1987; Dukler et al., 1984), own data and comparing the results with pressure drop correlations given in literature (e.g.: Feind, 1960; Teutsch, 1964; Hetsroni, 1982; Billet and Schultes, 1991), the gas-liquid interaction parameter in counter-current flow was correlated as:

$$\Psi_{G-L} = \sinh \left[ \frac{34 \times 10^{-15} (1-\theta^2)^7}{(\cos \alpha)^9} \frac{Re_L Re_G^{1.5} \rho_L \eta_L}{Re_L^2 Ga_p^2 \rho_G \eta_G} \right] = \sinh \left[ \frac{34 \times 10^{-15} a_p h}{(\cos \alpha)^9 \epsilon_0^7 (h_0)^6} \frac{h}{\rho_G \eta_G} \right] \quad (3.23)$$

Here  $h$  represents the liquid film thickness, which can be expressed as:  $h = 0.5 (1-\theta^2) r_0$ . The sinus hyperbolic form is used because the friction factor in a pipe flow increases exponentially with increasing surface roughness (see, e.g.: Nunner, 1956). The exponential form can also be justified as an increase in the turbulent viscosity (Datta, 1993), which is closely related to the interface roughness. When either the gas or liquid flow gets small, the gas-liquid interaction parameter of equation (3.23) becomes small as well and the undisturbed situation remains. In the next section the correlation will be tested using pressure drop in both random and structured packing. In chapter 5 of this thesis the relation will be connected with the mass transfer coefficients in contact equipment.

Calculation Procedure

At given liquid load, specified by equation (3.6), and given gas load, specified by equation (3.11), the film thickness, interface velocity, frictional pressure drop and total pressure drop have to be determined. These quantities can be solved using the velocity at the interface, expressed in equation (3.8), and the relations for the friction factor (3.12) and the total pressure drop (3.23). However, the parameters can not be expressed explicitly, so that the relations are to be solved using an iteration procedure. The calculation is started using initial estimates for the variables mentioned and continues until a satisfactory agreement between the subsequently calculated values is reached. The calculation procedure, including the initial calculations, is shown in figure 3.7.

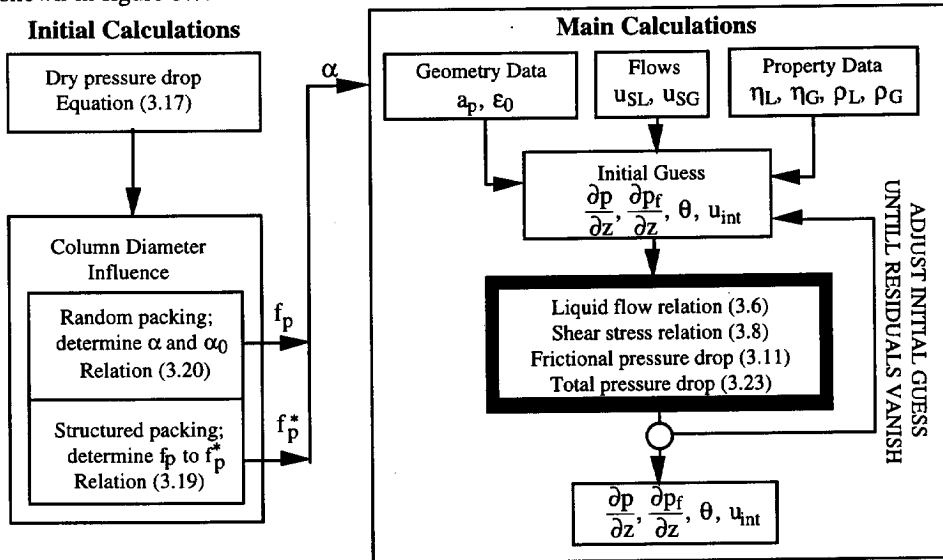


FIGURE 3.7: Block diagram showing the calculation method for the implicit flow parameters and the secondary parameters as column diameter corrections and the effective inclination angle.

RESULTS AND DISCUSSION

Following the above strategy it is possible to calculate all parameters of the flow. This has subsequently been done for a number of different systems of which experimental data were available. Literature data were used to investigate and develop the model, while mainly own measurements were used for the validation. The physical properties and the properties of the packing structure are given in appendix 3.A for all configurations used.

The Structured Packing Liquid Hold-Up

Figure 3.8 shows the measured and predicted liquid hold-up for two commercial structured packings (Montz B series) as function of the superficial liquid mass velocity at zero gas velocity. The measurements were carried out on the test rig of the packing manufacturer at

ambient conditions using water as liquid phase. The results support the idea of the falling film within a packing structure using an effective inclination angle.

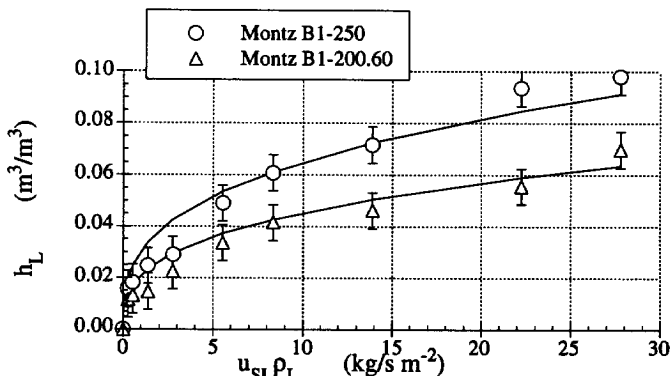


FIGURE 3.8: A comparison of the measured (this study) and predicted relative volumetric liquid hold-up at zero gas load in a bed with corrugated sheet packing as function of the liquid load.

By taking the interfacial friction equal to the friction of a smooth pipe a key assumption was made. Since this assumption, stated in equation (3.11) to (3.12), directly affects the interfacial velocity, the assumption can be verified by measuring the behaviour of the liquid hold-up as function of the gas velocity. The simplest geometry in which this can be verified is the vertical pipe. Figure 3.9 shows the predicted film thickness and the measured film thickness (Dukler et al., 1984) as function of the gas load in a vertical pipe with inner diameter of 50.8 mm.

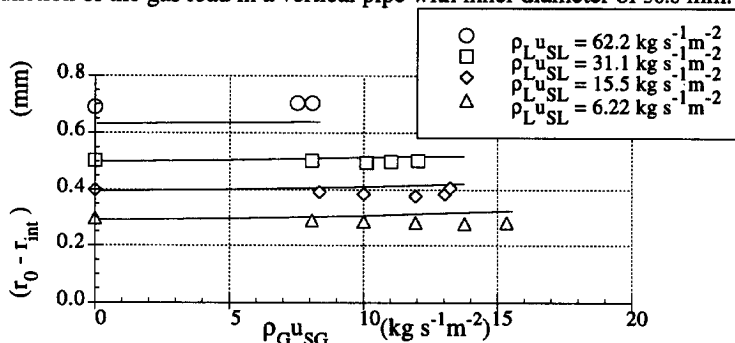


FIGURE 3.9: The calculated and measured (Dukler et al., 1984) liquid film thickness in a vertical pipe as function of the gas throughput for four liquid loads.

The graph shows that the liquid hold-up is well predicted over the whole gas load range. The model predicts a small increase of the film thickness with increasing gas load. Figures 3.10 A and B show the liquid hold-up as function of the gas load for a column with structured gauze packing. The shape of the curve is predicted well over the whole range of gas throughput, validating the assumption that the parallel shear on the liquid film is approximately identical to the shear of a gas flow in a smooth pipe. The absolute deviations in these cases are most likely

caused by the fact that a relatively small column diameter was used in combination with a gauze packing. This last fact could simply lead to an additional static hold-up in the packing structure and to a different flow angle for the gas and for the liquid flow.

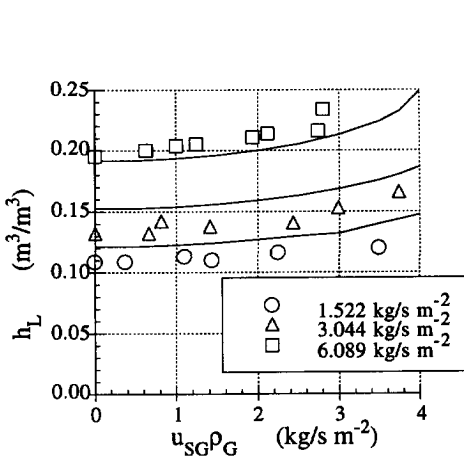


FIGURE 3.10A: The measured (this study) and calculated hold-up for glycol-air system, as function of the gas throughput for structured gauze packing.

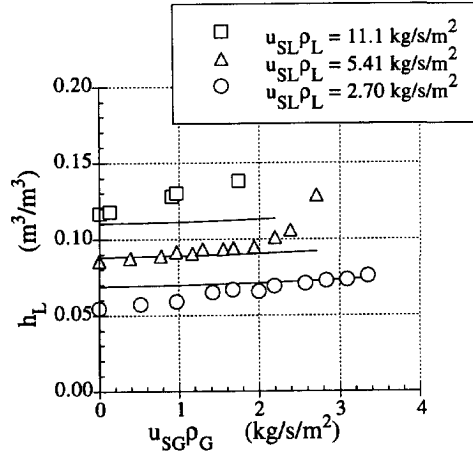


FIGURE 3.10B: The measured (this study) and calculated hold-up for water-air system, as function of the gas throughput for metal sheet structured packing.

**Specific Area and Column Diameter**

In the presented model information on specific surface area, column diameter, etc. has been transformed to a channel diameter and effective inclination angle for the gas flow. This angle has to be taken identical for the flows of both phases. When the corrections for diameter influence are carried out an identical effective inclination angle should be found for similar types of packing. Table III.I and III.II show the results for the Montz B1 series as function of the specific surface area and column diameter.

TABLE III.I: The effect of the specific area of the packing on the effective inclination angle for a Montz B1 packing constructed at 45° and a 30°.

$a_p$ $m^2/m^3$	$\alpha$ (45° construction)	$\alpha$ (30° construction)
110	39.8	27.0
123	39.7	26.9
190	38.2	27.1
258	39.9	26.3

TABLE III.II The effect of the column diameter on the effective inclination angle for Montz B1-250.

D m	$\alpha$ (45° construction)
0.48	40.0
0.79	39.9
1.57	38.9
2.75	38.9

The tables show that the approach used to calculate the geometrical effects are valid. However, one should remain careful with the column diameter influence on the pressure drop, because effects like changes in space between packing and column wall, careful installation of the packing elements, etc., can ruin the effect of scale-up rules easily.

### Random Packing Pressure Drop

Figure 3.11 shows the comparison of predicted and measured pressure drops for a packed bed consisting of ceramic berl saddles. Since no direct dry pressure drop data were available the pressure drops were calculated with the effective inclination angle found of the Ergun relation.

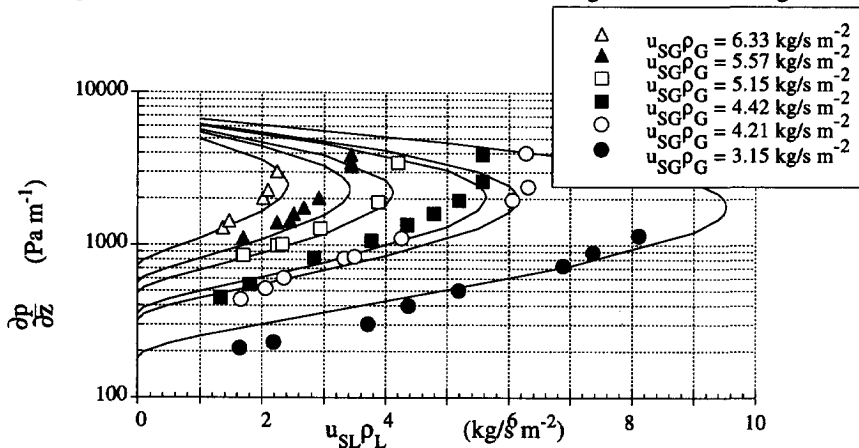


FIGURE 3.11: The measured (Krehenwinkel, 1987) and calculated pressure drops as function of the liquid load for various gas throughputs in a column with ceramic berl saddles.

An interesting result is the existence of two mathematically stable solutions for the pressure drop corresponding to two different liquid hold-ups. In a gas liquid system only the lower solution results in a stable counter-current film flow. However, the upper and lower stable pressure drops, more often represented as a small and a large hold-up of one phase, are indeed found in liquid-liquid extractions. The stable configuration is then dependent on the start-up procedure. In other words, because of its generality, the proposed model is also valid for liquid-liquid systems provided the flow is annular. Given that no exact data were used for the calculation of the effective inclination angle the results are rather good. The model predicts the steep increase of the pressure drop before the flooding point relatively accurately.

Figure 3.12 shows the calculated and measured pressure drops in a packed bed consisting of plastic pall rings. To determine the effective inclination angle use has been made of the dry pressure drop as measured by Krehenwinkel et al. (1987). The calculated pressure drops are within an accuracy of 10% of the measured values. The figure shows that the liquid flow does not reach the end of the calculated pressure drop line and flooding occurs at an earlier stage. To our opinion this could indicate two different mechanisms for flooding; i.e.: the entrainment of

droplets in the gaseous phase (figure 3.12) and a mechanism that is determined by the friction of the gas on the liquid film effectively increasing the hold-up (figure 3.11). One could say that there is a macroscopic and a microscopic cause for the occurrence of flooding, which depends on the physical properties of the fluids and the packing characteristics.

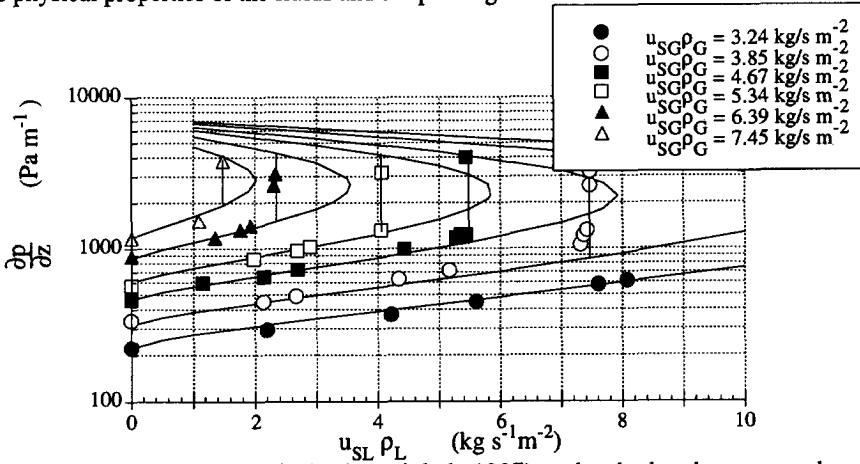


FIGURE 3.12: The measured (Krethwinkel, 1987) and calculated pressure drops as function of the liquid load for various gas throughputs in a column with plastic pall ring.

#### Structured Packing Pressure Drop

The prediction of the pressure drops of a structured packing at various gas and liquid loads using the given model are shown in figures 3.13 and 3.14 for the water-air system at ambient conditions, as measured in this study. Figure 3.13 shows the measurements and calculations for a packing with an inclination angle of  $30^\circ$  and specific area of  $260 \text{ m}^2/\text{m}^3$ , while figure 3.14 shows the results for a packing with an inclination angle of  $45^\circ$  and a specific area of  $110 \text{ m}^2/\text{m}^3$ . Both figures show that the dry pressure drop can be described using the packing dimensions and an effective inclination angle only. The liquid loads in these cases are relatively large, which makes it possible to evaluate some elementary phenomena. It can be seen that the liquid flow causes a non zero pressure drop at zero gas velocity in the model, indicating that the gas is dragged down by the liquid flow at the interface. The maximum deviations for systems with design angle of  $45^\circ$  were determined in the pre-loading range as +50%, while those for an angle of  $30^\circ$  were determined as +30%. The pressure drop increase caused by the loading in the packing is not predicted well for the packing with an inclination angle of  $30^\circ$ . The reason for this could be that the structured packing behaves as a demister, recollecting entrained droplets.

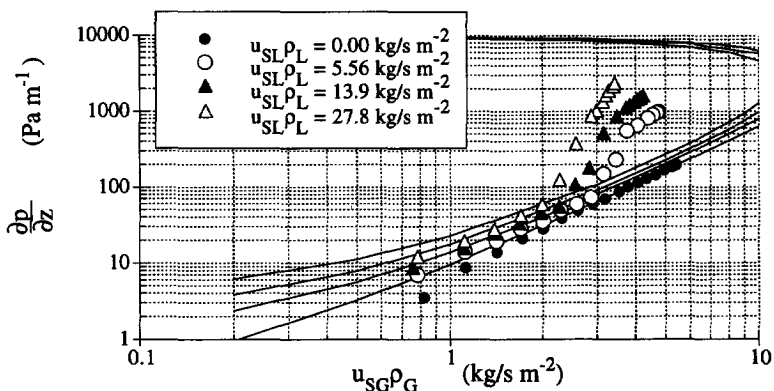


FIGURE 3.13: The measured and calculated pressure drops as function of the gas throughput for three liquid loads and the dry pressure drop in a structured packing with an effective inclination angle of 26.3 and specific surface of 260m<sup>2</sup>/m<sup>3</sup> (see also appendix 3.A).

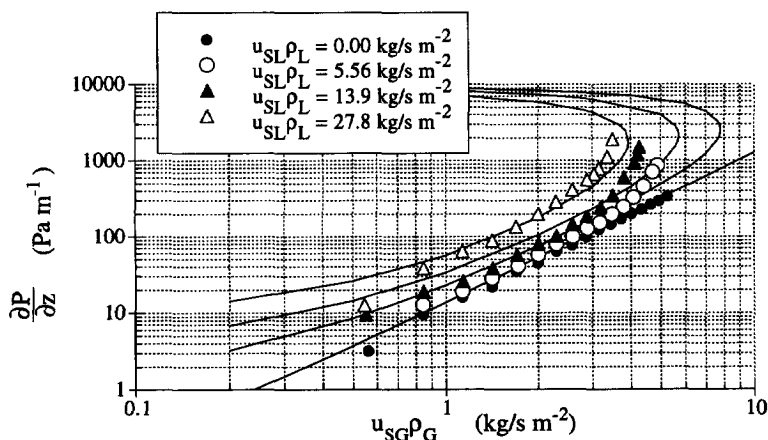


FIGURE 3.14: The measured and calculated pressure drops as function of the gas throughput for three liquid loads and the dry pressure drop in a structured packing with an effective inclination angle of 39.9 and specific surface of 110 m<sup>2</sup>/m<sup>3</sup>.

### Vertical Pipe Pressure Drop

In the preceding sections the pressure drops in packing geometries were predicted using the developed model. However, the model was based on the vertical pipe, which is an important test for relation (3.23), since the influence of the gas-liquid interaction parameter is shown directly. Figure 3.15 shows a comparison of the pressure drops as calculated with the correlation given by Feind (1960) and the pressure drop as calculated using equation (3.23). The comparison shows that relation (3.23) is close to the Feind correlation for the range as given by this study.



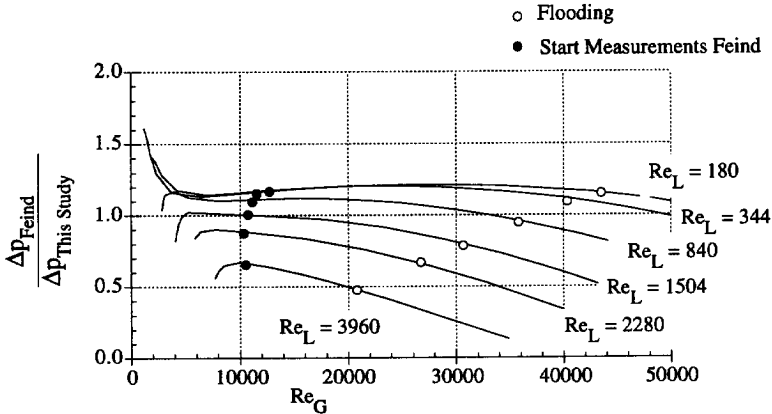


FIGURE 3.15: The ratio of the calculated pressure drops according to Feind (1960) and this study, as function of the gas Reynolds number for six liquid Reynolds numbers. The flooding points and the gas flow limits given by Feind are indicated.

The correlations of Feind are based on gas Reynolds numbers which are not taken relative towards the interface velocity. The presented model uses a gas velocity relative to the interface velocity. This gas liquid interaction parameter becomes close to zero for small liquid or gas Reynolds number. This approach will therefore especially lead to reliable pressure drop predictions for small liquid or gas loads. The deviations for large liquid Reynolds numbers are not surprising, because in our model a laminar flow model for the liquid was used.

### CONCLUDING REMARKS

A model has been presented that is able to describe two phase film flow systems for various physical properties. The presented model is based on a laminar liquid film, which totally wets the packing. This is an idealised situation, which already lead to deviations for structured packing pressure drop due to entrainment. Clearly it is not possible to predict deviations from idealised behaviour with the presented model, but the model provides a tool to identify these deviations.

As already postulated by Hutton et al., (1974), the pressure drop model revealed the likely existence of two principal flooding mechanisms, of which one is caused by the drag on the liquid film while the other mechanism has its base in the entrainment of droplets. Deviations of the measured and calculated pressure drops in the loading regime indicate a transition to a still counter-current flow with an increasing entrainment. The comparison of the measured and calculated pressure drop in packings and vertical pipes showed that the used interaction description for the gas and the liquid could describe both the frictional as geometrical increase of the pressure drop. This last fact offers the possibility to predict the mass transfer in packed beds using the friction factor in a Chilton-Colburn like relation. The whole strategy and the

subsequent results suggest possibilities of predicting the mass transfer rates by a friction factor related mass transfer model. This possibility will be explored in chapter 5 of this thesis.

The model presented has a sound physical basis. However, the description of the gas-liquid interactions taking into account the increase of the surface roughness (relation (3.23)), is largely an empirical relation. It has been tried to use the relation in a clear and unambiguous way and although it reasonably predicts the pressure drop, it can likely be improved.

### APPENDIX 3.A

The physical properties used to analyse the hydrodynamic relations. Next to the physical properties of the systems the packing characteristics are shown together with the column diameter.

Reference	$\rho_L$ kg/m <sup>3</sup>	$\rho_G$ kg/m <sup>3</sup>	$\eta_L$ mPa s	$\eta_G$ mPa s	$\sigma$ N/m	$a_p$ m <sup>2</sup> /m <sup>3</sup>	$\epsilon_0$ m <sup>3</sup> /m <sup>3</sup>	$\alpha$ °	$D_{col}$ mm
Figure 3.8	998	1.205	1.002	0.0182	0.0728	260	0.975	40	790
Figure 3.8	998	1.205	1.002	0.0182	0.0728	190	0.978	27	790
Figure 3.9	998	1.205	1.002	0.0182	0.0728	78.7	1.0	0.0	50.8
Figure 3.10A	1090	1.205	8.1	0.0182	0.048	650	0.98	29	38
Figure 3.10B	998	1.205	1.002	0.0182	0.0728	580	0.96	38	38
Table III.I	998	1.205	1.002	0.0182	0.0728	-	-	-	790
Table III.II	998	1.205	1.002	0.0182	0.0728	260	0.975	-	-
Figure 3.11	830	27.39	1.393	0.0154	0.0268	303	0.59	56	155
Figure 3.12	826	13.48	1.274	0.0156	0.0264	375	0.846	58.5	155
Figure 3.13	998	1.205	1.002	0.0182	0.0728	260	0.975	26.3	790
Figure 3.14	998	1.205	1.002	0.0182	0.0728	110	0.987	39.9	790
Figure 3.15	998	1.205	1.002	0.0182	0.0728	-	1.0	0.0	-

### NOTATION:

Symbol	Description	Unit
$a_p$	Specific packing surface area .....	m <sup>2</sup> /m <sup>3</sup>
$D_{col}$	Column diameter .....	m
$f$	Smooth pipe friction factor .....	
$f_g$	Geometrical friction factor.....	
$f_l$	Laminar part of the packing friction factor .....	
$f_p$	Friction factor of the packing .....	
$f_p^*$	Friction factor of packing corrected for column diameter.....	
$f_\infty$	Friction factor of packing at "infinite" flow rate .....	
$g$	Gravitational acceleration.....	m/s <sup>2</sup>
$H_{col}$	Column height .....	m
$h_L$	Liquid hold-up.....	m <sup>3</sup> /m <sup>3</sup>

$h$	Film thickness .....	m
$h_0$	Free falling film thickness.....	m
$l_t$	Channel length.....	m
$r$	Radial co-ordinate .....	m
$r_{int}$	Interface radius .....	m
$r_0$	Hydraulic radius.....	m
$u_{int}$	Interface velocity .....	m/s
$u_G$	Gas velocity .....	m/s
$u_L$	Liquid velocity.....	m/s
$u_{SG}$	Superficial gas velocity .....	m/s
$u_{SL}$	Superficial liquid velocity .....	m/s
$z$	Axial co-ordinate .....	m
$\alpha$	Effective inclination angle .....	°
$\alpha_0$	Effective inclination angle at infinite column diameter .....	°
$\Delta\rho$	Density difference .....	kg/m <sup>3</sup>
$\partial p/\partial z$	Pressure drop over packed bed ( $\partial p/\partial z = \partial p_f/\partial z + \partial p_g/\partial z$ ).....	Pa/m
$\partial p_f/\partial z$	Frictional pressure drop .....	Pa/m
$\partial p_g/\partial z$	Geometrical pressure drop .....	Pa/m
$\epsilon_{irr}$	Irrigated bed porosity .....	m <sup>3</sup> /m <sup>3</sup>
$\epsilon_0$	Void fraction .....	m <sup>3</sup> /m <sup>3</sup>
$\eta_G$	Dynamic gas viscosity .....	Pa s
$\eta_L$	Dynamic liquid viscosity .....	Pa s
$\theta$	Relative interface position .....	
$\rho_G$	Gas density.....	kg/m <sup>3</sup>
$\rho_L$	Liquid density.....	kg/m <sup>3</sup>
$\sigma$	Surface tension .....	N/m
$\Psi_{G-L}$	Gas-liquid interaction parameter.....	
$Ga_p$	Packing Galileo number .....	$Ga_p = \frac{4\Delta\rho\rho_L g \cos \alpha}{3\eta_L^2 a_p^3}$
$Re_G$	Gas phase Reynolds number.....	$Re_G = \frac{\rho_G \left( \frac{u_{SG}}{\theta^2 \epsilon_0 \cos \alpha} - u_{int} \right) 2\theta r_0}{\eta_G}$
$Re_L$	Liquid phase Reynolds number.....	$Re_L = \frac{4\rho_L u_{SL}}{\eta_L a_p}$
$Re_p$	Packing Reynolds number .....	$Re_p = Re_G \cos \alpha$

## REFERENCES:

- [1] Billet, R., and Schultes, M., (1991), *Modelling of Pressure Drop in Packed Columns*, Chem. Ing. Technol., **14** pp. 89-95.
- [2] Brauer, H., (1960), *Widerstandsgesetze für innen berieselte und gasdurchströmte senkrechte Rohre*, Chem. Ing. Techn., **32** (11), 719-725.
- [3] Datta, R., (1993), *Eddy Viscosity and Velocity Distribution in Turbulent Pipe Flow Revisited*, AIChE Journal, **39** (7), 1107-1112.
- [4] Dukler, A.E., Smith, L., and Chopra, A., (1984), *Flooding and Upward Film Flow in Tubes - I*, Int. J. Multi-phase Flow, **10** 585-597.
- [5] Feind, K., (1960), *Strömungsuntersuchungen bei Gegenstrom von Rieselfilmen und Gas in lotrechten Rohren*, VDI-Forsch. Heft 481, Düsseldorf.
- [6] Hetsroni, G., (1982), *Handbook of Multi-phase Systems*, Washington: Hemisphere Publishing Corporation.
- [7] Hikita, H., and Ishimi, K., (1976), *Frictional Pressure Drop for Laminar Gas Streams in Wetted-Wall Columns with Co-Current and Counter-Current Gas-Liquid*, J. Chem. Eng. Japan **9** pp. 351-362.
- [8] Hutton, B.E.T., Leung, L.S., Brooks, P.C., and Nicklin, D.J., (1974), *On Flooding in Packed Columns*, Chem. Eng. Sci., **29** pp. 493-500.
- [9] Imura, H., Kusuda, H., and Funetsu, S., (1977), *Flooding in a Counter-Current Annular Two-Phase Flow*, Chem. Eng. Sci. **32** pp. 79-87.
- [10] Kaiser, V., (1993), *Flooding in Packed Columns Correlated Another Way*, AIChE Spring National Meeting, March/April 1993, Houston (see also: Chem. Eng. Progr. **90** (6) pp. 55-59 (1994)).
- [11] Kister, H.Z. *Distillation Design*, McGraw-Hill, New York (1992).
- [12] Krehenwinkel, H., and H. Knapp, *Pressure Drop and Flooding in Packed Columns Operating at High Pressures*, Chem. Eng. Tech. **10**, 231-242 (1987).
- [13] Nunner, W., (1956), *Wärmeübergang und Druckabfall in rauhen Rohren*, VDI-Forsch. Heft 455, Düsseldorf.
- [14] Perry, R.H., and Green, D.W., (1984), *Perry's Chemical Engineering Handbook*, 6<sup>th</sup> ed. New York: McGraw-Hill.
- [15] Suess, P., and Spiegel, L., (1992), *Hold-Up of Mellapak Structured Packing*, Chem. Eng. Process., **31** pp. 119-124.
- [16] Teutsch, T., (1964), *Druckverlust in Füllkörperschüttungen bei hohen Berieselungsdichten*, Chem. Ing. Techn., **36** (5) pp. 496-503.
- [17] Wallis, G.B., (1969), *One-Dimensional Two-Phase Flow*, New York: McGraw-Hill.
- [18] Zabaras, G., Dukler, A.E., and Moalem-Maron, D., (1986), *Vertical Upward Co-current Gas-Liquid Annular Flow*, AIChE J., **32** (5) pp. 829-843.
- [19] Zogg, M., (1972), *Strömungs- und Stoffaustauschuntersuchungen an der Sulzergewebepackung*, Diss. No. 4886 Technische Hochschule Zürich.

## A Capacity Model for Packed Columns Based on Entrainment

Liquid flow reversal or flooding in counter-current falling film operations has been a subject of experimental and analytical study for over half a century. Perhaps the most common counter-current flow situation where flooding is important is in packed towers. Despite many research activities, there are still uncertainties on various aspects concerning the influences on the flood point, e.g.: equipment size, gas inlet and outlet configurations, operating conditions, and physical properties of the system. This is caused by the fact that the physical mechanisms governing the process of flooding are not completely understood even for the simplest geometry of a vertical pipe. This study intends to bridge flooding correlations in vertical tubes and the correlations for packed towers. Although it will not be possible to address all difficulties related to the flooding mechanism, some influences concerning physical properties and geometry will be elucidated, by applying data analysis and theoretical considerations.

In this study the definition of flooding as used by Hewitt and Wallis (1963) will be applied. They considered that flooding took place when the whole liquid flow is disrupted and expelled from the top of the equipment.

Flooding is caused by the frictional forces of the gas phase on the liquid phase and is often initiated by an increase of the liquid hold-up at constant liquid load with increasing gas load. The hold-up increase is called the loading of the column. Because of the frictional forces on the liquid interface waves are formed. These instabilities are considered as the most plausible flooding mechanism (Whalley, 1996). An analysis using the Kelvin-Helmholtz equation calculates the wave instabilities and subsequently leads to a prediction of entrainment in simple geometries at certain conditions (Taitel et al., 1980, Barnea and Taitel, 1993). However, it does not explain various aspects of packing behaviour, i.e.: the influence of the inclination angle of the packing surface, the relative insensitivity of the flood point for surface tension, etc. Although the wave instability approach can predict a point at which droplets are created, this does not mean that the droplets are carried by the gas. When most droplets are deposited on the falling film the condition at which droplets are generated, does not mark the flood point. An engineer would like to know the point at which liquid is carried up against gravity with the gas flow.

The capacity of a packed column is not directly related to the mass transfer, but the flood point determines the upper limit for good interphase mass transfer in a counter-current column. Therefore it is of crucial importance for the column designer to know precisely the capacity

limits of a given case. Here a general model is developed for predicting the flooding point in packed columns. The starting point is the simple vertical pipe.

### GENERAL FLOODING CONSIDERATIONS

The vertical pipe geometry is a starting point to investigate flooding in more complex geometries. Following the work of Govan et al., (1991) a recent experimental study of Jeong and No (1996) showed the dependence of the flood point in vertical pipes on inlet and outlet geometry, pipe length and gas entrance. These studies showed that the onset of flooding in a vertical pipe is very sensitive to the test-section geometry. Flooding data obtained in vertical pipes is often correlated using the Wallis type equation (see, e.g.; Wallis 1969):

$$\sqrt{U_G^*} + m\sqrt{U_L^*} = C \quad (4.1)$$

Here  $m$  and  $C$  are dimensionless constants and the dimensionless superficial velocities are related to the superficial gas velocity  $u_{SG}$  as:

$$U_G^* = u_{SG} \left( \frac{\rho_G}{2r_0 g(\rho_L - \rho_G)} \right)^{0.5}, \quad (4.1a)$$

and the superficial liquid velocity  $u_{SL}$  as:

$$U_L^* = u_{SL} \left( \frac{\rho_L}{2r_0 g(\rho_L - \rho_G)} \right)^{0.5} \quad (4.1b)$$

Here  $r_0$  represents the radius of the tube. The basic form of equation (4.1) was also applied by Crawford and Wilke (1951) to analyse the flood limits for extraction applications in packed beds. The capacity in counter-current equipment is usually showed as function of the flow parameter ( $\Phi$ ), which is defined as:

$$\Phi = \frac{U_L^*}{U_G^*} = \frac{u_{SL}}{u_{SG}} \sqrt{\frac{\rho_L}{\rho_G}} \quad (4.2)$$

By isolating the dimensionless gas velocity of equation (4.1),

$$U_G^* = \frac{C^2}{(1+m\sqrt{\Phi})^2}, \quad (4.3)$$

and by multiplication with the root of the product of the pipe diameter and the gravitational constant, the relation that generally is used for packed columns is found,

$$C_G = u_{SG} \sqrt{\frac{\rho_G}{\rho_L - \rho_G}} = \sqrt{2r_0 g} \frac{C^2}{(1+m\sqrt{\Phi})^2} \quad (4.4)$$

Here  $C_G$  represents the gas capacity factor. Figure 4.1 shows experimental flood points expressed as dimensionless gas velocities as function of the dimensionless liquid velocity for vertical tubes and packing structures. For the packing structures the hydraulic radius ( $r_0=2\epsilon_0/a_p$ ) is applied. The basic form of equation (4.1) is often applied for liquid-liquid extraction correlations (see, e.g., Laddha and Degaleesan, 1976).

The figure 4.1 shows the large difference between the capacity limits of the two vertical pipe configurations. Especially the square-edged bottom configuration causes a local increase of the

liquid hold-up that promotes the flooding phenomena (Govan et al., 1991; Jeong and No, 1996). The data show the sensitivity of flooding for subtle aspects of the flow configuration. It is likely that packed beds are sensitive to aspects as gas inlet and packing arrangement as well.

- Mellapak 250Y
- ▲ Berl Saddles ( $a_p = 392, \epsilon_0 = 0.59$ )
- Vertical pipe (rounded outlet and inlet)
- △ Vertical pipe (square-edged outlet and inlet)

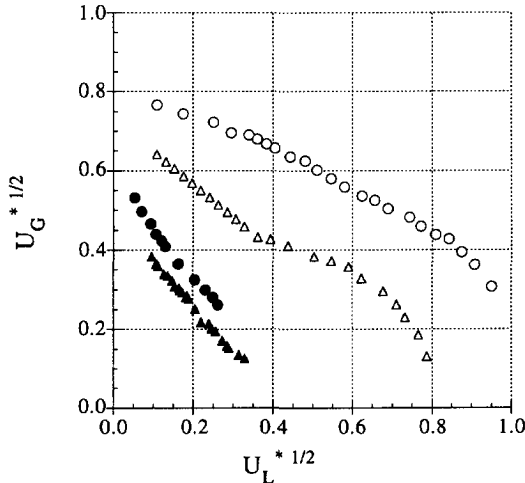


FIGURE 4.1: Maximum square root of the dimensionless superficial gas velocity as function of the square root of the dimensionless superficial liquid velocity, in a vertical one meter tube (Jeong and No, 1996), structured packing (Sulzer 1989) and random packing (Krehenwinkel 1987).

Several authors have attempted to justify the success of equation (4.1), but its general shape is still not completely understood. The most successful theoretical models describing the flooding mechanism in vertical tubes are based on the frictional forces on each phase (see McQuillan and Whalley 1984). However, given that liquid-liquid extraction application can be written also in the form of equation (4.1), the latter indicates that an approach based on droplet entrainment could also be effective. Taking the liquid-liquid extraction point of view for gas-liquid application the dispersed phase is formed by the entrained liquid droplets, while the continuous gas phase should be taken relative towards the interface velocity.

#### THE FORCES ON THE DROPLETS

Considering our work in regard to the pressure drop, we believe that the onset of flooding is in most cases due to entrainment of droplets in the gaseous phase. However, under some conditions the friction of the gas with the liquid itself can cause enough upward force to prevent the liquid from flowing down. Five entrainment mechanisms are distinguished that could create droplets in a vertical pipe (Ishii and Grolmes 1975), i.e.: roll wave shear off, wave undercut (Hewitt and Hall-Taylor 1970), bubble burst, liquid impingement, and liquid bulge

disintegration. Some of these mechanisms are not possible with thin films. Besides this, the structure of a packed bed will create droplets as well (see, e.g., Fair and Bravo 1990). In this study it is assumed that due to a mechanism that we will not address, droplets will enter the gas phase. Figure 4.2 illustrates that a droplet in the gaseous phase is exposed to three forces. These are the gravitational force  $F_g$ , the drag force  $F_d$ , and the rotational or lift force  $F_l$ . Only the gravitational and drag force are used normally to describe the flooding in existing theories.

The lift force on the droplets is caused by the acceleration of the gas phase and is always directed towards the centre of the tube. The lift force as drawn in figure 4.2 has a component opposite to gravity. However, the droplets created in the upper half of the cross section have a net component directed along the gravity.

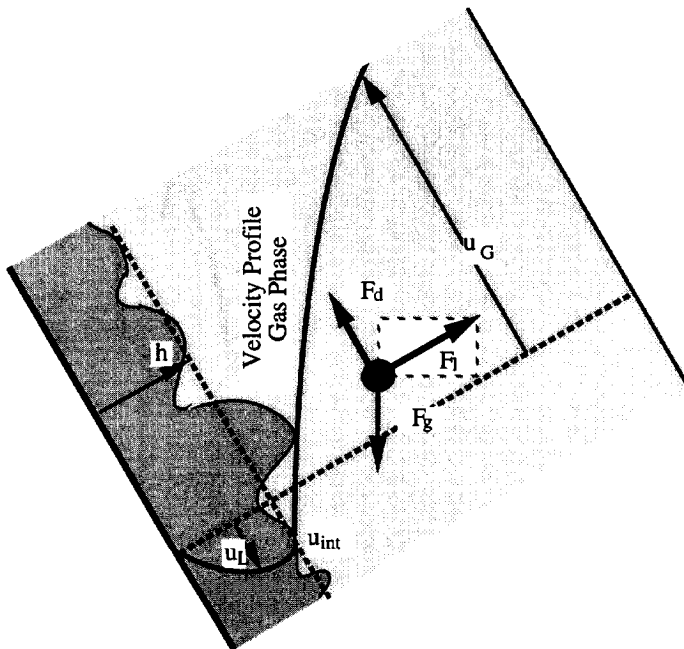


FIGURE 4.2: The three forces on the liquid film. Showing the lift force, the gravitational force and the drag force.

In case droplets created at the bottom part of the gas flow, they will be exposed to a lift force which has an upwards directed component. This means the droplets created at the bottom of the channel will be the first which will cause the entrainment. For an ideal fluid the lift force can be calculated by determining the rotation over the droplet (see, e.g.: Sabersky et al., 1989; Feynman et al., 1963; Rayleigh, 1877). For real fluids the phenomenon is more complex and related to the formation of an asymmetric wake at one side of the droplet as shown in figure 4.3 (see, e.g.: Clift et al., 1978).



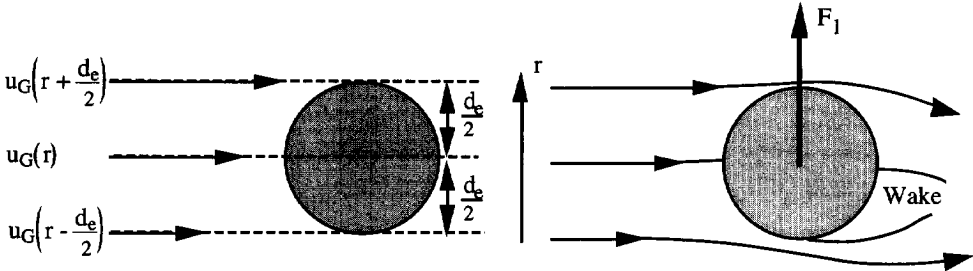


FIGURE 4.3: A droplet in a gradient velocity field (left hand side) and the by this field caused flow pattern and force on the droplet (right hand side).

We will not attempt to describe the full lift phenomena, but apply a simple method to quantify its size. With Bernoulli's relation a balance over an entrained droplet is given by:

$$p_1 + \frac{1}{2} \rho_G u_G^2 \Big|_{r - \frac{d_e}{2}} = p_2 + \frac{1}{2} \rho_G u_G^2 \Big|_{r + \frac{d_e}{2}}, \quad (4.5)$$

from the pressure difference resulting over the droplet the lift force can be approximated as:

$$\begin{aligned} \frac{1}{2} \rho_G \left( u_G(r) - u'(r) \frac{d_e}{2} \right)^2 - \frac{1}{2} \rho_G \left( u_G(r) + u'(r) \frac{d_e}{2} \right)^2 &= p_2 - p_1 \\ \rho_G u_G(r) u'(r) d_e &= \frac{F_1}{\frac{\pi}{4} d_e^2} \Rightarrow F_1 = \frac{\pi}{4} \rho_G u_G(r) u'(r) d_e^3 \end{aligned} \quad (4.6)$$

Here the  $u_G(r)$  represents the velocity of the gas compared with the velocity of the droplet. Due to the product of the local velocity and the gradient of the velocity the force will have a maximum. To approximate the product of the local velocity and the gradient of the local velocity in a turbulent flow, the universal velocity profile correlation of Datta (1993) is applied. Using the universal profile, which is expressed as function of the maximum velocity, the force in the bottom of the tube can be rewritten as:

$$F_1 = \rho_G \frac{\pi}{4} d_e^3 \left( \frac{u_{SG}}{\epsilon_0 \theta^2 \cos \alpha} - u_{int} \right) \frac{C_t}{r_{int}} \left( \frac{u_{SG}}{\epsilon_0 \theta^2 \cos \alpha} - u_d \right), \quad (4.7)$$

where  $C_t$  represents a dimensionless parameter, which depends on the relative position and the gas Reynolds number. In equation (4.7)  $u_d$  represents the droplet velocity and  $u_{int}$  the interface velocity. Figure 4.4 shows the dependence of the coefficient on the Reynolds number and radial position. Given the gas Reynolds numbers normally applied in a packed bed the value of the maximum value of the parameter  $C_t$  will be in the range of 3-6.

The drag force can be expressed in a number of ways, which are related to the type of flow and the droplet size. A constant friction factor of 0.44 can be applied for particles in a turbulent stream (see, e.g.: Clift, et al. 1978; Coulson and Richardson, 1978), such that the drag force  $F_d$  on an entrained droplet can be expressed as:

$$F_d = 0.055 \pi d_e^2 \rho_G \left| \frac{u_{SG}}{\epsilon_0 \theta^2 \cos \alpha} - u_d \right| \left( \frac{u_{SG}}{\epsilon_0 \theta^2 \cos \alpha} - u_d \right) \quad (4.8)$$

Taking the pressure drop into account the gravitational force can be written as:

$$F_g = \frac{1}{6} \pi d_e^3 \left( \rho_L - \rho_G + \frac{1}{g} \frac{\partial p}{\partial z} \right) g \quad (4.9)$$

When the gas flow is upwards, the pressure drop is negative, so that in that case the effective gravitational force decreases.

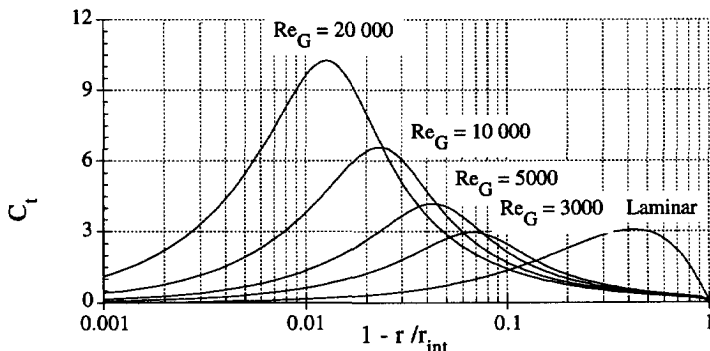


FIGURE 4.4: The coefficient as defined in equation (4.7) for zero droplet and interface velocity as function of the dimensionless radius and the Reynolds number.

Taking the gas flows at an inclination angle  $\alpha$ , the forces balance in the direction along the gravity reads:

$$F_d \cos \alpha + F_l \sin \alpha = F_g, \tag{4.10}$$

The boundary condition for flooding is defined as a critical gas velocity at which the velocity of the droplet becomes zero ( $u_{SG}^{crit}; u_d = 0$ ). Equation (4.10) can be rewritten using this condition so that the balance reads:

$$\left( \frac{u_{SG}^{crit}}{\epsilon_0 \theta^2 \cos \alpha} \right)^2 \frac{\cos \alpha}{d_e} + \frac{C_t}{0.22} \left( \frac{u_{SG}^{crit}}{\epsilon_0 \theta^2 \cos \alpha} - u_{int} \right) \left( \frac{u_{SG}^{crit}}{\epsilon_0 \theta^2 \cos \alpha} \right) \frac{\sin \alpha}{r_{int}} = 3g \left( \frac{\rho_L - \rho_G + \frac{1}{g} \frac{\partial p}{\partial z}}{\rho_G} \right). \tag{4.11a}$$

Substitution of an average coefficient as: ( $\bar{C}_t = 1.75$ ), this results in

$$\rho_G \left( \frac{u_{SG}^{crit}}{\epsilon_0 \theta^2 \cos \alpha} \right)^2 \left( \frac{\cos \alpha}{d_e} + \frac{8 \sin \alpha}{r_{int}} \left( 1 - \frac{u_{int} \epsilon_0 \theta^2 \cos \alpha}{u_{SG}} \right) \right) = 3 \left( \rho_L - \rho_G + \frac{1}{g} \frac{\partial p}{\partial z} \right) g. \tag{4.11b}$$

This average value agrees with the lower cross section part of the gas channel. Given the rough approach of the presented model a more accurate determination of the coefficient cannot be justified. By neglecting the interface velocity the critical capacity factor can be isolated from equation (4.11b):

$$C_{G}^{crit} = u_{SG}^{crit} \sqrt{\frac{\rho_G}{\rho_L - \rho_G}} = \epsilon_0 \theta^2 \cos \alpha \sqrt{\frac{3g}{\frac{\cos \alpha}{d_e} + \frac{4a_p}{\epsilon_0 \theta} \sin \alpha}} \sqrt{\frac{\rho_L - \rho_G + \frac{1}{g} \frac{\partial p}{\partial z}}{\rho_L - \rho_G}}. \tag{4.12}$$

### THE DROPLET SIZE

The capacity factor relation (4.12) includes a characteristic droplet diameter. Several approaches can be applied to determine a droplet diameter. Again much will depend on the view one has on

how the droplets are formed. However, here it is assumed that the droplets have entered the gas phase and therefore the gas phase behaviour will determine the size of the droplets. In a packing the mechanisms for break-up could either be caused by velocity gradients or by the turbulence of the flow. Both mechanisms were discussed by Hinze (1955). When it is assumed that the drop size is determined by the velocity gradients, a critical Weber number related to the maximum stable drop diameter  $d_{\max}$  is used;

$$We_{\text{crit-1}} = \frac{\rho_G \left( \frac{u_{SG}}{\epsilon_0 \theta^2 \cos \alpha} - u_{\text{int}} \right)^2 d_{\max}}{\sigma} \quad (4.13)$$

In most applications a typical critical Weber numbers of 10 to 22 is found (Hinze 1955; Ishii and Grolmes, 1975; Taitel et al., 1980). The second mechanism for droplet break-up is caused by the turbulent flow. Assuming isotropic homogeneous turbulence, the average velocity of the eddies ( $\bar{v}$ ) on the scale of the droplet can be obtained by integrating the general Kolmogorov energy distribution law up to the maximum size of the droplets (see, e.g., Hinze, 1975) as:

$$\bar{v}^2 = \int_{d_{\max}^1}^{\infty} \gamma_1 \epsilon^{2/3} k^{-5/3} dk = \frac{3}{2} \gamma_1 (\epsilon d_{\max})^{2/3} = 3(\epsilon d_{\max})^{2/3} \quad (4.14)$$

In this equation  $\epsilon$  represents the dissipated energy and  $\gamma_1$  is the general turbulence constant, which is taken equal to 2 (Batchelor, 1951). Hinze (1955) used this average velocity to obtain a critical Weber number;

$$We_{\text{crit-2}} = \frac{\rho_G \bar{v}^2 d_{\max}}{\sigma} = 3 \frac{\rho_G (\epsilon d_{\max})^{2/3} d_{\max}}{\sigma} \quad (4.15)$$

Applying experimental data he found a critical Weber number that was a little larger than unity for the maximum stable droplet. The sizes of the droplets are distributed and the maximum droplet size needs to be connected with an entrained droplet size. Here an average entrained droplet diameter is taken as one fourth of the maximum entrained droplet calculated with equation (4.15). The average entrained droplet now can be expressed as:

$$\begin{aligned} d_e &= \frac{d_{\max}}{4} = \frac{0.725}{4} \left( \frac{\sigma}{\rho_G} \right)^{0.6} \epsilon^{-0.4} = \frac{0.725}{4} \left( \frac{\sigma}{\rho_G} \right)^{0.6} \left( \frac{\frac{\partial p}{\partial z} \left( \frac{u_{SG}}{\epsilon_0 \theta^2} - u_{\text{int}} \cos \alpha \right)}{\rho_G} \right)^{-0.4} \\ &= \frac{0.725}{4} \left( \frac{\sigma}{\rho_G} \right)^{0.6} \left( \frac{\theta r_0}{f_p (1 + \psi_{G-L}) \left| \frac{u_{SG}}{\epsilon_0 \theta^2} - u_{\text{int}} \cos \alpha \right|^3} \right)^{0.4} \end{aligned} \quad (4.16)$$

A general relation for the total dissipated kinetic energy in the gas phase is used, where  $f_p$  represents the packing friction factor and  $\psi_{G-L}$  the gas-liquid interaction parameter. This expression has to be used in equation (4.12). The choice of 1/4 of the maximum droplet diameter is not crucial, but it appears a logical selection (see, e.g.: Baird and Lane, 1973) and as will be shown it is in accordance with the flooding relation in a vertical pipe.

RESULTS

Equation (4.16) can be used in combination with equation (4.12), so that the critical capacity factor can be written as:

$$C_G^{crit} = \left( \frac{3(\epsilon_0 \theta^2 \cos \alpha)^2 \left( g + \frac{1}{(\rho_L - \rho_G)} \frac{\partial p}{\partial z} \right)}{\frac{4}{0.725} \left( \frac{f_p a_p (1 + \psi_{G-L}) \left| \frac{u_{SG}^{crit}}{\epsilon_0 \theta^2} - u_{int} \cos \alpha \right|^3 \right)^{0.4}}{2\theta \epsilon_0}} \left( \frac{\rho_G}{\sigma} \right)^{0.6} \cos \alpha + \frac{4a_p \sin \alpha}{\theta \epsilon_0} \right)^{0.5} \quad (4.17)$$

Unfortunately, it cannot be justified to neglect certain terms, so that it is not possible to obtain an explicit expression for the critical capacity factor. In equation (4.17) the pressure drop could be expressed using the friction factor and the velocities, but the term can often be neglected compared with the gravitational acceleration. When equation (4.17) is used for a vertical pipe the equation simplifies as:

$$C_G^{crit} = 0.737 \theta^2 \left( \frac{\sigma}{\rho_G} \right)^{0.3} \left( \frac{\theta r_0}{f(1 + \psi_{G-L}) \left| \frac{u_{SG}^{crit}}{\theta^2} - u_{int} \right|^3} \right)^{0.2} \left( g + \frac{1}{(\rho_L - \rho_G)} \frac{\partial p}{\partial z} \right)^{0.5} \quad (4.18)$$

where the packing friction factor is replaced by the friction factor of a smooth pipe. Figure 4.5 shows measured flood points of Jeong and No (1996) in comparison with the estimated curve of equation (4.18).

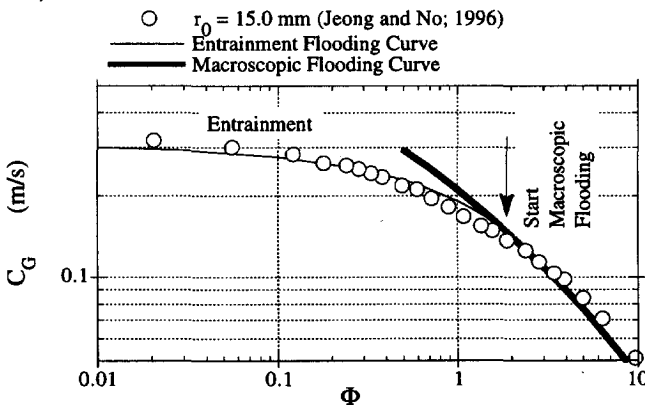


FIGURE 4.5: The critical capacity factor as function of the flow parameter. The data is measured in a vertical pipe of one meter height with smooth inlet and outlet. The thin line represents the curve calculated with equation (4.18), while the bold line indicates the macroscopic flood point due to frictional forces (see chapter 3).

Firstly it should be noticed that this analysis is related to a rounded pipe inlet and outlet. This is not surprising since the model uses idealised flow conditions and the square edged configuration causes an additional liquid hold-up due to contraction of the gas flow. Secondly, as indicated in the graph a relative smooth transition to macroscopic flooding is found after which the flooding curve is still predicted correctly. Kister (1992) refers to the macroscopic

flooding mechanism as the system limit. As explained in chapter 3, at macroscopic flooding the liquid film can no longer flow downwards due to the frictional forces and the pressure drop over the internals.

For thin films the interface velocity and the pressure drop in equation (4.18) can be neglected. So that the critical capacity factor can be written in the explicit form:

$$C_G^{crit} = 1.135\theta^2 \sqrt{g\theta r_0} \left( \frac{\sigma}{\theta^2 r_0^2 g(\rho_L - \rho_G)} \right)^{3/16} \left( \frac{Re_G^{1/4}}{1 + \psi_{G-L}} \right)^{1/8} \quad (4.19)$$

Here use has been made of the Blasius friction factor for smooth pipes. This equation enables a direct comparison with existing correlations and therefore an evaluation of the influence of the physical properties. When for instance the equation is rewritten as a Kutateladze number (see: Pushkina and Sorokin, 1969), it becomes close to the empirical relation given by Alekseev et al. (1972) and modified by McQuillan and Whalley (1984).

Again it has to be emphasised that flooding is a sensitive phenomenon and the initiation in a vertical pipe is already influenced by the length of the pipe (Govan et al., 1991). This sensitive behaviour is pronounced because the flooding phenomenon exhibits a large hysteresis (Celata et al. 1990), meaning that after the start of flooding one has to decrease the liquid or gas flows substantially to obtain de-flooding. Flooding therefore occurs over a flow range. A full description of flooding would require the prediction of both the flood point and the de-flood point. Nevertheless, relation (4.17) contains much information on the behaviour of packed beds about packing characteristics and physical properties. Figure 4.6 shows the comparison of the calculated curves for several packing geometries with an effective inclination angle of 38° and the correlation given by Sulzer (1989) for Mellapak 250Y.

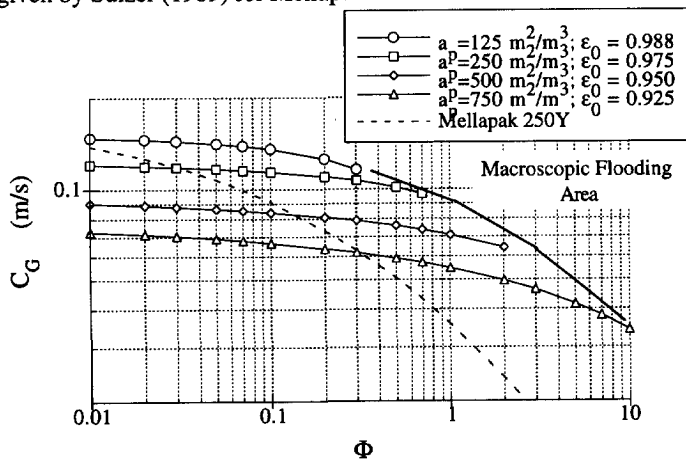


FIGURE 4.6: The critical capacity factor as function of the flow factor for packing with an inclination angle of 38° calculated with the equation (4.12) and (4.16) and the correlation given by Sulzer (1989).

The packing characteristics for the calculations are based on the Mellapak series of Sulzer. The used inclination angle is determined from dry pressure drop. Although the shapes of the calculated curves are approximately identical for all packing sizes, the slopes of the measured and estimated curves are quite different. The measured critical capacity factor curve can be represented in analogy with equation (4.4) by:

$$C_{G, \text{meas.}}^{\text{crit}} = C_r \frac{0.173}{(1 + 1.2 \sqrt{\Phi})^2}, \quad (4.20)$$

while the critical capacity curve up to the macroscopic flooding area as calculated with the model can be correlated as:

$$C_{G, \text{model}}^{\text{crit}} = C_r \frac{0.122}{(1 + 0.15 \sqrt{\Phi})^2}. \quad (4.21)$$

The capacity of a different geometry is represented by the relative capacity factor  $C_r$ , which compares the packing with a well-studied geometry. In principle we can only speculate on the difference between the estimated curves and the measured curves, but it could be explained by the fact that in packing beds several locations in the geometry can cause a local increase of the liquid hold-up. These obstructions for the gas flow cause a local increase of the gas velocity, pressure drop and liquid entrainment. Due to these disturbances the flooding phenomenon starts sooner than predicted with the model of equation (4.17), that is related to an undisturbed flow. However, when the disturbed capacity remains connected with the undisturbed capacity, it is plausible that the relative capacity factor ( $C_r$ ) can be estimated using the undisturbed capacity model. The relative capacity factor of a packing geometry with specific area, void fraction and effective inclination angle can be determined by the relation;

$$C_r = \frac{C_{G, \text{meas.}}^{\text{crit}}(\text{Type})}{C_{G, \text{meas.}}^{\text{crit}}(250Y)} = \frac{C_{G, \text{model}}^{\text{crit}}(\text{Type})}{C_{G, \text{model}}^{\text{crit}}(250Y)}. \quad (4.22)$$

Here Mellapak 250Y is used as reference. Hypothesis (4.22) can be tested by comparing flooding data for different geometries and systems with other physical properties.

#### Geometrical Influences on the Flood Point

Table IV.I shows a comparison of the measured relative capacity factors, reported by Sulzer (1989) for the Mellapak series and the estimated relative capacity factors applying equation (4.17) in hypothesis (4.22). No substantial deviations from the reported values are found, so that at first instance hypothesis (4.22) appears valid. The principle should remain valid for random packing. Table IV.II shows a list of random packing elements and their characteristic parameters (Treybal, 1980). The effective inclination angles are taken as  $55^\circ$  except for the raschig rings where an effective inclination angle of  $65^\circ$  was applied. The bold values in this table indicate macroscopic flooding.

The estimated relative capacity parameters for random packing show more deviations than those calculated for structured packing, but they still agree reasonably well with the measured

values. When flooding is caused by the macroscopic mechanism one should double check the outcome of the critical capacity factor. Although most ring packings have similar effective inclination angles, it is not a general result. Sherwood et al., (1938) for instance, increased the capacity for a packed column by a factor 2.3 using stacked rings. This means a reduction of the effective inclination angle by approximately 30°.

TABLE IV.I: The estimated relative critical capacity factors for various packing sizes using equation (4.17) and (4.22), compared with the data given by the supplier (Sulzer, 1989). The estimated values are obtained using a water-air system in a column with a diameter of 0.5m. Also indicated are the specific surface areas, void fractions and the effective inclination angle as determined from the pressure drop.

Type Mellapak	$a_p$ ( $m^2/m^3$ )	$\epsilon_0$ ( $m^3/m^3$ )	$\alpha$ (°)	$C_r$	$C_{r,model}$	$\Delta C$ %
125X	125	0.988	26	1.50	1.54	2.9
125Y	125	0.988	38	1.25	1.21	-3.1
170X	170	0.983	26	1.51	1.43	-5.2
170Y	170	0.983	38	1.14	1.12	-1.4
M2X	200	0.980	26	1.41	1.37	-3.1
M2Y	200	0.980	38	1.09	1.07	-1.6
250X	250	0.975	26	1.25	1.27	1.8
250Y	250	0.975	38	1.00	1.00	-0.4
350X	350	0.965	26	1.10	1.12	2.1
350Y	350	0.965	38	0.85	0.87	2.8
500X	500	0.950	26	1.00	0.96	-4.1
500Y	500	0.950	38	0.70	0.74	5.9
750Y	750	0.925	38	0.63	0.59	-5.9

TABLE IV.II: Characteristic parameters of various types of random packing. Indicated are the element size, the void fraction and the specific area. The relative capacity parameter (Treybal, 1980) is compared with the relative capacity parameter estimated with equation (4.22) at a flow parameter of 0.03. In these calculations use is made of an effective inclination angle of 55° and a column diameter of 0.5m.

Size mm	$\epsilon_0$ $m^3/m^3$	$a_p$ $m^2/m^3$	$C_r$ -	$C_{r,model}$ -	$\Delta C_r$ %
------------	---------------------------	--------------------	------------	--------------------	-------------------

Berl Saddles (Ceramic)

6	0.60	899	0.17	0.18	8
13	0.63	466	0.33	0.28	-14
19	0.66	269	0.39	0.40	1
25	0.69	249	0.49	0.44	-10
38	0.75	144	0.63	0.61	-4
50	0.72	105	0.76	<b>0.68</b>	-11

Raschig Rings (Metal Wall)

6	0.69	774	0.19	<b>0.18</b>	-7
13	0.84	420	0.29	<b>0.33</b>	<b>13</b>
19	0.88	274	0.41	<b>0.43</b>	<b>6</b>
25	0.92	206	0.48	<b>0.52</b>	<b>9</b>

Size mm	$\epsilon_0$ $m^3/m^3$	$a_p$ $m^2/m^3$	$C_r$ -	$C_{r,model}$ -	$\Delta C_r$ %
------------	---------------------------	--------------------	------------	--------------------	-------------------

Pall Rings (Metal)

16	0.93	341	0.61	0.59	-3
25	0.94	206	0.74	0.75	3
38	0.95	128	0.96	0.90	-6
50	0.96	102	1.14	<b>1.07</b>	<b>-6</b>

Pall Rings (Plastic)

16	0.87	341	0.52	0.53	2
25	0.90	206	0.71	0.69	-3
38	0.91	128	0.81	0.82	2
50	0.92	102	1.02	<b>0.95</b>	<b>-7</b>
89	0.92	85	1.27	<b>1.00</b>	<b>-21</b>

As mentioned before, flooding is influenced by a number of parameters and one that is often neglected is the influence of the column diameter. In the presented model the column diameter mainly affects the pressure drop and therefore the dissipated energy. As a consequence the dissipated energy will effect the maximum droplet size and therefore the flood point. Figure 4.7 illustrates the influences on the flood point caused by the column diameter for structured and random packing. The change in capacity factor is compared with the capacity factor obtained for infinite column diameter. Although the changes are not substantial, the figure again illustrates the dependence of the flood point for various parameters. The opposite effect of the column diameter on structured and random packing is caused by the decrease of the effective inclination angle for random packing with decreasing column diameter, so that the total pressure drop reduces, while for structured packing the pressure drop increases with decreasing column diameter (see equations (3.19) and (3.20) of chapter 3).

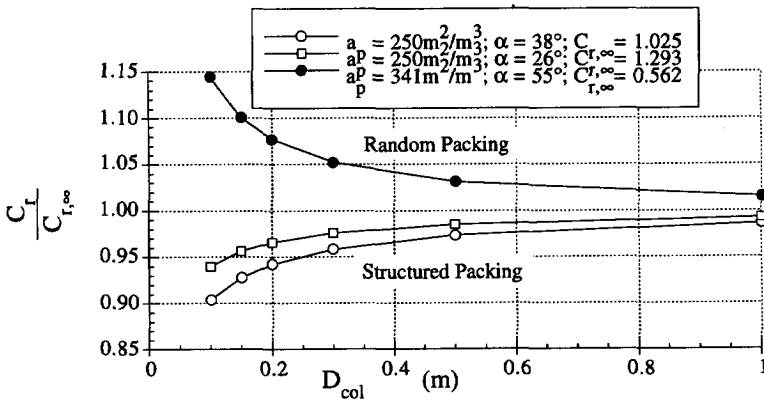


FIGURE 4.7: The relative influence of the column diameter on the critical capacity factor for structured packing and random packing. The influence is obtained by comparing them with the indicated critical capacity factor at infinite column diameter.

**Influence of Physical Properties on the Flood Point**

In addition to the packing characteristics, the physical properties will influence the critical capacity factor. Since all properties are covered by equation (4.17), the described influence of the physical properties should agree with those found in literature, so that the prediction of the relative capacity factor as function of the physical properties should be possible. In literature these influences on the capacity are often described by applying a relative power function. The influence of the liquid viscosity and the surface tension on the relative capacity parameter is described using a correction ( $C_{cor}$ ) factor as:

$$C_{cor} = \frac{C_G^{crit}(\sigma, \eta_L)}{C_G^{crit}(\sigma_{ref}, \eta_{L-ref})} = \frac{C_{G, model}^{crit}(\sigma, \eta_L)}{C_{G, model}^{crit}(\sigma_{ref}, \eta_{L-ref})} = C_{cor, \sigma} C_{cor, \eta_L} = \left( \frac{\sigma}{\sigma_{ref}} \right)^{m_1} \left( \frac{\eta_L}{\eta_{L-ref}} \right)^{m_2}, \quad (4.23)$$



where  $m_1$  and  $m_2$  are constants. In most cases the reference conditions are taken equal to those of a water-air system. As shown by equation (4.23) the physical property correction factor for a certain packing can also be estimated using the presented model. The physical property correction factor of equation (4.23) therefore enables a comparison with correlations reported in literature.

*The Surface Tension*

Equation (4.19) shows a surface tension influence on the critical capacity factor for a vertical pipe as:  $m_1=3/16=0.1875$ . This value is well in the range of the predicted dependences using theoretical consideration, which normally leads to a value of:  $m_1=0.25$  (see, e.g., Wallis, 1961; Ishii and Grolmes, 1975; Taitel et al., 1980) and published correlations (Alekseev et al., 1972; McQuillan and Whalley, 1985;  $m_1=0.155$ ). For packed columns the reported influence of the surface tension on the critical capacity varies considerably. Most studies neglect the influence (Sherwood et al., 1938; Mersmann 1965; Sulzer 1989), but surface tension effects are reported by for instance Norton 1993, ( $m_1=0.16$ ) and for liquid-liquid extraction by Dell and Pratt, 1951,  $m_1= 0.125$  and Crawford and Wilke, 1951 ( $m_1=0.20$ ). The results of the presented model, condensed in equation (4.22), are shown in figure 4.8. The calculated points are fitted using the power correlation

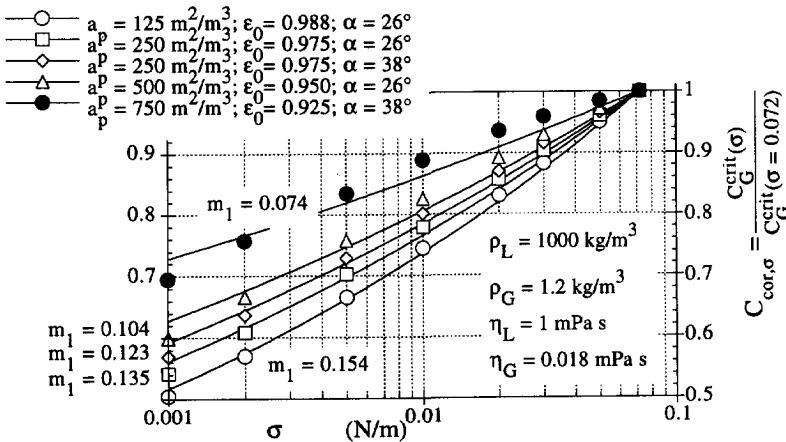


FIGURE 4.8: The relative influence of the surface tension on the critical capacity factor for various types of packing for constant other physical properties as calculated with equations (4.23) and (4.17). Indicated are the on the calculated data points fitted powers.

The figure shows that influence of the surface tension can be described reasonably well by using a power term. Interesting enough it also shows that the power coefficient depends on both the surface area and the inclination angle of the packing geometry. This effect was observed by Venkataraman and Laddha (1960) for liquid-liquid extractions in randomly packed columns. When applying a large specific area for the separation, the flood point is hardly influenced by the surface tension. For random packing the surface tension has only a limited

influence on the critical capacity factor, because of the large effective inclination angle. The calculations were carried out at a flow parameter of 0.03, but the choice of the flow parameter hardly affects the surface tension influence on the estimated capacity factor.

*The Liquid Viscosity.*

Equation (4.17) predicts a viscosity effect on the critical capacity factor mainly by the square of the reduced hydraulic diameter ( $\theta^2$ ). This factor reduces the total void fraction and therefore increases the gas velocity. Some reported power values for packed columns are: Sulzer (1989): not reported; Coulson et al. 1985:  $m_2=-0.05$ ; Sherwood et al., 1938:  $m_2=-0.1$ ; Norton 1993:  $m_2=-0.11$ ; Mersmann 1965:  $m_2=-0.17$ . Figure 4.9 shows the influence as estimated by our model over a wide viscosity range.

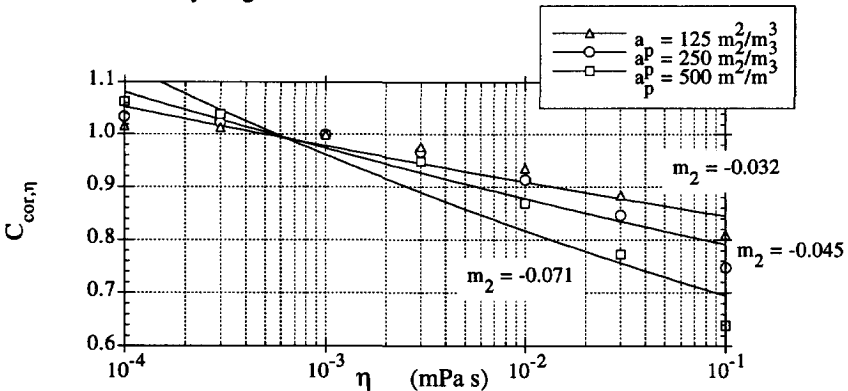


FIGURE 4.9: The relative influence of the liquid viscosity on the capacity factor for three packing types with inclination angle of  $38^\circ$ . The indicated power terms are fitted on the calculated relative values of  $C_{cor,\eta}$ . The points are obtained at a flow parameter of 0.1.

The normalised power term for the viscosity is not as effective as for the interfacial tension, which could explain the large deviations for the reported parameter. The viscosity in the presented model affects the critical capacity parameter in two ways. In addition to the effect on the void fraction, an opposite influence on the capacity is caused by the interface velocity. A larger viscosity decreases the interface velocity and therefore reduces the pressure drop over the packing, so that larger droplets can exist in the gas phase. This effect is most pronounced for packing with relative small specific area. The effective inclination angle hardly affects the viscosity influence, so that an estimated value for a packing with identical specific surface area, but different inclination angles, nearly coincide. The effect of the viscosity on the critical capacity factor is also shown in figures 4.10 A & B. Figure 4.10A shows the measured critical capacity factors, while the right graph shows the normalised critical capacity factors. Although the surface tension also has some influence in this case, the differences are mainly caused by the square of the reduced interface radius ( $\theta^2$ ), which is strongly influenced by the viscosity.

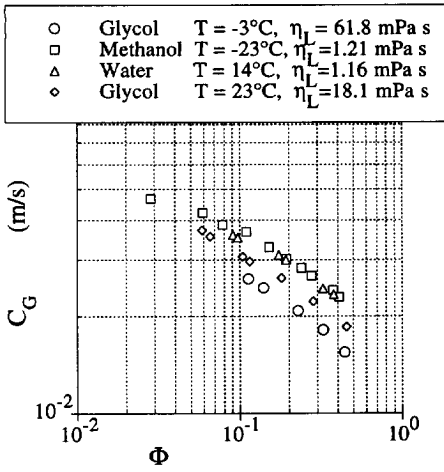


FIGURE 4.10A: The measured critical capacity factors of ceramic berl saddles, ( $a_p=303\text{m}^2/\text{m}^3$ ,  $\epsilon_0=0.59$ ,  $\alpha=55$ ) as reported by Krehenwinkel and Knapp (1987).

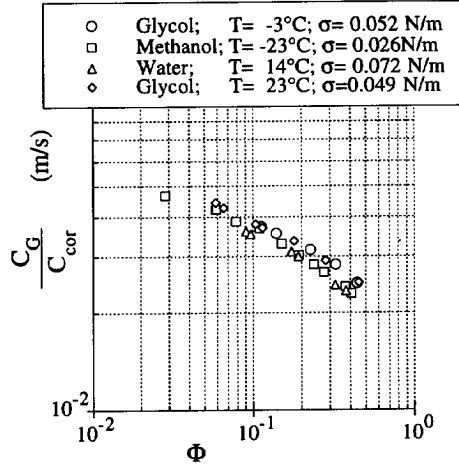


FIGURE 4.10B: The corrected critical capacity factors of ceramic berl saddles, for various liquids with different viscosities and surface tensions as reported by Krehenwinkel and Knapp (1987).

*The Gas Density*

One of the main considerations for applications at elevated pressures is the influence of the gas density on the capacity of the columns. By substituting equation (4.16) into equation (4.16), the influence of the gas density can be evaluated. Figures 4.11A & B show the relative change of the critical capacity factor in comparison with a gas of density  $1.2\text{kg}/\text{m}^3$  for two flow parameters.

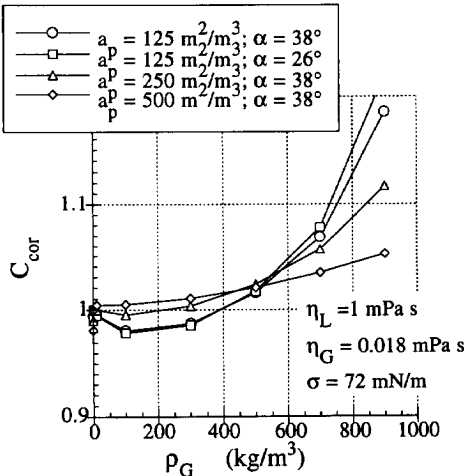


FIGURE 4.11A: The relative influence of the gas density on the critical capacity factor for a series of structured packing at constant flow parameter ( $\Phi=0.01$ ).

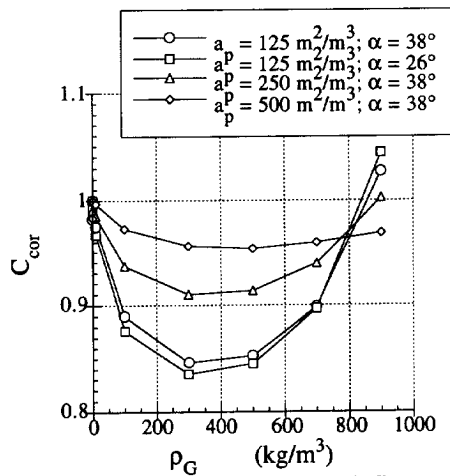


FIGURE 4.11B: The relative influence of the gas density on the critical capacity factor for a series of structured packing at constant flow parameter ( $\Phi=0.1$ ).

The figure shows that the gas density has a major influence on the critical capacity factor only for relative small specific area and effective inclination angle. The decrease of the presented curves at "low" gas density is caused by the interface velocity. The interface velocity relatively increases towards the gas velocity when the gas density is increased. Since the dissipated kinetic energy depends on the third power of the velocity, this parameter decreases at "large" gas densities, so that the drop size and the critical gas velocity will increase. Only limited data are reported on the change of the flood point with increasing gas density. Krehenwinkel and Knapp (1987) measured pressure drops and flood points at high pressures for various random packing systems. They did not find any change of the critical capacity factor for pressures up to 100bar in packed columns for ceramic Berl saddles ( $a_p=386$ ,  $\epsilon_0=0.59$ ) and for ceramic Raschig rings ( $a_p=309$ ,  $\epsilon_0=0.68$ ). They used a methanol-nitrogen flow system. When the critical capacity factors are estimated using equation (4.17) a change of less than one per cent is found over the applied density compared with the relative critical capacity factor for an ambient water-air system. The model therefore again is consistent with the reported results.

#### *The Gas/Bulk Viscosity*

Since the flow of the bulk gas phase is turbulent the influence of the gas viscosity in equation (4.17) is incorporated by making use of the smooth pipe friction factor. The relative effect of this parameter on the estimated critical capacity factor with constant other properties is limited and it seldom causes a change in the critical capacity factor over five per cent.

In liquid-liquid contactors an influence of the continuous bulk phase viscosity can be expected. Indeed some correlations suggest a dependence on the bulk phase viscosity (Breckenfeld and Wilke,  $(\eta_G/\eta_{ref})^{-0.33}$ , 1950; Hoffing and Lockhart,  $(\eta_G/\eta_{ref})^{-0.125}$ , 1954), but most don't (Crawford and Wilke, for  $Re_G > 50$ , 1951; Venkataraman and Laddha, 1960; Dell and Pratt, 1951).

#### CONCLUDING REMARKS

It has been found that flooding can be described by either liquid entrainment or by macroscopic drag on the liquid surface. This confirms the indications found in chapter 3. The results in this study show that entrainment appears the main cause of flooding. The presented model provides an estimation method that describes the relative changes of flood point with the physical properties and geometry of the packing. This has been accomplished by taking into account the lift force,  $F_l \sim d_e^3 \rho_G \cdot u_G(r) \cdot \partial u_G(r) / \partial r$ , on entrained droplet. Using this additional force it has been possible to predict several observed phenomena concerning physical properties and geometry of the packing. More elaborate descriptions concerning all influences on a droplet in a velocity field, distinguish even more forces on the droplet (see, e.g., van der Geld, 1997). However, most of these forces include a gas velocity and a gas velocity gradient and can be written similar to the expression used. It therefore appears justified to conclude that the

presented description provides a more fundamental basis for the flooding phenomena than correlations reported earlier and consequently predicts several of the observed flooding phenomena. The presented estimation method also has been tested with systems involving a supercritical fluid. In chapter 7 it will be shown that the model can predict the flood point over a wide range of physical properties.

The presented model predicts and explains some of phenomena concerning flooding. However, it does certainly not clear all uncertainties about the flooding phenomena. Although some circumstantial evidence is presented, the dependence of the critical capacity curve on the flow parameter remains partly unexplained. The most likely cause of local liquid entrainment and obstruction of the gas does not provide a better connection with theory, so that comparison with a well-known geometry remains necessary. The dependence of the critical capacity factor on subtle factors as the pipe length and a smooth gas and liquid entrance (Govan, et al., 1991) in a vertical pipe geometry, indicates the necessity of research in the hysteresis of the flooding phenomena, so that these secondary influences can be controlled.

NOTATION:

Symbol	Description	Unit
$a_p$	Specific packing area.....	$m^2/m^3$
$C$	Constant in Wallis correlation.....	
$C_G$	Capacity factor.....	m/s
$C_G^{crit}$	Critical capacity factor .....	m/s
$C_{G, meas.}^{crit}$	Measured critical capacity factor.....	m/s
$C_{G, model}^{crit}$	Critical capacity factor calculated with the model.....	m/s
$C_{orr}$	Correction factor for physical properties .....	
$C_r$	Relative capacity factor .....	
$C_t$	On position dependent parameter of the lift force.....	
$D_{col}$	Column diameter .....	m
$d_e$	Entrained drop diameter .....	m
$d_{max}$	Maximum stable drop diameter .....	m
$F_d$	Drag force on entrained droplet .....	N
$F_g$	Gravitational force on entrained droplet .....	N
$F_l$	Lift force on entrained droplet .....	N
$f$	Smooth pipe friction factor.....	
$f_p$	Friction factor of the packing .....	
$G''$	Gas load .....	$kg/s/m^2$
$g$	Gravitational acceleration.....	$m/s^2$

$H_{col}$	Column height.....m
$h$	Liquid film thickness.....m
$h_L$	Liquid hold-up.....m <sup>3</sup> /m <sup>3</sup>
$L''$	Liquid load.....kg/s/m <sup>2</sup>
$m$	Constant in Wallis correlation.....
$m_1$	Power constant for surface tension correction.....
$m_2$	Power constant for liquid viscosity correction.....
$p_{1,2}$	Pressure.....Pa
$r$	Radial co-ordinate.....m
$r_{int}$	Interface radius ( $r_{int} = \theta r_0$ ).....m
$r_0$	Hydraulic radius.....m
$u_d$	Drop velocity.....m/s
$u_{int}$	Interface velocity.....m/s
$u_G$	Gas velocity.....m/s
$u_{SG}$	Superficial gas velocity.....m/s
$u_{SG}^{crit}$	Critical superficial gas velocity.....m/s
$u_{SL}$	Superficial liquid velocity.....m/s
$U_G^*$	Dimensionless superficial gas velocity.....
$U_L^*$	Dimensionless superficial liquid velocity.....
$\alpha$	Effective inclination angle.....°
$\Delta\rho$	Density difference.....kg/m <sup>3</sup>
$\partial p/\partial z$	Pressure drop over equipment.....Pa/m
$\epsilon$	Dissipated kinetic energy.....m <sup>2</sup> /s <sup>3</sup>
$\epsilon_0$	Void fraction.....m <sup>3</sup> /m <sup>3</sup>
$\gamma_1$	General turbulence constant ( $\gamma_1=1.8$ ).....
$\eta_G$	Dynamic gas viscosity.....Pa s
$\eta_L$	Dynamic liquid viscosity.....Pa s
$\theta$	Relative interface position.....
$\Phi$	Flow parameter.....
$\rho_G$	Gas density.....kg/m <sup>3</sup>
$\rho_L$	Liquid density.....kg/m <sup>3</sup>
$\sigma$	Surface tension.....N/m
$\bar{v}$	Velocity of turbulent eddies.....m/s
$\psi_{G-L}$	Gas-liquid interaction parameter.....
$Bo$	Bond number..... $Bo = \frac{2r_{int}^2 g (\rho_G - \rho_L)}{\sigma}$
$K_G$	Gas Kutateladze number..... $K_G = u_{SG} \left( \frac{\rho_G^2}{g\sigma(\rho_G - \rho_L)} \right)^{0.25}$

Re<sub>G</sub> Gas phase Reynolds number.....  $Re_G = \frac{\rho_G \left( \frac{u_{SG}}{\theta^2 \epsilon_0 \cos \alpha} - u_{int} \right) 2\theta r_0}{\eta_G}$

Re<sub>L</sub> Liquid phase Reynolds number.....  $Re_L = \frac{4\rho_L u_{SL}}{\eta_L a_p}$

We<sub>crit-1</sub> Critical Weber number .....  $We_{crit-1} = \frac{\rho_G \left( \frac{u_{SG}}{\epsilon_0 \theta^2 \cos \alpha} - u_{int} \right)^2 d_{max}}{\sigma}$

We<sub>crit-2</sub> Critical Weber number .....  $We_{crit-2} = \frac{3\rho_G (\epsilon d_{max})^{2/3} d_{max}}{\sigma}$

REFERENCES:

[1] Alekseev, V.P., Poberezkin, A.E., and Gerasimov, P.V., (1972), *Determination of Flooding Rates in Regular Packing*, Heat Transfer Soviet Res., **4** pp. 159-163.

[2] Barnea, D., and Taitel, Y., (1993), *Kelvin-Helmholtz Stability Criteria for Stratified Flow: Viscous versus Non-Viscous Approaches*, Int. J. Multiphase Flow, **19** (4) pp. 639-649.

[3] Baird, M.H.I., and Lane, S.J., (1972), *Drop size and Hold-up in a Reciprocating Plate Extraction Column*, Chem. Eng. Sci., **28** pp. 947-957.

[4] Batchelor, D.C., (1951), Proc. Cambridge Phil. Soc., **47** pp. 359.

[5] Breckenfeld, R.R., and Wilke, C.R., (1950), Chem. Eng. Prog., **46** pp. 187.

[6] Celata, G.P., Cumo, M., Farello, G.E., and Setaro, T., (1991), *Hysteresis Effect in Flooding*. Int. J. Multiphase Flow, **17** (2) pp. 283-289.

[7] Clift, R., Grace, J.R., and Weber, M.E., (1978), *Bubbles, Drops, and Particles.*, Academic Press, New York..

[8] Coulson, J.M., and Richardson, J.F., (1978), *Chemical Engineering*, Vol. 2, 3<sup>rd</sup> ed. Oxford: Pergamon Press.

[9] Coulson, J.M., and Richardson, J.F., (1985), *Chemical Engineering (Design)*, Vol. 6. Oxford: Pergamon Press.

[10] Crawford, J.W., and Wilke C.R., (1951), *Limiting Flows in Packed Extraction Columns.*, Chem. Eng. Prog., **47** (8) pp. 423-431.

[11] Datta, R., (1993), *Eddy Viscosity and Velocity Distribution in Turbulent Pipe Flow Revisited*. AIChE Journal, **39** (7), 1107-1112.

[12] Dell, F.R., and Pratt, H.R.C., (1951), Trans. Inst. Chem. Eng., **29**, p89.

[13] Fair, J.R., and Bravo, J.L., (1990), *Distillation Columns Containing Structured Packing*. Chem. Eng. Prog., **86** pp.19-29.

[14] Feynman, R.P., Leighton, R.B., Sands, M., (1964), *Lectures on Physics*. Massachusetts: Addison-Wesley Publishing Com..

[15] Geld, van der C.W.M., (1997), *Measurement and prediction of solid sphere trajectories in accelerated gas flow*, Int. J. Multiphase Flow, **23** pp. 357-376.

[16] Govan, A.H., Hewitt, G.F., Richter, H.J., Scott, A., (1990), *Flooding and Churn Flow in Vertical Pipes*, Int. J. Multiphase Flow, vol. **17**, no. 1, pp. 27-44.

[17] Hewitt, G.F., and Wallis, G.B., (1963), *Flooding and Associated Phenomena in Falling Film Flow in a Tube.*, UKAERE Report, R-4022.

[18] Hewitt, G.F., and Hall-Taylor, N.S., (1970), *Annular Two-Phase Flow*, Pergamon Press, New York.

[19] Hiller, N., Schiemann, H., Weidner, E., and Peter, S., (1993), *Interfacial Tension in Systems with a Supercritical Component at High Pressures*, Chem. Eng. Technol., **16** pp. 206-212.

- 
- [20] Hinze, J.O. (1954), *Fundamentals of the Hydrodynamic Mechanism of Splitting in Dispersion Processes*, AIChE J., **1** pp. 289-295.
- [21] Hinze, J.O. (1975), *Turbulence*, 2<sup>nd</sup> ed, McGraw-Hill, New York.
- [22] Hoffing, E.H., and Lockhart, F.J., (1954), *A Correlation of Flooding Velocities in Packed Columns*, Chem. Eng. Prog., **50** pp. 94-103.
- [23] Ishii, M., and Grolmes, M.A., (1975), *Inception Criteria for Droplet Entrainment in Two-Phase Concurrent Film Flow*, AIChE J., **21** pp. 308-317
- [24] Krehenwinkel, H., and H. Knapp, *Pressure Drop and Flooding in Packed Columns Operating at High Pressures*, Chem. Eng. Tech. **10**, 231-242 (1987).
- [25] Laddha, G.S., and Degaleesan, T.E., (1976), *Transport Phenomena in Liquid Extraction*, McGraw-Hill Publishing Co. Ltd., New Delhi.
- [26] McQuillan, K.W. and Whalley, P.B. (1984), *A comparison Between Flooding and Experimental flooding Data for Gas-Liquid Flow in Vertical Circular Tubes*, Chem. Eng. Sci., **40** pp. 1425-1440.
- [27] Mersmann, A., (1965), *Zur Berechnung des Flutpunktes in Füllkörperschüttungen*, Chem. Ing. Techn., **37** (3) pp. 218-226.
- [28] Norton Chemical Process Products Corporation, (1993), *Intalox High-Performance Structured Packing*, Information Bulletin.
- [29] Pushkina, O.L., and Sorokin, Yu. L., (1969), *Breakdown of Liquid Film Motion in Vertical Tubes.*, Heat Transfer Soviet Res., **1** pp. 56-64.
- [30] Rayleigh, Lord, (1878), Proc. London Math. Soc., **10** pp.4-13.
- [31] Sabersky, R.H., Acosta, and A.J., Hauptmann, E.G., (1989), *Fluid Flow*, 3<sup>rd</sup> ed. New York: MacMillan Publishing Company.
- [32] Sherwood, T.K., Shipley, G.H., and Holloway, F.A., (1938), *Flooding Velocity in Packed Columns*, Ind. Eng. Chem., **30** pp. 765-769.
- [33] Sulzer Brother Ltd., (1989), *Separation Columns for Distillation and Absorption*. Information Bulletin.
- [34] Taitel, Y., Bornea, D., and Dukler, A.E., (1980), *Modelling Flow Pattern Transitions for Steady upward Gas-Liquid flow in Vertical Tubes*, AIChE J., **26** (3) pp. 345.
- [35] Treybal, R.E., (1980), *Mass Transfer Operations*, 3<sup>rd</sup> ed, Wiley Series in Chemical Engineering, New York.
- [36] Venkataraman, G., and Laddha, G.S., (1960), AIChE J., **6** pp. 355
- [37] Wallis, G.B., (1961), *Flooding Velocities for Air and Water in Vertical Tubes.*, Report AEEW-R123.
- [38] Wallis, G.B., (1969), *One-Dimensional Two-Phase Flow*, New York: McGraw-Hill.
- [39] Whalley, P.B., (1996), *Two-Phase Flow and Heat Transfer*, Oxford University Press, Oxford.
-



## Mass Transfer in Packed Columns, a Description Based on Hydrodynamics

An important objective of separation technology is the design and prediction of the performance of the equipment involved. This thesis focuses on packed columns, in which hydrodynamics dominates the equipment potentials. The thermodynamic description used normally, is based on equilibrium. However, the actual separation can be achieved only by creating a continuous non equilibrium between the phases, so that mass transfer can take place from one phase to the other. To enable a prediction of the column performance, information on thermodynamics, physical properties, hydrodynamics and mass transfer have to be combined.

Separation of components of a homogeneous liquid mixture can be performed in packed columns by contacting the liquid with an auxiliary gas phase in which certain compounds preferably will dissolve. When equilibrium is established the distribution of a component (i) over the phases is described as:

$$K_i = \frac{y_i}{x_i}, \quad (5.1)$$

where  $y_i$  is the molar fraction in the gas phase and  $x_i$  is the molar fraction in the liquid phase.

To obtain a molecular diffusion flux  $J_i$  of a component from one phase in the other, non equilibrium between the bulk of the phases is required resulting in a mass transfer through the interface. According to the film model for mass transfer it is assumed that the molecules in the two phases at the interface reach equilibrium instantaneously. This is shown in figure 5.1.

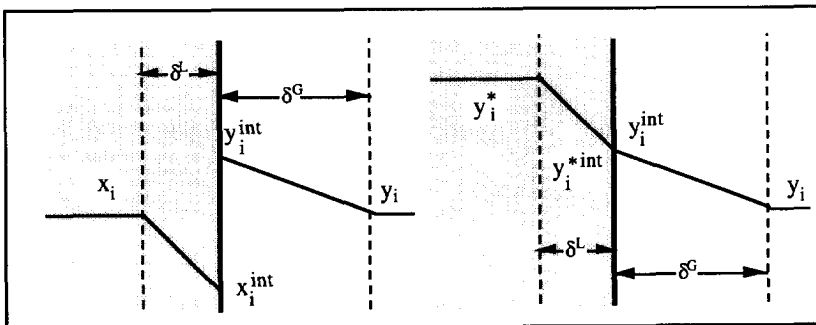


FIGURE 5.1: Non equilibrium over an interface shown in a film model with indicated thicknesses in the gas ( $\delta^G$ ) and liquid ( $\delta^L$ ) phase. The left drawing shows the real concentration level, while the second shows the corrected profile in a hypothetical one phase system.

When using the normal notation for the gas and liquid phase, the flux of a component from the interface to the gas phase can be described by means of the difference in concentration at the interface and the bulk concentration in the gas phase as:

$$J_i^G = k_i^G c_t^G (y_i^{int} - y_i), \quad (5.2)$$

where  $c_t^G$  is the total molar concentration in the gas phase and  $k_i^G$  is the gas phase mass transfer coefficient representing the rate of the molecular transport. When the equilibrium line, expressing the concentrations in the gas and liquid phase, is linearised as function of the liquid concentration an apparent equilibrium gas concentration ( $y_i^*$ ) can be defined (see, e.g., Treybal, 1980; Taylor and Krishna, 1993) as:

$$y_i^* = \frac{\partial y_i^*}{\partial x_i} x_i + b_i = m_i x_i + b_i, \quad (5.3)$$

where  $m_i$  is the slope of the equilibrium line. This expression can be used to describe the diffusion flux  $J_i^L$  from the liquid bulk to the interface in terms of gas concentrations as:

$$J_i^L = k_i^L c_t^L (x_i - x_i^{int}) = k_i^L c_t^L \left( \frac{y_i^* - b_i}{m_i} - \frac{y_i^{int} - b_i}{m_i} \right) = k_i^L \frac{c_t^L}{m_i} (y_i^* - y_i^{int}), \quad (5.4)$$

where  $k_i^L$  is the liquid mass transfer coefficient,  $c_t^L$  is the total molar concentration in the liquid and the star superscript indicates that it concerns an apparent gas concentration. Equation (5.4) uses the interface equilibrium condition. The derivative of the equilibrium curve ( $m_i$ ) remains in the analysis, while the constant  $b_i$  is eliminated from further calculations. When equimolar diffusion is assumed, the molar fluxes in the liquid and gas phase must be equal. The interface concentration therefore can be eliminated and one obtains:

$$(y_i^* - y_i) = J_i \left( \frac{1}{k_i^G c_t^G} + \frac{m_i}{k_i^L c_t^L} \right) = \frac{J_i}{c_t^G} \left( \frac{1}{k_i^G} + m_i \frac{c_t^G}{c_t^L k_i^L} \right) = \frac{J_i}{c_t^G k_i^{OG}} \quad (5.5)$$

In this equation  $k_i^{OG}$  is the overall gas phase mass transfer coefficient. Similar to equation (5.2) the molar flux can be expressed as:

$$J_i = k_i^{OG} c_t^G (y_i^* - y_i). \quad (5.6)$$

### MASS TRANSFER COEFFICIENTS

When the mass transfer can be described by the film model (see figure 5.1) the above equations can be applied. However, to develop a consistent mass transfer model it is required to obtain characteristic thicknesses of gas ( $\delta^G$ ) and liquid ( $\delta^L$ ) film. To describe these characteristic thicknesses for each component Sherwood numbers ( $Sh$ ) are used. The Sherwood number relates the mass transfer to a macroscopic size of the flow and is defined as the ratio of the total mass transport and the diffusive molecular transport. When the liquid phase is a film with thickness  $h$ , the characteristic mass transfer film thickness can be expressed using the liquid Sherwood number as:

$$Sh_i^L = \frac{k_i^L h}{D_i^L} \quad \Rightarrow \quad \delta_i^L = \frac{h}{Sh_i^L} \quad (5.7)$$

where the denominator of the Sherwood number represents the diffusion coefficient. By replacing the superscripts an analogous Sherwood number for the gas phase can be used to express the characteristic mass transfer film thickness by using the macroscopic flow dimension of the gas flow as:

$$\text{Sh}_i^G = \frac{k_i^G 2\theta r_0}{D_i^G} \Rightarrow \delta_i^G = \frac{2\theta r_0}{\text{Sh}_i^G} \quad (5.8)$$

where  $2\theta r_0$  represents the for channel flow characteristic macroscopic diameter. In this equation  $\theta$  represents the ratio of the interface radius over the hydraulic radius ( $r_0$ ) of the packing (see also chapter 3).

### The Gas Phase Mass Transfer Coefficients

At normal conditions in a packed column, the gas phase Sherwood number mainly describes the mass transfer enhancement due to the turbulence of the gas flow. The turbulence can be calculated from different models describing the flow profile in a duct (Sideman and Pinczewski, 1975). In a pipe the analogy between transfer of momentum and mass can be described well with the Chilton-Colburn relation (1934). This analogy, also valid for heat transfer, relates the Sherwood number with the smooth pipe friction factor ( $f$ ), the gas Reynolds number ( $\text{Re}_G$ ) and the Schmidt number ( $\text{Sc}_i^G$ ) as (Linton and Sherwood, 1950):

$$\text{Sh}_i^G = \frac{f}{2} \text{Re}_G \text{Sc}_i^{G0.33} = 0.023 \text{Re}_G^{-0.2} \text{Re}_G \text{Sc}_i^{G0.33}$$

where  $\text{Re}_G = \frac{\rho_G 2\theta r_0}{\eta_G} \left| \frac{u_{SG}}{\theta^2 \epsilon_0 \cos \alpha} - u_{int} \right|$

and  $\text{Sc}_i^G = \frac{\eta_G}{\rho_G D_i^G}$  (5.9)

Here  $u_{int}$  represents the interface velocity of the liquid and  $\alpha$  the effective inclination angle of the gas flow. The success of this empirical relation lies in the fact that it describes the boundary layer of a turbulent flow over a wide range of Schmidt numbers (Fletcher et al., 1982).

Given the channel type gas flow in a packed bed, equation (5.9) consequently appears a logical starting point to express the mass transfer in the gas phase. To enable a comparison, packed bed correlations reported in literature for mass transfer in the gas phase will be written similar to equation (5.9). The relation requires a description of the Reynolds number relative towards the interface. However, most of the correlations reported neglect the interface velocity and only use the superficial gas velocity  $u_{SG}$ . For comparison the gas Reynolds number is therefore rewritten as:

$$\text{Re}_G = \frac{\rho_G \left| \frac{u_{SG}}{\theta^2 \epsilon_0 \cos \alpha} - u_{int} \right| 2\theta r_0}{\eta_G} = \frac{\rho_G \left| \frac{u_{SG}}{\theta^2 \epsilon_0 \cos \alpha} - u_{int} \right| 4\theta \epsilon_0}{a_p \eta_G} \approx \frac{4}{\theta \cos \alpha} \frac{\rho_G u_{SG}}{a_p \eta_G} \quad (5.10)$$

Here use has been made of the flow radius as defined using the specific packing area  $r_0 = 2\epsilon_0/a_p$ , where  $\epsilon_0$  is the porosity of the packing. The simplification of equation (5.10) is justified for low

liquid loads and small gas densities. The first correlation that is considered, is reported by Onda et al., (1968) for random packing. The authors distinguish small ( $d_p < 12$  mm) and large packing sizes ( $d_p > 12$  mm). When their correlation is rewritten in the form of the Chilton-Colburn analogy and applying simplification (5.10), it reads:

$$Sh_i^G = \frac{4\theta\epsilon_0}{(a_p d_p)^2} \left( \frac{\theta \cos \alpha}{4} \right)^{0.7} A Re_G^{-0.3} Re_G Sc_i^{G,0.33} \quad \text{where} \quad \begin{matrix} A = 2.00 & \text{for } d_p < 12\text{mm} \\ A = 5.23 & \text{for } d_p > 12\text{mm} \end{matrix} \quad (5.11)$$

A second relation, applied to structured packing, is reported by Bravo et al., (1985). They correlate their data as:

$$Sh_i^G = 0.0338 Re_G^{-0.2} Re_G Sc_i^{G,0.33} \quad (5.12)$$

The relation is similar to the relation given in equation (5.9). All correlations are written so that the friction factor can be isolated readily. In figure 5.2 they are compared to the Blasius friction factor for smooth pipes.

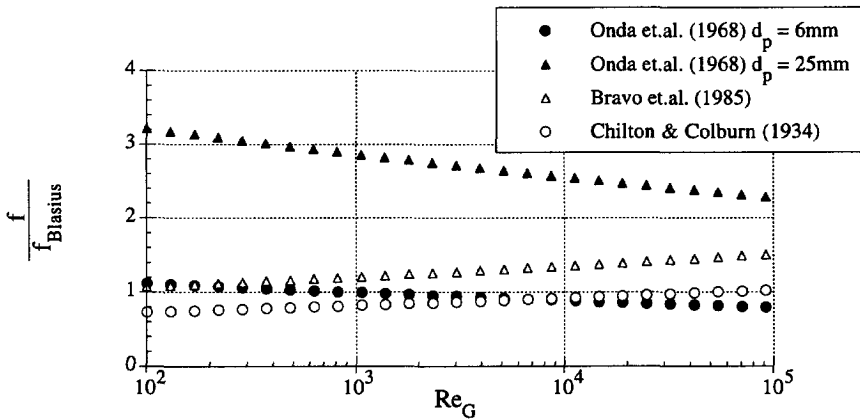


FIGURE 5.2: Comparison of the friction factors from various mass transfer models. For the Onda model use has been made of data (Treybal, 1980) for ceramic Raschig rings, a flow angle ( $\alpha$ ) of  $54.9^\circ$  and a dimensionless radius ( $\theta$ ) of 0.95.

The figure shows that the smooth Blasius curve is approximated well by the friction factor of the Chilton-Colburn analogy. Although the results are in the same range, the Onda relation (5.11) shows substantial deviations for large packing elements.

Considering the above results, it is likely that the gas mass transfer in structured packing can be described analogue to duct flow mass transfer. The pressure gradient in a packed column is calculated normally in the z-direction of the column. Because the gas in a packed bed flows at an angle, a cosine term needs to be incorporated to take into account the larger flow path, which effectively increases the friction factor. The friction factor also depends on the roughness of the pipe. When the friction factor increases by the interaction of the gas and liquid phase the mass transfer will increase. The increase of the friction factor is described in chapter 3 using the gas-liquid interaction parameter  $\psi_{G-L}$ . Here this parameter can be used to describe the increase of the smooth friction factor ( $f$ ) and therefore the increase of the Sherwood number as:

$$Sh_i^G = \frac{f}{2} \frac{1+\psi_{G-L}}{\cos \alpha} \left( \frac{\rho_G \left| \frac{u_{SG}}{\theta^2 \epsilon_0 \cos \alpha} - u_{int} \right| 2\theta r_0}{\eta_G} \right) Sc_i^{G0.33} \quad (5.12)$$

When at first instance the gas-liquid interaction parameter is neglected, equation (5.12) can be used directly to interpret the gas phase correlation of Bravo et al., (1985). It is found that both correlations are identical for an effective inclination angle of  $\arccos(0.023/0.0338) = 47^\circ$ . Equation (5.12) can be used to express the mass transfer coefficient, defined by equation (5.8), as:

$$k_i^G = \frac{f}{2} (1+\psi_{G-L}) \frac{|u_{SG} - u_{int} \theta^2 \epsilon_0 \cos \alpha|}{\theta^2 \epsilon_0 \cos^2 \alpha} Sc_i^{G-0.66} \quad (5.13)$$

The smooth pipe friction factor  $f$  in this relation can be taken as the Blasius relation or any better. The square cosine term in equation (5.13) is caused by the increase of the Reynolds number and the increase of the friction factor per unit column height.

### Review of the Liquid Phase Mass Transfer Coefficients

Because the major part of the mass transfer resistance is located often in the gas phase the assumption made for the liquid phase is less vital in most separations using gas-liquid mass transfer. However, when a volatile component is stripped from a viscous stream, the liquid mass transfer coefficient can become the dominant factor.

Although the liquid film on the packing structure is assumed laminar, the description of the mass transfer in the liquid phase is still the most difficult. This is caused by the fact that the mass transfer within the laminar film is influenced by secondary flow effects such as wave formation and the packing structure, generating surface renewal.

The basis of most relations for the liquid mass transfer is the film penetration theory, which requires the solution of the non stationary diffusion equation derived from the conservation of mass;

$$c_t^L \frac{\partial x_i}{\partial t} + \frac{\partial J_i^L}{\partial r} = 0 \quad \Rightarrow \quad \frac{\partial x_i}{\partial t} = D_i^L \frac{\partial^2 x_i}{\partial r^2} \quad (5.14)$$

In this equation the radial term  $J_i^L/r$  is neglected. The solution of this differential equation is given in several engineering and mathematical textbooks (see, e.g.: Bird et al., 1960, Coulson and Richardson, 1977, Boyce and DiPrima, 1977, Spiegel, 1967). Two equivalent series solutions are found (Toor and Marchello, 1958):

$$J_i^L = \sqrt{\frac{D_i^L}{\pi t}} \left( 1 + 2 \sum_{n=1}^{\infty} \exp\left(-\frac{n^2 h^2}{D_i^L t}\right) \right) c_t^L(x_i - x_i^{int}) = \frac{D_i^L}{h} \left( 1 + 2 \sum_{n=1}^{\infty} \exp\left(-\frac{n^2 \pi^2 D_i^L t}{h^2}\right) \right) c_t^L(x_i - x_i^{int}) \quad (5.15)$$

In the exponential terms of the equations the Fourier number is found;

$$Fo_i^L = \frac{D_i^L t}{h^2} \quad (5.16)$$

The first series solution of relation (5.15) converts rapidly for small Fourier numbers, while the second series convert rapidly for large Fourier numbers. The above solution considers a non

flowing situation. However, in case of a falling film, as within packed columns, the velocity of film causes an increase of the mass transfer. Johnstone and Pigford (1942) showed that this increase is equal to a factor 3.41 for large Fourier numbers. Equation (5.15) leads to a time dependent liquid mass transfer coefficient  $k^L(t)$ . To overcome this problem a time averaged value is introduced. The model of Higby (1935) is based on the assumption that all the fluid elements reside at the interface for the same time and the average mass transfer coefficient is found by integrating over the exposed time ( $t_e$ ) as:

$$\bar{k}_f^L = \frac{1}{t_e} \int_0^{t_e} \sqrt{\frac{D_i^L}{\pi t}} \left( 1 + 2 \sum_{n=1}^{\infty} \exp\left(-\frac{n^2 h^2}{3.41^2 D_i^L t}\right) \right) dt \quad (5.17)$$

Figure 5.3 shows the average Sherwood number as calculated with equation (5.7) and (5.17) as function of the Fourier number. The figure shows that the series for the average mass transfer coefficient can be approximated for long and small Fourier numbers. The two limited solutions therefore often are used up to and after a characteristic Fourier number. Dobbins (1956) suggested a function that interpolates the whole series of equation (5.17). The two interpolation functions are written as:

$$\begin{aligned} \text{Limit Values} \quad \bar{k}_f^L &= 2 \sqrt{\frac{D_i^L}{\pi t_e}} & \text{for} \quad \text{Fo}_i^L < \left(\frac{2}{3.41}\right)^2 \frac{1}{\pi} \approx 0.1 & (a) \\ \bar{k}_f^L &= 3.41 \frac{D_i^L}{h} & \text{for} \quad \text{Fo}_i^L > \left(\frac{2}{3.41}\right)^2 \frac{1}{\pi} \approx 0.1 & \\ \text{Dobbins} \quad \bar{k}_f^L &= 2 \sqrt{\frac{D_i^L}{\pi t_e}} \coth \sqrt{\frac{4h^2}{(3.41)^2 \pi D_i^L t_e}} & & (b) \end{aligned} \quad (5.18)$$

Figure 5.4 shows the deviations of these approximation functions from the integral of equation (5.17). Most mass transport models (see, e.g.: Bravo et al., 1985, de Haan, 1991) use the limit values to describe the liquid mass transport coefficient. This is rather peculiar, because next to the advantages of a continuous function the Dobbins interpolation also has considerably smaller deviations from the real solution as shown in figure 5.4.

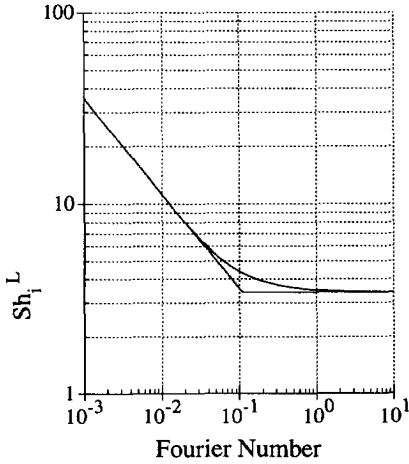


FIGURE 5.3 The effective liquid Sherwood number, for transport into the free surface of a falling film.

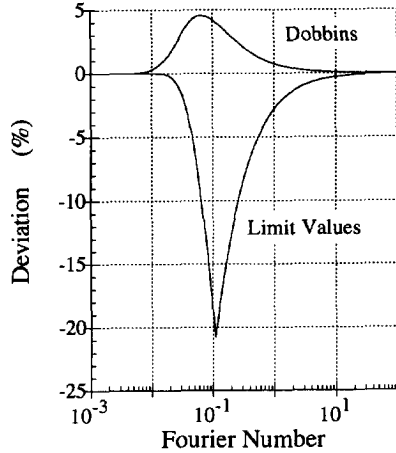


FIGURE 5.4: The deviation of the approximation relations (5.18a & 5.18b) from the integral relation (5.17).

The mass transfer from gas to liquid, or visa versa, occurs through the interface. The exposure time therefore can be paraphrased as an exposure length divided by the interface velocity (See, e.g., Sherwood and Pigford, 1952; Singh and von Stockar, 1996);

$$\ell_e = |u_{int}| t_e \tag{5.19}$$

The interpretation of this is physically simpler, since its limit value is always known as the height of the geometry. Besides, for simple geometries like a vertical pipe, its value is determined exactly, so that an evaluation is unambiguous. The essential step in modelling the liquid mass transfer is therefore condensed in the determination of the exposure length. Before evaluating reported liquid mass transfer data, the correlations in literature are rewritten in a uniform way.

The Reynolds number for a liquid mass flow per cross sectional area  $L''$  of the column is recalled (Perry 1985, Bird et al., 1962):

$$Re_L = \frac{4\rho_L |u_L| h}{\eta_L} = \frac{4\rho_L h}{\eta_L} \frac{|u_{SL}|}{a_p h} = \frac{4\rho_L |u_{SL}|}{\eta_L a_p} = \frac{4|L''|}{\eta_L a_p} \tag{5.20}$$

and is used to express the free falling liquid film thickness,

$$h_0 = \left( \frac{3\eta_L}{\Delta\rho\rho_L g \cos \alpha} \frac{|L''|}{a_p} \right)^{\frac{1}{3}} = \frac{1}{a_p} \left( \frac{3\eta_L^2 a_p^3}{4\Delta\rho\rho_L g \cos \alpha} \frac{4|L''|}{\eta_L a_p} \right)^{\frac{1}{3}} = \frac{1}{a_p} \left( \frac{Re_L}{Ga_p} \right)^{\frac{1}{3}} \tag{5.21}$$

and the free falling film interface velocity ( $u_{0-int}$ ),

$$|u_{0-int}| = \frac{3}{2} \frac{|L''|}{\rho_L a_p h_0} = \frac{3}{8} \frac{a_p \eta_L}{\rho_L} Re_L^{0.66} Ga_p^{0.33} \tag{5.22}$$

In these equations the packing Galileo number ( $Ga_p$ ) is introduced. The above quantities will be used as references for the evaluation.

As shown in equation (5.18), the average liquid mass transfer coefficient for large Fourier times is determined by the film thickness ( $h$ ) and the influence of the exposure time ( $t_e$ ) is then marginal. The exposure length therefore can only be evaluated using experimental mass transfer data for small Fourier times. By rewriting the Sherwood using the expressions for a free falling film,

$$\begin{aligned} Sh_1^L &= \frac{k_1^L h}{D_1^L} \approx \sqrt{\frac{4h_0^2}{\pi D_1^L t_e}} \approx \sqrt{\frac{4h_0^2 u_{0-int}}{\pi D_1^L \ell_e}} = \sqrt{\frac{3}{2\pi} \frac{4h_0 \bar{u}_L \rho_L}{\eta_L} \frac{\eta_L}{\rho_L D_1^L} \frac{h_0}{\ell_e}} \\ &= \sqrt{\frac{3}{2\pi} Re_L Sc_1^L \frac{h_0}{\ell_e}} = \sqrt{\frac{3}{2\pi} \frac{Re_L^{1.33} Sc_1^L}{Ga_p^{0.33} \ell_e a_p}} \end{aligned} \quad (5.23)$$

the reciprocal exposure length is isolated;

$$\frac{1}{\ell_e} = a_p \frac{2\pi}{3} \frac{Sh_1^L{}^2 Ga_p^{0.33}}{Re_L^{1.33} Sc_1^L} \quad (5.24)$$

All reported correlations can be formulated so that they give an expression for the exposure length. To compare these correlations, they are written in the form of the right hand side of equation (5.24), so that a relation for the reciprocal exposure length can be isolated. Table V.I shows the obtained relations for the reciprocal exposure length for three types of geometrical structures. In these expressions the needed effective flow angle for the Galileo number is neglected and in some relations a liquid density is replaced by a density difference. In contrast to the gaseous mass transfer models, the table shows several configurations and no tendency towards one specific model can be observed (see also, e.g., Semmelbauer, 1967). However, some characteristics can be detected in the correlations.

The two correlations for the vertical pipe geometry, given by Vivian and Paeceman (1956), and Lamourelle and Sandell (1972) appear complementary in respect to the Reynolds number range. Vivian and Paeceman report a dependence close to the theoretical value of the pipe length and no significant dependence on the liquid Reynolds number. However, according to Emmet and Pigford (1954) the liquid mass transfer may be substantially larger than this near theoretical relation, due to ripples and waves which form at  $Re_L > 25$ .

Most available data for the liquid mass transfer in packed beds are measured in randomly packed beds. The reported correlations for this geometry often apply the size of an individual packing element ( $d_p$ ) in the relation. These sizes can be related to the specific surface area of the packing, e.g.: the product ( $a_p d_p$ ) is typically equal to 5 and the sphere diameter ( $d_s$ ) used by Shulman and Ullrich (1955) has a product ( $a_p d_s$ ) with its specific surface area, which normally is equal to 3. It is interesting that only the relation of Semmelbauer (1967) does not show any dependence on the packing Galileo number, while the two relations of Onda et al., (1959 and 1968) show a direct dependence (see also; van Krevelen and Hoftijzer, 1948). Shulman and Ullrich (1955), (see also, Sherwood and Holloway, 1940) report a reciprocal dependence.



For structured packing Bravo et al., (1985) use a simple approach by employing the channel side of a structured packing element as characteristic flow length. By doing so the authors state that the liquid is mixed completely flowing over each ridge in the structured packing. Given the way that liquid flows through a structured packing (Olujic et al., 1993) this length appears on the short side. The last equation of table V.I will be discussed in the following section.

TABLE V.I: Expressions for the reciprocal exposure length as correlated by different authors for vertical pipes, random packing and structured packing, expressed as function of dimensionless numbers<sup>†</sup>.

Author	Relation for $\frac{1}{\ell_e}$	Comments
Vertical pipe		
Vivian & Paeceman (1956)	$\frac{0.535}{Z} Re_L^{0.13}$	$Re_L < 2200$ Z is the pipe length.
Lamourelle & Sandell (1972)	$\frac{a_p}{1.54 \cdot 10^9} Re_L^{1.68} Ga_p^{0.33}$	$1300 < Re_L < 8000$
Random Packing		
Shulman & Ullrich (1955)	$\frac{379}{d_s} \frac{Re_L^{0.23}}{Ga_p^{0.33} (d_s a_p)^{0.1}}$	$d_s$ is size of sphere with a surface area identical to a packing element.
Onda et al. (1959)	$\frac{a_p}{44} Re_L^{0.31} Ga_p^{0.33}$	
Semmelbauer (1967)	$\frac{a_p}{24} Re_L^{0.51} (d_p a_p)^{0.1}$	Coeff. for Raschig rings. $d_p$ size of packing element.
Onda et al. (1968)	$\frac{a_p}{238} Re_L^{0.66} Ga_p^{0.33} (d_p a_p)^{0.4}$	The equation is used in combination with wetted area of the packing.
Structured Packing		
Bravo et al. (1985)	$\frac{1}{s}$	s is the corrugation side
Generalised Relation		
This study	$\frac{a_p}{2 \cdot 10^{14}} \frac{Re_L Re_G^2}{\epsilon_0^7 \cos^9 \alpha} \frac{\rho_L}{\rho_G} + \frac{1}{Z_p}$	$Z_p$ is the characteristic length of the packing geometry.

<sup>†</sup> The effective flow angle and density difference, introduced by the Galileo number are incorporated without changing the constants, since their influences in the literature models are small.

It is illustrative to compare the relations of table V.I with an example. This is done in figure 5.5 for a packed column of 2 meters, in which internals are applied all with a specific surface area of 250 m<sup>2</sup>/m<sup>3</sup>, a void fraction of 0.9 m<sup>3</sup>/m<sup>3</sup> and a flow angle of 45°. The system has physical properties equal to those of air and water at 25°C and to avoid the possibility of using

the correlations beyond the flooding point it is "operated" at a low gas load ( $G = 0.5 \text{ kg/m}^2/\text{s}$ ). The sizes of the packing element are replaced with the specific surface area, using the earlier mentioned relations.

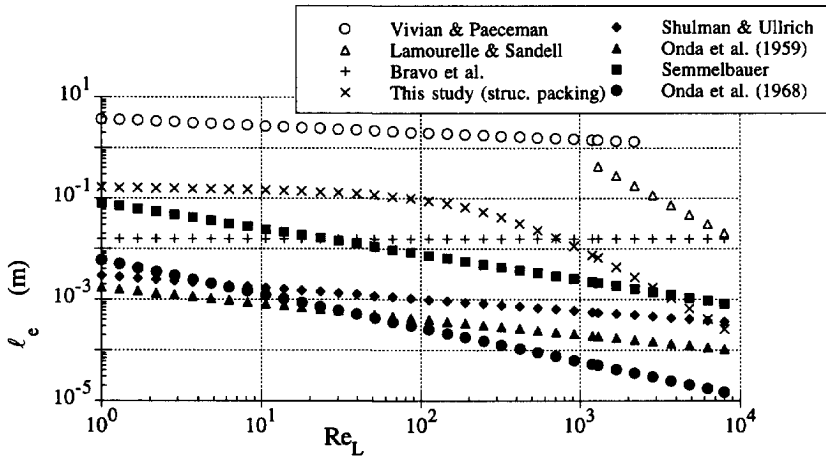


FIGURE 5.5: Comparison of the exposure lengths for the models given in table V.I as function of the liquid Reynolds number for an ambient water air system at ambient conditions.

The figure shows that the correlations for the exposure lengths differ by a factor hundred for random packing. However, the exposure length is not the measured variable and it is for that reason that the average liquid mass transfer coefficients are calculated using equations (5.18b), (5.19) and (5.22). Figures 5.6A and 5.6B show that all systems have the same solution at low Reynolds number. The inflection point in each curve is caused by the difference of the solution for short and long Fourier times. Although the resulting mass transfer coefficients are of course closer together than the obtained exposure length, a deviation between correlations of a factor fifty can still be qualified as substantial. The deviation observed, can be explained partly by the fact that Onda et al., use estimated wetted specific areas in his liquid mass transfer correlations instead of the total specific area of the packing.

As indicated in figures 5.6A and 5.6B, this study shows three distinguishable regions for the liquid mass transfer coefficients. Each region is dominated by a characteristic length. The first region is found in all models and represents the long time solution of equation (5.14), causing a direct dependence of the liquid mass transfer on the liquid film thickness. The second and third regions are subsequently dominated by the packing geometry and the waves on the liquid interface. These influences will be discussed in the following sections.

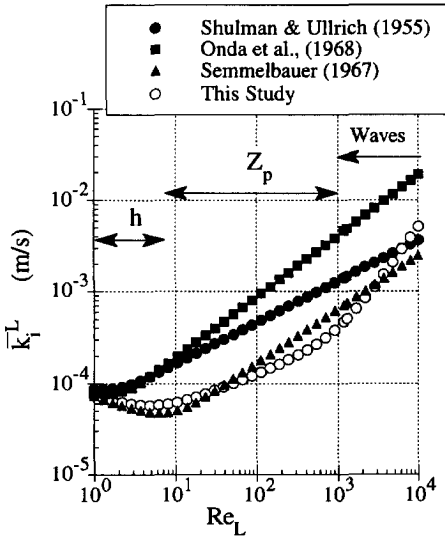


FIGURE 5.6A: Comparison of the liquid mass transfer coefficients for an ambient air-water system using the Dobbins equation for random packing. The lengths that dominate a mass transfer region are indicated.

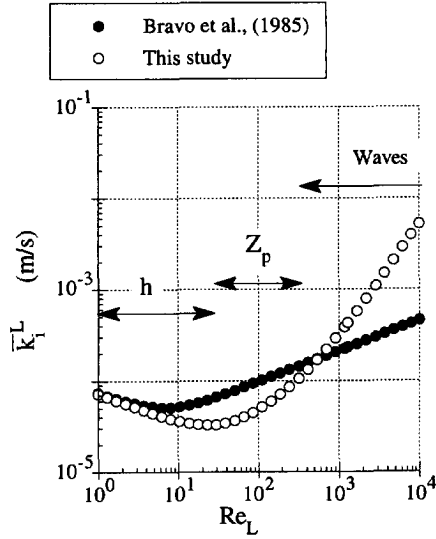


FIGURE 5.6B: Comparison of the liquid mass transfer coefficients for an ambient air-water system using the Dobbins equation for structured packing. The lengths that dominate a mass transfer region are indicated.

### A COMBINED THEORY AND MODEL FOR LIQUID PHASE MASS TRANSFER

The diversity in the correlations for the liquid mass transfer coefficients is in our opinion due to a series of effects that influence the mass transfer. Depending on the selected components and the applied geometry one can obtain substantially different mass transfer results. However, it will be shown that these effects can be described in a uniform way by distinguishing between the influences of the waves on the interface and the geometrical influences of the packing structure.

#### Waves on the Gas-Liquid Interface

The waves on the interface cause an additional friction between the gas and the liquid. The increased friction factor directly causes an increase of the pressure drop of the system. It is therefore to be expected that the behaviour of the pressure drop, carries information about the structures on the interface. The energy of the waves is dissipated in the liquid film, thereby mixing the liquid and consequently increasing the mass transfer within the liquid. In the following a wavelength of the liquid interface is determined, which is characterised by the dissipated energy in the liquid film. The wavelength also determines the elliptical trajectory of a microscopic volume element in the liquid film (see, e.g.: Main, 1993) and it therefore represents a measure for the exposure length of the surface elements.

In Appendix 5.B it is shown that the ratio of dissipated kinetic energy ( $\epsilon_{kin}$ ) and the kinetic energy ( $e_{kin}$ ) leads to a damping factor being a reciprocal time ( $1/\tau$ ), which expresses the decrease of the wave amplitude due to the dissipation of the energy in the liquid film. This decrease is a function of the wave number ( $k$ ) and the film thickness;

$$\frac{1}{\tau} = \frac{\epsilon_{kin}}{e_{kin}} = 2v_L k^2 \frac{\sinh kh \cosh kh - kh}{\sinh kh \cosh kh} \approx 2v_L k^2 \left( 1 - \frac{kh}{kh \left( 1 + \frac{1}{2} (kh)^2 \right)} \right) = v_L k^4 h^2 \quad (5.25)$$

Here the kinematic viscosity  $v_L$  of the liquid is used. The damping factor represents the time in which the wave loses its energy by a factor ( $1/e$ ). The hyperbolic functions of equation (5.25) can be expanded, when the wave length is much larger than the liquid film thickness (typically one finds liquid film thicknesses, which are  $h \sim 200\mu\text{m}$ , while the smallest unstable wavelengths as calculated with the Kelvin-Helmholtz stability are  $\lambda \sim 2\text{mm}$ , so that  $h \ll \lambda$ ). The Kolmogorov time ( $t_{kol}$ ) also represents a characteristic time required for the absorption of the kinetic energy within the eddy of a flow;

$$\frac{1}{t_{kol}} = \sqrt{\frac{\epsilon_{kin}}{v_L}}, \quad (5.26)$$

The crucial step in this analysis is the hypothesis that the Kolmogorov time can be related to the damping factor of the waves. Although the first describes the energy dissipation in a two dimensional structure, while the other applies to a three dimensional structure, they both describe the time required for the decrease of wavy structures in a flow. For this reason it is assumed that they are of the same order of magnitude for equal dissipated energies;

$$t_{kol} \equiv \tau. \quad (5.27)$$

When the above assumption is valid, equations (5.25) and (5.26) can be used to express the kinetic energy as:

$$\sqrt{\frac{\epsilon_{kin}}{v_L}} = \frac{\epsilon_{kin}}{e_{kin}} \Rightarrow \frac{\epsilon_{kin}}{e_{kin}} = \frac{\epsilon_{kin}}{v_L} \Rightarrow e_{kin} = v_L^2 k_e^4 h^2, \quad (5.28)$$

where  $k_e$  represent a characteristic wave number, which can be used as average reciprocal exposure length. As shown in appendix 5.B, the kinetic energy of a wave also can be related to its amplitude ( $A$ ), wavelength and wave velocity ( $c$ ) (see also, e.g.: Brekhovskikh and Goncharov, 1993) as:

$$e_{kin} = \frac{k_e A^2 (u_L - c)^2}{4h \tanh k_e h} \approx \frac{k_e A^2}{4h \tanh k_e h} \left( \frac{\rho_G u_G}{\rho_L \coth k_e h} \right)^2 \approx \frac{k_e^2 A^2 \rho_G^2 u_G^2}{4\rho_L^2} \quad (5.29)$$

The equation uses the real part of the wave velocity ( $c$ ),

$$c = \frac{\rho_L \coth kh u_L + \rho_G u_G}{\rho_L \coth kh + \rho_G} \approx u_L + \frac{\rho_G u_G}{\rho_L \coth kh}, \quad (5.30)$$

which can be calculated with the Kelvin-Helmholtz relation for waves on film, see Appendix 5.A. The expressions (5.28) and (5.29) for the kinetic energy yield a characteristic wave length,

$$k_e = \frac{A \rho_G u_G}{2\rho_L v_L h} \Rightarrow \lambda_e = \frac{4\pi \rho_L v_L h}{A \rho_G u_G} \approx \frac{h}{A} \frac{\eta_L}{\eta_G} \frac{16\pi \epsilon_0 \theta}{Re_{Ga}}, \quad (5.31)$$

which is representative for the dissipation of the energy in the liquid. Here the gas Reynolds number is used to replace the gas velocity. The only unknown parameter in equation (5.31) is the amplitude (A) of the waves, but when it is assumed that the waves are experienced as a solid surface by the gaseous phase, the amplitude can be expressed using the friction factor relations for smooth and rough surfaces. When the friction factor for rough surfaces ( $f_r$ ) is expressed as a friction factor of smooth surfaces (f) with a correction term, it is found that up to Reynolds numbers of 20 000 the usual pipe friction correlations (see, e.g.: Coulson and Richardson, 1977) can be rewritten as:

$$f_r = f \left( 1 + 0.30 \operatorname{Re}_G^{0.5} \left( \frac{e}{2\theta r_0} \right) \right) = f \left( 1 + 0.30 \operatorname{Re}_G^{0.5} \left( \frac{2A}{2\theta r_0} \right) \right) \quad (5.32)$$

Here the absolute surface roughness (e) is replaced by the amplitude (A). The friction factor was also expressed using the description of the pressure drop and the gas liquid interaction parameter as:

$$f_r = f (1 + \Psi_{G-L}) \quad (5.33)$$

From these two equations the amplitude can be isolated and connected with the pressure drop correction of equation (3.23) of chapter 3 as:

$$A = \frac{10}{3} \theta r_0 \Psi_{G-L} \operatorname{Re}_G^{-0.5} \quad (5.34)$$

The characteristic wavelength can now be isolated from equations (5.31) and (5.34) as:

$$\lambda_e = \frac{24\pi h \operatorname{Re}_G^{0.5}}{5 r_0 \Psi_{G-L}} \frac{\eta_L}{\eta_G \operatorname{Re}_G} \frac{\varepsilon_0}{a_p} = \frac{12\pi h}{5 \Psi_{G-L}} \frac{\eta_L}{\eta_G \operatorname{Re}_G^{0.5}} \quad (5.35)$$

The expression for the gas liquid interaction is a sine hyperbolic, by taking the first term of the series expansion,

$$\Psi_{G-L} = 34 \cdot 10^{-15} \frac{a_p h}{(\cos \alpha)^9 \varepsilon_0^7} \left( \frac{h}{h_0} \right)^6 \frac{\eta_L \rho_L}{\eta_G \rho_G} \operatorname{Re}_G^{1.5} \operatorname{Re}_L \quad (5.36)$$

equation (5.35) is rewritten as:

$$\lambda_e = 222 \cdot 10^{12} \frac{\rho_G (\cos \alpha)^9 \varepsilon_0^7}{\rho_L a_p \operatorname{Re}_G^2 \operatorname{Re}_L} \left( \frac{h_0}{h} \right)^6 \approx 222 \cdot 10^{12} \frac{\rho_G (\cos \alpha)^9 \varepsilon_0^7}{\rho_L a_p \operatorname{Re}_G^2 \operatorname{Re}_L} \quad (5.37)$$

In this equation the film thickness for small gas loads at first instance is approximated with the free falling film thickness, so that the ratio of the film thicknesses becomes equal to unity. Equation (5.37) represents a wave length describing the characteristic size of the currents in which the energy in the liquid is dissipated.

Reviewing the reported equations of table V.I it can be concluded that the non molecular transport in the liquid flow most likely is caused by a combination of the waves on the interface and the size and arrangement of the internals. This would lead to a hybrid equation for the exposure length. Combining the result of equation (5.37) and the conclusion that the arrangement of the internals also will influence the exposure length the following equation is proposed:

$$\frac{1}{\ell_e} = \frac{1}{222 \cdot 10^{12}} \frac{a_p \text{Re}_G^2 \text{Re}_L}{(\cos \alpha)^9 \epsilon_0^7 \rho_G} + \frac{1}{Z_p} \tag{5.38}$$

Here  $Z_p$  represents a characteristic length of the packing. This equation is derived from the general pressure drop correlation and should also be applicable for the vertical pipe geometry. For a vertical pipe the influence of the characteristic length of the geometry is simply the length of the pipe, so that for this configuration the exposure length is established. Figure 5.7 shows a comparison of equation (5.38) and the two reported correlations for an ambient air water system.

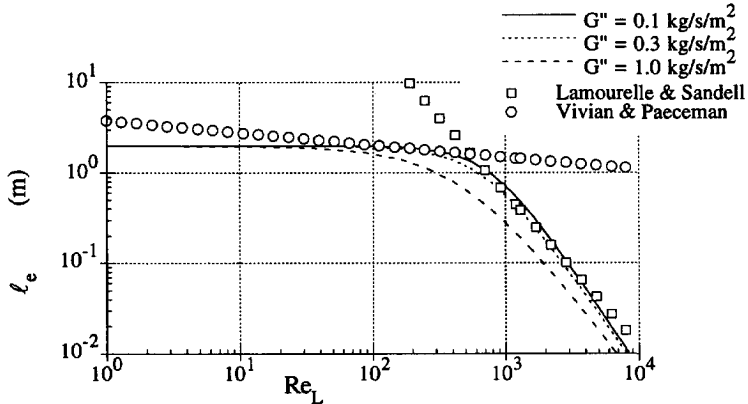


FIGURE 5.7: Comparison of the reported correlations and the by our model estimated exposure lengths in a 16mm diameter vertical pipe of two meter as function of the liquid Reynolds number for an ambient air-water system. Equation (5.38) is applied for three different gas loads.

The figure shows that the theory matches the empirical correlations for the vertical pipe geometry remarkable well. Although expression (5.38) is rather different from the reported correlations, the result is approximately equal. The hypothesis stating the equivalents of the Kolmogorov time scale and the reciprocal damping factor for waves as formulated in equation (5.26) therefore appears to be correct.

The influence of the gas Reynolds number in equation (5.38) appears large, but figure 5.7 only shows a moderate influence of the gas load on the exposure length. The reason for this can be elucidated when the gas Reynolds number is rewritten into a pure gas load and a pure liquid load dependent term as:

$$\text{Re}_G \approx \frac{\rho_G \left| \frac{u_{SG}}{\theta^2 \epsilon_0 \cos \alpha} - u_{0-int} \right| 2\theta r_0}{\eta_G} = \frac{4G''}{\theta \cos \alpha a_p \eta_G} + \frac{3}{2} \frac{v_L}{v_G} \theta \epsilon_0 \text{Re}_L^{0.66} \text{Ga}_P^{0.33} \tag{5.39}$$

Here the free falling film interface velocity of equation (5.22) has been used as approximation. By applying a gas velocity relative to the interface velocity, the gas Reynolds number is largely determined by the liquid load. This is especially the case in the range where the waves on the

interface dominate the liquid mass transfer mechanism. It therefore largely explains the absence of the gas Reynolds numbers in the correlations given in table V.I.

When expression (5.38) is written in liquid Reynolds numbers only, an exposure length is found;  $\ell_e = a_0(\text{Re}_L + a_1\text{Re}_L^{1.66} + a_2\text{Re}_L^{2.33})$ , which shows a major dependency on the liquid Reynolds number close to the expression of Lamourelle and Sandell. This explains the good fit of the slope in figure 5.7.

#### The Characteristic Geometrical Length for Structured Packing

The major reason for the variations in the reported mass transfer coefficients is the influence of the packing structure itself. An important problem of equation (5.38) therefore remains the definition of the geometrical exposure length ( $Z_p$ ). For structured packing three geometrical contributions to the exposure length will be distinguished.

The first contribution to the exposure length is the height of a packing element ( $H_p$ ), at which the liquid falls into the normally perpendicularly arranged next element. The height of a packing element is for most structured packing approximately 0.20m.

A second contribution is caused by the diameter ( $D_{col}$ ) of the column. At the edge of the packing the liquid film turns, which will cause droplets (Fair and Bravo, 1990) and a renewal of the exposed liquid surface. The influence of the column diameter depends on the path of the liquid film. If the liquid film follows the channel as the gas phase, the column diameter should be incorporated in the description. However, if the film flows downward with gravity over the sheets, surface renewal can only be caused by the packing structure.

In structured packing surface renewal is generated when the liquid flows into a contact-point of the adjacent corrugated sheets (see figure 5.8A). A liquid surface element flows undisturbed from one ridge that has contact-points to an other ridge that has contact-points over a certain length ( $\ell_0$ ). At this point the surface element has a possibility to mix. Bravo et al., effectively sets this possibility equal to one. In our opinion this probability depends on the width of a mixing element ( $\Delta$ ) and the distance between these mixing elements ( $b_0$ ). This last parameter can be expressed as (see figure 5.8A):

$$b_0 = \frac{\pi}{2} \frac{2r_0}{\cos \alpha}, \quad (5.40)$$

where the factor  $\pi/2$  accounts for curved surface of the packing geometry. The probability that the liquid flow will be mixed is equal to the ratio of both lengths. The average number ( $N_e$ ) of unit distances ( $\ell_0$ ) that the liquid escapes a mixing step can be expressed as:

$$N_e = \sum_{n=0}^{\infty} \left(1 - \frac{\Delta}{b_0}\right)^n = \frac{1}{1 - \left(1 - \frac{\Delta}{b_0}\right)} = \frac{b_0}{\Delta} \quad (5.41)$$

so that the average free path ( $\bar{z}$ ) of a surface element before it collides with a mixing element becomes:

$$\bar{z} = \ell_0 N_e = \frac{\pi}{2} \frac{2r_0}{\sin \alpha} \frac{b_0}{\Delta} \quad (5.42)$$

This reduces the problem of finding an expression for the mixing width  $\Delta$ . Figures 5.8B & C, illustrate two possible configurations for a structured packing geometry with an inclination angle of  $45^\circ$ . The mixing width for a sharp edge (see figure 5.8B) only depends on the film thickness  $h$ , while the mixing width for a rounded ridge (see figure 5.8C) also depends on a contact radius  $r_c$ .

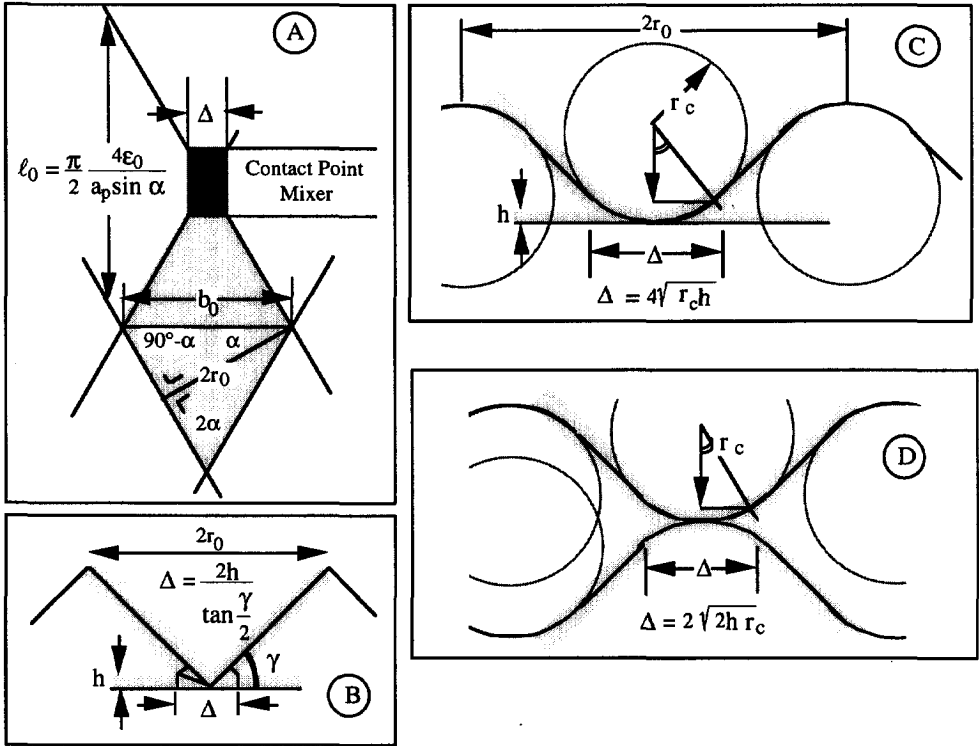


FIGURE 5.8: Geometrical arrangements in structured packing. Indicated are the gas flow cross-section (figure A) and three mixing elements in different configurations.

In the latter case the total mixing width as function of the inclination angle can be expressed as:

$$\Delta = \frac{\sqrt{8h r_c}}{\cos \alpha} \quad (5.43)$$

Figure 5.8D shows the extreme case of the geometry when the two corrugated sheets are parallel. The contact radius of the packing is a design parameter, which can be altered to decrease the exposure length. The average free path of a surface element in the configuration of figure 5.8C can be written as:



$$\bar{z}_1 = \pi \frac{r_0}{\sin \alpha} \frac{\pi r_0}{\sqrt{8h} r_c} = \pi^2 \frac{r_0}{\sin \alpha} \sqrt{\frac{r_0}{2h}} = \frac{2\pi^2 \epsilon_0^{1.5} (Ga_p)^{\frac{1}{6}}}{a_p \sin \alpha (Re_L)} = \frac{20\epsilon_0^{1.5} (Ga_p)^{\frac{1}{6}}}{a_p \sin \alpha (Re_L)} \quad (5.44)$$

Here we applied as typical contact radius one fourth of the packing radius ( $4r_c = r_0$ ).

Figure 5.8B illustrates the extreme situation, in which the contact point between the two corrugated sheets form a sharp edge. For this case the average length before a surface element is renewed, can be expressed as:

$$\bar{z}_2 = \pi \frac{r_0}{\sin \alpha} \frac{\pi r_0}{2h \tan \frac{\gamma}{2}} = \frac{4\pi^2 \epsilon_0^2 (Ga_p)^{\frac{1}{3}}}{5a_p \sin \alpha (Re_L)} = \frac{8\epsilon_0^2 (Ga_p)^{\frac{1}{3}}}{a_p \sin \alpha (Re_L)} \quad (5.45)$$

where the angle ( $\gamma$ ) as indicated in figure 5.8B is taken as  $45^\circ$ . Equations (5.44) and (5.45) are two possible ways to describe the average free path of a surface element. Equation (5.44) yields in nearly all cases a substantially shorter average length. The above approach does not take into account static liquid hold-up, capillary activity of the contact point and the packing surface roughness. These effects will most likely increase the size of the mixing elements. In practice the constants 20 and 8 represent an indication only. It is interesting that the exposure length can be influenced, by either altering the angle of the geometry or the radius of the contact point. The overall expression for the characteristic packing length ( $Z_p$ ), describing the influence of geometry of the packing can be considered as composed by two parts. In our opinion these are the height of a packing element and the contact points. Combined with equation (5.38) describing the waves on the interface the exposure length can be expressed as:

$$\begin{aligned} \frac{1}{\ell_e} &= \frac{1}{222 \cdot 10^{12}} \frac{a_p Re_G^2 Re_L}{(\cos \alpha)^9 \epsilon_0^7 \rho_G} + \frac{1}{Z_p} \\ &= \frac{1}{222 \cdot 10^{12}} \frac{a_p Re_G^2 Re_L}{(\cos \alpha)^9 \epsilon_0^7 \rho_G} + \frac{\cos \alpha}{H_p} + \frac{a_p \sin \alpha}{20\epsilon_0^{1.5}} \left( \frac{Re_L}{Ga_p} \right)^{\frac{1}{6}} \end{aligned} \quad (5.46)$$

The cosine in the height of the packing element ( $H_p$ ) has been incorporated, to take into account the increased flow length.

The liquid mass transfer model for structured packing is compared with model of Bravo et al., (1985) in figure 5.6B. In the typical operating range ( $10 < Re_L < 500$ ) the presented model predicts substantially smaller mass transfer coefficients.

### The Characteristic Geometrical Length for Random Packing

Although the correlations for random packing do not point to an identical characteristic packing height, the characteristic exposure length shown in figure 5.5 indicates that it will be in the range of one individual element. This means that when the liquid falls on the next element, the flow is sufficiently disturbed to mix the surface element. We will use the size of a packing element ( $d_p$ ) as an exposure length. In addition, contact points similarly to those for structured packing are present in random packing. When an element is surrounded by other elements as in a cubical structure, each element has six contact points. The top and bottom elements do not

cause an additional mixing, since they mark a start or end of the element itself. This leaves four contact points on the outside of the element, but on the inside of an element the flow is undisturbed. This on average leaves two effective contact points. The expression for the exposure length (equation (5.38)) for random packing therefore is written as:

$$\begin{aligned} \frac{1}{\ell_e} &= \frac{1}{222 \cdot 10^{12}} \frac{a_p \text{Re}_G^2 \text{Re}_L}{(\cos \alpha)^9 \epsilon_0^7 \rho_G} \frac{\rho_L}{Z_p} + \frac{1}{Z_p} = \frac{1}{222 \cdot 10^{12}} \frac{a_p \text{Re}_G^2 \text{Re}_L}{(\cos \alpha)^9 \epsilon_0^7 \rho_G} \frac{\rho_L}{d_p} + \frac{1}{d_p} + 2 \frac{a_p \sin \alpha}{20 \epsilon_0^{1.5}} \left( \frac{\text{Re}_L}{G a_p} \right)^{\frac{1}{6}} \\ &= \frac{1}{222 \cdot 10^{12}} \frac{a_p \text{Re}_G^2 \text{Re}_L}{(\cos \alpha)^9 \epsilon_0^7 \rho_G} \frac{\rho_L}{4 \epsilon_0} + \frac{a_p}{4 \epsilon_0} + \frac{a_p \sin \alpha}{10 \epsilon_0^{1.5}} \left( \frac{\text{Re}_L}{G a_p} \right)^{\frac{1}{6}} \end{aligned} \quad (5.47)$$

Here the size of the packing element is approximated by the hydraulic diameter of the packing. The element contribution in equation (5.47), influences the mass transfer far more than the contact points. Expression (5.47) should be combined with equation (5.38) to obtain the exposure length of a surface element for random packing.

A comparison of the liquid mass transfer coefficient for random packing is given in figure 5.6A. The results of the presented model are close to the correlation of Semmelbauer (1967). The disagreement with the correlation of Onda et al., is largely caused by the fact that this correlation uses a wetted area in the liquid mass transfer coefficient, which is a strong function of the liquid load.

#### COMPARISON OF STRUCTURED PACKINGS

Several brochures of suppliers show the performance of their packings. This is normally done by reporting the height equivalent of a theoretical plate (HETP). This quantity can be expressed in mass transfer terms as:

$$H_i^{\text{etp}} = \frac{\ln(S_i)}{(S_i - 1)} \frac{u_{SG}}{k_i^{\text{OG}} \theta a_p} \quad (5.48)$$

where  $S_i$  is the stripping factor. The equation is derived in numerous textbook (see also Appendix 5.C). In equation (5.48)  $k_i^{\text{OG}}$  represents the on the gas phase based overall mass transfer coefficient, which has been defined in equation (5.5) of this chapter. The dimensionless radius  $\theta$  in equation (5.48), is applied to take into account the decrease of the interfacial area with increasing film thickness. This factor is derived by rewriting the interface radius and the porosity of the irrigated bed (see chapter 3 of this thesis), leading to a specific interface area of  $\theta a_p$ . The concept of HETP becomes ambiguous for multi-component systems (see, e.g. Taylor and Krishna, 1993). Nevertheless it is a useful tool for the characterisation of a packing performance. However, it should always be realised that a comparison of HETP values requires: identical components, identical column dimensions and identical process conditions. In the following the properties of the system ethylbenzene - chlorobenzene will be applied for calculating the performance of certain packing geometries. The estimated properties for a system, that mainly consists of ethylbenzene, are shown in table V.II.

TABLE V.II: The estimated physical properties for a system consisting of 99.9% of ethylbenzene and 0.1% of chlorobenzene.

$\rho_L$	756	815	836	kg/m <sup>3</sup>
$\rho_G$	3.28	0.378	0.103	kg/m <sup>3</sup>
$\eta_L$	0.231	0.407	0.547	mPa s
$\eta_G$	8.33	6.74	6.07	$\mu$ Pa s
$D^L$	7.76	3.91	2.74	n m <sup>2</sup> /s
$D^G$	4.04	28.50	93.80	$\mu$ m <sup>2</sup> /s
$\sigma$	16.7	22.9	25.4	mN/m

p	1013	100	25	mbar
T	136.4	67.3	37.5	°C
$m_i$	1.13	1.19	1.24	mol <sup>2</sup> /mol <sup>2</sup>

This system can be distilled at various temperatures. Depending on the operating pressure a different HETP is obtained. Figure 5.9 shows the calculated number of theoretical plates per meter of packing at total reflux for the system ethylbenzene - chlorobenzene. This graph also shows reported values of Sulzer BX packing (Sulzer, 1989). The BX gauze packing has the advantage that the surface area is completely wetted, so that the mass transfer characteristics are not disturbed by incomplete wetting. Although the brochure does not report the applied composition, the measured values are in the correct range and show the detected tendencies. In distillation applications, as the given example, the mass transfer resistance is mainly located in the gas phase, the trends for other systems therefore will be similar.

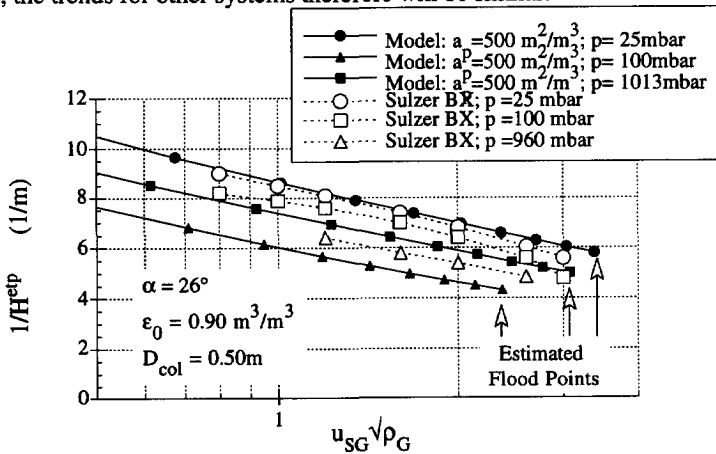


FIGURE 5.9: Measured and estimated number of theoretical plates per meter packing as function of the gas load factor for various distillation conditions. The arrows indicate the estimated flood points.

When the HETP is calculated for a different type of packing geometry, the result becomes quite different. Figure 5.10 shows the predicted result for the Sulzer Mellapak series with different specific areas.

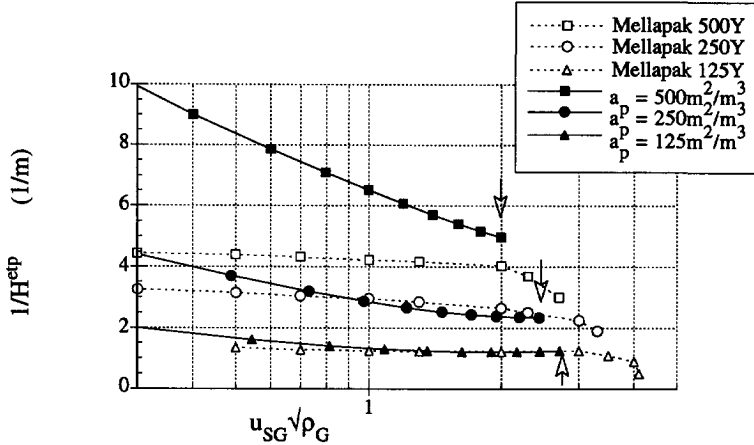


FIGURE 5.10: Measured and estimated number of theoretical plates per meter packing for the distillation of an ethylbenzene - chlorobenzene at 100mbar as function of the gas load factor for various specific surface areas. The arrows indicate the estimated flood points.

The agreement for surface areas smaller than  $250 \text{ m}^2/\text{m}^3$  is good, but the model overestimates the number theoretical plates per meter column for larger surface areas. The deviations become so substantial for large specific areas that we are obliged to address them. In the next chapter of this thesis it will be demonstrated that they are caused by insufficient wetting of the packing.

### CONCLUDING REMARKS

Both gas and liquid phase models have been connected with the pressure drop relation of chapter 3 of this thesis. This makes it possible to evaluate the pressure drop relation not only from pressure drop data, but also on basis of experimental mass transfer coefficients. This especially applies for simple geometries like the vertical pipe.

It has been shown that the gas phase mass transfer can be described using the Chilton-Colburn relation for different types of packed beds, by incorporation of the effective inclination angle. The liquid mass transfer coefficient is described using a hyperbolic function, which is a continuous description of the average non stationary solution for the diffusion equation. The influences of the geometry and the waves on the liquid mass transfer have been described applying a reciprocal exposure length contributions summation. The different contributions to the liquid mass transfer dominate certain regions of the liquid Reynolds numbers. The regions are depending on the application and the geometry of the packing. At low liquid Reynolds numbers (typically, structured packing:  $Re_L < 20$ ; random packing:  $Re_L < 5$ ) the film thickness dominates the mass transfer in the liquid phase, while at larger Reynolds numbers the surface renewal dominates the liquid mass transfer. At large liquid Reynolds numbers (typically, structured packing:  $Re_L > 200$ ; random packing:  $Re_L > 1000$ ) the liquid waves are the major cause of the surface renewal, while at intermediate liquid Reynolds numbers (typically, structured

packing:  $20 < Re_L < 200$ ; random packing:  $5 < Re_L < 1000$ ) the geometry of the packing dominates the surface renewal.

The dissipation of the energy in the liquid waves characterised by the reciprocal damping factor has been connected with the Kolmogorov time scale. This lead to a characteristic wavelength that could be used as average exposure length. The obtained expression describes the reported empirical correlations well for various gas loads. Further, it is interesting that the description using a single wavelength is successful. This implies that a total determination of the interface, describing the energy dissipation over all wave lengths can be avoided at first instance.

Although the description has been quite successful so far it was shown that the theory does not include wetting at low liquid Reynolds numbers. This causes a decrease of the measured overall mass transfer coefficient and will be discussed in chapter 6 of this thesis.

APPENDIX 5.A (*The Kelvin-Helmholtz relation*)

The Kelvin-Helmholtz relation determines the stability of a nonviscous flow. The derivation of this relation is covered in numerous textbooks (see, e.g.,: Drazin and Reid, 1981; Landau and Lifshitz, 1987). However, because of the central role of this theory in the derivation of the wave influence it is reproduced below.

If there are two flows as indicated in figure 5.A1, with a small disturbance on the surface it can be shown that any type of disturbance can be composed using a Fourier series. It will therefore be sufficient to analyse the disturbance of only one wave ( $\xi$ ) going in the x direction with amplitude A. This wave can be symbolised as:

$$y = \xi(x,t) = A e^{i(kx - \omega t)} \tag{5.A1}$$

and its propagation direction will be on the interface of the two substances indicated with roman numbers. The Kelvin-Helmholtz stability will be calculated for a Cartesian co-ordinate system.

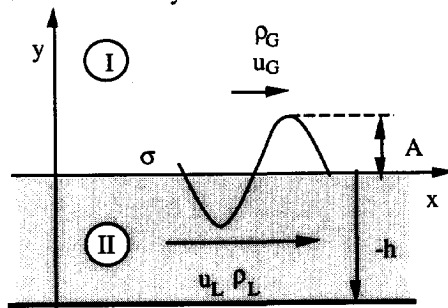


FIGURE 5.A1: Geometry of the Kelvin-Helmholtz instability, with an open boundary condition and a limited boundary condition.

The velocity field can be expressed with a potential field as:

$$\vec{u} = \nabla\phi \tag{5.A2}$$

In case the flows are incompressible the Laplace's equation is found;

$$\nabla \cdot \vec{u} = \nabla^2 \phi = 0 \tag{5.A3}$$

When a surface wave is considered, a potential field can be defined as a function of the  $x$  and  $y$  to describe a single wave. This has been indicated in figure 5.A1. Following the definition of the disturbance, the function,

$$\phi = F(y) G(x) = F(y) e^{i(kx - \omega t)} \tag{5.A4}$$

is chosen for the potential field, in which  $F$  is an arbitrary function. Equations (5.A3) and (5.A4) lead to the differential equation:

$$\frac{\partial^2 F}{\partial y^2} - k^2 F = 0 \tag{5.A5}$$

Dividing the potential field into a part above the average surface and a part below the surface (where the surface will be located at  $y = 0$ ), the boundary conditions can be used to solve equation (5.A5). A solution for (5.A5) is readily recognised as:

$$F = C_1 e^{-ky} + C_2 e^{ky} \tag{5.A6}$$

Where  $C_1$  and  $C_2$  are constants. Since the function must be limited for both regions, it follows that the second term of the solution for the gas region is zero, so that the solution becomes:

$$\phi_G = B_G e^{-ky} e^{i(kx - \omega t)} \tag{5.A7}$$

where the arbitrary constant  $B_G$  equals the constant  $C_1$ . For the liquid region the velocity in the  $y$  direction must be zero at any point located at the plane  $y = -h$ . Then the second constant can be expressed as:

$$\begin{aligned} \frac{\partial \phi}{\partial y} \Big|_{y=-h} &= (-kC_1 e^{-ky} + kC_2 e^{ky}) e^{i(kx - \omega t)} = 0 \\ -kC_1 e^{kh} + kC_2 e^{-kh} &= 0 \\ C_2 &= C_1 e^{2kh} \end{aligned} \tag{5.A8}$$

The potential field in the liquid region therefore becomes:

$$\begin{aligned} \phi_L &= (C_1 e^{-ky} + C_1 e^{2kh} e^{ky}) e^{i(kx - \omega t)} \\ &= \frac{C_1 (e^{-ky} + e^{2kh} e^{ky})}{e^{-kh}} e^{i(kx - \omega t)} \\ &= \frac{2C_1}{e^{-kh}} \cosh k(y + h) e^{i(kx - \omega t)} \\ &= B_L \cosh k(y + h) e^{i(kx - \omega t)} \end{aligned} \tag{5.A9}$$

Equations (5.A7) and (5.A9) are general solutions for the potential field in the two areas. They can also be written as a leading potential field on which a small disturbance ( $\phi^\circ$ ) is superimposed. The total potential field can be written as:

$$\begin{aligned} \phi_G &= u_G x + \phi_G^\circ & y > 0 \\ \phi_L &= u_L x + \phi_L^\circ & y < 0 \end{aligned} \tag{5.A10}$$

The interface of the two flows is material in nature, meaning that the fluid particles must move the interface without the two phases occupying the same point at the same time and without a

---

cavity forming between the phases. The vertical velocity therefore is given by (see, e.g., Drazin and Reid, 1981)

$$\frac{\partial \phi_i}{\partial y} = \frac{\partial \xi}{\partial t} + \frac{\partial \phi_i}{\partial x} \frac{\partial \xi}{\partial x} + \frac{\partial \phi_i}{\partial z} \frac{\partial \xi}{\partial z} \quad i = G, L \quad (5.A11)$$

When equation (5.A11) is linearised and the double cross terms are neglected, the relations between the amplitude and the constants  $B_G$  and  $B_L$  are found. The condition for the first region leads to:

$$\begin{aligned} \frac{\partial \phi_G^0}{\partial y} &= \frac{\partial \xi}{\partial t} + \left( u_G + \frac{\partial \phi_G^0}{\partial x} \right) \frac{\partial \xi}{\partial x} \\ \frac{\partial \phi_G^0}{\partial y} &= \frac{\partial \xi}{\partial t} + u_G \frac{\partial \xi}{\partial x} \\ -k B_G e^{-ky} e^{i(kx - \omega t)} &= -i\omega A e^{i(kx - \omega t)} + ik u_G A e^{i(kx - \omega t)} \\ -k B_G e^{-ky} &= -i\omega A + ik u_G A \quad \Rightarrow \quad B_G = \frac{iA(ku_G - \omega)}{-k} \end{aligned} \quad (5.A12)$$

where the boundary condition at  $y = 0$  is taken. The second boundary condition leads to:

$$\begin{aligned} k B_L \sinh k(y+h) e^{i(kx - \omega t)} &= -i\omega A e^{i(kx - \omega t)} + ik u_L A e^{i(kx - \omega t)} \\ k B_L \sinh k(y+h) &= -i\omega A + ik u_L A \quad \Rightarrow \quad B_L = \frac{iA(ku_L - \omega)}{k \sinh kh} \end{aligned} \quad (5.A13)$$

The dynamic boundary condition states that the pressure must be continuous at the surface. When the pressure is also written as a leading pressure and a disturbance,  $P = P^0 + p$ , where the leading pressure is symbolised by a capital letter, the Bernoulli equation can be used to solve the equations for both regions. This subsequently leads to the relations:

$$\frac{\partial \phi_G}{\partial t} + \frac{1}{2} (\nabla \phi_G)^2 + g\xi + \frac{P_G}{\rho_G} = \frac{1}{2} u_G^2 + \frac{P_G^0}{\rho_G} \quad (5.A14-G)$$

$$\frac{\partial \phi_L}{\partial t} + \frac{1}{2} (\nabla \phi_L)^2 + g\xi + \frac{P_L}{\rho_L} - \sigma \frac{\partial^2 \xi}{\partial x^2} = \frac{1}{2} u_L^2 + \frac{P_L^0}{\rho_L} \quad (5.A14-L)$$

When the double cross terms are neglected again, the equations (5.A14-G & 5.A14-L) can be written as:

$$\rho_G \frac{\partial \phi_G^0}{\partial t} + \rho_G u_G \frac{\partial \phi_G^0}{\partial x} + \rho_G g \xi + P_G = 0 \quad (5.A15-G)$$

$$\rho_L \frac{\partial \phi_L^0}{\partial t} + \rho_L u_L \frac{\partial \phi_L^0}{\partial x} + \rho_L g \xi + P_L - \sigma \frac{\partial^2 \xi}{\partial x^2} = 0 \quad (5.A15-L)$$

Using the condition that the pressure must be equal at the interface ( $P_G = P_L$ ) for  $y = 0$ , equations (5.A15-G and 5.A15-L) reduces to:

$$i B_L \rho_L \cosh kh (ku_L - \omega) + i B_G \rho_G (\omega - k u_G) + gA(\rho_L - \rho_G) + k^2 \sigma A = 0 \quad (5.A16)$$

In combination with formula (5.A12) and (5.A13) a second order equation in  $\omega$  can be written as:

$$\rho_L \coth kh (ku_L - \omega)^2 + \rho_G (\omega - ku_G)^2 - gk(\rho_L - \rho_G) - k^3 \sigma = 0 \quad (5.A17)$$

Solving this equation and dividing by  $k$  the wave velocities  $c_{1,2}$  are found as:

$$c_{1,2} = \frac{\omega}{k} = \frac{u_G \rho_G + u_L \rho_L \coth kh}{\rho_G + \rho_L \coth kh} \pm \left[ \frac{g(\rho_L - \rho_G) + \sigma k}{\rho_G + \rho_L \coth kh} - \rho_G \rho_L \coth kh \frac{(u_G - u_L)^2}{(\rho_G + \rho_L \coth kh)^2} \right]^{\frac{1}{2}} \quad (5.A18)$$

The flow becomes unstable when the root of equation (5.A18) is complex. To calculate this instability the complex argument of the circle frequency has to be taken.

$$\text{Im}(\omega)_{\text{carrh}} = kg(\rho_L - \rho_G) + \sigma k^3 - k^2 \rho_G \rho_L \coth kh \frac{(u_G - u_L)^2}{\rho_G + \rho_L \coth kh} \quad (5.A19)$$

This functions approximately is a third order polynomial in  $k$  with three points equal to zero, being: zero and a negative and positive wave number. Given that the wave number has to be positive only one relevant zero point remains, which is the smallest unstable wavelength.

A similar derivation can be made using cylindrical co-ordinates. This leads to a similar expression for the wave velocity of:

$$c_{1,2} = \frac{\omega}{k} = \frac{u_G \rho_G^\circ + u_L \rho_L^\circ}{\rho_G^\circ + \rho_L^\circ} \pm \left[ \frac{g(\rho_L - \rho_G) + \sigma k}{\rho_G^\circ + \rho_L^\circ} - \rho_G^\circ \rho_L^\circ \frac{(u_G - u_L)^2}{(\rho_G^\circ + \rho_L^\circ)^2} \right]^{\frac{1}{2}} \quad (5.A20)$$

where the densities are expressed as:

$$\rho_G^\circ = \rho_G \frac{I_0(k\theta_{r0})}{I_1(k\theta_{r0})} \quad \text{and} \quad \rho_L^\circ = \rho_L \frac{I_0(k\theta_{r0}) K_1(kr_0) + I_1(kr_0) K_0(k\theta_{r0})}{I_1(kr_0) K_1(k\theta_{r0}) - I_1(k\theta_{r0}) K_1(kr_0)} \quad (5.A21)$$

Here  $I_0$ ,  $I_1$ ,  $K_0$  and  $K_1$  are modified Bessel functions. When the  $h \ll \theta_{r0}$ , this result is close to the result derived for Cartesian co-ordinates.

#### APPENDIX 5.B (Energy Dissipation in Waves)

The generated waves due to the gas liquid interaction don't have an unlimited lifetime, but their energy is dissipated by the viscosity of the liquid. When the waves are not fed with new energy they will vanish after a time. The dissipation of the wave energy in an incompressible fluid can be derived using the relation for the kinetic energy dissipation (Landau and Lifshitz, 1987) as:

$$\dot{E}_{\text{kin}} = -\frac{1}{2} \eta_L \iiint \left( \frac{\partial u_x}{\partial y} + \frac{\partial u_y}{\partial x} \right)^2 dV = -2\eta_L \iiint \left( \frac{\partial^2 \phi}{\partial x \partial y} \right)^2 dV \quad (5.B1)$$

where  $\phi$  represents the potential field and  $V$  stands for the enclosed volume. In a system undergoing small oscillations the mean kinetic and potential energies are equal. Therefore the total mechanical energy can be calculated as twice the kinetic energy, which can be calculated as:

$$E_{\text{kin}} = \frac{1}{2} \rho_L \iiint \vec{u}^2 dV = \frac{1}{2} \rho_L \iiint \left[ \left( \frac{\partial \phi}{\partial x} \right)^2 + \left( \frac{\partial \phi}{\partial y} \right)^2 \right] dV \quad (5.B2)$$

The potential field used in the relations (5.B1) and (5.B2) can for the Cartesian co-ordinate be written as (see appendix 5.A, equation (5.A9)):

$$\phi_L = \frac{A(u_L - c)}{\sinh kh} \cosh k(y+h) \cos(kx - \omega t) \quad (5.B3)$$



Here  $c$  represents the wave velocity. Using this potential field, the volume integrals can be solved, so that the energy dissipation can be calculated as:

$$\begin{aligned}
 \dot{E}_{kin} &= -\frac{2\eta_L A^2 k^4 (u_L - c)^2}{\sinh^2 kh} \int_{-h}^0 \sinh^2 k(y+h) dy \iint_0^\lambda \sin^2(kx - \omega t) dx dz \\
 &= -\frac{2\eta_L A^2 k^4 (u_L - c)^2}{\sinh^2 kh} \left( \frac{1}{2k} \sinh kh \cosh kh - \frac{1}{2} h \right) \frac{\lambda}{2} \int_0^{z_0} dz \\
 &= -\frac{\eta_L A^2 k^3 (u_L - c)^2 \lambda}{2 \sinh^2 kh} (\sinh kh \cosh kh - kh) z_0 \quad (5.B4)
 \end{aligned}$$

and the kinetic energy as:

$$\begin{aligned}
 E_{kin} &= \frac{\rho_L k^2 A^2 (u_L - c)^2}{2 \sinh^2 kh} \iiint_0^\lambda \sinh^2 k(y+h) \cos^2(kx - \omega t) + \cosh^2 k(y+h) \sin^2(kx - \omega t) dx dy dz \\
 &= \frac{\rho_L k^2 A^2 (u_L - c)^2 \lambda}{4 \sinh^2 kh} \iint_{-h}^0 \sinh^2 k(y+h) + \cosh^2 k(y+h) dy dz \\
 &= \frac{\rho_L k^2 A^2 (u_L - c)^2 \lambda}{4 \sinh^2 kh} \frac{\cosh kh \sinh kh}{k} \int_0^{z_0} dz = \frac{\rho_L k A^2 (u_L - c)^2 \lambda z_0}{4 \sinh^2 kh} \cosh kh \sinh kh \quad (5.B5)
 \end{aligned}$$

The damping coefficient ( $\tau^{-1}$ ) of the wave is defined as the change in energy divided by the total energy. By using equation (5.B4) and equation (5.B5) it can be expressed as:

$$\frac{1}{\tau} = -\frac{\dot{E}_{kin}}{E_{kin}} = \frac{2\eta_L k^2}{\rho_L} \frac{\sinh kh \cosh kh - kh}{\sinh kh \cosh kh} \quad (5.B6)$$

This approximately is the kinematic viscosity multiplied with the square of the wave number. The second half of the right expression is for small wave numbers equal to one and for large wave numbers equal to a half. Equation (5.B6) can be integrated,

$$\frac{\partial E_{kin}}{\partial t} = -\frac{1}{\tau} E_{kin} \quad \Rightarrow \quad E_{kin} = E_{kin}(t_0) \exp\left(-\frac{t}{\tau}\right) \quad (5.B7)$$

to describe the decrease of the kinetic energy in time. The total kinetic energy of a wave per unit of mass ( $e_{kin}$ ) can be calculated using equation (5.B5) and is given by the relation:

$$e_{kin} = \frac{E_{kin}}{\rho_L \lambda h z_0} = \frac{k A^2 (u_{int} - c)^2}{4h \tanh kh} \quad (5.B8)$$

Because this quantity is responsible for the additional mixing in the liquid it is a measure for the wave influence on the mass transfer.

#### APPENDIX 5.C (Height Equivalent to a Theoretical Plate)

Over 70 years ago, Peters (1922) provided the theoretical basis behind the concept of a Height Equivalent to a Theoretical Plate (HETP). Despite this early development the derivations given in literature are not always unambiguous and often apply intermediate definition. It is for this reason that the derivation of the HETP is reproduced here.

When a separation is accomplished using a counter-current packed column, a overall balance over the equipment is made. Figure 5.C1 shows the balance and the notation of a component over a counter-current flow element. The proper signs in the balance over an element is essential. When the molar flows ( $G_m, L_m$ ) are applied positive and the molar flux ( $J_i$ ) through the surface is positive for the gas phase, a balance over a slice of packing with interface area  $dA$ , leads to:

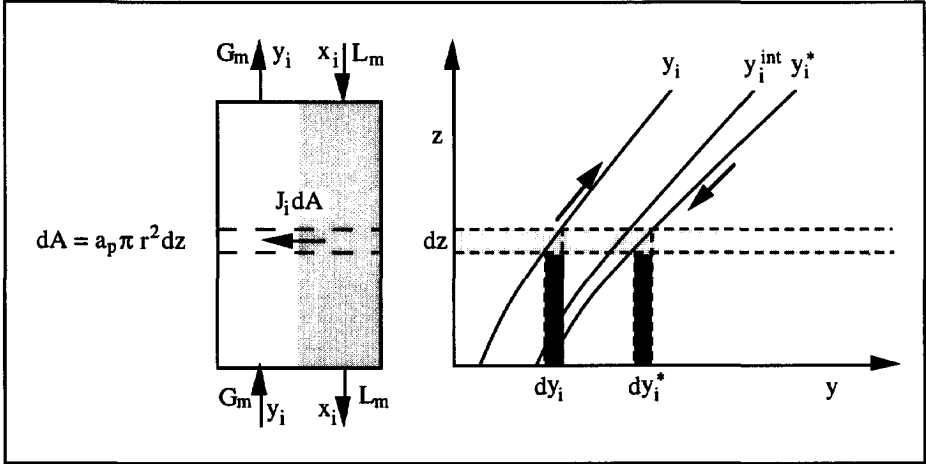


FIGURE 5.C1: The nonequilibrium over an apparatus element with specific interfacial area. The left drawing shows a hypothetical concentration profile over the apparatus.

$$\begin{aligned}
 L_m x_i - J_i dA &= L_m (x_i - dx_i) & \text{or} & & J_i dA &= L_m dx_i & \text{(a)} \\
 G_m y_i + J_i dA &= G_m (y_i + dy_i) & & & J_i dA &= G_m dy_i & \text{(b)}
 \end{aligned}
 \tag{5.C1}$$

These relations can be transformed using the molar flux relations. These relations are given in first section of this chapter and can be based on either the liquid or the gas phase;

$$J_i = k_i^{OG} c_t^G (y_i^* - y_i) = k_i^{OL} c_t^L (x_i - x_i^*) \tag{5.C2}$$

The equilibrium relation ( $y_i^* = m_i x_i + b_i$ ), where  $m_i$  is the derivative of the equilibrium line, can be used to express the concentrations of either the liquid or the gas phase in apparent concentrations of the other phase. When this is combined with the expression for the molar flux, one can express the differential equations (5.C1) as:

$$\begin{aligned}
 dx_i &= \frac{k_i^{OL} c_t^L (x_i - x_i^*) a_p \pi r^2 dz}{L_m} & \text{(a)} & \Leftrightarrow & dy_i^* &= \frac{k_i^{OL} c_t^L (y_i^* - y_i) a_p \pi r^2 dz}{L_m} & \text{(c)} \\
 dy_i &= \frac{k_i^{OG} c_t^G (y_i^* - y_i) a_p \pi r^2 dz}{G_m} & \text{(b)} & \Leftrightarrow & dx_i^* &= \frac{k_i^{OG} c_t^G (x_i - x_i^*) a_p \pi r^2 dz}{G_m} & \text{(d)}
 \end{aligned}
 \tag{5.C3}$$

In these equations the infinitesimal packing surface area ( $dA$ ) is replaced by  $a_p \pi r^2 dz$ , where  $a_p$  is the specific surface area of the packing per unit volume. The equations can be expressed in either the gas or liquid phase concentration. The equations (5.C3b and 5.C3c) can be subtracted from each other, so that a simple differential equation for the gas phase is obtained (Colburn, 1941) as:

$$\begin{aligned}
 \frac{d(y_i^* - y_i)}{(y_i^* - y_i)} &= \frac{k_i^{OL} c_t^L a_p \pi r^2 dz}{L_m} - \frac{k_i^{OG} c_t^G a_p \pi r^2 dz}{G_m} \\
 &= \frac{m_i k_i^{OG} c_t^G a_p \pi r^2 dz}{L_m} - \frac{k_i^{OG} c_t^G a_p \pi r^2 dz}{G_m} \\
 &= \left( \frac{m_i}{L_m} - \frac{1}{G_m} \right) k_i^{OG} c_t^G a_p \pi r^2 dz \\
 &= \left( m_i \frac{G_m}{L_m} - 1 \right) \frac{k_i^{OG} c_t^G}{G_m} a_p \pi r^2 dz
 \end{aligned} \tag{5.C4}$$

If this equation is integrated over a concentration trajectory, such that the out-going gas stream is at equilibrium with the out-going liquid stream, a height is obtained, which is referred to as the height equivalent to a theoretical plate (HETP). An illustrated is given in figure 5.C2.

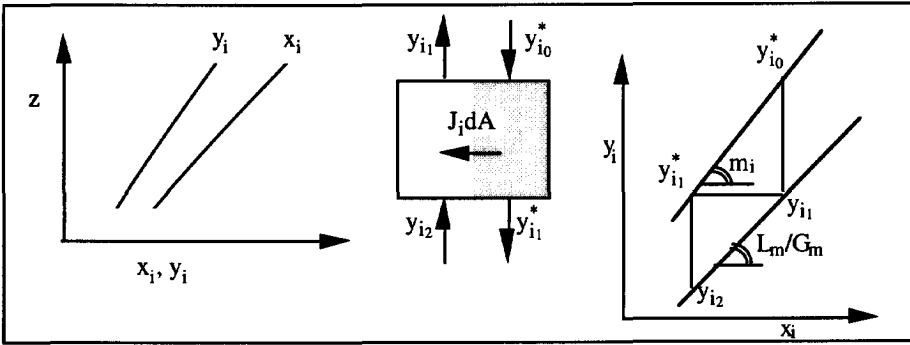


FIGURE 5.C2: The mass transfer over one theoretical plate of an apparatus. The left drawing shows a hypothetical concentration profile over the apparatus.

Using the notation of figure 5.C2, this means that the condition  $y_{i1}^* = y_{i1}$  needs to be satisfied. The integration of equation (5.C4) is now performed as:

$$\begin{aligned}
 \int_{y_{i2}}^{y_{i1}} \frac{d(y_i^* - y_i)}{(y_i^* - y_i)} &= \int_0^{H_i^{etp}} \left( m_i \frac{G_m}{L_m} - 1 \right) \frac{k_i^{OG} c_t^G}{G_m} a_p \pi r^2 dz \\
 \ln \left( \frac{y_{i0}^* - y_{i1}}{y_{i1}^* - y_{i2}} \right) &= \left( m_i \frac{G_m}{L_m} - 1 \right) \frac{k_i^{OG} c_t^G}{G_m} a_p \pi r^2 H_i^{etp} \\
 H_i^{etp} &= \frac{\ln \left( m_i \frac{G_m}{L_m} \right)}{\left( m_i \frac{G_m}{L_m} - 1 \right)} \frac{u_{SG}}{k_i^{OG} a_p} = \frac{\ln(S_i)}{(S_i - 1)} \frac{u_{SG}}{k_i^{OG} a_p}
 \end{aligned} \tag{5.C5}$$

Here the stripping factor  $S_i$  is introduced, which is the ratio of the slope of the equilibrium line and the slope of the operating line. The concentrations used in the integration is equal to the stripping factor. This result can be found by a component balance over the apparatus as:

$$\begin{aligned}
 x_{i0} L_m + y_{i2} G_m &= x_{i1} L_m + y_{i1} G_m \Rightarrow \frac{L_m}{G_m} (x_{i0} - x_{i1}) = y_{i1} - y_{i2} \Rightarrow \\
 \frac{L_m}{G_m} (y_{i0}^* - y_{i1}^*) &= m_i (y_{i1} - y_{i2}) \Rightarrow \frac{(y_{i0}^* - y_{i1}^*)}{(y_{i1} - y_{i2})} = \frac{(y_{i0}^* - y_{i1}^*)}{(y_{i1}^* - y_{i2})} = m_i \frac{G_m}{L_m}
 \end{aligned} \tag{5.C6}$$

The superficial gas velocity,

$$u_{SG} = \frac{G_m}{c_t^G \pi r^2}, \quad (5.C7)$$

is used to replace the molar gas flow in equation (5.C5).

When the equations (5.C3a and 5.C3d) are used, a similar relation based on the liquid mass transfer phase can be derived.

## NOTATION

Symbol	Description	Unit
A	Constant in the Onda et al., correlation .....	
A	Wave amplitude.....	m
A	Interface area.....	m <sup>2</sup>
a <sub>p</sub>	Specific packing area.....	m <sup>2</sup> /m <sup>3</sup>
b <sub>0</sub>	Distance between two contact points .....	m
b <sub>i</sub>	Constant in equilibrium curve.....	mol/mol
c	Wave velocity .....	m/s
c <sub>t</sub> <sup>G</sup>	Total gas concentration .....	mol/m <sup>3</sup>
c <sub>t</sub> <sup>L</sup>	Total liquid concentration.....	mol/m <sup>3</sup>
D <sub>col</sub>	Column diameter .....	m
D <sub>i</sub> <sup>G</sup>	Gas diffusion coefficient .....	m <sup>2</sup> /s
D <sub>i</sub> <sup>L</sup>	Liquid diffusion coefficient .....	m <sup>2</sup> /s
d <sub>p</sub>	Size of a packing element.....	m
d <sub>s</sub>	Size of a sphere with identical surface area as a packing element....	m
Ė <sub>kin</sub>	Dissipated kinetic energy .....	J/s
e	Surface roughness.....	m
e <sub>kin</sub>	Kinetic energy per unit mass.....	J/kg
f	Smooth pipe friction factor.....	
f <sub>r</sub>	Rough pipe friction factor .....	
G''	Gas flux .....	kg/m <sup>2</sup> /s
G <sub>m</sub>	Molar gas flow.....	mol/s
g	Gravitational acceleration.....	m/s <sup>2</sup>
H <sub>i</sub> <sup>etp</sup>	Height of an equivalent theoretical plate .....	m
H <sub>p</sub>	Height of a structured packing element .....	m
h	Liquid film thickness.....	m
h <sub>0</sub>	Free falling film thickness.....	m
J <sub>i</sub> <sup>G</sup>	Molar gas diffusion flux.....	mol/m <sup>2</sup> /s
J <sub>i</sub> <sup>L</sup>	Molar liquid diffusion flux .....	mol/m <sup>2</sup> /s

---

$K_i$	Distribution factor .....	mol/mol
$k$	Wave number .....	$m^{-1}$
$k_e$	Characteristic wave number for the exposure length .....	$m^{-1}$
$k_i^G$	Gas mass transfer coefficient .....	m/s
$k_i^L$	Liquid mass transfer coefficient .....	m/s
$k_i^{OG}$	Overall gas transfer coefficient.....	m/s
$k_i^{OL}$	On liquid phase based overall mass transfer coefficient .....	m/s
$L''$	Liquid flux .....	$kg/m^2/s$
$L_m$	Molar liquid flow.....	mol/s
$\ell_0$	Distance between two packing turns .....	m
$\ell_e$	Exposure length .....	m
$m_i$	Derivative of the equilibrium line.....	mol/mol
$N_e$	Average number of unit distances of free path.....	
$r_0$	Hydraulic radius.....	m
$S_i$	Stripping factor $S_i = m_i G_m/L_m$ .....	
$s$	Corrugated spacing.....	m
$t$	Time.....	s
$t_e$	Exposure time.....	s
$t_{kol}$	Kolmogorov time scale .....	s
$u_{0-int}$	Interface velocity of free falling film .....	m/s
$u_{int}$	Interface velocity .....	m/s
$u_G$	Average gas velocity .....	m/s
$u_L$	Average liquid velocity .....	m/s
$u_{SG}$	Superficial gas velocity .....	m/s
$u_{SL}$	Superficial liquid velocity .....	m/s
$V$	Volume .....	$m^3$
$x$	Horizontal co-ordinate .....	m
$x_j$	Mol fraction in the liquid phase .....	mol/mol
$x_i^{int}$	Liquid interface mol fraction .....	mol/mol
$x_i^*$	Apparent liquid mol fraction .....	mol/mol
$y$	Vertical co-ordinate.....	m
$y_i$	Mol fraction in the gas phase.....	mol/mol
$y_i^{int}$	Gas interface mol fraction .....	mol/mol
$y_i^*$	Apparent gas mol fraction .....	mol/mol
$Z$	Pipe length .....	m
$Z_p$	Total Geometrical contribution to the exposure length.....	m
$z$	Axial co-ordinate .....	m
$\bar{z}$	average free path of a surface element .....	m

---

$z_0$	Integration distance.....	m
$\alpha$	Effective inclination angle .....	°
$\beta$	Angle with the liquid film .....	°
$\gamma$	Angle with the liquid film .....	°
$\delta^G$	Characteristic gas film thickness for the mass transfer.....	m
$\delta^L$	Characteristic liquid film thickness for the mass transfer .....	m
$\Delta$	Wide of a contact point .....	m
$\Delta\rho$	Density difference .....	kg/m <sup>3</sup>
$\epsilon_{kin}$	Dissipated kinetic energy per unit mass.....	m <sup>2</sup> /s <sup>3</sup>
$\epsilon_0$	Void fraction .....	m <sup>3</sup> /m <sup>3</sup>
$\eta_G$	Dynamic gas viscosity .....	Pa s
$\eta_L$	Dynamic liquid viscosity .....	Pa s
$\theta$	Relative interface position .....	
$\lambda$	Wavelength.....	m
$\lambda_e$	Exposure wavelength .....	m
$\nu_G$	Kinematic gas viscosity.....	m <sup>2</sup> /s
$\nu_L$	Kinematic liquid viscosity.....	m <sup>2</sup> /s
$\xi$	Wave function .....	m
$\rho_G$	Gas density.....	kg/m <sup>3</sup>
$\rho_L$	Liquid density.....	kg/m <sup>3</sup>
$\sigma$	Surface tension .....	N/m
$\tau$	Damping time .....	s
$\phi$	Potential field of the velocity .....	s <sup>-1</sup>
$\Psi_{G-L}$	Gas-liquid interaction parameter.....	
$\omega$	Circle frequency .....	s <sup>-1</sup>
$Fo_i^L$	Fourier number .....	$Fo_i^L = \frac{D_i^L t}{h^2}$
$Ga_p$	Packing Galileo number .....	$Ga_p = \frac{4\Delta\rho\rho_L g \cos \alpha}{3\eta_L^2 a_p^3}$
$Re_G$	Gas phase Reynolds number.....	$Re_G = \frac{\rho_G \left( \frac{u_{SG}}{\theta^2 \epsilon_0 \cos \alpha} - u_{int} \right) 2\theta r_0}{\eta_G}$
$Re_L$	Liquid phase Reynolds number.....	$Re_L = \frac{4L''}{\eta_L a_p}$
$Sc_i^G$	Gaseous Schmidt number .....	$Sc_i^G = \frac{\eta_G}{\rho_G D_i^G}$

---

$Sc_i^L$	Liquid Schmidt number.....	$Sc_i^L = \frac{\eta_L}{\rho_L D_i^L}$
$Sh_i^G$	Gaseous Sherwood number.....	$Sh_i^G = \frac{k_i^G 2\theta r_0}{D_i^G}$
$Sh_i^L$	Liquid Sherwood number .....	$Sh_i^L = \frac{k_i^L h}{D_i^L}$

---

## REFERENCES

- [1] Bird, R.B., Stewart, W.E., and Lightfoot, E.N., (1960), *Transport Phenomena*, New York: Wiley.
  - [2] Boyce, W.E., and DiPrima, R.C., (1977), *Elementary Differential Equations and Boundary Value Problems*, 3<sup>rd</sup> ed., New York: Wiley.
  - [3] Brekhovskikh, L.M., and Goncharov, V., (1993), *Mechanics of Continua and Wave Dynamics*, 2<sup>nd</sup> ed., Berlin: Springer-Verlag
  - [4] Bravo, J.L., Rocha, J.A., and Fair, J.R., (1985), *Mass Transfer in Gauze Packings*, Hydrocarbon Processing, 91-95.
  - [5] Chilton, T.H., and Colburn, A.P., (1934), *Mass Transfer Co-efficients - Production from data on heat transfer and fluid friction*, Ind. Eng. Chem., **26** pp. 1183.
  - [6] Coulson, J.M., and Richardson, J.F., (1977), *Chemical Engineering*, Vol. 1, 3<sup>rd</sup> ed. Oxford: Pergamon Press.
  - [7] Dobbins, W.E., (1956), in McCabe, J., and Eckenfelder, W.W., (Eds.) *Biological Treatment of Sewage and Industrial Wastes*, New York: Reinhold.
  - [8] Drazin, P.G., Reid, W.H., (1981), *Hydrodynamic Stability*. London: Cambridge University Press.
  - [9] Emmet, R.E., and Pigford, R.L., (1954), *A study of Gas Absorption in Falling Liquid Films*, Chem. Eng. Prog., **50** pp. 87.
  - [10] Fair, J.R., and Bravo J.L., (1990), *Distillation Columns Containing Structured Packing*, Chem. Eng. Prog., **86** pp. 19-29.
  - [11] Fletcher, D.F., Maskell, S.J., and Patrick, M.A., (1982), *Theoretical Investigation of the Chilton-Colburn Analogy*, Trans. Inst. Chem. Engrs., **60** pp. 122-125.
  - [12] Haan, de A.B. (1991). *Supercritical fluid extraction of liquid hydrocarbon mixtures*. PhD Thesis, Delft: Delft University Press.
  - [13] Higbie, R., (1935), *The Rate of Absorption of a Pure Gas into a Still Liquid During Short Periods of Exposure*, Trans. Am. Inst. Chem. Engrs., **31** pp. 365-389.
  - [14] Johnstone, H.F., and Pigford, R.L., (1942), *Distillation in Wetted Wall Columns*, Trans. Am. Inst. Chem. Engrs., **38** pp. 25-51.
  - [15] Krevelen, D.W., and Hoftijzer, P.J., (1948), , Chem. Eng. Prog., **44** pp. 529.
  - [16] Lamourelle, A.P., and Sandall, O.C., (1972), *Gas Absorption into a Turbulent liquid*, Chem. Eng. Sci., **27** pp. 1035.
  - [17] Landau, L.D., Lifshitz, E.M. (1987). *Fluid Mechanics*, 2nd ed. Oxford: Pergamon Books Ltd.
  - [18] Linton, W.H., and Sherwood, T.K., (1950), *Mass transfer from solid shapes to water in streamline and turbulent flow*, Chem. Eng. Prog., **46** pp. 258.
  - [19] Main, I.G., (1993), *Vibrations and Waves in Physics*, 3<sup>rd</sup> ed., Cambridge: Cambridge University Press.
  - [20] Onda, K., Takeuchi, H., and Okumoto, Y., (1968), *Mass Transfer Coefficients between Gas and Liquid Phases in Packed Columns*, J. Chem Eng Jpn., **1** pp. 56-62.
  - [21] Onda, K., Sada, E., and Murase, Y., (1959), *Liquid-Side Mass Transfer Coefficients in Packed Towers*, AIChE J., **5** pp. 235-239.
-

- [22] Olujic, Z., Stoter, F., and Graauw, de J., (1993), *Liquid Distribution Performance of Structured Packings with Different Surface Characteristics*, AIChE Spring National Meeting, March/April 1993, Houston.
- [23] Perry, R.H., and Green, D.W., (1984), *Perry's Chemical Engineering Handbook*, 6th ed. New York: McGraw-Hill.
- [24] Semmelbauer, R., (1967), *Die Berechnung de Schütthöhe bei Absorptionsvorgängen in Füllkörperkolonnen*, Chem. Eng. Sci., **22** pp. 1237.
- [25] Sideman, S., and Pinczewski, W.V., (1975), in Gutfinger, C. (Ed.) *Topics in Transport Phenomena*, New York: Halstead Press.
- [26] Singh, P.C., and Stockar, U. von, (1996), *A somplified penetration model for mass transfer in packed beds and strings of spheres*, Chem. Eng. Proc., **35** 343-347.
- [27] Sherwood, T.K., and Holloway, F.A.L., (1940), *Performance of Packed Towers-Liquid film data for several packings*, Trans. Am. Inst. Chem. Engrs., **36** pp. 2940.
- [28] Sherwood, T.K., and Pigford, R.L., (1952), *Absorption and Extraction*, 2<sup>nd</sup> ed., New York: McGraw-Hill Book Company.
- [29] Sulman, H.L., and Ulrich, C.F., (1955), *AIChE J.*, **1** p 253.
- [30] Sulzer Brother Ltd., (1989), *Separation Columns for Distillation and Absorption*. Information Bulletin.
- [31] Spiegel, M.R., (1967), *Applied Differential Equations*, 2<sup>nd</sup> ed., Englewood Cliffs, N.J.: Prentice-Hall, Inc.
- [32] Taylor, R., and Krishna, R., (1993), *Multi-Component Mass Transfer*, Wiley Series in Chemical Engineering, New York.
- [33] Toor, R., Kooijman, H.A., and Woodman, M.R., (1992), *Industrial Applications of a Nonequilibrium Model of Distillation and Absorption Operations*, The institution of Chemical Engineers Symposium Series No. 128, pp. A415-A427.
- [34] Treybal, R.E., (1980), *Mass Transfer Operations*, 3<sup>rd</sup> ed, Wiley Series in Chemical Engineering, New York.
- [35] Vivian, J.E., and Paeceman, B.W., (1956), *Liquid-Side Resistance in Gas Absorption*, *AIChE. J.*, **2** pp. 437-443.



## Packing Design for Specific Applications

Numerous types of packing are encountered in separation processes in practice. In these processes mass transfer takes place within the column between gas and liquid phase. The intensity of the mass transfer is dependent on the applied packing. The models presented in chapter 3 to 5 describing pressure drop, mass transfer and column capacity, distinguishes adjustable geometrical packing parameters. By changing the geometrical packing parameters in the models, the potential performance of a packed bed configuration can be evaluated and the result can be used to design separation columns for specific applications.

As has been shown in chapter 5 the models developed simplify the situation in packing geometries in several ways. First, it assumes total wetting, which is valid only for certain conditions and it depends on the type of packing used (see, e.g. Fair and Bravo, 1990, Billet, 1986). Second, it does not account for the liquid and gas back mixing or axial dispersion, a phenomenon that for instance becomes important near the flood point. Third, the model does not account for large scale maldistribution in the column (see, e.g. Hoek, 1983; Stoter, 1993; Klemas and Bonilla, 1995). It is not intended to address all these influences here, but given the large effect of wetting on the mass transfer in packed beds, we will extend the model for the possibility of partial wetting in this part of the thesis. The other factors are also important for the performance of a packed column and should be considered when designing a separation, but they essentially do not influence the potential of a packed bed geometry.

When wetting is incorporated in the model, it becomes possible to optimize the geometry of the packing to obtain the best operating column. The best column implies here the lowest investment costs or it could concern a column with the lowest pressure drop for the separation. The models will be used to determine the costs of packed columns for two different applications, along the lines described in the pioneering work by Billet (1992). However, in this work we will not only optimize surface geometry, but the effective inclination angle of the packing will be evaluated as well. At the end of this chapter it will be shown that it is possible to further optimize the packing geometry, by changing another basic parameter of a corrugated sheet.

### MODEL EXTENSION AND VALIDATION

For the evaluation of the models two different systems will be used. The total reflux distillation of ethylbenzene - chlorobenzene (Sulzer, 1989) represents a system where the mass transfer is mainly located in the gaseous phase. The second case is the vacuum stripping of isopropyl

alcohol (IPA) from ethylene glycol using carbon dioxide at 200 mbar as stripping agent. In this system a considerable mass transfer resistance is located in the liquid phase. Although this system contains three components, only IPA will be distributed over both phases, so that each phase can be treated as a binary system. The estimated physical properties of the applied systems are listed in tables VI.I and VI.II.

TABLE VI.I: The estimated physical properties for a system consisting of 99.9% of ethylbenzene and 0.1% of chlorobenzene.

p	1013	100	25	mbar
T	136.4	67.3	37.5	°C
$m_i$	1.13	1.19	1.24	
$\rho_L$	756	815	836	kg/m <sup>3</sup>
$\rho_G$	3.28	0.378	0.103	kg/m <sup>3</sup>
$\eta_L$	0.231	0.407	0.547	mPa s
$\eta_G$	8.33	6.74	6.07	$\mu$ Pa s
$D^L$	7.76	3.91	2.74	n m <sup>2</sup> /s
$D^G$	4.04	28.50	93.80	$\mu$ m <sup>2</sup> /s
$\sigma$	16.7	22.9	25.4	mN/m

TABLE V.II: The estimated physical properties and equilibrium for a system consisting of equal molar fractions of ethylene glycol and carbon dioxide combined with 5%mol IPA.

p	200	200	200	mbar
T	0	20	40	°C
$m_i$	0.125	0.503	1.662	
$x_{IPA}$	0.088	0.067	0.038	mol/mol
$y_{IPA}$	0.011	0.034	0.062	mol/mol
$\rho_L$	1075	1074	1076	kg/m <sup>3</sup>
$\rho_G$	0.390	0.366	0.346	kg/m <sup>3</sup>
$\eta_L$	19.8	9.6	5.3	mPa s
$\eta_G$	13.2	13.8	14.3	$\mu$ Pa s
$D^L$	0.081	0.176	0.328	n m <sup>2</sup> /s
$D^G$	23.3	29.0	35.7	$\mu$ m <sup>2</sup> /s
$\sigma$	44.3	43.7	43.3	mN/m

Before determining the wetting of the packing, the totally wetted packing performance will be evaluated as function of the specific surface area and the effective inclination angle. These parameters are considered as the principle design parameters of the current generation of internals. Since total wetting is assumed the following evaluation in principle describes the potential of metal gauze packing which, as shown in the previous chapter, appears to wet the packing surface completely.

#### *The surface area influence*

The major packing design parameter is of course the specific surface area of the packing. Figure 6.1 shows the effect of the specific surface area on the predicted HETP for the ethylbenzene - chlorobenzene system operated at total reflux ( $G'' = L''$ ). The right hand graph shows the product of the specific area and the HETP. This can be seen as the specific area per equilibrium stage. The curves for the different specific areas don't correspond totally at low load conditions. This is due to the smaller interfacial velocities for larger packing areas and the influences of the dimensionless radius  $\theta$ . The decrease of the HETP at larger loads is caused by the influence of the gas-liquid interaction ( $\psi_{G-L}$ ), which causes interface waves and extra gas friction.

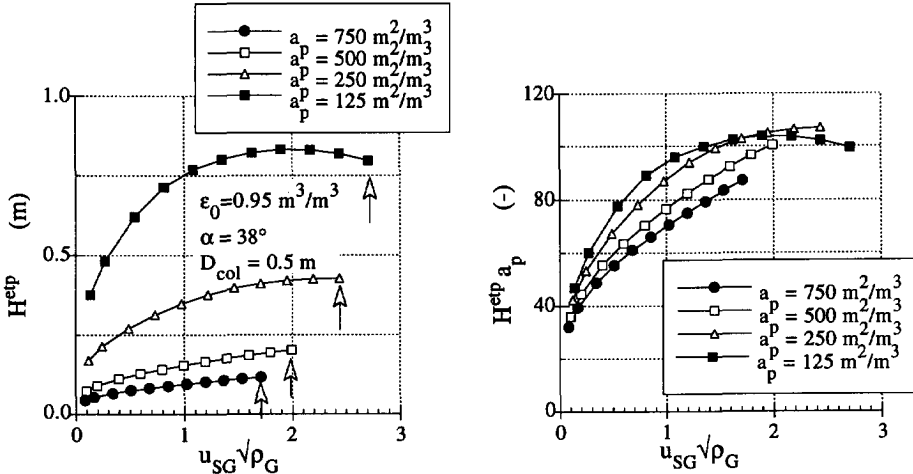


FIGURE 6.1: Estimated height equivalent to a theoretical stage for ethylbenzene - chlorobenzene at atmospheric pressure as function of the gas load factor for various specific packing areas. The arrows indicate the estimated flood points. The right hand side graph shows the required specific surface area in the flow direction for an equivalent to a theoretical plate.

For the liquid side controlled system the calculations have been based on the condition of equal molar flows in gas and liquid phases ( $G''_m = L''_m$ ). The used liquid mass flow therefore is approximately 1.4 ( $= 62/44$ ) times larger than the used gas mass flow. By applying this condition the stripping factor ( $S_i$ ) is equal to the molar distribution coefficient. When a system also has a resistance in the liquid phase, the HETP will always be larger than for a system where no important liquid mass transfer resistant is present. The general shape of the HETP curves does not change significantly as shown in figure 6.2. However, due to the additional liquid phase resistance the differences between the required area per HETP for various packings become smaller (see figure 6.2 RHS).

#### *The effective inclination angle influence*

Another parameter that can be varied is the effective inclination angle of the packing. Its influence is shown in figure 6.3 for the atmospheric ethylbenzene - chlorobenzene system. Again, the most interesting graph is the normalised one. It shows that for small loads the influence of the gas liquid interaction is small, but that the interaction becomes significant for high loads. The graph indicates that if one intends to minimize the volume of a column, the best choice would be the packing with the largest effective inclination angle. Although the flooding velocity of the  $55^\circ$  packing is only half of the  $25^\circ$  packing, the HETP is approximately one third of the value found for the smaller effective inclination angle.

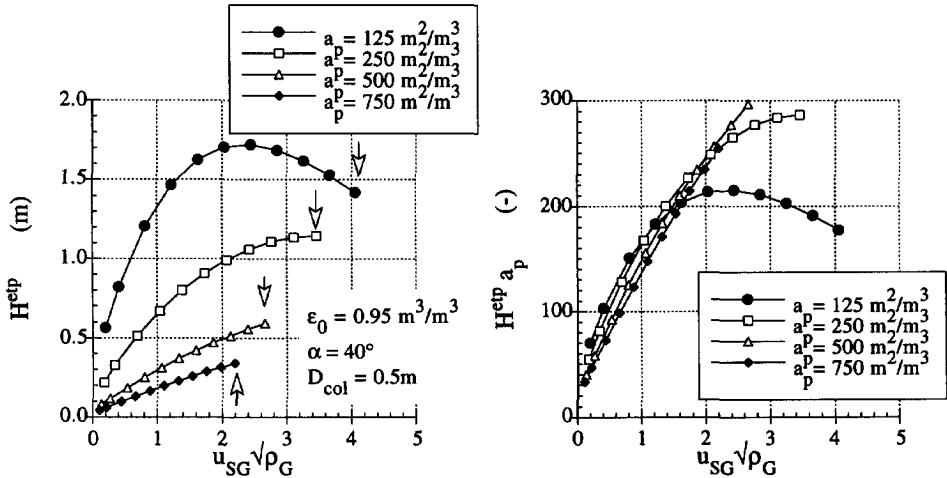


FIGURE 6.2: Estimated HETP for IPA - ethylene glycol - carbon dioxide at 200 mbar and 40°C as function of the gas load factor for various specific packing areas. The arrows indicate the estimated flood points. The right hand graph shows the required specific surface area for one height equivalent to a theoretical plate.

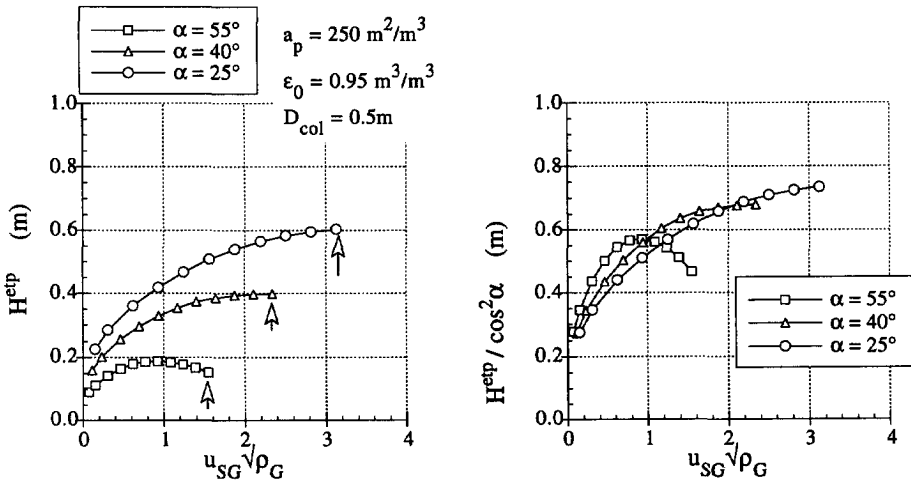


FIGURE 6.3: Estimated height equivalent to a theoretical plate for ethylbenzene-chlorobenzene at atmospheric pressure as function of the gas load factor for various packing effective inclination angles. The arrows indicate the estimated flood points. The right hand side graph shows a HETP normalised for the effective inclination angle.

If the Mellapak metallic sheet packing type X and Y are compared, the reported HETP's for the Mellapak Y series are a factor 1.25 to 1.5 smaller. The expected ratio would be  $(\cos 26^\circ / \cos 38^\circ)^2 = 1.3$ . Although this value seems to be reasonable, it shows that the model monitors trends, but that deviation with measurements can occur rapidly. Much depends on additional factors as liquid distributors, wetting, maldistribution, adjustment of the packing elements, column dimensions, etc.

*The wetting of the packing*

In all the following calculations the porosity of the packing decreases with increasing specific surface area as:  $\epsilon_0 = 1 \cdot 10^{-4} a_p$ , which is equivalent to 0.2mm sheets.

As shown in chapter 5 the model predicts the mass transfer performance very well for metal gauze packing (figure 5.9), but the model predictions of the HETP's for metal sheet packing with surface areas larger than  $250 \text{ m}^2/\text{m}^3$  show substantial deviations (figure 5.10). It is likely that these deviations are caused by insufficient wetting i.e. rivulet formation on the packing. The inefficient use of the installed packing surface causes a decrease of the mass transfer and a consequently larger HETP. Billet (1986) showed that the wetting can be described well on basis of the liquid Reynolds number. Since normally the mass transfer is the measured quantity, we will use the total geometrical area ( $a_p$ ) of the packing and multiply the whole expression for the HETP with a function describing the wetting to obtain an effective height of an equilibrium stage  $H_{\text{eff}}^{\text{etp}}$ .

When the wetting is plotted on a logarithmic scale as function of the Reynolds number, a straight line is found (see, e.g., Fair and Bravo, 1991). We therefore have looked for a simple power function of the liquid Reynolds number, that also correctly describes the extreme wetting behaviour (for:  $Re_L = 0$ ; and  $Re_L = \infty$ ) to modify the calculated HETP. The result is:

$$H_{\text{eff}}^{\text{etp}} = H^{\text{etp}} \left( \left( \frac{Re_{L-W50}}{Re_L} \right)^{0.5} + 1 \right) \quad (6.1)$$

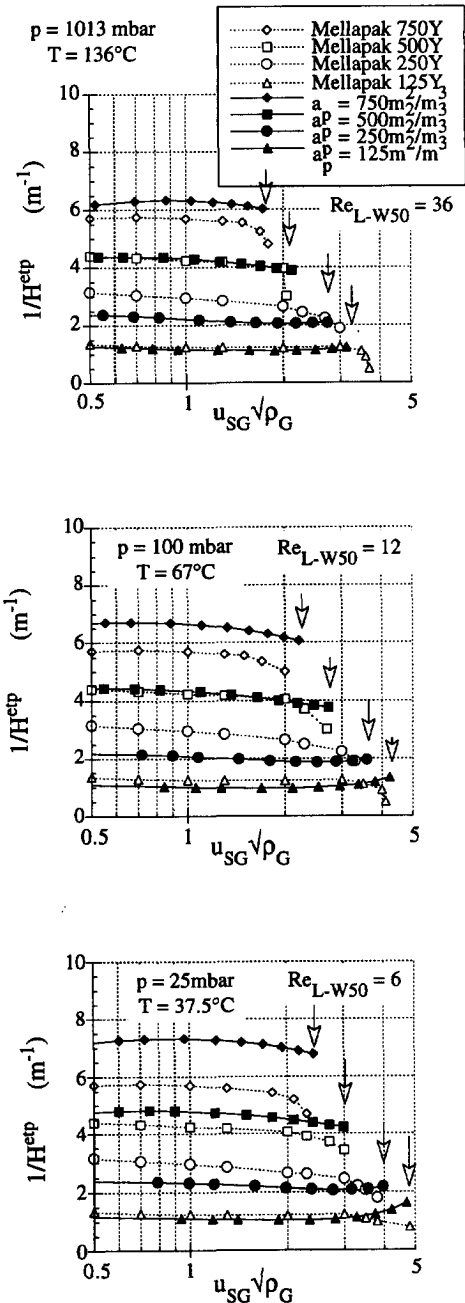


FIGURE 6.4: Comparison of measured and for wetting corrected estimated number of theoretical stages per meter packing for the distillation at total reflux of an ethylbenzene - chlorobenzene system.

In this expression  $Re_{L-W50}$  is a liquid Reynolds number at which the packing performance is 50% of the predicted value. This number is characteristic for packing type and application. Figure 6.4 shows three typical results obtained with equation (6.1). The comparison shows that the calculated HETP's agree well with the reported values (Sulzer, 1989). In addition, the graphs show that the flood point is predicted well for the different pressures. To obtain this result the value of  $Re_{L-W50}$  had to be determined for each operating pressure. Since the fitted values of  $Re_{L-W50}$  proved to be proportional to the square root of the systems gas density, it is possible to rewrite equation (6.1) as function of the gas density, so that a more general wetting relation ( $f_{wet}$ ) can be formulated;

$$H_{eff}^{etp} = H^{etp} f_{wet} = H^{etp} \left( \left( \frac{Re_{W50}}{Re_L} \left( \frac{\rho_G}{\rho_L} \right)^{0.5} \right)^{0.5} + 1 \right) \quad (6.2)$$

Here the liquid density was used to obtain a dimensionless expression. Using correlation (6.2) the general wetting number at which 50% of the model performance is reached now becomes for all three pressure:  $Re_{W50} = 550$ . This value is valid for the system ethylbenzene - chlorobenzene, applied on one of the Mellapak Y series. Given the condition  $L'' = G''$  at total reflux, the equation equivalently could have been formulated as depending on the gas load. This means that the correlation can be written as a function that depends on the percentage of flood. This construction was, as a first approximation, suggested by Fair and Bravo, (1990).

#### *Evaluation of performance on basis of column and packing dimensions*

The choice of a packing will depend on the main objective. For vacuum distillation the pressure drop per stage is an important parameter. In case of a revamp the dimensions of the column are fixed and the capacity or the purity of the components should be optimised. In case of a new column the normal constrains are the load and the required number of stages and the objective is the construction of the cheapest column. In the following only new columns are evaluated and for simplicity the operating temperature and pressure will be fixed as well.

A criterion to select a packing type would be the minimisation of the equipment volume ( $V_{col}$ ). The total volume of the equipment can be written using the packing characteristics as:

$$\begin{aligned} V_{col} &= H_{col} \frac{\pi}{4} D_{col}^2 = N H_{eff}^{etp} \frac{G}{u_{SG} \rho_G} = N \frac{\ln S_i}{S_i - 1} f_{wet} \frac{u_{SG}}{k_i^{OG} \theta_{ap}} \frac{G}{u_{SG} \rho_G} \\ \Rightarrow V_{col} &\sim v_v = \left. \frac{f_{wet}}{k_i^{OG} \theta_{ap}} \right|_{\text{for } N, G, S_i \text{ are constant}} \quad (6.3) \end{aligned}$$

In this equation the height of a column is taken equal to the required number of equilibrium stages ( $N$ ) times the HETP. The diameter is expressed using the required gas throughput ( $G$ ). Because the stripping factor and the gas throughput are fixed for given separation conditions, the performance of a packing therefore is summarised by the wetting divided by the overall mass transfer coefficient and the specific surface area. Billet (1992) refers to this parameter as the specific column volume  $v_v$ . The smaller the specific column volume the larger the volumetric efficiency of a packed bed will be.

The model is validated further by comparing measured overall mass transfer data, which includes the wetting of the packing, with model predictions. Figure 6.5 shows measured data reported by Billet (1992), the correlation given by Billet (1992), and the mass transfer coefficients calculated by our model as function of the specific surface area of the packing at 80% of the flood point. Obviously the transfer coefficients estimated by our model correlate the data well. The curve generated by the model shows a slower decrease of the mass transfer coefficient at larger packing areas than an extrapolation of correlation of Billet. The reciprocal mass transfer coefficient can be interpreted as the degree of exploitation of geometrically installed surface area (Billet, 1992). The diagram shows a decrease of the exploitation area with increasing geometrical area.

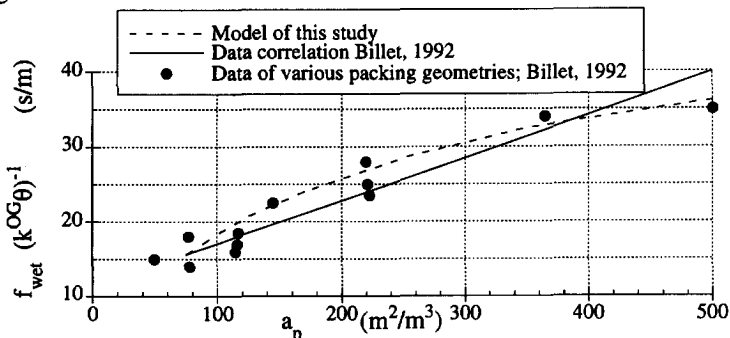


FIGURE 6.5: Comparison of the performance related area at 80% of the flood point. Indicated are data points for various packing geometries, the correlation given by Billet, (1992) and the curve resulting from this study.

### THE SPECIFIC DESIGN OF A PACKED COLUMN

In most cases the engineer would like to design the cheapest column. We therefore need to estimate the installed column costs. The column costs are a combination of the purchase equipment costs of the column shell ( $K_S$ ) and the packing ( $K_P$ ). The installed column costs ( $K_{col}$ ) are obtained by multiplying the purchase costs by an appropriate factor. These factors are not identical for the column shell and the packing. The size of the shell directly influences: equipment erection, piping, process structures, site development and ancillary buildings, while the packing influences the equipment erection only. Using the factors listed by Coulson et al., (1985), a factor 2.5 is found for the column shell and a factor 1.5 is found for the installation of the packing including liquid distributors. The installed column costs are estimated by multiplying the sum with a factor 2;

$$K_{col} = 2.0 (2.5 K_S + 1.5 K_P) = 5 (35000 + 3000 D_{col} H_{col}^{1.1}) + 3 a_p \left( 25 + \frac{7}{D_{col}} \right) V_{col} \quad (6.4)$$

Here the expression for the costs of the stainless steel packing is taken identical to the one given by Billet, (1992). The purchase costs of the carbon steel column are correlated as function of the diameter and height (Webci, 1995), using data for columns in the range:  $0.5m < D_{col} < 4m$  and  $5m < H_{col} < 40m$ . All costs are expressed in Dutch guilders ( $f$ ).

In the following design studies for packed columns our main objective is the minimisation of equation (6.4). As examples we will use the total reflux distillation of the ethylbenzene-chlorobenzene system and the stripping of IPA from ethylene glycol using an equimolar amount of carbon dioxide so that  $L = 1.4G$ .

*The specific area and effective inclination angle influence*

In figure 6.6A the specific column volume is shown as function of the specific surface area for the stripping of IPA from ethylene glycol and the distillation of ethylbenzene-chlorobenzene, for total wetting and partial wetting. Equation (6.2) is used to calculate the wetting for both applications, applying a characteristic wetting number of  $Re_{w50} = 550$ . The calculations are carried out at 80% of the flood point, using a gas load of 3kg/s. For total wetting the specific column volume decreases much faster for both applications. The specific volume for the application with liquid phase resistance clearly is larger than in the case of the application with gas phase resistance only. To obtain comparable column sizes the number of stages for the distillation is taken as:  $N=50$ , while the number of stages for the stripping is taken as:  $N=20$ . Figure 6.6B shows the calculated dimensions of the columns using the partial wetted specific column volume.

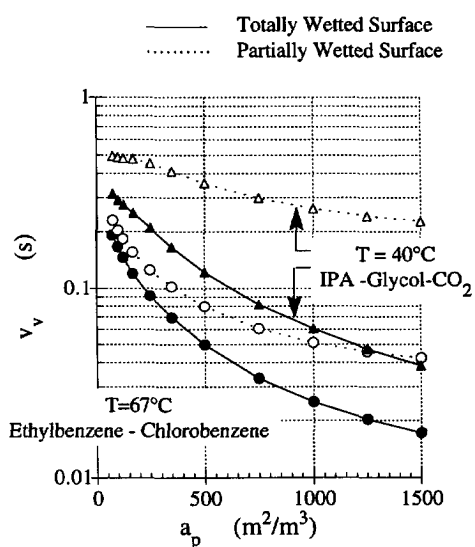


FIGURE 6.6A: Estimated performance at 80% of the flood point as function of the specific area, for totally and partially wetted surfaces using an effective inclination angle of  $\alpha = 40^\circ$  and a gas load of  $G = 3\text{kg/s}$ .

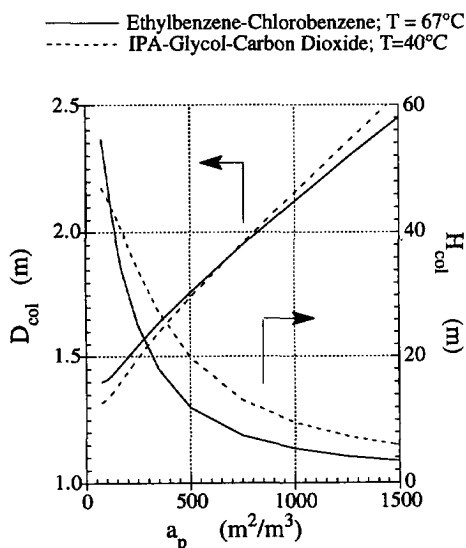


FIGURE 6.6B: Estimated column diameter and height at 80% of the flood point as function of the specific area, for partially wetted surfaces using fixed gas throughput, stripping factors and stages,  $N=50$  for distillation and  $N=20$  for stripping.



The next parameter that influences the column sizes is the effective inclination angle. Figure 6.7A shows the specific column volume as function of the effective inclination angle at 80% of the flood point. The graph shows a maximum around an effective inclination angle of  $\alpha = 30^\circ$ . The decrease of the required volumes at intermediate effective inclination angles ( $30^\circ < \alpha < 60^\circ$ ), is caused by the influence of the gas-liquid interaction ( $\Psi_{G-L}$ ), which slowly becomes more pronounced in this region. At effective inclination angles exceeding  $60^\circ$  the required specific column volume increases again. This is due to a change of flooding mechanism from entrainment flooding to flooding initiated by drag. Drag flooding causes a faster decrease of the column capacity. The graph indicates that by increasing the effective inclination angle from  $30^\circ$  to  $60^\circ$  the required volume for the separation decreases by the same order as increasing the specific surface area by a factor 2. The shaded area indicates the extrapolation of the model to effective inclination angles not available in practice. These effective inclination angles are typically found for random packings. Figure 6.7B shows the dimensions of the column as function of the effective inclination angle.

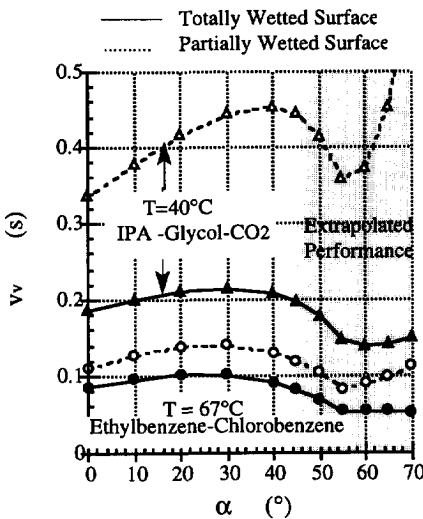


FIGURE 6.7A: Estimated performance of packing configuration as function of the effective inclination angle for totally and partially wetted surfaces using a specific surface area of  $a_p=250 \text{ m}^2/\text{m}^3$  and a gas load of  $G = 3 \text{ kg/s}$ .

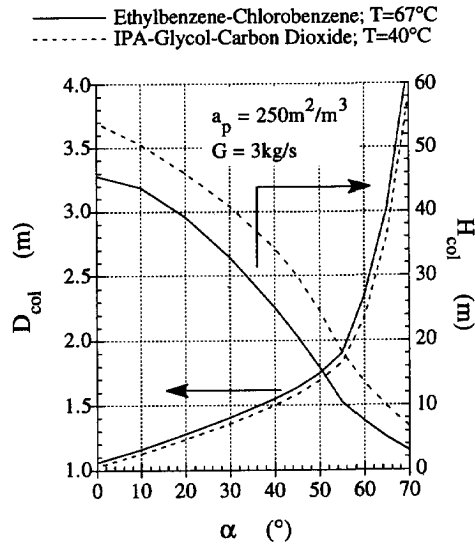


FIGURE 6.7B: Estimated column diameter and height at 80% of the flood point as function of the effective inclination angle, for partially wetted surfaces using fixed gas throughput, stripping factors and number stages,  $N=50$  for distillation and  $N=20$  for stripping.

The two applications are further analysed by calculating the costs and the total required pressure drop for the application. In the figures 6.8 and 6.10 the installed costs as function of the geometrical area and as function of the effective inclination angle are shown, while in figures 6.9 and 6.11 the total required pressure drop for the cases is given.

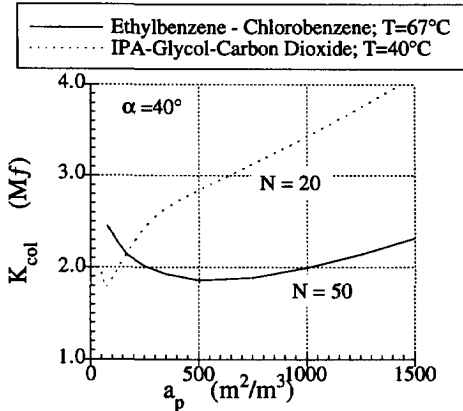


FIGURE 6.8: Investment costs in million guilders for a distillation column of ethylbenzene-chlorobenzene at  $67^\circ C$  and 100mbar and a stripping column operated at  $40^\circ C$  and 200mbar for the removal of IPA from glycol using  $CO_2$  as stripping agent as function of the specific surface area. Using:  $G=3kg/s$  and indicated stages.

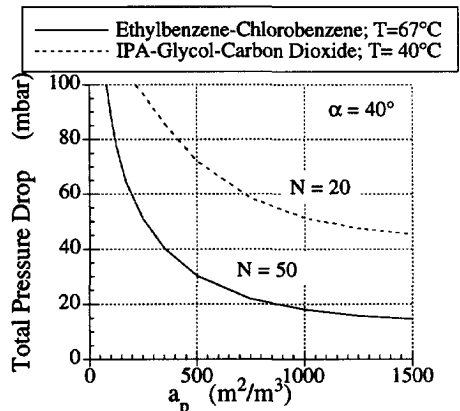


FIGURE 6.9: Estimated total pressure drop for a distillation column of ethylbenzene-chlorobenzene at  $67^\circ C$  and 100mbar and a stripping column operated at  $40^\circ C$  and 200mbar for the removal of IPA from glycol using  $CO_2$  as stripping agent as function of the specific surface area. Using:  $G=3kg/s$  and indicated stages.

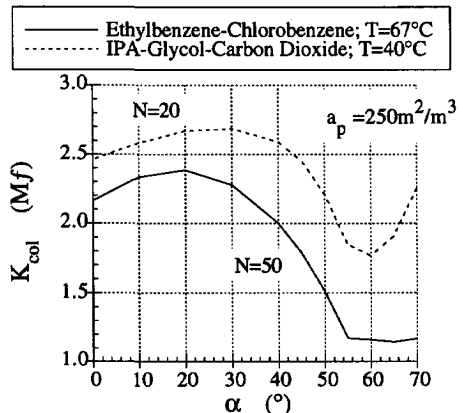


FIGURE 6.10: Investment costs in million guilders for a distillation column of ethylbenzene-chlorobenzene at  $67^\circ C$  and 100mbar and a stripping column operated at  $40^\circ C$  and 200mbar for the removal of IPA from glycol using  $CO_2$  as stripping agent as function of the effective inclination angle. Using:  $G=3kg/s$  and indicated stages.

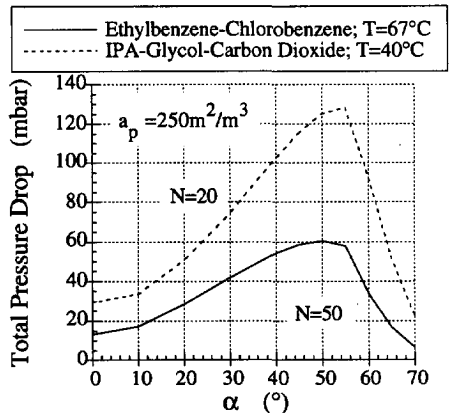


FIGURE 6.11: Estimated total pressure drop for a distillation column of ethylbenzene-chlorobenzene at  $67^\circ C$  and 100mbar and a stripping column operated at  $40^\circ C$  and 200mbar for the removal of IPA from glycol using  $CO_2$  as stripping agent as function of the effective inclination angle. Using:  $G=3kg/s$  and indicated stages.

First it is interesting that the distillation case shows a tendency to large specific surface areas. Billet found a most cost effective specific geometrical surface area near  $250 m^2/m^3$ , our optimum values typically are two times larger. This is mainly caused by the price of the column shell. When a more expensive type of steel was used for the column the most cost effective surface areas would even tend to larger specific areas. The most cost effective geometrical areas

for the stripping case are found in the low range;  $a_p = 100\text{m}^2/\text{m}^3$ . This is mainly caused by the fact that the gas-liquid interactions increase at low geometrical areas. The developed waves on the interface strongly contribute to a decrease of the liquid phase resistance and therefore to a less steep increase of column height with decreasing specific surface area (see figure 6.6B). An interesting result is found for the total pressure drop as function of specific surface area (see, figure 6.9). The lowest pressure drops for both applications are located at large specific surface areas. Figure 6.10 shows the costs for the columns as function of the effective inclination angle. Both applications have a minimum near  $\alpha = 55^\circ$ . This angle was also found earlier for the specific column volume. As illustrated in figure 6.11, the lower investment costs are paid for by an increased total pressure drop over the equipment.

*The capacity of the application*

The capacity of the separation also influences the selection of the packing. For throughputs the specific column volume will not change significantly, but as shown in figure 6.12 the installed costs of the column as function of gas throughputs do.

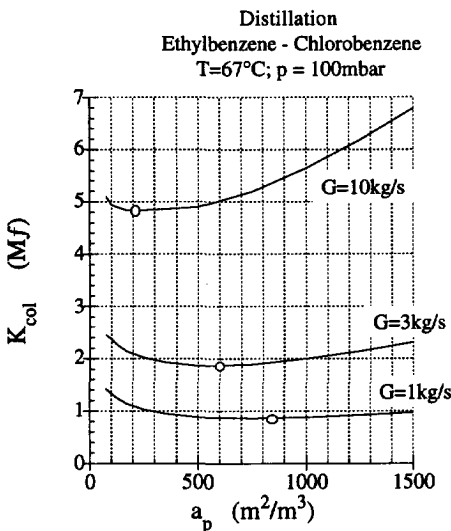


FIGURE 6.12: Investment costs in million guilders for a distillation column of ethylbenzene-chlorobenzene at 67°C as function of the packing specific surface area for indicated gas loads using an effective inclination of  $\alpha = 40^\circ$ .

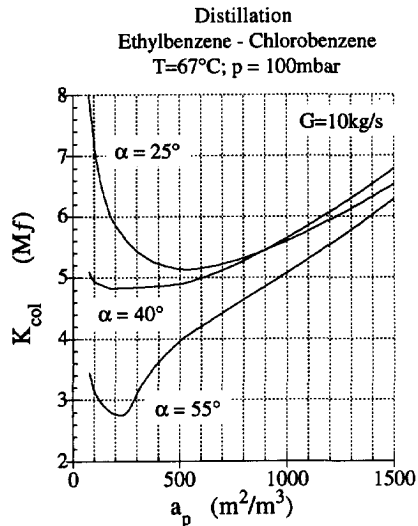


FIGURE 6.13: Investment costs in million guilders for a distillation column of ethylbenzene-chlorobenzene at 67°C as function of the packing specific surface area for indicated effective inclination at a gas load of  $G=10\text{kg/s}$ .

Figure 6.12 shows the normal tendencies for the most costs effective surface area with increasing capacity. The larger the column the smaller the specific surface area should be. Figure 6.13 shows for the large throughput the costs for three different effective inclination angles. The figure illustrates that the column with the larger inclination angle is the most cost effective. The graph of the packing of  $55^\circ$  shows a pronounced minimum at a specific surface

area of  $250\text{m}^2/\text{m}^3$ , which is 40% lower than all other options. This minimum has a different origin than those found at inclination angles of  $25^\circ$  and  $40^\circ$ . It is caused by the increased gas-liquid interaction, which improves the mass transfer. Figure 6.14 shows the pressure drop for the three effective inclination angles. The maximum pressure drop for a packing with effective inclination angle of  $\alpha = 55^\circ$  is found near the minimum costs of the column. The improved mass transfer is paid for by a larger total pressure drop over the column. When using a packing with inclination angle of  $40^\circ$ , an increase of the surface area from 250 to  $500\text{m}^2/\text{m}^3$  decreases the total pressure drop from 50 to 30mbar. However, the investment costs are hardly affected. The smaller inclination angle of  $25^\circ$  shows a lower pressure drop characteristic at normally applied specific surface areas, but the column is also more expensive.

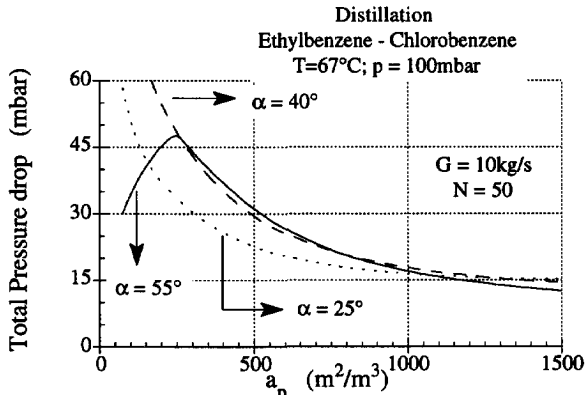


FIGURE 6.14: Total required pressure drop for a column operated at 80% of the flood point, for accomplishing required separation for various effective inclination angles as function of the specific surface area of the packing.

### SUGGESTIONS TO IMPROVE THE PACKING GEOMETRY

An important factor in the selection of the packing is the pressure drop per theoretical stage. It determines the pressure and temperature at the bottom of the column and thus the level of energy consumption. In addition, if the principle of heat pump is applied, the total pressure drop between the head and the foot of the column determines the economics of the separation process (Billet, 1983).

The operating characteristic of the packing is another criterion for that selection. Some products tend to foul or corrode the packing in a column. Experience has shown that simple geometries and smooth packing surfaces prevent fouling and corroding. The corrugated sheet therefore is one of the best bases for column internals.

The important parameters of the packing described so far are the specific surface area and the effective inclination angle. The specific area can be increased up to a point where the wetting becomes important. The effective inclination angle can be optimized and a significant improvement can be achieved by applying effective inclination angles near  $55^\circ$ . Also a decrease of the effective inclination angle improves the specific column volume (see figure 6.7A), but

when decreasing the effective inclination angle one has to overcome problems concerning the liquid distribution, since maldistribution will then continue through the whole column and is not smoothed by the packing. The question is: can the packing geometry be improved without changing the successful characteristics of the corrugated sheet?

To improve the packing performance one needs to focus on the parameters of a packing geometry. The description of packing geometry has been relatively successful because most packings are constructed in the same manner. Therefore the observed effects can be described similarly for different packing geometries. Most structured packings are made of sinuous shaped sheets, which are placed with opposite angles towards each other (see figure 6.15). The overall shape of these sheets changes hardly. Typically, the corrugation base is three times larger than the corrugation corrugation height. However, increasing the amplitude, or corrugation height, of the metal sheets has a clear advantage. To construct a packing with normal amplitude sheet and the same surface area two sheets are required compared with one sheet in the case where the amplitude is increased by a factor two (see figure 6.15). This construction has the advantage that the number of gas-gas contact planes decreases also by a factor two. According to Stoter, et al., (1993) a decrease of the gas-gas friction will substantially decrease the total friction factor. Next to this the total number of corrugated sheets decreases by a factor two, so that it simplifies the construction. This configuration has direct advantages for vacuum distillation (Woerlee, 1997).

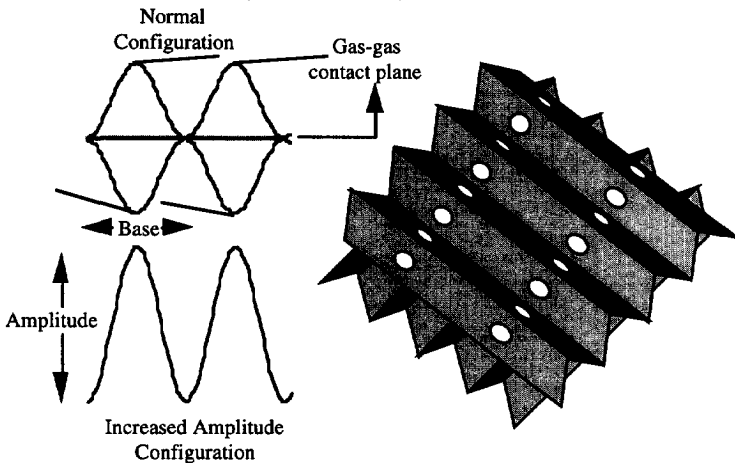


FIGURE 6.15: Shape of individual packing sheets and structured packing configuration.

The total friction is determined in equation (3.17), but the gas-gas contribution to the friction is accounted for in the constant, 0.6556, of this equation. To evaluate the potential of the increased amplitude packing this constant will be reduced with a factor 3 in the following calculations. Practically this means that the amplitude becomes twice the height of the base.

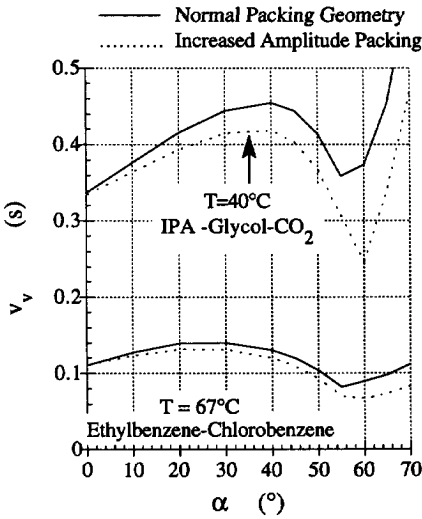


FIGURE 6.16: Estimated effective column volume at 80% of the flood point as function of the effective inclination angle for partially wetted surfaces using a specific surface area of  $a_p=250 \text{ m}^2/\text{m}^3$  and  $G=10\text{kg/s}$ .

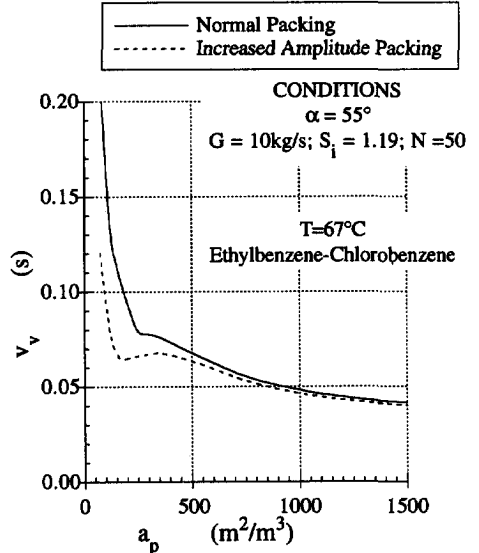


FIGURE 6.17: Estimated effective column volume at 80% of the flood point as function of the specific area, for partially wetted surfaces using an effective inclination of  $\alpha = 55^\circ$  and  $G=10\text{kg/s}$ .

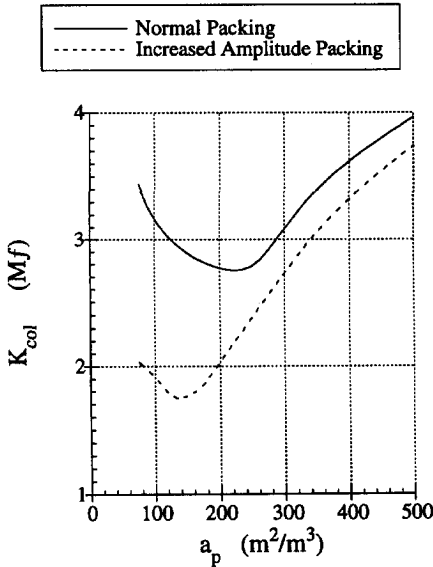


FIGURE 6.18: Investment costs for the distillation of ethylbenzene-chlorobenzene at 67°C as function of the packing specific surface area for  $G=10\text{kg/s}$  using: an effective inclination of  $\alpha = 55^\circ$  and  $N=50$ .

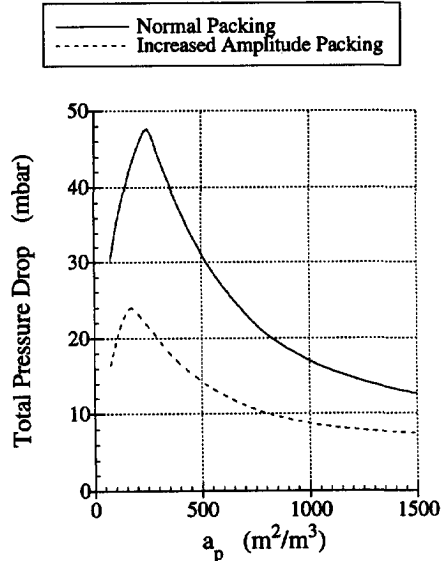


FIGURE 6.19: Pressure drop for the distillation of ethylbenzene-chlorobenzene at 67°C as function of the packing specific surface area for  $G=10\text{kg/s}$  using an effective inclination of  $\alpha = 55^\circ$  and  $N=50$ .

---

First the specific column volume as a function of the effective inclination angle is calculated. The result is shown in figure 6.16. Both cases show an improvement of the effective column volume, that increases with increasing effective inclination angle. The increased amplitude configuration is therefore evaluated as function of the specific surface area at an effective inclination angle of  $55^\circ$ , since the most pronounced differences will be found at large effective inclination angles. Figure 6.17 indicates an additional minimum caused by the increased friction factor at specific surface areas near  $250\text{m}^2/\text{m}^3$ . Flooding due to form drag is postponed due to the reduction of the total pressure drop, so that the column can be operated at larger gas loads. However, the gas-liquid interaction increases substantially in this region, which means an improved overall mass transfer characteristic.

More interesting for the user of the column are of course the total investment costs. Figure 6.18 shows the capital investment for the increased amplitude packing as function of the surface area. Due to the further decrease of the minimum caused by the gas liquid interaction a maximum cost reduction is found at a specific surface area of  $150\text{m}^2/\text{m}^3$ . At this point the investments are reduced over 50% compared with the previous situation, which certainly can be called substantial.

Pronounced is the reduction of the required pressure for the separation. Figure 6.19 shows that the pressure drop is reduced by a factor 2 compared with the normal packing configuration. Compared with the pressure drop of a normal packing with an effective inclination of  $25^\circ$ , the increased amplitude packing with an effective inclination angle of  $55^\circ$  has a 30% lower pressure drop. Clearly the above calculations are based on model considerations only and should be validated by experiments.

When applying larger effective inclination angles, the pressure drop caused by the column wall is increased substantially (see equation (3.19)). It is for this reason that the presented calculations are carried out for large columns. The effect of the column wall is important for two reasons. It is realised that the pressure in radial directions of the column is unlikely and even undesired to vary substantially. This means that the superficial gas velocity has to decrease near the column wall and increases in the centre of the column. This causes a gas maldistribution. Second, the wall causes a form drag that increases the pressure drop over the column and decreases the macroscopic flood point. It is therefore advantageous to reduce the wall effects of the column, especially for small columns and for large effective inclination angles.

The wall effects can for instance be balanced by increasing the number of holes in the packing sheets in the wall zone, so that the effective inclination angle is decreased and a more smooth turn for the gas phase is created. Another possibility would be to insert additional metal sheets between the corrugated plates near the column wall only.

**CONCLUDING REMARKS**

In this chapter the model proposed, connecting the pressure drop over packed beds with the mass transfer in both the liquid and the gaseous phase as developed in chapters 3 to 5, has been extended to account for effective wetting and then used for a performance and economical evaluation of packed beds.

The wetting quality of a packing has been described using a characteristic wetting Reynolds number at which the efficiency is 50% of the potential at total wetting. A density correction term is used to account for operating pressure effects, so that the characteristic wetting Reynolds number can be used for a series of packing geometries.

The model was validated using data of packing suppliers. The analysis revealed the influences of the specific surface area and the effective inclinations on the mass transfer. This is done for a system with mainly mass transfer resistance in the gas phase and for a system with additional mass transfer resistance in the liquid phase. The analysis was used to optimize the design of packed columns for different applications. It appears possible to find the most cost effective packed column by optimising the packing geometry. The most cost effective column design will depend on the components involved and the application size. When applying a carbon steel shell, the cheapest column for the application with liquid phase resistance is with small specific surface areas ( $a_p \approx 100\text{m}^2/\text{m}^3$ ), while for the application with only gas phase resistance the most cost effective column uses relatively large specific surface areas ( $a_p \approx 500\text{m}^2/\text{m}^3$  at medium capacities and  $a_p \approx 300\text{m}^2/\text{m}^3$  at very large capacities). However, the economics here depend strongly on the construction materials used. The analysis also showed that packing with a large effective inclination angle ( $\alpha \approx 55^\circ$ ) is the most cost effective. This is caused by the increasing contribution of the gas-liquid interaction. However, these inclination angles therefore also will have the largest pressure drop.

Finally this study indicated the potential for a real improvement of the packing geometry. Most promising modification seems to be increasing the amplitude of the corrugations. In this case the capital investment could be decreased by approximately 50%, while 50% reduction of the pressure drop appears possible.

**NOTATION**

Symbol	Description	Unit
$a_p$	Specific packing area.....	$\text{m}^2/\text{m}^3$
$D_{\text{col}}$	Column diameter .....	m
$D_i^G$	Gas diffusion coefficient .....	$\text{m}^2/\text{s}$
$D_i^L$	Liquid diffusion coefficient .....	$\text{m}^2/\text{s}$
$f_{\text{wet}}$	Wetting function.....	



G	Gas flow.....	kg/s
G"	Gas flux .....	kg/m <sup>2</sup> /s
G" <sub>m</sub>	Molar gas flux .....	mol/m <sup>2</sup> /s
H <sup>etp</sup>	Height of an equivalent theoretical stage.....	m
H <sup>etp</sup> <sub>eff</sub>	Effective height of an equivalent theoretical plate for wetting .....	m
H <sub>col</sub>	Height of the column.....	m
K <sub>col</sub>	Installed costs of a column .....	f
K <sub>S</sub>	Purchase costs of the column shell.....	f
K <sub>p</sub>	Purchase costs packing .....	f
k <sub>i</sub> <sup>OG</sup>	On gas phase based overall mass transfer coefficient .....	m/s
L	Liquid flow.....	kg/s
L"	Liquid flux .....	kg/m <sup>2</sup> /s
L" <sub>m</sub>	Molar liquid flux.....	mol/m <sup>2</sup> /s
m <sub>i</sub>	Derivative of the equilibrium line.....	mol/mol
N	Number of equilibrium stages .....	
p	Pressure .....	Pa
S <sub>i</sub>	Stripping factor S <sub>i</sub> = m <sub>i</sub> G <sub>m</sub> /L <sub>m</sub> .....	
T	Temperature.....	K
u <sub>int</sub>	Interface velocity .....	m/s
u <sub>SG</sub>	Superficial gas velocity .....	m/s
u <sub>SL</sub>	Superficial liquid velocity .....	m/s
V <sub>col</sub>	Volume of the column .....	m <sup>3</sup>
v <sub>v</sub>	Specific column volume .....	s
x <sub>i</sub>	Mol fraction in the liquid phase.....	mol/mol
y <sub>i</sub>	Mol fraction in the gas phase.....	mol/mol
α	Effective inclination angle .....	°
ε <sub>0</sub>	Void fraction .....	m <sup>3</sup> /m <sup>3</sup>
η <sub>G</sub>	Dynamic gas viscosity .....	Pa s
η <sub>L</sub>	Dynamic liquid viscosity .....	Pa s
θ	Relative interface position .....	
ρ <sub>G</sub>	Gas density.....	kg/m <sup>3</sup>
ρ <sub>L</sub>	Liquid density.....	kg/m <sup>3</sup>
σ	Surface tension .....	N/m
Ψ <sub>G-L</sub>	Gas-liquid interaction parameter.....	

Re<sub>G</sub> Gas phase Reynolds number..... 
$$Re_G = \frac{\rho_G \left( \frac{u_{SG}}{\theta^2 \epsilon_0 \cos \alpha} - u_{int} \right) 2\theta r_0}{\eta_G}$$

$Re_L$	Liquid phase Reynolds number.....	$Re_L = \frac{4L''}{\eta_L a_p}$
$Re_{L-w50}$	Liquid Reynolds number at which the packing performance is 50%.....	
$Re_{w50}$	Dimensionless number at which the packing performance is 50% .....	

---

REFERENCES

- [1] Billet, R., (1983), *Energieeinsparung bei thermische Stofftrennverfahren, Anwendungen im Technologischen Umweltschutz*, Dr. Alfred Hüthig Verlag, Heidelberg.
- [2] Billet, R., (1986), *Packed Column Analysis and Design*, Glitsch, Inc., Dallas, TX (1986).
- [3] Billet, R., (1992), *State of the Art in Development of Column Packings and their Optimal Surface Geometries*. *Fat Sci. Technol.* **94** (12) pp 571-579.
- [4] Fair, J.R., and Bravo J.L., (1990), *Distillation Columns Containing Structured Packing*, *Chem. Eng. Prog.*, **86** (1) pp. 19-29.
- [5] Hoek, P.J., (1983), *Large and Small Scale Liquid Maldistribution in Packed Towers*, Ph.D. thesis, Delft Technical University, Delft.
- [6] Klemas, L., and Bonilla, J.A., (1995), *Accurate Assess Packed Column Efficiency*, *Chem. Eng. Prog.*, **92** (7) pp. 27-45.
- [7] Sulzer Brother Ltd., (1989), *Separation Columns for Distillation and Absorption*. Information Bulletin.
- [8] Stoter, F., Olujic, Z., and de Graauw, J., (1993), *Modelling of Measurements of gas flow distribution in corrugated sheet structured packings*, *Chem. Eng.J.*, **53** pp. 55-66.
- [9] Stoter, F., (1993), *Modelling of Maldistribution in Structured Packings*, Ph.D. thesis, Delft Technical University, Delft.
- [10] Webci and Wubo, (1995), *Dutch Association of Cost Engineers-Prijzenboekje*, Misset, Leidschendam, The Netherlands.
- [11] G.F. Woerlee, *Gestructureerde pakking voor stof- en/of warmte-uitwisseling tussen vloeistof en een gas, alsmede houder voorzien van een dergelijke pakking* Dutch application NL 1005990, priority date 6.5.1997.

## Hydrodynamics and Mass Transfer in Packed Columns using Supercritical Fluids

One of the main objectives of this thesis is the description of column hydrodynamics in supercritical fluid applications. In the previous chapters it was not intended to obtain the most accurate description of counter-current flow in packed beds, but to acquire general hydraulic packed bed relations, which can be extended to supercritical conditions. This has been achieved by using few empirical relations at specific points in the developed theories and models. The previous chapters, might have seem not specifically related to supercritical applications, but in essence they are. Here we will harvest from our efforts of the earlier general hydrodynamic and mass transfer description and show that the obtained design rules for normal gas liquid separations can be used at supercritical conditions.

So far only limited data for the hydrodynamic behaviour at supercritical conditions are available. To our knowledge the only other research group studying hydraulics with similar objectives and methods is at the Technische Universität Hamburg-Harburg (Meyer and Brunner, 1994). They state "adapting correlations that were derived for normal operation pressure and high temperature applications is unsafe". Our extensive study on hydrodynamics and mass transfer shows that we share their opinion. The following experimental study on hydrodynamic at supercritical conditions is therefore one of the first and no comparable data are available at this moment. The hydrodynamic data are collected using the experimental set-up described in detail in chapter 2.

Given the larger investment costs of supercritical applications, a good mass transfer understanding at supercritical condition would be very welcome. Although more experimental studies on mass transfer than for hydraulics in supercritical applications are available (Carmelo et al., 1993; Bernad et al, 1993; de Haan, 1991; Brunner, 1991), no direct comparison of the mass transfer data is possible because each study uses different compounds. Moreover, the use of small columns with limited number of equilibrium stages does not increase the clarity. It is for this reason that we have started to compare all the available data at more (see, e.g., Sulzer, 1986) and less (see, e.g., Krehenwinkel, 1986) conventional conditions in order to be able to develop more reliable design rules. In the following chapter it will be shown that no unexplained deviations with the in chapter 3 to 6 presented models and theories are found.

## FLOODING AND PRESSURE DROPS IN SUPERCRITICAL SYSTEMS

Flood point measurements at supercritical conditions encounter several difficulties. One difficulty is caused by the often substantial solubility of the supercritical solvent in the liquid phase and the solubility of the liquid in the solvent phase. These effects change the load factor within the column and cause changes in the physical properties of both the liquid and solvent phase. Flood points are often obtained by increasing either the gas flow at constant liquid flow or the reverse. Since the flood point is sensitive to small system changes, the procedure of changing one load only, often leads to the most reproducible results. Besides this an evaluation of pressure drop as function of an increasing gas load at constant liquid load or vice versa is simple. When the liquid and gas are insoluble into each other, the method results in an approach of the critical capacity curve, which is illustrated in figure 7.1 by the two arrows.

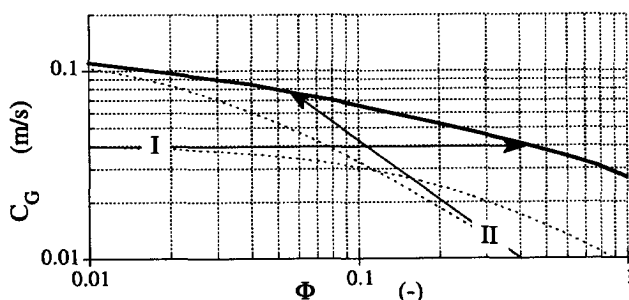


FIGURE 7.1: Approaching the capacity curve by increasing the liquid (case I) and the gas load (case II). The dotted lines indicate the effect of this approach when using partly soluble components.

When using a supercritical fluid, one would like to apply the method of changing only one load as well. However, it is nearly impossible because when the liquid load is increased only, the gas will dissolve in the liquid phase, thus increasing the liquid flow and decreasing the gas flow and as a result the flooding point will not be reached. The dotted line of figure 7.1 (case I) illustrates this situation. When only the gas load is increased, liquid will dissolve in the gas phase, which can cause an approach of the critical capacity curve as indicated in figure 7.1 (case II). Systems of commercial interest obviously have a gas phase solubility. Flooding data therefore have to be collected by both increasing the liquid and the gas load.

In chapter 4 the influence of the physical properties on the critical capacity factor was studied by changing only one property. In reality all properties are closely connected. Severe physical property changes occur when using supercritical fluids. Since the physical properties in a supercritical fluid can only rarely be measured directly, the mutual solubilities require estimation methods for the physical properties. The problems described above can be avoided to a large extent, using a water-carbon dioxide system. The solubilities of these components into each other are limited, so that the system can be approximated by treating the components as

insoluble. The flood points are determined by analysing the pressure drop over the packing. A sudden increase of the pressure drop characterises the flood point. Illustrations of the pressure drop curves measured in with the CO<sub>2</sub>-water system and the subsequently determined flood points are shown in the figure 7.2 for various "extraction" pressures.

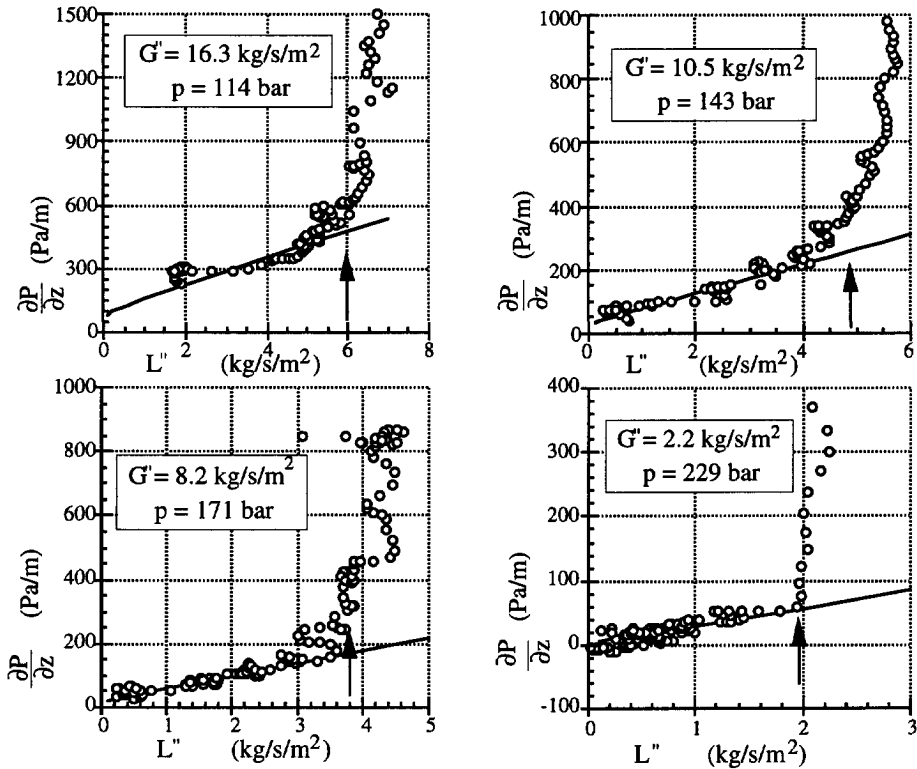


FIGURE 7.2: Measured (points) and calculated (continuous lines) pressure drops over gauze packing ( $a_p=660\text{m}^2/\text{m}^3$ ,  $\varepsilon_0=0.97$ ,  $\alpha=30^\circ$ ,  $D_{\text{col}}=36\text{mm}$ ) as function of the liquid load (water) for given gas flow at 50°C. The arrows indicate the observed flood points.

The calculated pressure drops, using the method presented in chapter 3, show a good agreement with the experimental results. The pressure drop over the packing is small compared with pressure drops measured at atmospheric pressure. This is primarily caused by the smaller density difference between the phases. The inaccuracy of the differential pressure measurements accuracy approximately was 30Pa/m. However, the white noise could easily be filtered out by using a triangle shaped moving average filter over 5 or 7 data points (see, e.g., Oppenheim et al., 1983) so that the inaccuracy of each data point was improved to 10Pa/m. An interesting point is the small contribution of the gas-liquid interaction term ( $\psi_{G-L}$ ) in the pre-loading range. The pressure drop is hardly affected by this factor.

During the experiments both liquid raffinate and the liquid feed streams are measured, so that the hold-up can be determined by subtracting the integrated values in time. A dynamic liquid hold-up curve, measured at 171 bar and the calculated curve are shown in figure 7.3. The arrow in figure 7.3 indicates the flood point. The left hand part of the hysteresis loop is caused by an arbitrary reduction of the liquid pump. In this system the flooding started at the bottom of the column, so that at flooding the liquid accumulates in the packing.

The de-flooding can be analysed by plotting the bottom flow of the column against the liquid feed (see figure 7.4). This method can be used also for determination of the flood point and therefore verifies the pressure drop method. The liquid bottom flow first reaches the values of the flood point, in this case a value of  $3.7 \text{ kg/s/m}^2$ , which is within the accuracy of the value ( $3.8 \pm 0.3 \text{ kg/s/m}^2$ ) found with the pressure drop method, where after it drops to a stable bottom flow of  $3.1 \text{ kg/s/m}^2$ . This is the de-flood point and illustrates the flow hysteresis of the system.

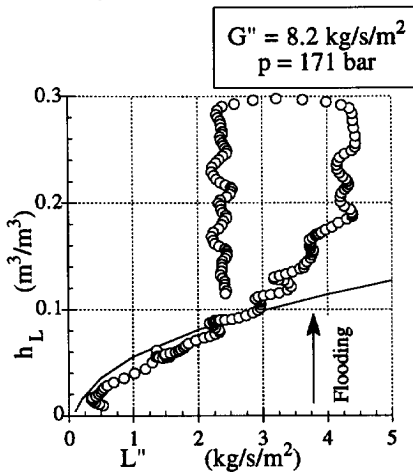


FIGURE 7.3: Measured and calculated (continuous lines) liquid hold-up in the column as function of the liquid load.

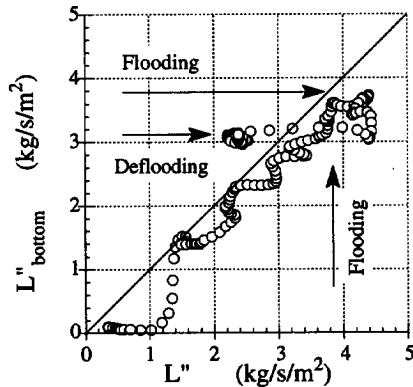


FIGURE 7.4: The feed flow and the bottom or "raffinate" flow. The flood and de-flood point are indicated.

All measured critical capacity factors at supercritical conditions for the system water carbon dioxide are shown in the figures 7.5A. The experimental data and used physical properties are given in appendix A. Figure 7.5A also shows some data points obtained at atmospheric pressure applying a water-air system. The low pressure data are close to the critical capacity curve using the estimated relative critical capacity factor of:  $C_r = 0.766$ . The data collected at elevated pressures are 50-70% lower than the predicted value. This is possibly due to the pulsations of the used membrane pump for the carbon dioxide flow. At small density differences and large flow parameters (see measurements at  $p=229 \text{ bar}$ ) the measured flood points are even less than 30% of the predicted value. This phenomenon was also observed by Meyer and Brunner, (1993). Whether this concerns a systematic deviation or erratic data cannot be decided at this point.

The system hexadecane-carbon dioxide has a reasonable mutual solubility and as a result the physical properties of especially the liquid phase change considerably. Figure 7.5B shows measured flood points for system hexadecane-carbon dioxide. Also for this system the measured flood points are below the predicted ones, but they follow the critical capacity curve well. This is rather odd, since the data are not corrected for the different physical properties of the system, which change dramatically at the given conditions.

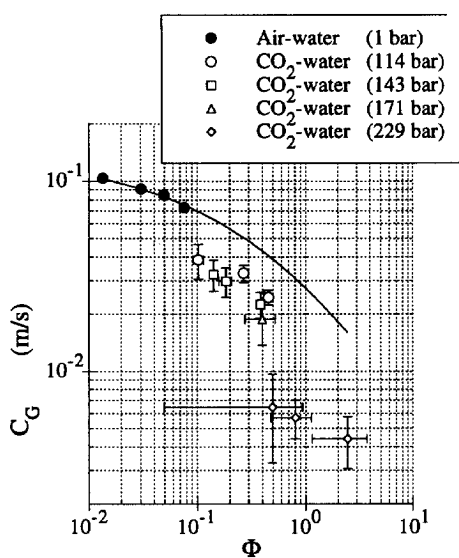


FIGURE 7.5A: The measured and estimated (line) critical capacity factors as found for water-CO<sub>2</sub> at 50°C and various pressures. The experimental accuracies are indicated.

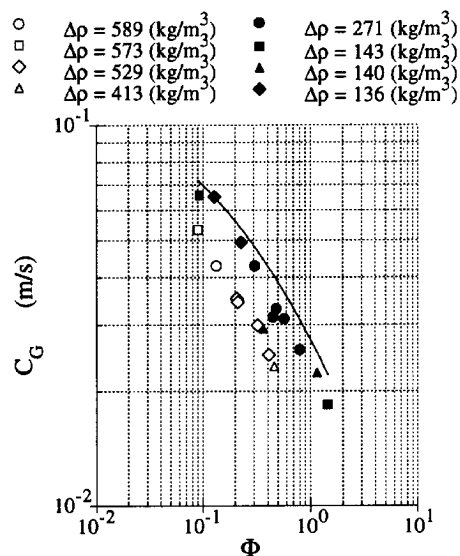


FIGURE 7.5B: The measured critical capacity factors for hexadecane-CO<sub>2</sub> at various densities. The continuous line indicates the overall correlation.

This system shows no large deviations of the measured and predicted critical capacity factor for small density differences and large flow parameters. The opposite is even observed when the measured data points are "corrected" for the physical properties using equation (4.23). This is shown in figure 7.6. The hexadecane-carbon dioxide data can be split in two series. The first series is approximately at 80% of the original flooding curve while the second series at larger gas densities lies approximately at 135% of the original capacity curve. We believe that the reason for this phenomenon is the solubility of the hexadecane in the gaseous carbon dioxide phase. When hexadecane dissolves in the fresh carbon dioxide in the bottom of the column, the capacity factor moves along the dotted line of figure 7.1 (case II) at the bottom of the column. In the extreme case all the liquid dissolves in the gas phase so that the flow factor becomes zero. When only a substantial part of the liquid dissolves, this effect stabilises the bottom part of the column. It is therefore intriguing that the capacity factors measured with hexadecane for high densities are more stable than the values obtained at lower gas densities. This supercritical

system seems to stabilise the most unstable part of the column by natural means. Given these results it is therefore our opinion that the observed deviations at large flow parameters for the water-CO<sub>2</sub> system are caused by the sensitivity of the system for local disturbances.

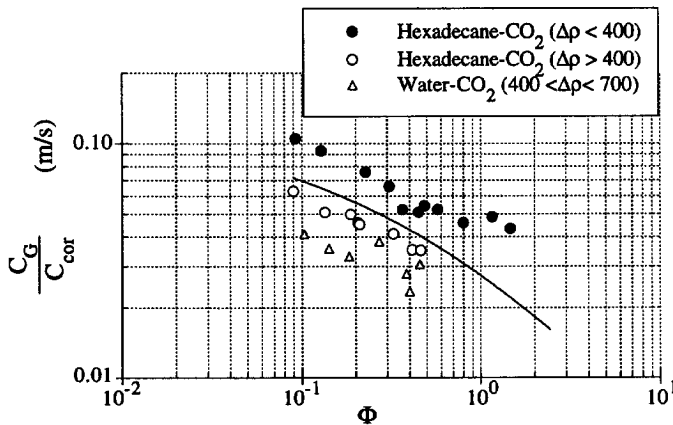


FIGURE 7.6: The corrected (equation (23)) measured critical capacity factors for hexadecane-CO<sub>2</sub> at various densities. The continuous line indicates the overall correlation.

Hiller et al., (1993) reported the disintegration of a liquid falling film, generating a mist of tiny droplets, at molar carbon dioxide concentrations of 70 to 80% in the liquid phase. Although these concentrations are applied in this study as well, no mist was observed. One also would expect a decrease of the capacity when a mist is generated. Given the presented results, no evidence for this phenomenon was observed in this study.

#### MASS TRANSFER AT SUPERCRITICAL CONDITIONS

Although the number of mass transfer studies is larger than the number of studies on hydraulics, the complexity of the problem is such that the knowledge on the phenomena is even more limited than on hydraulics. This is caused by a large number of experimental uncertainties i.e.: the entrance effects of the solvent feed and the product feed into the extraction column, the use of different separation systems, the thermodynamic equilibrium sensitivity of these systems for small variations in temperature and pressures, multi-component diffusion aspects, dramatic changes of the physical properties of especially the liquid phase, different gas-liquid ratios at different points in the column, recycled components in the solvent phase and the limited height and diameter of the experimental column. Moreover the interpretation of the results using earlier reported models for structured packed beds will be extremely difficult if not impossible when a liquid mass transfer resistance is present.



To avoid some of the above mentioned experimental problems we have selected two three component systems of which sufficient independent thermodynamic data were available. The first has strong mass transfer resistance in the liquid phase. Stripping experiments were carried out with the system isopropyl alcohol (IPA) - 1,2-ethanediol (ethylene glycol) and carbon dioxide (CO<sub>2</sub>) at a pressure of 125bar and a temperature of 50°C. The liquid feed contained 26.3%mol of IPA in ethylene glycol and was pumped into a packed column containing wired gauze packing to ensure total wetting. The IPA concentration in the raffinate stream was analysed so that the number of equilibrium stages could be established using the approach given in appendix B. To enable these calculations a sufficient knowledge of the thermodynamic behaviour is required. Independent binary vapour-liquid equilibrium data from literature were used to determine the binary interaction of the components. These were used to model the ternary system with the Peng-Robinson (1976) equation of state. The binary system IPA - ethylene glycol was described using reported data given by Gmehling et al., (1990). Data of Kaminishi et al., (1989) was used to describe the systems carbon dioxide - ethylene glycol and data of Radosz (1986) was used to describe the binary system carbon dioxide - isopropyl alcohol. The found binary interaction parameters agree well with equilibrium measurements carried out at our experimental set-up. Appendix 7.C shows the pure component data, the established binary interaction parameters, the column characteristics, and the estimated physical properties. The measured and estimated heights of theoretical equilibrium stages are shown in the parity plots of figures 7.8A and 7.8B. In these figures two possible liquid exposure lengths are evaluated. The triangle symbols represent an exposure length similar to the one proposed by Bravo et al., (1985) and the dots show the estimated values using an exposure length that is proposed in chapter 5 by equation (5.46). The model of this study estimates the mass transfer resistance in the gas phase on approximately 1/3 of the total mass transfer resistance. Clearly, the measured number of equilibrium stages are relatively close to the values estimated. The measured mass transfer coefficients are still smaller than the estimated values. Several causes can be suggested for these deviations, e.g.: estimated physical properties, thermodynamic deviations, liquid maldistribution, back mixing of the gas phase due to larger density in the top of the column, larger HETP for exit and entrance stage. Considering the possible uncertainties of the applied system the outcome is reasonable good. Due to the solubility of the solvent in the liquid phase and vice versa, the calculation of the HETP from the experimental data is not straightforward. To avoid an interruption of our main objective, being the evaluation of the deduced design rules, a justification and full report of the data analysis is given in appendix 7.C. However, the in this appendix described methods are essential for a correct experimental analysis.

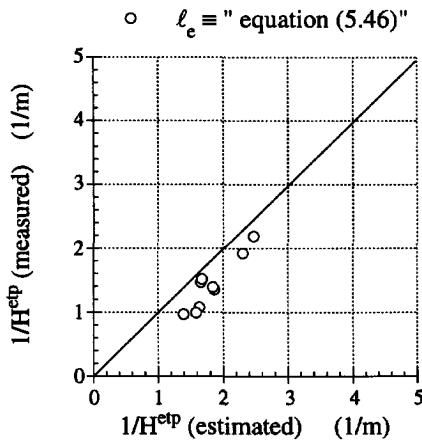


FIGURE 7.8A: Parity plot of the average measured number of equilibrium stages per meter with the average estimated number using the model presented in chapter 5. The data is presented in appendix 7.C.

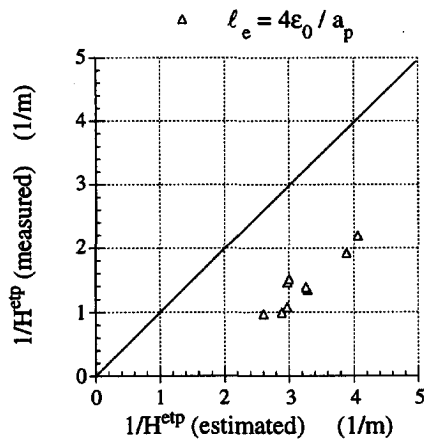


FIGURE 7.8B: Parity plot of the average measured number of equilibrium stages per meter with the average estimated number using the model of Bravo et al., (1985).

Other experiments on the same column were conducted to analyse the mass transfer at supercritical conditions, when the resistance is mainly located in the gas phase. The system 2-methyl naphthalene - hexadecane - carbon dioxide was selected for these experiments. Data of the Haan, (1991) were used to model the thermodynamic behaviour of the system. In this system the mass transfer resistance is for 90% located in the gaseous phase. The ternary system is also modelled using the Peng-Robinson equation of state. The system has the disadvantage that it is extremely sensitive for temperature and pressure. A temperature difference of less than 1°C changes the equilibrium derivative ( $m_i$ ) with more than 20%. Depending on the applied stripping factor, the inaccuracy in the measured HETP can easily exceed 100%. A reasonable accuracy of the measured HETP can only be obtained when a stripping factor larger than 0.8 is applied. Experiments were carried out at three conditions. The main results of the experiments are shown in the parity plot of figure 7.9. This figure only shows data with an estimated experimental error less than 15%. A reasonable agreement with the estimated HETP is found. A justification and full report of the data analysis, results and the applied physical properties are given in appendix 7.D. Again the described methods in this appendix are essential for a correct experimental analysis.

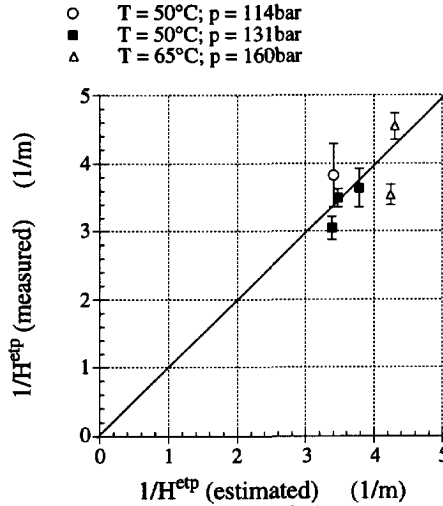


FIGURE 7.9: Parity plot of the average measured number of equilibrium stages per meter with the average estimated number of equilibrium stages for the system 2-methyl naphthalene - hexadecane - carbon dioxide. Full data are given in appendix D.

The presented comparison is carried out using Fick type approach towards the mass transfer, were the entrance effects were avoided by adding two equilibrium stages of average height. However, the HETP of the entrance stage for the CO<sub>2</sub> and entrance stage for the liquid feed of the IPA-ethylene glycol-CO<sub>2</sub> system are probably larger due to a larger liquid diffusivity. The HETP of the entrance stages for the 2-methyl naphthalene - hexadecane - CO<sub>2</sub> system, are probably smaller due to the little resistance in the liquid phase. A multi-component approach would be required to clarify the entrance effects in detail. However, the experimental data show that the models developed in this thesis also describe the mass transfer at supercritical conditions.

#### THE DESIGN OF A PACKED SUPERCRITICAL SEPARATION COLUMN

Given the larger capital investments for pressure applications the objective of the engineer designing a supercritical application would nearly always be the design of the cheapest column. When the extraction conditions are established the designer can select a packing. In the case of a pressure application the costs of the column shell will be dependent on the mass of the column. The mass of the column  $m_{col}$  is calculated using the column wall thickness  $t_{col}$  (see e.g., Coulson et al., 1985), the column diameter  $D_{col}$ , and the height of the column  $H_{col}$ , as:

$$m_{col} = t_{col} \pi D_{col} H_{col} \rho_S = \frac{p D_{col}}{2\sigma} \pi D_{col} H_{col} \rho_S = 2 \frac{p \rho_S}{\sigma} V_{col} \quad (7.1)$$

Here  $\rho_S$  represents the density of the steel,  $p$  is the operating pressure and  $\sigma$  represents the design shear stress of the steel. The total costs ( $K_{col}$ ) of a packed column are the sum of the purchase costs of the column shell ( $K_S$ ) and the purchase costs of the packing ( $K_p$ ), multiplied

with appropriate factors (see chapter 6). The investment costs expressed in Dutch guilders ( $f$ ) of an installed pressure column ( $p > 50\text{bar}$  and  $V_{\text{col}} > 3\text{m}^3$ ) made of 316L steel can be correlated as function of the diameter and height (Billet, 1992, chapter 6, chapter 9):

$$K_{\text{col}} = 2 \left( 2.5K_S + 1.5 K_p \right) = 5 (65000 + 160 p_{\text{bar}} V_{\text{col}}) + 3 a_p \left( 25 + \frac{7}{D_{\text{col}}} \right) V_{\text{col}} \quad (7.2)$$

Here the pressure should be expressed in bar. Equation (7.2) is similar to the equation (6.4), but it shows a stronger influence of the column diameter, so that the whole expression is nearly linearly dependent on the column volume. This means that the costs of a column are nearly directly related with the specific column volume.

Equation (7.2) can be used to evaluate the costs of supercritical application, as has been done in chapter 6. Here the removal of methyl naphthalene from hexadecane using carbon dioxide as solvent will be analysed. The necessary physical and thermodynamic properties are listed in table VII.DII. For the calculations the stripping factor is taken as  $S_i=1$ . Using the molar densities and the derivative of the equilibrium line;  $m_i=0.15$ , the mass liquid flow is established as 24% of the gas stream, which will be taken as:  $G=3\text{kg/s}$ . This means that approximately 1 te/h of hexadecane is treated in this application. The specific column volume is shown in figure 7.10A, while the column diameter and height are shown in figure 7.10B.

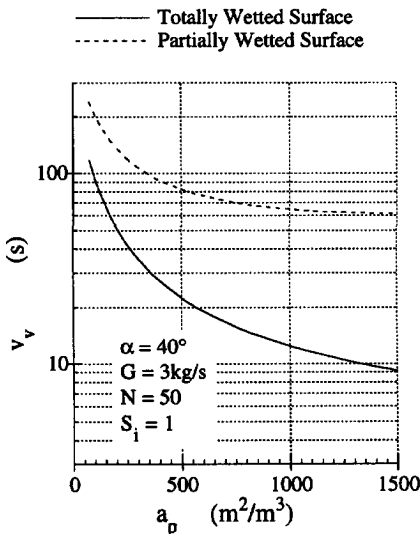


FIGURE 7.10A: Estimated performance at 80% of the flood point as function of the specific area, for totally and partially wetted surfaces for 2-methyl naphthalene - hexadecane -  $\text{CO}_2$  at  $60^\circ\text{C}$  and 160 bar.

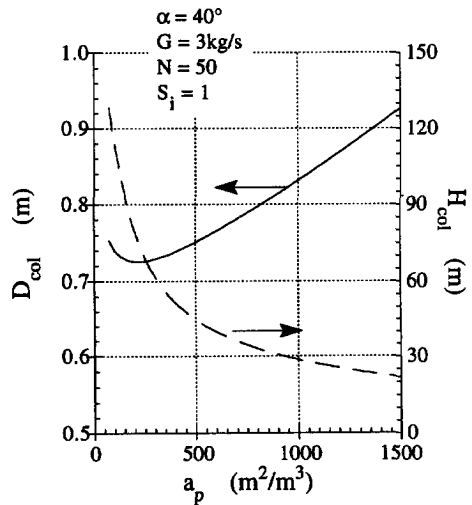


FIGURE 7.10B: Estimated column diameter and height at 80% of the flood point as function of the specific area, using partially wetted surfaces for the system 2-methyl naphthalene - hexadecane -  $\text{CO}_2$  at  $60^\circ\text{C}$  and 160 bar.

Figure 7.10A shows the results for partial wetted and totally wetted surfaces. To enable a comparison with the results of chapter 6 a characteristic wetting number of  $\text{Re}_{w50} = 550$  is used

in equation (6.2). Due to the large gas density in this application the use of this value causes a relative significant difference between partial wetted and totally wetted specific column volumes. The specific column volume nearly is three times larger than for a totally wetted column.

A somewhat different type of curve is obtained when evaluating the specific column volume as function of the effective inclination angle. This is shown in figure 7.11A, while the resulting column dimensions are shown in figure 7.11B.

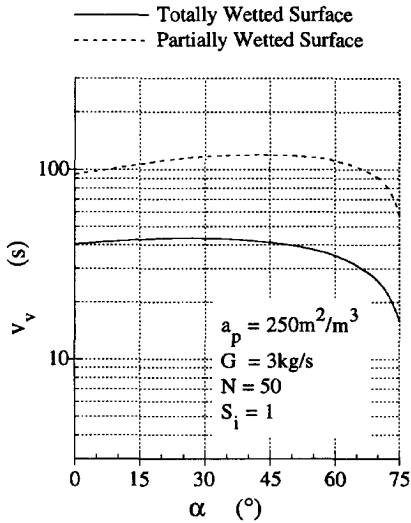


FIGURE 7.11A: Estimated performance of packing configuration as function of the effective inclination angle for totally and partially wetted surfaces for the system 2-methylnaphthalene-hexadecane- $\text{CO}_2$  at  $60^\circ\text{C}$  and 160 bar.

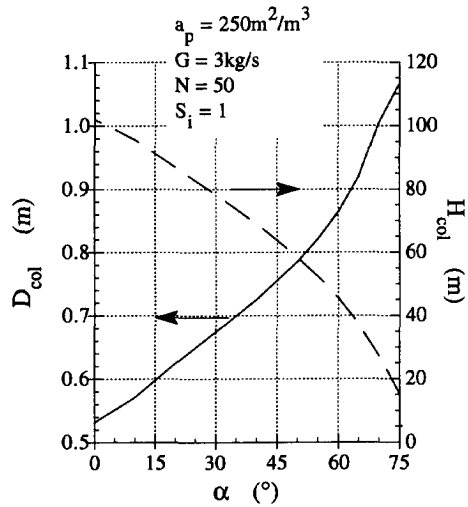


FIGURE 7.11B: Estimated column diameter and height at 80% of the flood point as function of the effective inclination angle using partially wetted surfaces for the system 2-methylnaphthalene-hexadecane- $\text{CO}_2$  at  $60^\circ\text{C}$  and 160 bar.

Figure 7.11A differs from figure 6.7A in the fact that the minimum is located at even larger effective inclination angles ( $\alpha = 75^\circ$ ). It is only at these effective inclination angles that the gas liquid interaction becomes important for the specific column volume. The predicted quality of the model has not been tested at these large effective inclination angles, so that it should be considered as an extrapolation only. However, given the fact that these effective inclination angles are found for random packings, it indicates that the use of random packing for this application can be defended.

This tendency is also observed when the installed costs of the column are calculated. Figure 7.12 shows the costs of an installed column for this application as function of the applied specific areas for different effective inclination angles using partially wetted surfaces. Although a cost minimum is found for a large effective inclination angle, the difference is not so pronounced as found with the distillation of ethylbenzene-chlorobenzene (see figures 6.10 and

6.13). This is due to fact that hardly no use is made of the mass transfer increase due to the gas liquid interaction. Clearly, the costs of a supercritical extraction column would significantly improve when a surface is installed with total wetting characteristics.

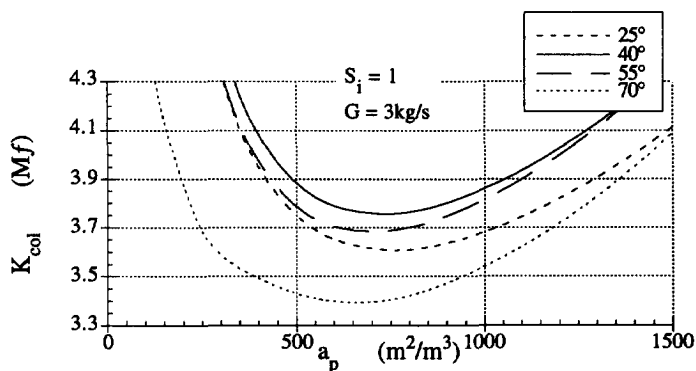


FIGURE 7.12: Investment costs in million guilders for the supercritical extraction of 2-methyl naphthalene - hexadecane -  $CO_2$  at  $60^\circ C$  and 160 bar as function of the packing specific surface area for indicated effective inclinations angles.

The above calculations are based on assumptions that cannot be fully validated at this moment. They nevertheless show tendencies which can be valuable for designing supercritical separation. Chapter 8 will show that next to the cost effective design of the separation column there are also other options to reduce the costs of a supercritical separation.

### CONCLUDING REMARKS

In the previous chapters general approaches are used to describe the hydrodynamic behaviour of packed beds. In these approaches it is tried to rely on empirical corrections as few as possible. When required this has been done on specific places, being equation (3.23) for the gas liquid interaction describing the pressure drop, equation (4.16) applying 1/4 of the maximum droplet size and equation (6.2) describing the wetting efficiency of the packing. In the previous chapters the models have been tested for systems with rather conventional physical properties. In this chapter the developed models are used and tested in a two phase system of which one will be a supercritical fluid. This causes an extreme variation of the physical properties. It is especially here, as always has been the intention, that we have harvested from our previous efforts.

The in chapter 4 developed estimation method for the flood point needed a wider experimental verification, which has been presented in this chapter. It has been found that the model is consistent with the experimental determined flood points in supercritical applications. It has been validated successfully for systems with varying gas viscosity (range: 15-73  $\mu Pa s$ ),

liquid viscosity (range: 0.2-60 mPa s), surface tension (range: 0.4-73 mN/m) and density difference (range: 130-1100 kg/m<sup>3</sup>). However, it also has been made clear that flooding remains a subtle phenomenon, which depends strongly on its hysteresis, while secondary influences can easily take over control.

In this chapter it has been shown that the measured mass transfer in supercritical separation is in excellent agreement with the developed theory. The connection with hydrodynamic behaviour proves to hold at the extremely varying conditions of supercritical fluids. Finally it has been shown with an example that the method of optimising the packing geometry can also be applied for supercritical applications.

APPENDIX 7.A

Measured flooding data at supercritical conditions. Indicated are the process conditions, the estimated physical properties, the applied gas and liquid flows and the measured and estimated correction factors. Besides this, the table for hexadecane-carbon dioxide also shows the mass solubilities, and the pure liquid and gas load.

p bar	T °C	$\eta_L$ mPa s	$\eta_G$ $\mu$ Pa s	$\rho_G$ kg/m <sup>3</sup>	$\rho_L$ kg/m <sup>3</sup>	$\sigma$ mN/m	$G''$ kg/s/m <sup>2</sup>	$L''$ kg/s/m <sup>2</sup>	$C_{cor}$ meas	$C_{cor}$ est
Water- Carbon Dioxide										
114	50	0.582	36.9	537	1000	34.78	12.20	7.60	0.61	0.80
114	50	0.582	36.9	537	1000	34.78	16.30	6.00	0.65	0.86
114	50	0.582	36.9	537	1000	34.78	19.20	2.70	0.56	0.94
143	50	0.585	49.1	679	1000	27.95	10.50	4.90	0.52	0.81
143	50	0.585	49.1	679	1000	27.95	13.90	3.10	0.52	0.90
143	50	0.585	49.1	679	1000	27.95	15.10	2.60	0.51	0.90
171	50	0.590	56.4	742	1000	25.27	8.20	3.80	0.44	0.80
229	50	0.595	67.8	817	1000	22.34	1.70	4.60	0.27	0.55
229	50	0.595	67.8	817	1000	22.34	2.20	1.96	0.19	0.71
229	50	0.595	67.8	817	1000	22.34	2.50	1.36	0.17	0.77

Gauze Packing Characteristics		
$a_p$	660	m <sup>2</sup> /m <sup>3</sup>
$\epsilon_0$	0.97	m <sup>3</sup> /m <sup>3</sup>
$\alpha$	30°	
$D_{col}$	36	mm
$H_p$	0.17	m

p bar	T °C	$\eta_L$ mPa s	$\eta_G$ $\mu$ Pa s	$\rho_G$ kg/m <sup>3</sup>	$\rho_L$ kg/m <sup>3</sup>	$\sigma$ mN/m	$G''$ kg/s/m <sup>2</sup>	$L''$ kg/s/m <sup>2</sup>	$C_{cor}$ meas	$C_{cor}$ est	X-HD kg/kg	Y-HD kg/kg	F'' kg/s/m <sup>2</sup>	$G''_0$ kg/s/m <sup>2</sup>
Hexadecane-CO <sub>2</sub>														
80	40	0.41	20	288	817	6.6	13.70	4.76	0.63	0.76	0.688	0.0013	3.27	13.67
80	40	0.41	20	288	817	6.6	13.40	4.76	0.62	0.76	0.688	0.0013	3.27	13.37
80	40	0.41	20	288	817	6.6	11.65	6.35	0.64	0.73	0.688	0.0013	4.37	11.63
80	40	0.41	20	288	817	6.6	9.73	6.75	0.59	0.71	0.688	0.0013	4.64	9.72
80	50	0.54	19	226	799	9.2	19.18	3.23	0.74	0.85	0.760	0.0007	2.46	19.16
80	60	0.61	19	197	786	10.7	14.59	3.92	0.67	0.84	0.802	0.0007	3.14	14.57
114	40	0.33	56	697	833	1.0	15.15	3.75	0.92	0.65	0.614	0.0755	2.18	13.29
114	40	0.33	56	697	833	1.0	20.01	2.81	1.00	0.70	0.614	0.0755	1.64	17.55
114	50	0.31	41	547	818	2.3	16.44	6.17	0.89	0.65	0.631	0.0298	3.82	15.66
114	50	0.31	41	547	818	2.3	12.69	7.49	0.84	0.61	0.631	0.0298	4.64	12.09
114	50	0.31	41	547	818	2.3	12.06	6.61	0.77	0.61	0.631	0.0298	4.09	11.49
114	50	0.31	41	547	818	2.3	11.94	8.37	0.85	0.59	0.631	0.0298	5.19	11.38
114	50	0.31	41	547	818	2.3	9.91	9.69	0.83	0.56	0.631	0.0298	6.00	9.44
114	60	0.37	27	389	802	4.7	14.83	3.98	0.64	0.74	0.689	0.0081	2.73	14.65
114	60	0.37	27	389	802	4.7	9.33	6.16	0.58	0.66	0.689	0.0081	4.23	9.22
143	50	0.25	58	689	832	0.6	9.15	3.68	0.66	0.56	0.564	0.0929	1.91	7.64
143	50	0.25	58	689	832	0.6	7.02	8.93	0.89	0.46	0.564	0.0929	4.64	5.87
173	60	0.21	60	688	828	0.4	20.35	2.06	0.92	0.62	0.526	0.1168	0.96	15.83
173	60	0.21	60	688	828	0.4	5.72	9.14	0.83	0.42	0.526	0.1168	4.23	4.45

APPENDIX 7.B (*Determination of the Experimental Number of Stage*)

Due to the mutual solubilities of the components the determination of the height of a theoretical stage for an extraction is more complicated than for distillation. This is caused by the changes in the flows. The most simple way to determine the height of a theoretical stage is by considering the column as a stripping column. In figure 7.B1 a stripping column is shown. To calculate the overall behaviour of the system one needs to know the load and composition of three main streams. Normally one has knowledge of the feed ( $F$ ), the solvent flow ( $G_0^*$ ), and the raffinate ( $L_0$ ). Using the given loads one calculates the composition and size of the extract flow ( $G_{ex}$ ) by applying an overall balance,  $G_{ex} = F + G_0^* - L_0$ . Next to the loads and composition one needs knowledge of the thermodynamic behaviour of the system to determine the concentrations;

$$y_{i,0} = K_{i,0}x_{i,0} \quad \text{for } i = 1 \dots n$$

$$x_{i,N+1} = \frac{y_{i,N+1}}{K_{i,N+1}} \quad \text{for } i = 1 \dots n \tag{7.B1}$$

These expressions can be used to calculate the main streams in the system over each segment.

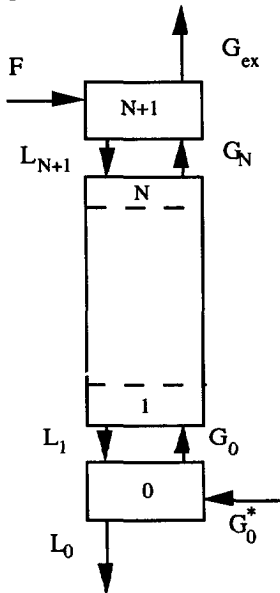


FIGURE 7.B1: Schematic representation of a stripping column with indicated main flows.

In the top of the column the feed becomes saturated with solvent. The total balance of the top segment,

$$F + G_N = G_{ex} + L_{N+1} \tag{7.B2}$$

and the solvent component balance,

$$x_{s,F}F + y_{s,N}G_N = y_{s,N+1}G_{ex} + x_{s,N+1}L_{N+1} \tag{7.B3}$$

are used to express the liquid flow  $L_{N+1}$ . When the solvent fraction in the solvent flow remains nearly identical ( $y_{s,N} \approx y_{s,N+1}$ ), the liquid flow can be isolated as:

$$L_{N+1} = \left( \frac{y_{s,N+1} - x_{s,F}}{y_{s,N+1} - x_{s,N+1}} \right) F = \left( \frac{1 - \frac{x_{s,F}}{y_{s,N+1}}}{1 - K_{s,N+1}} \right) F \tag{7.B4}$$

The top segment is in this approach considered as one equilibrium stage. The gas flow  $G_N$  can then be calculated using the overall balance. Often the feed does not contain any solvent, so that the relation becomes relatively simple.

The bottom segment is treated likewise, using one equilibrium stage, the total balance,

$$G_0^* + L_1 = G_0 + L_0 \tag{7.B5}$$

and the solvent balance,



$$y_{s,0}G_0^* + x_{s,1}L_1 = y_{s,0}G_0 + x_{s,0}L_0 \quad (7.B6)$$

In this case it is assumed that the solvent dissolved in the liquid phase remains approximately equal,  $x_{s,0} \approx x_{s,1}$ , so that the flow  $G_0$  can be expressed in terms as:

$$G_0 = \frac{(y_{s,0} - x_{s,0})}{(y_{s,1} - x_{s,0})} G_0^* \quad (7.B7)$$

Using this equation the total balance over the bottom stage is determined and the component balances can be calculated using the thermodynamically equilibrium relations. When the thermodynamic data are known, the ratio of two components in the feed and raffinate or extract is enough to determine the whole system.

The number of stages in the column can now be evaluated. The most simple approach is the use of the Kremser relation to determine the number of equilibrium stages in the middle section of the column and add two equilibrium stages to take into account the top and bottom section of the separation column. The total number of stages is therefore:

$$N = \frac{\ln \left( \frac{(x_{i,N+1} - x_{i,0}) \left(1 - \frac{1}{S_i}\right) + \frac{1}{S_i}}{(x_{i,1} - x_{i,0})} \right)}{\ln S_i} + 2 \quad (7.B8)$$

#### APPENDIX 7.C (Approach and data, system IPA - ethylene glycol - carbon dioxide)

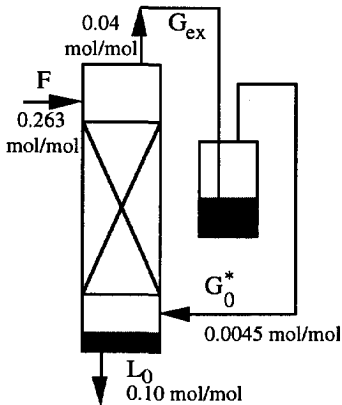


FIGURE 7.C1: Experimental stripping set-up with typical IPA concentrations.

The data was obtained by pumping a mixture of IPA (0.263mol%) and ethylene glycol into the top of the column that was operated at 125bar and approximately 50°C. The mixture was counter-currently contacted with carbon dioxide, so that in principle the IPA was removed from the ethylene glycol. The carbon dioxide was pumped into the bottom of the column. The enriched solvent flow was depressurized to 50 bar and heated to approximately 30°C after which the solvent was recycled. Due to the recycling step, the fresh solvent contained IPA. Using the composition

of the top of the column the concentration IPA was determined as 0.0045mol/mol at 30°C and 50 bar. This values was used as IPA concentration in the feed, except in the cases were fresh carbon dioxide was used. The experimental set-up with the IPA concentrations is shown in figure 7.C1. The used physical properties and the experimental data are given in tables VII.CI and VII.CII. Table VII.CII shows the measured flows and concentrations and the calculated streams in the top and bottom section. By either applying the the flows in the bottom section

( $G_0$  and  $L_1$ ) or in the top section ( $G_N$  and  $L_{N+1}$ ) in the column with the subsequent equilibrium conditions, two measured and estimated number of equilibrium stages are determined, so that an experimental error is found.

TABLE VII.CI: Property data of pure components, the PREOS binary interaction parameters, the characteristics of the packing, the column characteristics, the estimated physical properties at given conditions and composition. The concentration of the IPA in the recycles solvent stream at different temperatures at 50 bar is also given.

## Pure Component properties

No.	CO <sub>2</sub> i	Glycol j	IPA k
M (g/mol)	44.01	62.069	60.096
P <sub>c</sub> (bar)	73.83	89.00	47.60
T <sub>c</sub> (K)	304.21	718	508.3
$\omega$	0.239	0.588	0.665

## PREOS Binary interaction parameters

ij	k <sub>ij</sub>	l <sub>ij</sub>
12	0.059	0
13	0.093	-0.004
23	-0.059	0

## Packing Characteristics

a <sub>p</sub>	660	m <sup>2</sup> /m <sup>3</sup>
H <sub>p</sub>	0.165	m
$\epsilon_0$	0.97	m <sup>3</sup> /m <sup>3</sup>
$\alpha$	30	°

## Column Characteristics

D <sub>col</sub>	0.036	m
Z (packing)	2.03	m

## Conditions:

T	50	°C
p	125	bar

## Physical Properties

D <sup>G</sup>	2.37E-08	m <sup>2</sup> /s
D <sup>L</sup>	5.84E-10	m <sup>2</sup> /s
$\rho_L$	1021	kg/m <sup>3</sup>
$\rho_G$	656	kg/m <sup>3</sup>
$\eta_L$	1.86	mPa s
$\eta_G$	50.07	$\mu$ Pa s
c <sup>L</sup>	17.41	kmol/m <sup>3</sup>
c <sup>G</sup>	14.71	kmol/m <sup>3</sup>
$\sigma$	0.0072	N/m

## Applied Column Composition:

x <sub>i</sub> :	0.170	mol/mol
y <sub>i</sub> :	0.964	mol/mol
x <sub>j</sub> :	0.642	mol/mol
y <sub>j</sub> :	0.003	mol/mol
x <sub>k</sub> :	0.188	mol/mol
y <sub>k</sub> :	0.033	mol/mol

## Solvent IPA flow

T	y <sub>0</sub> -IPA
°C	mol/mol
20	0.0027
25	0.0036
<b>30</b>	<b>0.0045</b>
35	0.0057

TABLE VII.CII: Measured temperature, solvent flow, feed flow, raffinate flow, and IPA concentration in the bottom flow and the IPA concentration in the solvent flow. For each measurement the following quantities were calculated: the top liquid and gas flows ( $L''_{N+1}$  and  $G''_N$ ), the bottom liquid and gas flows ( $L''_1$  and  $G''_0$ ), the equilibrium derivative ( $m_i$ ), stripping factor ( $S_i$ ), measured number of equilibrium stages ( $N$ ), estimated number of stages ( $N_E$ ). For all the calculations the thermodynamic and physical properties at 50°C and 125bar were used.

T °C	$G''_0$ mol $s^{-1}m^{-2}$	$F''$ mol $s^{-1}m^{-2}$	$L''_0$ mol $s^{-1}m^{-2}$	$y_{IPA,0}$ mol/mol	$x_{IPA,0}$ mol/mol	$L''$ kg $s^{-1}m^{-2}$	$G''$ kg $s^{-1}m^{-2}$	$m_i$ mol/mol	$S_i$	$N$ $m^{-1}$	$N_E$ $m^{-1}$
47.8	373.8	71.2	66.6	0.0000	0.082	-5.25 -4.35	17.72 16.86	0.216 0.201	0.956 1.041	1.48 1.45	1.59 1.73
47.5	193.8	40.3	36.4	0.0000	0.068	-3.07 -2.34	9.40 8.71	0.227 0.200	0.903 0.998	2.29 2.09	2.31 2.63
47.8	360.2	71.4	69.5	0.0046	0.104	-5.31 -4.48	17.05 16.26	0.219 0.202	0.918 0.975	1.52 1.50	1.61 1.74
47.6	399.6	68.4	66.8	0.0046	0.109	-4.94 -4.38	18.59 18.07	0.210 0.204	1.039 1.113	1.08 1.08	1.60 1.67
47.1	302.8	60.2	57.8	0.0046	0.109	-4.46 -3.74	14.35 13.69	0.217 0.203	0.915 0.984	1.36 1.34	1.80 1.94
47.4	206.1	45.7	43.5	0.0046	0.103	-3.48 -2.78	9.94 9.30	0.226 0.202	0.841 0.897	1.96 1.88	2.19 2.43
48.2	312.1	60.2	57.5	0.0046	0.105	-4.45 -3.72	14.77 14.09	0.217 0.203	0.943 1.018	1.40 1.38	1.78 1.92
49.9	408.9	74.3	72.6	0.0046	0.119	-5.36 -4.77	19.07 18.53	0.210 0.205	0.981 1.052	0.99 0.99	1.55 1.62
50.1	502.8	90.4	88.5	0.0046	0.119	-6.51 -5.83	23.42 22.80	0.209 0.205	0.990 1.060	0.96 0.96	1.37 1.43

APPENDIX 7.D(Approach and data, system 2-methyl naphthalene-hexadecane-carbon dioxide)

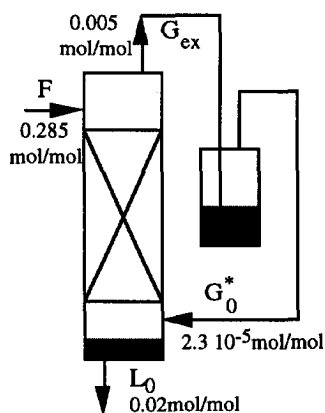


FIGURE 7.D1: Experimental stripping set-up with typical 2-methyl naphthalene concentrations.

The data were obtained by pumping a mixture of 2-methyl naphthalene (0.285mol%) and hexadecane into the top of the column that was operated at 114bar and 131bar and 50°C and at 160bar and 65°C. The mixture was counter-currently contacted with carbon dioxide, so that in principle the 2-methyl naphthalene was removed from the hexadecane. The carbon dioxide was pumped into the bottom of the column. The enriched solvent flow was depressurized to 50 bar and heated to approximately 30°C after which the solvent was recycled. Due to the recycling step, the fresh solvent contained a limited amount of 2-methyl naphthalene.

Using the composition of the top of the column the concentration 2-methyl naphthalene was determined as  $2.3 \cdot 10^{-5}$  mol/mol at 30°C and 50 bar. This value was used as 2-methyl naphthalene concentration in the solvent feed. The experimental set-up with the 2-methyl naphthalene concentrations are shown in figure 7.D1. The used physical properties and the experimental data are given in table VII.DI and VII.DII. Table VII.DII shows the measured flows and concentrations and the calculated streams in the top and bottom section. The calculated streams and different stripping factors are used to calculate two measured ( $N$ ) and estimated ( $N_E$ ) number of equilibrium stages. The experimental error in these measurements  $\Delta N$  was estimated by calculating the equilibrium conditions at a temperature that was 0.5°C lower than the measured value and by recalculating the experimental number of transfer units. The order of magnitude for the relative experimental error obtained in this way was:  $(N/N_{T-0.5^\circ} - 1)$ .

TABLE VII.DI: Data of the system 2-methyl naphthalene - hexadecane - carbon dioxide. Indicated are the pure component properties, the PREOS binary interaction parameters, the characteristics of the packing, the column characteristics, and the estimated physical properties at given conditions and composition.

Pure Component properties				Physical Properties			Physical Properties			Physical Properties		
No.	CO <sub>2</sub> i	Hex j	2MN k	D <sup>G</sup>	16 10 <sup>-9</sup>	m <sup>2</sup> /s	D <sup>G</sup>	13 10 <sup>-9</sup>	m <sup>2</sup> /s	D <sup>G</sup>	14 10 <sup>-9</sup>	m <sup>2</sup> /s
				D <sup>L</sup>	4.7 10 <sup>-9</sup>	m <sup>2</sup> /s	D <sup>L</sup>	4.8 10 <sup>-9</sup>	m <sup>2</sup> /s	D <sup>L</sup>	5.1 10 <sup>-9</sup>	m <sup>2</sup> /s
				ρ <sub>L</sub>	754	kg/m <sup>3</sup>	ρ <sub>L</sub>	760	kg/m <sup>3</sup>	ρ <sub>L</sub>	745	kg/m <sup>3</sup>
				ρ <sub>G</sub>	570	kg/m <sup>3</sup>	ρ <sub>G</sub>	673	kg/m <sup>3</sup>	ρ <sub>G</sub>	625	kg/m <sup>3</sup>
				η <sub>L</sub>	0.23	mPa s	η <sub>L</sub>	0.20	mPa s	η <sub>L</sub>	0.18	mPa s
				η <sub>G</sub>	42.93	μPa s	η <sub>G</sub>	54.16	μPa s	η <sub>G</sub>	51.34	μPa s
M (g/mol)	44.01	226.4	142.3	c <sub>t</sub> <sup>L</sup>	9.54	kmol/m <sup>3</sup>	c <sub>t</sub> <sup>L</sup>	10.29	kmol/m <sup>3</sup>	c <sub>t</sub> <sup>L</sup>	10.09	kmol/m <sup>3</sup>
P <sub>c</sub> (bar)	73.83	15.30	35.00	c <sub>t</sub> <sup>G</sup>	12.55	kmol/m <sup>3</sup>	c <sub>t</sub> <sup>G</sup>	14.25	kmol/m <sup>3</sup>	c <sub>t</sub> <sup>G</sup>	13.28	kmol/m <sup>3</sup>
T <sub>c</sub> (K)	304.21	734	761	σ	1.22	mN/m	σ	0.4	mN/m	σ	0.47	mN/m
ω	0.239	0.742	0.382	Applied Composition:			Applied Composition:			Applied Composition:		
PREOS Binary interaction parameters				x <sub>i</sub>	0.785	mol/mol	x <sub>i</sub>	0.818	mol/mol	x <sub>i</sub>	0.818	mol/mol
ij	k-ij	l-ij		y <sub>i</sub>	0.991	mol/mol	y <sub>i</sub>	0.979	mol/mol	y <sub>i</sub>	0.981	mol/mol
12	0.083	0.009		x <sub>j</sub>	0.166	mol/mol	x <sub>j</sub>	0.143	mol/mol	x <sub>j</sub>	0.142	mol/mol
13	0.062	-0.067		y <sub>j</sub>	0.006	mol/mol	y <sub>j</sub>	0.015	mol/mol	y <sub>j</sub>	0.014	mol/mol
23	-0.003	0.022		x <sub>k</sub>	0.049	mol/mol	x <sub>k</sub>	0.039	mol/mol	x <sub>k</sub>	0.040	mol/mol
Packing Characteristics				y <sub>k</sub>	0.003	mol/mol	y <sub>k</sub>	0.006	mol/mol	y <sub>k</sub>	0.006	mol/mol
a <sub>p</sub>	660	m <sup>2</sup> /m <sup>3</sup>		Operating Conditions:			Operating Conditions:			Operating Conditions:		
H <sub>p</sub>	0.165	m		T	50	°C	T	50	°C	T	65	°C
ε <sub>0</sub>	0.97	m <sup>3</sup> /m <sup>3</sup>		p	114.3	bar	p	131.4	bar	p	160	bar
α	30	°										
Column Characteristics												
D <sub>col</sub>	0.036	m										
Z(packing)	2.03	m										

TABLE VII.DII: Measured data are: temperature, solvent free 2-methyl naphthalene mass concentrations in the bottom ( $X_{2mn,0}$ ) and extract flow ( $Y_{2mn,N+1}$ ), solvent flow, feed flow, raffinate flow. Calculated are: the molar 2-methyl naphthalene concentration in the bottom flow, for each measurements the top liquid and gas flows ( $L''_{N+1}$  and  $G''_N$ ), the bottom liquid and gas flows ( $L''_1$  and  $G''_0$ ), the subsequent equilibrium derivative ( $m_i$ ), stripping factor ( $S_i$ ), and from data determined number of equilibrium stages ( $N$ ). Also indicated is the estimated number of equilibrium stages ( $N_E$ ) and an estimation of the experimental accuracy. The operating pressures for the three tables are respectively 114.3bar, 131.4bar, and 160bar.

T °C	$X_{2mn,0}$ kg kg <sup>-1</sup>	$Y_{2mn,N+1}$ kg kg <sup>-1</sup>	$G''_0$ mol s <sup>-1</sup> m <sup>-2</sup>	$F''$ mol s <sup>-1</sup> m <sup>-2</sup>	$L''_0$ mol s <sup>-1</sup> m <sup>-2</sup>	$x_{2mn,0}$ mol mol <sup>-1</sup>	$L''$ kg s <sup>-1</sup> m <sup>-2</sup>	$G''$ kg s <sup>-1</sup> m <sup>-2</sup>	$m_i$ mol mol <sup>-1</sup>	$S_i$	N m <sup>-1</sup>	$N_E$ m <sup>-1</sup>	$\Delta N/N$
---------	---------------------------------------	---	---	---	---	---	--	--	-----------------------------------	-------	----------------------	--------------------------	--------------

52.8	0.169	0.333	175.3	4.92	17.88	0.0525	-1.78	7.96	0.050	0.407	1.75	3.41	1.15
							-1.89	8.16	0.050	0.385	1.85	3.33	
50.1	0.132	0.301	225.2	4.90	12.80	0.0416	-1.81	10.39	0.065	0.668	3.61	3.40	0.63
							-1.77	10.67	0.064	0.677	3.39	3.34	
49.9	0.125	0.314	229.3	4.74	12.04	0.0394	-1.77	10.59	0.067	0.715	2.80	3.41	0.38
							-1.74	10.88	0.066	0.719	2.76	3.59	
50.3	0.132	0.320	201.1	4.31	12.52	0.0416	-1.60	9.23	0.063	0.654	3.13	3.47	0.74
							-1.65	9.50	0.063	0.632	3.68	3.57	
51.5	0.095	0.315	335.0	5.12	12.47	0.0303	-1.85	15.27	0.053	0.793	5.74	2.88	0.97
							-1.86	15.58	0.052	0.778	7.59	2.81	
49.5	0.096	0.307	255.2	4.77	10.43	0.0306	-1.79	11.81	0.071	0.828	3.50	3.38	0.25
							-1.72	12.14	0.069	0.843	3.33	3.31	
48.5	0.057	0.299	276.0	4.85	7.72	0.0185	-1.86	12.90	0.080	0.973	4.12	3.43	0.12
							-1.67	13.24	0.077	1.040	3.53	3.40	

T °C	$X_{2mn,0}$ kg kg <sup>-1</sup>	$Y_{2mn,N+1}$ kg kg <sup>-1</sup>	$G''_0$ mol s <sup>-1</sup> m <sup>-2</sup>	$F''$ mol s <sup>-1</sup> m <sup>-2</sup>	$L''_0$ mol s <sup>-1</sup> m <sup>-2</sup>	$x_{2mn,0}$ mol mol <sup>-1</sup>	$L''$ kg s <sup>-1</sup> m <sup>-2</sup>	$G''$ kg s <sup>-1</sup> m <sup>-2</sup>	$m_i$ mol mol <sup>-1</sup>	$S_i$	N m <sup>-1</sup>	$N_E$ m <sup>-1</sup>	$\Delta N/N$
---------	---------------------------------------	---	---	---	---	---	--	--	-----------------------------------	-------	----------------------	--------------------------	--------------

54.2	0.138	0.281	116.4	4.31	12.57	0.0433	-1.74	5.88	0.111	0.609	3.67	4.07	0.83
							-1.67	5.83	0.109	0.625	3.19	4.11	
51.5	0.042	0.270	167.8	4.27	6.97	0.0137	-1.84	8.74	0.144	1.081	3.64	3.76	0.08
							-1.71	8.57	0.134	1.082	3.64	3.81	
52.1	0.039	0.270	163.4	4.17	9.74	0.0127	-1.77	8.33	0.137	1.023	5.21	3.79	0.21
							-1.83	8.27	0.126	0.935	8.55	3.72	
53.2	0.028	0.235	226.9	4.78	0.78	0.0092	-1.99	11.79	0.122	1.166	3.51	3.18	0.06
							-1.39	11.31	0.114	1.539	2.60	3.59	
52.1	0.015	0.215	225.0	4.28	1.86	0.0050	-1.84	11.62	0.134	1.350	3.67	3.39	0.04
							-1.57	11.33	0.123	1.467	3.32	3.55	

T °C	$X_{2mn,0}$ kg kg <sup>-1</sup>	$Y_{2mn,N+1}$ kg kg <sup>-1</sup>	$G''_0$ mol s <sup>-1</sup> m <sup>-2</sup>	$F''$ mol s <sup>-1</sup> m <sup>-2</sup>	$L''_0$ mol s <sup>-1</sup> m <sup>-2</sup>	$x_{2mn,0}$ mol mol <sup>-1</sup>	$L''$ kg s <sup>-1</sup> m <sup>-2</sup>	$G''$ kg s <sup>-1</sup> m <sup>-2</sup>	$m_i$ mol mol <sup>-1</sup>	$S_i$	N m <sup>-1</sup>	$N_E$ m <sup>-1</sup>	$\Delta N/N$
---------	---------------------------------------	---	---	---	---	---	--	--	-----------------------------------	-------	----------------------	--------------------------	--------------

64.8	0.146	0.244	67.7	3.61	10.52	0.0457	-1.57	3.71	0.158	0.581	3.99	6.24	0.63
							-1.40	3.60	0.156	0.621	2.82	6.38	
65.9	0.124	0.255	109.8	4.24	9.42	0.0391	-1.81	5.88	0.145	0.738	2.39	4.89	0.17
							-1.60	5.72	0.142	0.801	2.17	5.03	
66.7	0.014	0.238	177.4	3.79	1.83	0.0046	-1.62	9.25	0.133	1.205	5.13	4.19	0.04
							-1.27	8.94	0.122	1.397	3.96	4.41	
66.9	0.025	0.238	179.8	3.54	3.72	0.0082	-1.52	9.20	0.130	1.255	3.53	4.25	0.04
							-1.44	9.06	0.121	1.250	3.55	4.24	

## NOTATION

Symbol	Description	Unit
$a_p$	Specific packing area.....	$m^2/m^3$
$C_G$	Capacity factor: $C_G = u_{SG} \sqrt{\frac{\rho_G}{\rho_L - \rho_G}}$ .....	$m/s$
$C_{orr}$	Correction factor for physical properties .....	
$C_r$	Relative capacity factor .....	
$c_t^G$	Total gas concentration .....	$mol/m^3$
$c_t^L$	Total liquid concentration.....	$mol/m^3$
$D_{col}$	Column diameter .....	$m$
$D_i^G$	Gas diffusion coefficient .....	$m^2/s$
$D_i^L$	Liquid diffusion coefficient .....	$m^2/s$
$F$	Feed flow.....	$mol/s$
$F''$	Molar feed flux .....	$mol/m^2/s$
$G$	Gas flow.....	$kg/s$
$G''$	Gas flux .....	$kg/m^2/s$
$G_0^*$	Gas feed .....	$mol/s$
$G_{ex}$	Extract gas flow .....	$mol/s$
$G_0^{*''}$	Molar solvent flux .....	$mol/m^2/s$
$G_m$	Molar gas flow.....	$mol/s$
$H_{col}$	Height of the column.....	$m$
$H^{etp}$	Height of an equivalent theoretical stage.....	$m$
$H_{eff}^{etp}$	Effective height of an equivalent theoretical stage for wetting .....	$m$
$H_p$	Height of a structured packing element .....	$m$
$K_{col}$	Installed costs of a column .....	$f$
$K_S$	Purchase costs of the column shell.....	$f$
$K_p$	Purchase costs of the packing.....	$f$
$K_i$	Distribution factor $K_i = y_i/x_i$ .....	
$k_{ij}$	Peng-Robinson binary interaction parameter.....	
$k_i^{OG}$	On gas phase based overall mass transfer coefficient .....	$m/s$
$L''$	Liquid flux .....	$kg/m^2/s$
$L_0$	Liquid raffinate flow .....	$mol/s$
$L_m$	Molar liquid flow .....	$mol/s$
$\ell_e$	Exposure length .....	$m$
$l_{ij}$	Peng-Robinson binary co-volume parameter .....	
$M$	Molar weight.....	$kg/kmol$

$m_{col}$	Mass of the column .....	kg
$m_i$	Derivative of the equilibrium line .....	mol/mol
$N$	Number of equilibrium stages .....	
$N_E$	Estimated number of equilibrium stages .....	
$p_c$	Critical pressure .....	Pa
$p$	Pressure .....	Pa
$r_0$	Hydraulic radius .....	m
$S_i$	Stripping factor $S_i = m_i G_m/L_m$ .....	
$T$	Temperature .....	K
$T_c$	Critical temperature .....	K
$t_{col}$	Thickness of column wall .....	m
$u_{int}$	Interface velocity .....	m/s
$u_{SG}$	Superficial gas velocity .....	m/s
$V_{col}$	Volume of the column .....	$m^3$
$x_i$	Mol fraction in the liquid phase .....	mol/mol
$y_i$	Mol fraction in the gas phase .....	mol/mol
$\alpha$	Effective inclination angle .....	$^\circ$
$\epsilon_0$	Void fraction .....	$m^3/m^3$
$\eta_G$	Dynamic gas viscosity .....	Pa s
$\eta_L$	Dynamic liquid viscosity .....	Pa s
$\theta$	Relative interface position .....	
$\rho_G$	Gas density .....	$kg/m^3$
$\rho_L$	Liquid density .....	$kg/m^3$
$\rho_s$	Steel density .....	$kg/m^3$
$\sigma$	Surface tension .....	N/m
$\sigma_s$	Normal design stress of the steel .....	$N/m^2$
$\Phi$	Flow parameter .....	
$\Psi_{G-L}$	Gas-liquid interaction parameter .....	
$Re_G$	Gas phase Reynolds number .....	$Re_G = \frac{\rho_G \left( \frac{u_{SG}}{\theta^2 \epsilon_0 \cos \alpha} - u_{int} \right) 2\theta r_0}{\eta_G}$
$Re_L$	Liquid phase Reynolds number .....	$Re_L = \frac{4L''}{\eta_L a_p}$
$Re_{W50}$	Dimensionless number at which the packing performance is 50% .....	

---

## REFERENCES

- [1] Bernard, L., Keller, A., Barth, D., and Perrut, M., (1993), *Separation of Ethanol From Aqueous Solutions by Supercritical Carbon Dioxide - Comparison between Simulations and Experiments*, J. of Supercritical Fluids, **6** pp.9-13.
- [2] Billet, R., (1992), *State of the Art in Development of Column Packings and their Optimal Surface Geometries*. Fat Sci. Technol. **94** (12) pp 571-579.
- [3] Bolles, W.L., and Fair, J.R., (1985), I. Chem. E. Symp. Ser., **56** p3.3/35.
- [4] Bravo, J.L., Rocha, J.A., and Fair, J.R., (1985), *Mass Transfer in Gauze Packings*, Hydrocarbon Processing, 91-95.
- [5] Brunner, G., Malchow, Th., Stürken, K., and Gottschau, Th.J., (1991), *Separation of Tocopherols from Deodorizer Condensates by Counter-Current Extraction with Carbon Dioxide*, J. of Supercritical Fluids, **4** pp.72-80.
- [6] Carmelo, P.J., Simoes, P., and Nunes da Ponte, M., (1994), *Supercritical fluid extraction of olive oils in counter-current extraction column: experimental results and modelling*, 3rd Int. Symposium on Supercritical Fluids, TOME 2 pp. 107- 112.
- [7] Coulson, J.M., and Richardson, J.F., (1985), *Chemical Engineering (Design)*, Vol. 6. Oxford: Pergamon Press.
- [8] Gmehling, J., Onken, U., and Rarey, J.R., (1990), *Vapour-Liquid Equilibrium data Collection, Alcohols and Phenols*, DECHEMA, Frankfurt, vol. 1, part 2f.
- [9] Haan, A.B. de, (1991), *Supercritical Fluid Extraction of Liquid Hydrocarbon Mixtures*, Ph.D. thesis, Delft Technical University, Delft.
- [10] Hiller, N., Schiemann, H., Weidner, E., and Peter, S., (1993), *Interfacial Tension in Systems with a Supercritical Component at High Pressures*, Chem. Eng. Technol., **16** pp. 206-212.
- [11] Kaminishi, G-I, Takano, S., Yokoyama, C., and Takahashi, S., (1989), *Concentration of triethylene glycol, diethylene glycol and ethylene glycol in supercritical carbon dioxide up to 16 MPa at 313.15 and 333.15K*, Fluid Phase Equilibria, **52**, pp 365-372.
- [12] Krehenwinkel, H., and H. Knapp, *Pressure Drop and Flooding in Packed Columns Operating at High Pressures*, Chem. Eng. Tech. **10**, 231-242 (1987).
- [13] Meyer, J.T. and Brunner, G., (1994), *Apparatus for the determination of hydrodynamic behaviour in counter-current columns and some experimental results*, 3rd Int. Symposium on Supercritical Fluids, TOME 2 pp. 217- 222.
- [14] Oppenheim, A.V., Willisky, A.S., and Young, I.T., (1983), *Signals and Systems*, Prentice-Hall International inc., London.
- [15] Peng, D.Y. and Robinson, D.B. (1976). Ind. Eng. Chem. Fundam., **15** p 59-64.
- [16] Radosz, M., (1986), *Vapour-Liquid Equilibrium for 2-propanol and Carbon Dioxide*, J. Chem. Eng. Data, **31** pp 43-45.
- [17] Sulzer Brother Ltd., (1989), *Separation Columns for Distillation and Absorption*. Information Bulletin.



## Overall Supercritical Process Design Considerations

Despite of the fact that it always has been presented as a promising alternative, supercritical fluid extraction (SFE) has not become a widely applicable separation technique. Breakthroughs were only found in extractions for which no conventional technique was available. In addition to the large investment costs, one of the main drawbacks of supercritical processes is the energy requirement for the recycle of the solvent stream. This is normally accomplished using compressors or pumps, of which the last should be combined with a condensation step using refrigeration. When the rich solvent leaves the extraction vessel after the extraction step, the product is normally recovered from the solvent by reducing the pressure. This product-solvent separation principle is based on the density decrease of the solvent, which reduces the solubility of the product. However, a density decrease can also be accomplished using a temperature change after the extraction process. The extraction conditions can be chosen so that in most cases a temperature increase, decreases the solvent density sufficiently and the separation of the rich solvent can be accomplished. This principle is generally known as isobaric retrograde condensation. The isobaric concept has the potential of reducing the energy requirements considerably. Although the isobaric process has been known in literature for quite some time and several papers can be found on retrograde condensation and crystallisation (see, e.g., Brunner and Peter, 1982; McHugh and Krukoni 1986; Johnston et al. 1987; Birtigh and Brunner, 1993), it is often only analysed from a thermodynamic equilibrium viewpoint, without considering the economical applicability.

This partly explains the often quoted drawbacks of supercritical extraction as being not cost effective on both the capital investment and energy requirements. However, both costs can be reduced substantially for most supercritical extraction processes when the isobaric features are well exploited. One of these features is the use of gravity as driving force for the circulation of the solvent flow, by placing the required heat exchangers on an appropriate position. In this way a static pressure in the process can be created. The static pressure will create the solvent circulation and the retrograde condensation cleans the solvent stream.

As will be shown, the isobaric operation can lead to a substantial reduction of capital and operating costs. To fully explore the potential of the isobaric supercritical separation process a typical separation problem will be studied. The analysis will especially address the possible separation of the components and the heat integration of the process. It will be shown that non polar compounds with a molar weight in the range of 200-500kg/kmol have a reasonable solubility in supercritical carbon dioxide and therefore have a high potential of being

economically fractionated using an isobaric supercritical separation process. To find the appropriate separation conditions, the typical solubility behaviour of components in carbon dioxide will be discussed, after which the engineering aspects will be analysed.

### GENERAL SOLVENT CYCLE CONSIDERATIONS

Since in a supercritical separation process the equipment sizes and operating costs are nearly proportional with the quantity of solvent recycled, the main objective in the optimization of the supercritical separation process will be the reduction of the required solvent. This has to be done by choosing conditions corresponding to maximum product solubility. However, the product also must be separated from the solvent. Both extraction conditions and solvent-product separation conditions determine the thermodynamic cycle of the solvent.

To examine possible solvent cycle methods one needs information on the solubility behaviour. Less soluble components are adequately described using an exponential function with solvent density (see, e.g.: Bartle et al., 1991; Smitt and Reid, 1985). This description often enables a quick evaluation of the solvent cycle. However, products with a large solubility in the solvent phase or products in which solvent dissolves substantially, are better described using a more complex equation of state. For this description the cubical Peng-Robinson equation of state (1976) is widely used. An example for the different solubility behaviour in carbon dioxide is given in figures 8.1A and 8.1B for toluene and hexadecane.

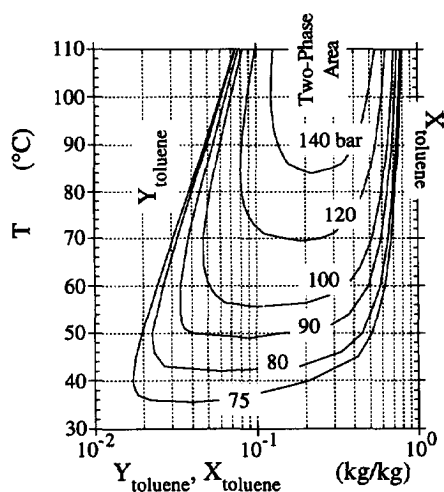


FIGURE 8.1A: The mass fractions of toluene in gas and liquid phase as function of the temperature for various pressures. The bottom of the loci indicates the lower critical solution temperature of the mixture. The curves are calculated using the PREOS with  $k_{ij}=0.09$  and  $l_{ij}=0$ , for all temperatures.

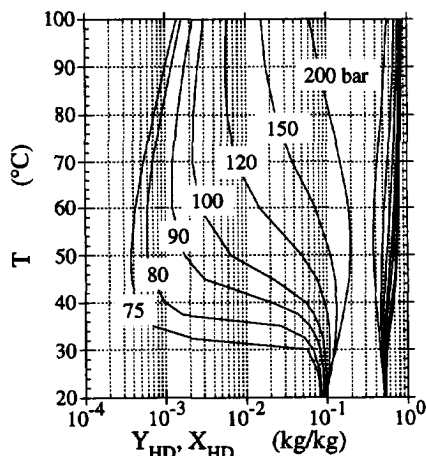


FIGURE 8.1B: The mass fractions of hexadecane in the gas and liquid phase as function of the temperature for various pressures. The curves are calculated using the PREOS with the binary interaction parameters  $k_{ij}=0.083$  and  $l_{ij}=0.009$ , for all temperatures.

Figure 8.2 illustrates three ideal process solvent cycles for a supercritical extraction process indicated in temperature entropy diagrams (T-S diagrams). In these diagrams the system is simplified to a pure solvent cycle. The enclosed shaded area in these diagrams represents the amount of work that in the ideal case can be done with the solvent cycle.

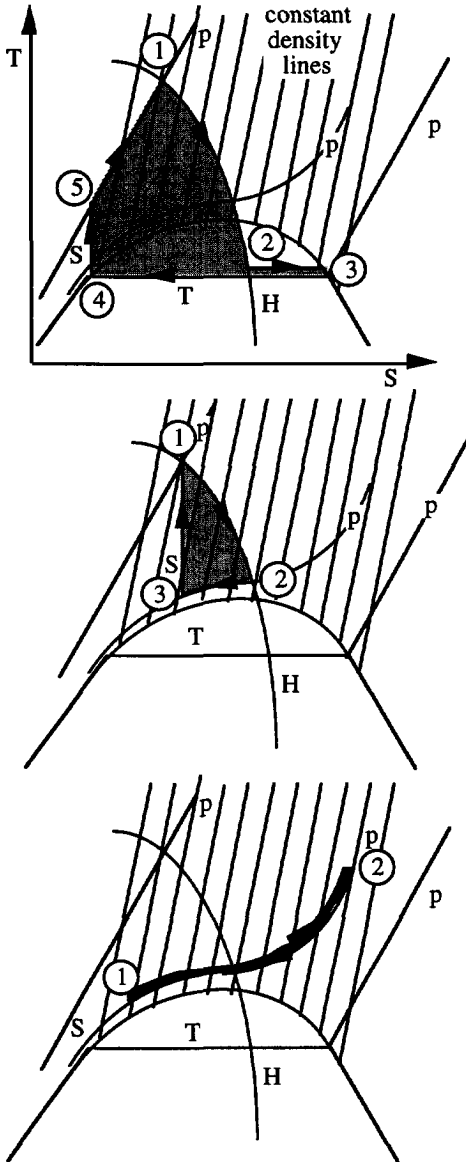


FIGURE 8.2: Three ideal temperature-entropy diagrams for the solvent recycling.

The top diagram shows an operation cycle in which the extract phase is adiabatically expanded into the two phase region (1-2), where the liquid solvent is evaporated (2-3) to separate it from the product and thereafter is condensed (3-4) to enable pumping (4-5) of the solvent to process pressure and finally is heated to extraction temperature (5-1). The advantage of this cycle is the possibility of using a simple pump to pressurise the solvent. Given the critical temperature of carbon dioxide, that is normally applied as solvent, chilled water will be required for the condensation, being a large disadvantage for this process cycle.

The middle diagram shows a process cycle that does not expand the solvent phase (1-2) into the two phase region, but just above this region. This strategy enables the use of cooling water (2-3) and direct compression (3-1) to operating conditions. Although this process uses a compressor it nearly always requires less energy and has lower utility costs than the first process. This is due to the behaviour of the constant enthalpy lines in this region, causing the vanishing of the distinction between compression and pumping.

The bottom diagram illustrates an isobaric process. The product is separated from the solvent by a temperature increase (1-2) causing the retrograde condensation of the product. Hereafter the solvent is

cooled (2-1) to extraction temperature. This process configuration has several advantages. To use these advantages a closer examination of the isobaric separation is required. The isobaric process has two possible solvent-product separation steps. The first possibility is the condensation of the product, which can be illustrated using figure 8.1A. Taking an extraction condition of 80 bar and 100°C the toluene can be separated from the solvent by cooling the rich solvent to 50°C, so that the solubility decreases from  $6 \times 10^{-2}$  to  $2 \times 10^{-2}$  kg/kg. This three fold solubility reduction is caused by the decrease of the toluene vapour pressure with temperature. The second possibility is retrograde condensation which is better suited for systems with a solubility behaviour similar to hexadecane (see figure 8.1B). Taking the extraction conditions at 90bar and 30°C the hexadecane can be separated from the solvent by increasing the temperature to 65°C, so that the solubility decreases from  $8 \times 10^{-2}$  to  $1 \times 10^{-3}$  kg/kg. This 80 fold solubility reduction is caused by the decrease of solvent density. The maximum retrograde condensation is found near the critical pressure of the solvent.

Retrograde condensation is also possible with toluene, operated at 80bar and 42°C the solubility can be decreased with a factor 3 by increasing the temperature to 50°C. However, the lower critical solution temperature limits the practical use of retrograde condensation for these components. Given the recycling of the solvent a high purity separation can in this case often only be accomplished by applying a pressure drop with a subsequent temperature decrease. Fortunately most of the considered components for supercritical extraction processes have the typical solubility behaviour as hexadecane, so that an isobaric solvent cycle is possible.

### THE ISOBARIC PROCESS

When an isobaric process can be used from a thermodynamic view point, the solvent circulations can be maintained by using a pump. However, the solvent circulation can also be designed using natural convection only. This can be done using the different solvent densities in the extraction and the product-solvent separation section. A typical isobaric extraction process is illustrated in figure 8.3, where the heat exchangers are placed at specific heights in the extraction process. To separate the product from the solvent the rich solvent stream from the column with density  $\rho_1$  is heated so that the density is reduced ( $\rho_2$ ). Hereafter the solvent is cooled to a density  $\rho_3$ . Combined with the heights ( $z$ ) the density differences create a static pressure difference ( $\Delta p$ ), which can be expressed as:

$$\Delta p = \rho_3 g (z_3 - z_1) - \rho_1 g (z_2 - z_1) - \rho_2 g (z_3 - z_2) \quad (8.1)$$

The static pressure difference can be enough to overcome the frictional pressure drops in extraction column, heat exchangers and pipes at maximum column capacity. Our estimate is that a driving force of 1bar is sufficient to balance these pressure drops. This corresponds to an effective installation height of 20m.

The items that consume most of pressure are the heat exchangers and the flow control valve. To be able to design the heat exchangers the other pressure drops need to be calculated. The

pressure drop over a structured packing at supercritical conditions will not exceed 800 Pa/m, so that the total pressure drop over a packing height of 12 meters is 0.1bar. Sufficient pressure difference therefore remains available for the heat exchangers.

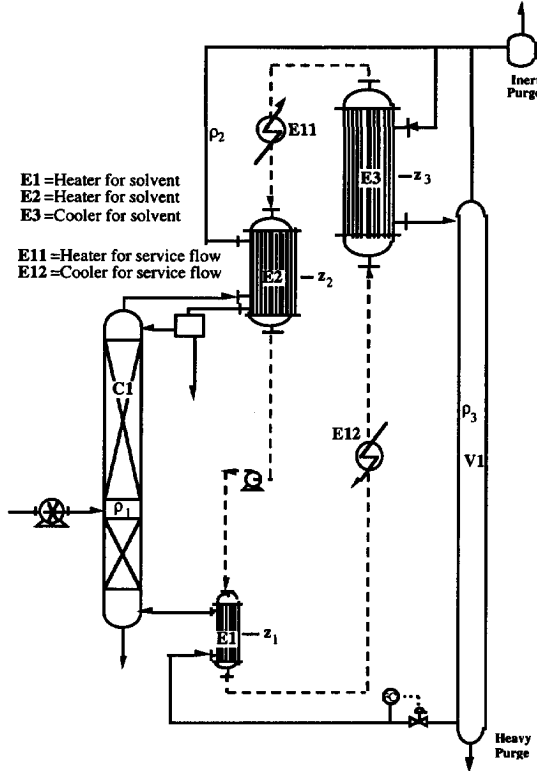


FIGURE 8.3: Proposed flowsheet for a supercritical extraction process, utilizing free convection to circulate the solvent stream. When heat integration is used the required energy consumption can be lowered further by the anti clockwise service flow.

#### Other Plant Lay-outs

In addition to the presented flowsheet in figure 8.3, two other general isobaric concepts are illustrated in the figures 8.4A & 8.4B. Some specific process examples using the illustrated processes are given by Woerlee (1992). Figure 8.4A shows the concept of the extraction of a component that is subsequently adsorbed on a substance that has a larger affinity to the product than the used solvent. In this case one could think of the use of activated carbon or mol sieves. This process is rather similar to the decaffeination process. In this process the caffeine is absorbed by a water absorption tower.

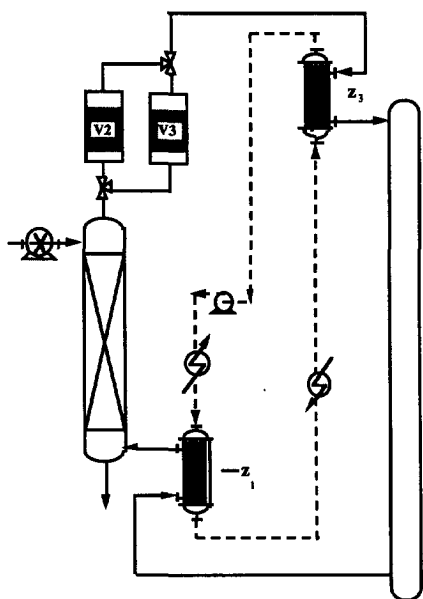


FIGURE 8.4A: Free convection process where the solvent is cleaned utilizing an absorption step.

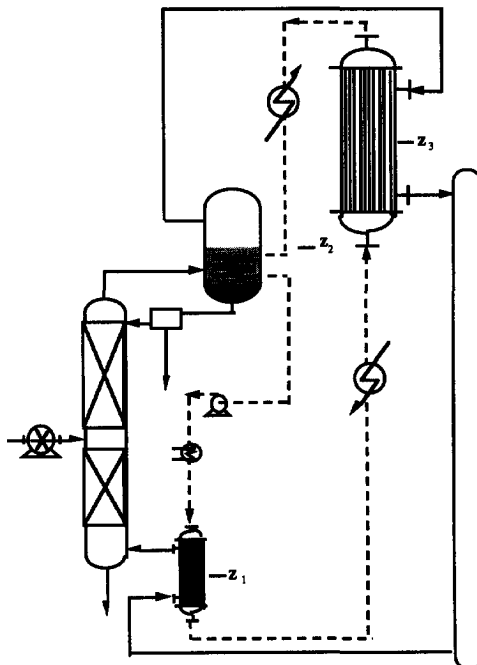


FIGURE 8.4B: Near critical free convection process, where an additional phase transition in the separator is created.

Figure 8.4B is basically the same process as drawn in figure 8.3 except for the fact that by using a near critical solvent an additional solvent rich phase can be created. Although the fugacities of the three phases are equal;

$$f^{L1} = f^{L2} = f^V \quad (8.2)$$

a better solvent-product separation can be achieved due to the density differences between the solvent vapour phase and the solvent rich liquid phase. This configuration therefore can be especially suitable for processes that have a tight raffinate specification, as will become apparent in the following example.

### ISOBARIC PROCESS EXAMPLES

In order to explore the possibilities of the isobaric separation further, we will design an isobaric process for the separation of hexadecane and octadecane using carbon dioxide as solvent. These model components have a typical solubility behaviour and it therefore will not be difficult replacing them with compounds of commercial interest. Important overall process design considerations, e.g.: recovery of the dissolved solvent from the end product streams, liquid settling, storage facilities, etc., will not be discussed here.

Hexadecane (component *i*; molecular weight 226.4) is separated from octadecane (component *j*; molecular weight 254.5) using the plant concept of figure 8.3. The product feed

contains 50%mol of hexadecane, which has to be purified to 99.5%mol and the recovery of hexadecane should be as large as possible. The Peng-Robinson equation of state is used to model the phase equilibria and the physical properties. The binary interaction parameters were determined as:  $k_{CO_2-HD} = 0.083$  and  $l_{CO_2-HD} = 0.009$  and  $k_{CO_2-OD} = 0.086$  and  $l_{CO_2-OD} = 0.022$  using solubility data of de Haan (1991).

If one intends to use the isobaric concept a pressure close to the critical pressure is required. It is for that reason that a process pressure of 90bar will be used. The solubility and selectivity as function of the temperature are given in figures 8.5A & 8.5B, both showing clearly the density changes of carbon dioxide and the usual trade-off between solubility and selectivity.

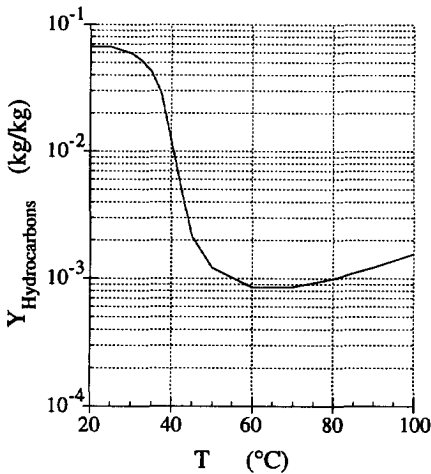


FIGURE 8.5A: The solubility of a 50/50wt hexadecane-octadecane mixture as function of the temperature at a pressure of 90 bar.

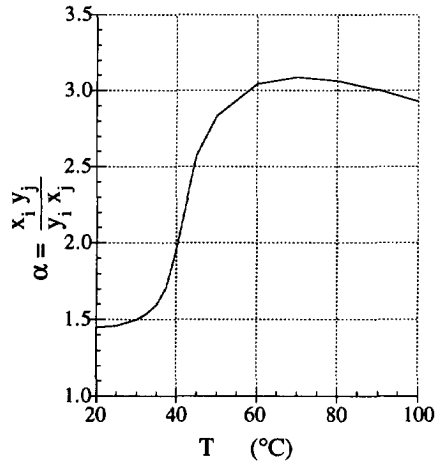


FIGURE 8.5B: The selectivity of hexadecane and octadecane as function of the temperature at a pressure of 90 bar.

The extraction temperature is set at 30°C, so that the solubility of pure hexadecane is 8.15%wt (see figure 8.1B) and the average selectivity is:  $\alpha_{ij} = 1.50$ . The best solvent-product separation is achieved at approximately 65°C at which hexadecane has a solubility of 0.12%wt (see figure 8.1B). These solubilities determine the possible separation that can be accomplished using the isobaric supercritical separation process at this pressure. We first calculate the minimum reflux ratio ( $R_{min}$ ) using the Underwood equation for a binary system (see e.g., Coulson and Richardson, 1987) as:

$$R_{min} = \frac{1}{\alpha_{ij} - 1} \left( \frac{x_{i,D}}{x_{i,F}} - \alpha_{ij} \frac{(1 - x_{i,D})}{(1 - x_{i,F})} \right) \quad (8.3)$$

Here  $x_{i,F}$  and  $x_{i,D}$  are the mol fractions of component  $i$  in the feed and extract stream. The reflux ratio is determined as:  $R = 5.53$  by applying  $R = 1.4R_{min}$ . The minimum hexadecane

concentration in the raffinate stream is obtained by assuming a constant hexadecane gas phase concentration in the bottom stage of the column. The hexadecane concentration in the raffinate is then calculated as:  $0.12/(8.15/1.50)/1.50 = 1.5\% \text{wt}$ . The total solvent to feed ratio is established using the solubility of hexadecane as:  $G_0/F=(R+1)D/y_{HD} = 6.53 \times 0.49/0.081 \approx 40$ . Finally the Smoker equation is applied to calculate the number of stages in the rectifying section ( $N_r = 23$ ) and the number of stages that still are effective in the stripping section of the column ( $N_s = 19$ ). Figure 8.6 shows the composition in the separation.

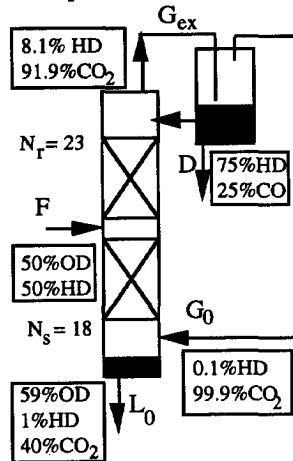


FIGURE 8.6: Schematic flowsheet for the separation of hexadecane and octadecane at 90bar and 30°C. Indicated are the compositions of the flows in weight percents.

The purity of the top flow is unlimited, but the purity of the bottom flow is dependent on the solvent-product separation in the heater (i.e.: E2 in figure 8.3). There are a few options using the configuration of figure 8.3, that can deal with a tighter bottom specification. The first option is the use of a different extraction pressure, which results in a different optimum separation temperature. The results for the separation at different extraction pressures using a temperature of 30°C are shown in table VIII.I.

TABLE VIII.I: The separation of hexadecane octadecane at isobaric process conditions. Indicated are the extraction pressure, the solvent-product separation temperature, the selectivity, the solubility in the solvent, the solvent free composition of the bottom flow, the solvent to feed ratio, the solvent free extract plus reflux flow and the enthalpy difference between extraction conditions and solvent-product separation conditions of pure carbon dioxide.

p bar	TE2 °C	$\alpha$	$Y_{HD}$ wt%	$X_{L0-OD}$ wt%	$G_0/F$ kg/kg	$(R+1)D$ kg	$\Delta H$ kJ/kg
75	50	1.62	5.64	99.3	48	2.73	151
80	55	1.56	6.66	99.1	44	2.97	163
90	65	1.50	8.15	98.5	40	3.27	178
100	75	1.45	9.26	97.5	37	3.57	191



The table shows that by using a lower extraction pressure a purity of 99%wt of octadecane can be achieved. As can be seen in figure 8.1B the increase in bottom purity is caused by the better separation at the top of the column using a temperature change. An other option would be the use of a second column with a separate solvent recycle. The feed of this column is the bottom stream of the first column. When this column mainly operates as stripping column and has a top stream that contains a fraction of hexadecane (e.g.: 10%wt), the purity can be increased with an order of magnitude.

For the isobaric supercritical separation process, hot water service flows are required for the heaters (E1) and (E2) and cooling water is required for heat exchanger (E3). These services are available at many sites at little costs. Table VIII.I shows the amount of energy required to heat up the solvent to solvent-product separation temperature. To design the heat exchangers at given conditions, the temperature as function of the enthalpy needs to be studied. Figure 8.7A shows the temperature profiles of carbon dioxide as function of the enthalpy for four pressures. Due to the behaviour of the specific heat of carbon dioxide near the critical temperature the lines are not linear. These effects should be considered within the design of the service flows. As an example the service flow around the 90bar isobar is drawn in figure 8.7B. When a minimum driving force of 2°C is applied the required temperature difference between the hot service flow and the cold service flow becomes 10°C.

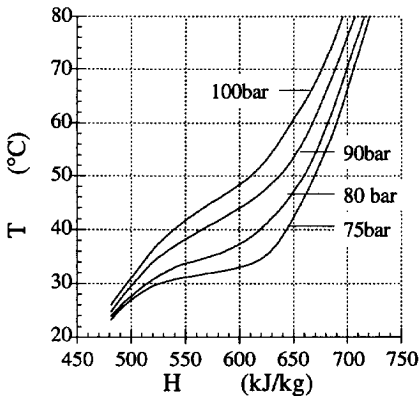


FIGURE 8.7A: The temperature of carbon dioxide as function of the enthalpy for four pressures.

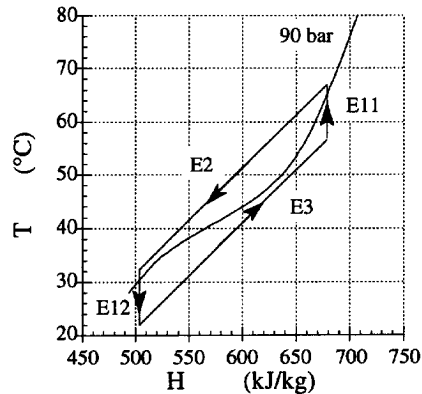


FIGURE 8.7B: The temperature of carbon dioxide as function of the enthalpy at a pressure of 90 bar enclosed by a heat transfer network.

To illustrate the differences of the service systems, a plant for the separation of hexadecane-octadecane using three service flow configurations will be designed. This will be done for a product feed of  $F=1\text{te/h}$  resulting in a solvent flow of  $G_0=40\text{te/h}$  when using an extraction pressure of 90bar. The three configurations will be based on the simplified flowsheet of figure

8.3, excluding heater (E1), since this main plant item is in principle not required for the operation. From table VIII.I it is found that at 90bar the amount of heat to increase the temperature of the solvent flow from 30 to 65°C is equal to:  $40 \cdot 178 = 7120 \text{ MJ/h} \equiv 1978 \text{ kW}$ . This energy is required for the solvent-product separation.

Configuration I considers the solvent cycle similar to the one illustrated in figure 8.3, but now the heating of the solvent and the cooling of the solvent cycle are carried out independently. The required amount of gauge steam for the heating of heater (E2) is equal to:  $7120/2257 = 3.15 \text{ te/h}$ . To control the temperature of the solvent stream, it is necessary to make-up hot water of 100°C, which is used in the heater (E2) and leaves the exchanger at 90°C. For the cooler (E3), cooling water at 20°C is used, which leaves the exchanger at 35°C. The required amount of cooling water for this duty is equal to:  $7120/(4.18 \cdot 15) = 113 \text{ m}^3/\text{h}$ . The sizes of the heat exchangers are estimated using an overall heat transfer coefficient of  $U_0 = 500 \text{ W/m}^2/^\circ\text{C}$  for all applications. The heater (E2) using hot water made from steam, has an average temperature difference of 50°C, so that the required area becomes  $A_{E2} = 1978/(0.5 \cdot 50) = 79 \text{ m}^2$ . The cooler has an average temperature difference of 12°C, so that the required area becomes  $A_{E3} = 1978/(0.5 \cdot 20) = 198 \text{ m}^2$ .

Configuration II uses the continuous service flow cycle as indicated in figure 8.3. The temperature of the service flow is controlled with an additional heater (E11) and cooler (E12). The temperature enthalpy cycle of the service flow and the solvent flow is illustrated in figure 8.7B. If water is used as service fluid the size of the service flow becomes  $7120/(4.18 \cdot 35) = 48.6 \text{ te/h}$ . The required heat input (E11) becomes  $48.6 \cdot 4.18 \cdot 10 = 2.03 \text{ MJ/h} \equiv 565 \text{ kW}$ . The necessary amount of steam for heater (E11) is therefore:  $2034/2257 = 0.902 \text{ te/h}$ . Since the average temperature difference is decreased to 5°C, the increasing energy efficiency requires larger surface areas for the heater (E2) and the cooler (E3). They both require a specific exchange area equal to  $A_{E2} = A_{E3} = 1978/(0.5 \cdot 5) = 791 \text{ m}^2$ .

At this stage it is interesting to evaluate the energy requirements for distilling hexadecane and octadecane. An indication can be found by assuming the required energy for this distillation equal to the sum of the total heat of condensation of the top vapour flow plus the energy required to heat the feed to its boiling point. Figure 8.8 shows the vapour pressure and selectivity for hexadecane and octadecane as function of the temperature (Reid et al., 1988). If the reboiler is operated at 225°C and 100mbar, the selectivity is equal to:  $\alpha_{ij} = 2.2$ . Using the Underwood relation (8.3) for the minimum reflux ratio, the top vapour flow is calculated as  $(1.4 \cdot 1.67 + 1) \cdot 0.5 \text{ te/h} = 1.67 \text{ te/h}$ . Applying a heat of condensation of 300kJ/kg this contribution becomes  $1.67 \cdot 300 = 500 \text{ MJ/h} \equiv 139 \text{ kW}$ . Applying a specific heat of 2.0kJ/kg/K, the energy required to heat the feed to its boiling temperature becomes  $(2.0 \cdot 200 \cdot 1000) = 400 \text{ MJ/h} \equiv 111 \text{ kW}$ . The total required energy for distilling hexadecane and octadecane therefore becomes:  $900 \text{ MJ/h} \equiv 250 \text{ kW}$ .

When comparing the required energy for the separation, one must conclude that distillation requires less energy than the supercritical separation. However, the energy consumption of the supercritical separation process can be improved when the thermal fluid used for the heating of the solvent flow is optimized. Clearly, the best fluid to follow the profile of the solvent is an equal amount of same solvent at the same conditions.

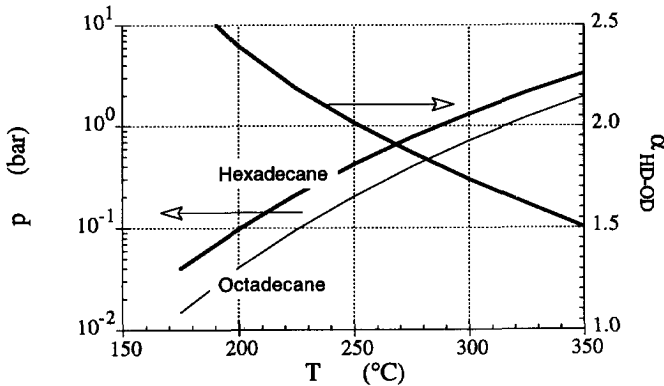


FIGURE 8.8: The vapour pressure and selectivity for hexadecane octadecane as function of the temperature.

This leads us to configuration III, which is illustrated in figure 8.9. In this case the solvent flow cannot be maintained using the pressure difference within the process. The solvent has to be circulated using an axial pump as indicated in the figure. Since the pressure differences of this process are almost balanced, the required energy for the pump to maintain the flow is small (i.e.: ~1.6kW for this application). The total energy used in the solvent stream will be made equal to the energy used for distillation (250kW). The energy in the solvent stream therefore becomes  $900/40 = 22.5\text{kJ/kg}$ . At 90bar this means an average temperature difference over the heat exchanger (E2) of 5°C. The required heat-transfer area therefore becomes equal to  $A_{E2} = 1978 / (0.5 \cdot 5) = 791\text{m}^2$ .

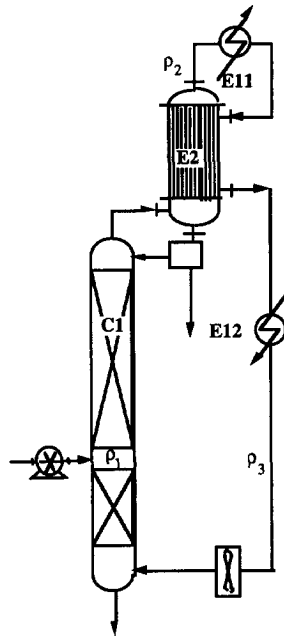


FIGURE 8.9: Configuration III. Simplified flowsheet of integrated solvent flow.

The for heater (E11) required amount of steam is now calculated as:  $900/2257 = 0.399\text{te/h}$ .

Given the rough approximations it is emphasised that this analysis only intends to show the potential of an nearly isobaric supercritical separation process. A temperature difference over the heat exchanger of  $5^\circ\text{C}$  might be too tight, but not impossible given the fact that the streams are equal. The analysis indicates that an isobaric supercritical fluid separation can be as energy effective as normal distillation. However, the type of energy used in supercritical separations is quite different. At many sites a service flow of approximately  $70^\circ\text{C}$  can often be made available from other processes at little costs. It therefore can be concluded that isobaric supercritical separation is potentially more energy efficient than vacuum distillation and steam distillation.

The real question does not concern the energy efficiency, but the economical feasibility of the process. The equipment costs and operating costs for the three configurations are listed in table VIII.II. The designs include recovery facilities for carbon dioxide, which is dissolved in the separated hexadecane and octadecane. Not included in this analysis are labour and maintenance. In the operating costs a distinction is made between normal steam and a waste energy stream available from an other process.

TABLE VIII.II: The costs of the main plant items, the operating costs, and the total costs for the isobaric supercritical separation of hexadecane octadecane at 90bar using carbon dioxide and three different service configurations and two options for the heat supply.

MPI Equipment Cost	Configuration I kf	Configuration II kf	Configuration III kf
E2	217	1185	1185
E3	432	1185	
E11		65	92
E12		188	187
E21 (hot water)	109	51	38
Pump (2kW)			20
<b>Sub Total Heat Services</b>	<b>758</b>	<b>2674</b>	<b>1522</b>
C1 (H=15m;D=1m)	763	763	763
Packing CY	226	226	226
P1 (5kW)	40	40	40
Degas pots extract/residue	15	15	15
Recompression (20kW)	195	195	195
<b>Sub total</b>	<b>1997</b>	<b>3913</b>	<b>2761</b>

**Operating Costs f/h**

Electrical f0.13/kWh	3.25	3.25	3.25	3.25	3.25	3.51	f/h
Steam f30/te	94.5		26.98		13.1		f/h
Waste Steam f5/te		15.75		4.50		2.18	f/h
Cooling water f0.10/m3	11.34	11.34	6.07	6.07	2.93	2.93	f/h

<b>Installed Equipment Costs</b>	<b>7406</b>	<b>7406</b>	<b>14763</b>	<b>14763</b>	<b>10355</b>	<b>10355</b>	<b>kf</b>
----------------------------------	-------------	-------------	--------------	--------------	--------------	--------------	-----------

Depreciation (15%/A)	1111	1111	2214	2214	1553	1553	kf/A
Operating Costs (kf/A)	873	243	290	111	154	69	kf/A
<b>Total</b>	<b>0.25</b>	<b>0.17</b>	<b>0.31</b>	<b>0.29</b>	<b>0.21</b>	<b>0.20</b>	<b>f/kg</b>

The most favourable configuration would be the independent heating and cooling system using a waste energy stream for the heating. Interesting enough the costs for this separation are in the same range as vacuum distillation. Despite of the fact that the configuration using a closed service system, uses only 25% of the energy of the non-closed service system, the investment costs are twice as large and it is therefore unlikely that this configuration will be used. However, configuration III is both cost effective with respect to energy use and investment.

### CONCLUDING REMARKS

In this chapter it has been shown that the supercritical separation process has the potential to become an energy effective process when the isobaric features are fully explored. It also showed that the required energy for isobaric supercritical separation can become similar to those for distillation applications. Besides this the process has the advantage of applying near ambient temperatures, so that waste heat streams of other processes can be used as energy sources. When the investment costs of an isobaric process are compared with a process using a pressure change, the isobaric process most likely has lower costs. The costs of an isobaric supercritical separation are in the same range as normal vacuum distillation of 20mbar.

The isobaric supercritical separation shows that the potential of the supercritical technology is still far from fully exploited.

### NOTATION

Symbol	Description	Unit
D	Extract flow .....	kg/s
$f^\beta$	Fugacity of phase $\beta$ .....	
F	Feed flow .....	kg/s
g	Gravitational acceleration .....	m/s <sup>2</sup>
G	Gas flow .....	kg/s
$G_0$	Solvent flow .....	kg/s
$G_{ex}$	Extract flow .....	kg/s
H	Enthalpy .....	J/kg
$k_{ij}$	Peng-Robinson binary interaction parameter .....	
$L_0$	Liquid raffinate flow .....	kg/s
$l_{ij}$	Peng-Robinson binary co-volume parameter .....	
$N_r$	Number of equilibrium stages in the rectifying section .....	
$N_s$	Number of equilibrium stages in the stripping section .....	
p	Pressure .....	Pa
R	Reflux ratio .....	
$R_{min}$	Minimum reflux ratio .....	

---

S	Entropy .....	
T	Temperature.....	K
$x_i$	Mol fraction in the liquid phase.....	mol/mol
$X_i$	Mass fraction in the liquid phase .....	kg/kg
$y_i$	Mol fraction in the gas phase.....	mol/mol
$Y_i$	Mass fraction in the liquid phase .....	kg/kg
$z$	Axial co-ordinate .....	m
$\alpha_{ij}$	Selectivity .....	
$\Delta p$	Static pressure differences.....	Pa

---

## REFERENCES

- [1] McHugh, M.A. & Krukonis, V.J., (1986). *Supercritical Fluid extraction: Principles and Practice*, Butterworths, Stoneham.
  - [2] Bartle, K.D., Clifford, A.A., Jaffar, S.A., Shilstone, G.F. (1991). *Solubilities of Solids and Liquids of Low Volatility in Supercritical Carbon Dioxide*. J.Phys.Ref. Data, **20**: 713 - 756.
  - [3] Birtigh, A. and Brunner, G., (1994), *Regeneration of loaded CO<sub>2</sub> by means of isobaric processes*, 3rd Int. Symposium on Supercritical Fluids, TOME 2 pp. 41- 46.
  - [4] Brunner, G., and Peter, S., (1982). *Sep. Sci. Techn.*, **17**: pp. 199.
  - [5] Coulson, J.M., Richardson, J.F., (1986). *Chemical Eneengineering Vol. 2*, 3rd ed, Pergamon Press, Oxford.
  - [6] Coulson, J.M. Richardson, J.F. & Sinnott, R.K., (1983). *Chemical Engineering Vol. 6: Design*, Pergamon Press, Oxford.
  - [7] Haan, de A.B. (1991). *Supercritical fluid extraction of liquid hydrocarbon mixtures*. PhD Thesis, Delft: Delft University Press.
  - [8] Johnston, K.P., Barry, S.E., Read, N.K., and Holcomb, T.R., (1987). *Separation of Isomers Using Retrograde Crystallization from Supercritical Fluids*, *Ind. Eng. Chem. Res.* **26** p2372-2377.
  - [9] Johnston, K.P., Peck, D.G. and Kim, S. (1989). *Ind. Eng. Chem. Res.*, **28** p1115.
  - [10] Peng, D.-Y., Robinson D.B., *Ind. Eng. Chem. Fundam.* **15** 59-64 (1976).
  - [11] Reid, R.C., Prausnitz, J.M., Poling, E.P., (1988). *The Properties of Gases & Liquids*, 4<sup>th</sup> ed. New York: McGraw-Hill.
  - [12] Schmitt, W.J., and Reid, R.C., (1985), *The influence of the solvent gas on solubility and selectivity in supercritical extraction*, Elsevier Science Publishers B.V., Amsterdam, *Supercritical Fluid Technology*, ed. by Penninger, Radosz, McHugh and Krukonis.
  - [13] Woerlee, G.F. (1992). *Process and Device for Separating a Mixture or Extracting a Material*. Int. Pub. No. WO 94/13377. Int. App. No. PCT/NL93/00264.
-

## The Removal of Undesirable Components from Edible Oils Using SFE

An edible oil is a complex mixture of hundreds of tri-glycerides. Crude vegetable oils are usually produced by grinding and pressing the seeds of plants such as rapeseed, soy bean or sunflower. They are then refined to yield edible oils. Beside the tri-glycerides, many components are still present in the crude oil which influence taste and colour. These components range from free fatty acids, phospholipids (slimes), sterols and pigments to Polycyclic Aromatic Compounds (PAC's) and pesticides. Some of these, like vitamins and natural antioxidants, should remain in the oil. Obviously, the last two have to be removed almost completely. The presence of pesticides is due to their use to protect the crops, while the presence of PAC's are caused by exhaust gases and slash and burn agricultural techniques.

Currently, the components are removed from the oil by stripping the oil using high temperature steam (180-270°C) at low pressure (5mbar). This deodorization process causes destruction of heat sensitive components (auto oxidation) and cis-trans transformations of the unsaturated fatty acids. Considering the present consumer awareness towards natural products, the high temperature renders this process unfavourable compared to a potential "green" process.

A non destructive alternative that removes the undesirable compounds without effecting the natural composition of the edible oil is supercritical carbon dioxide extraction. In this chapter a 100kte/A supercritical extraction plant is designed that removes the traces to a level well below 5ppb, while the temperature of the process should not exceed 120°C.

### PROCESS THERMODYNAMICS

For the design of an supercritical extraction process using carbon dioxide, solubility data of the involved components in carbon dioxide are required. Several methods are available to interpolate and extrapolate the data by using an equation of state. However, even more sophisticated equations, like the Peng-Robinson equation of state are not successful in fitting the data at all temperature and pressures for large molecules (see, e.g.: Yu et al., 1994) so that temperature dependent binary interaction parameters are required. This process design requires the description of the tri-glycerides solubility behaviour, which are large molecules. Several papers (see, e.g.: Johnston et al., 1981; Schmitt and Reid, 1985; Bartle et al., 1991) come to the conclusion that a correlation using an enhancement factor for the vapour pressure (Prausnitz et al., 1986) as function of the density is the best available route. This leads to an equation

which expresses the mass fraction  $Y_i$  of a component in the solvent phase at constant temperature as function of the solvent density  $\rho$ ,

$$\ln Y_i = A + B_0 \rho, \tag{9.1}$$

where  $A, B_0$  are constants. In this study it is found that the temperature dependency of the solubility can be taken into account when the equation is written as:

$$\ln Y_i = \frac{a}{T} + B_0 \rho \tag{9.2}$$

This effectively means that both the solvent density and the vapour pressure of a component can be described using an exponential function. When equation (9.2) is written as:

$$T \ln Y_i = a + b T_r \rho, \tag{9.3}$$

all data have to fit a straight line. In equation (9.3) the reduced temperature  $T_r = T/T_c$  of carbon dioxide is introduced, so that the x-axis will be close to the real solvent density. Figure 9.1 shows the solubility of a number of edible oils at different temperatures as reported by Quirin and Brunner (1982) and Brunner (1986) together with own measurements.

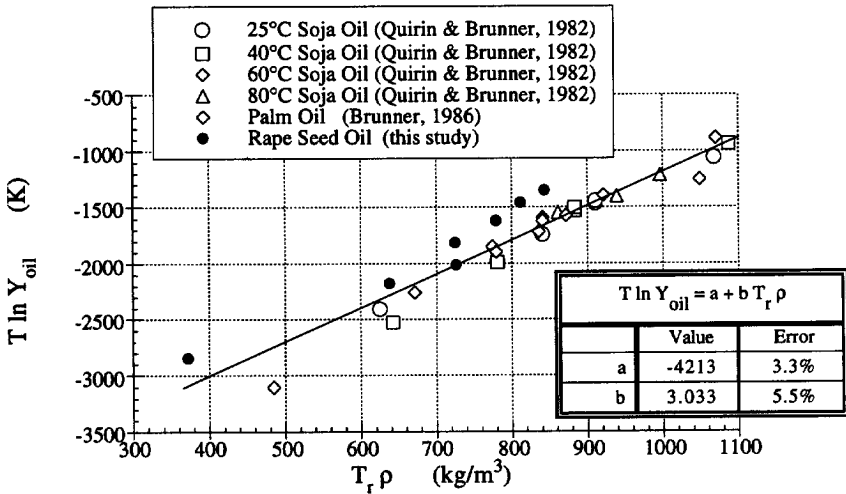


FIGURE 9.1: Solubility of edible oils in carbon dioxide as function of the density.

The quotient of the distribution factors, determining the selectivity can be approximated as:

$$\alpha = \frac{K_i}{K_j} = \frac{Y_i X_j}{X_i Y_j} \approx e^{(b_i - b_j) \rho} + (a_i - a_j) / T = e^{\Delta b \rho} + \Delta a / T \tag{9.4}$$

Relation (9.4) describes the selectivity as function of the temperature and density. It is useful to calculate the selectivity on a solvent free basis, so that one has direct insight in the viability of the separation. In this special case this is convenient since the concentration of the oil, on solvent free basis, in both the solvent and the liquid phase are close to unity. The selectivity of the dissolved contaminants therefore is practically equal to the distribution coefficient.

In this study the selectivities of trace contaminants in edible oils were investigated. To model the contaminated oil three polycyclic aromatic compounds, an organochlorine and an organo-



phosphorous pesticide (see table IX.I) were added to rape seed oil. To enable an analysis at our laboratory the feed concentration of the contaminants was made 100 ppm wt%. The selectivities of the components were measured for temperatures varying between 35 to 105°C and pressures up to 300 bar. This was done in a counter-current supercritical extraction column, which was described by de Haan (1991), using carbon dioxide as solvent. The concentrations in the extracted material were analysed using HPLC and GC equipment. The determined selectivities could be described using equations (9.4), an illustration is shown in the figures 9.2A and 9.2B. An overall data summary is given in table IX.I.

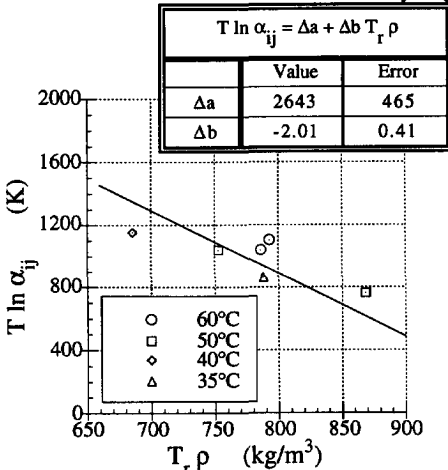


FIGURE 9.2A: The measured selectivity of phenanthrene - oil, shown as function for the carbon dioxide density for various temperatures.

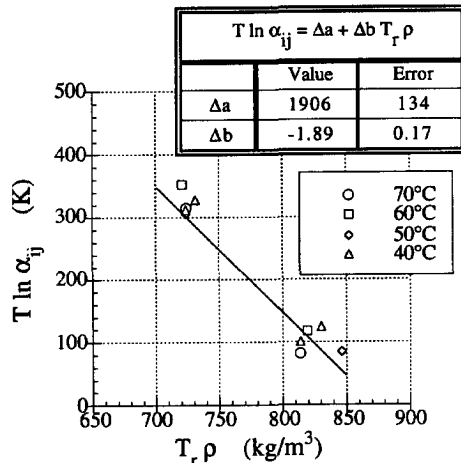


FIGURE 9.2B: The measured selectivity of benzo( $\alpha$ )pyrene - oil, shown as function for the carbon dioxide density for various temperatures.

TABLE IX.I: The used contaminants in rape seed oil, their chemical formulas and the experimentally determined selectivity parameters (accuracy approximately 10%). The last columns shows some typical selectivity values.

Component	Formula	M g/mol	$\Delta a$ ( $K^{-1}$ )	$\Delta b$ K m <sup>3</sup> /kg	$\alpha$ (100°C, 400 bar)
phenanthrene	C <sub>14</sub> H <sub>10</sub>	178	2643	-2.01	9.90
chrysene	C <sub>18</sub> H <sub>12</sub>	228	2446	-1.90	7.59
benzo( $\alpha$ )pyrene	C <sub>20</sub> H <sub>12</sub>	252	1906	-1.89	1.83
dimethoate	C <sub>5</sub> H <sub>12</sub> NO <sub>3</sub> PS <sub>2</sub>	229	5451	-4.30	78.18
lindane	C <sub>6</sub> H <sub>6</sub> Cl <sub>6</sub>	290	5259	-4.24	53.91

## PROCESS DESIGN

All poly-aromatic compounds need to be removed from the edible oils in the purification process. The heavier fraction of it can be removed by active carbon adsorption. In this section an extraction process is proposed for the removal of the more volatile poly-aromatic components (less than 5 benzene rings); chrysene is therefore taken as key component. For the design it is assumed that the edible oil contains 200 ppb of chrysene only. This needs to be

reduced to a concentration less than 5 ppb. The temperature of the process has not to exceed 120°C to avoid any thermal degradation of the oil. Carbon dioxide is used as solvent while the capacity of plant intake is taken as 100 kte/A.

*The solvent flow*

An important cost determining factor with SFE is the quantity of solvent through the column, since it determines the size of nearly all equipment and is largely responsible for the energy consumption. The solvent flow can be calculated by determining the extract stream (D) of the process (see figure 9.3). The extract stream is in this case in principle a waste oil stream and it therefore needs to be minimized. Due to the measured selectivities it is therefore required to create a reflux stream to accomplish this goal. When the selectivity is known, a minimum reflux  $R_{min}$  can be calculated using the Fenske equation (See, e.g., Coulson and Richardson, 1985). The total necessary top flow of oil  $G_{oil}$ , which is the quantity of oil that needs to be dissolved in the solvent, is then calculated as:

$$G_{oil} = (R + 1)D = (1.4 R_{min} + 1) D \tag{9.5}$$

By using the Smoker relations (See, e.g., Coulson and Richardson, 1985) it has been found that a reflux ratio of  $1.4 R_{min}$  leads to an optimum between the total number of required theoretical stages  $N$  (the height of the column) and the quantity of necessary solvent flow (the diameter of the column).

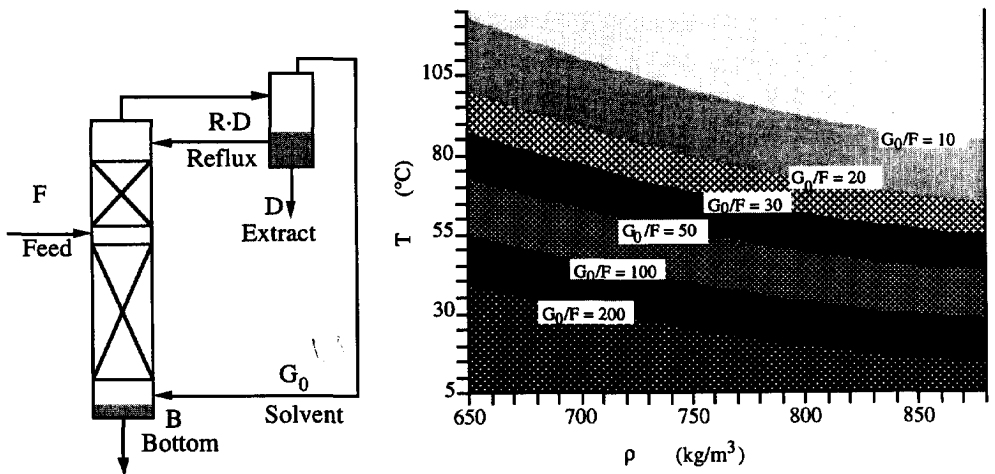


FIGURE 9.3 & 9.4 : The simplified process flowsheet with used notation and the solvent to feed ratio as function of the extraction temperature and density.

When the extract stream is decreased the reflux ratio has to be increased to accomplish the bottom specification. This has the nett result that the total quantity of top oil vapour flow is nearly constant and can therefore be expressed as function of the selectivity only;

$$G_{oil} = (R + 1) D = 2.551 \alpha^{-1.250} \quad (9.6)$$

The total solvent flow,

$$G_0 = \frac{G_{oil} (1 - Y_{oil})}{Y_{oil}} \quad (9.7)$$

can now be calculated via the earlier derived solubility for the edible oil (see figure 9.1) and the selectivity of the key component crysene (see table IX.I) using the equations (9.3), (9.4) and (9.7). The result of this exercise is shown in figure 9.4, where the solvent to feed ratio is shown as function of the temperature and the solvent density. It can be seen that a low solvent to feed ratio can be achieved only at relative high temperature. However, these higher temperatures require relative large pressures. Since the increase in pressure is less steep than the decrease of solvent to feed ratio, it pays off to design the process at higher temperatures.

### Column design

When the quantity of necessary solvent is known the capacity of the column diameter can be calculated. In this design the capacity is calculated via the relation given by Sulzer for BX packing, which expresses the maximum superficial vapour velocity  $u_{SG}$  (flooding limit),

$$u_{SG} = C_G^{crit} \sqrt{\frac{\rho_L - \rho_G}{\rho_G}} \quad (9.8)$$

as function of the flow parameter  $\Phi$ , (Sulzer, 1989)

$$\Phi = \frac{L}{G} \sqrt{\frac{\rho_G}{\rho_L}} \quad (9.9)$$

before flooding occurs. Equation (9.9) contains the load factor  $C_G^{crit}$  which is an empirical velocity given as function of the flow parameter for a particular type of packing (Sulzer, 1989) and is in this case of the order 0.1 m/s. The diameter of the column  $D_{col}$  is now calculated as:

$$D_{col} = 1.1 \sqrt{\frac{4G}{\pi \rho_G u_{SG}}} \quad (9.10)$$

The factor 1.1 assures that the design velocity is 80% of the flooding limit. The final costs of the column can now be estimated by calculating the mass of column ( $m_{col}$ ) necessary for construction. Calculating the wall thickness  $t_{col}$  in relation with the yield stress  $\sigma_S$  and the pressure the total mass of the column,

$$m_{col} = t_{col} \pi D_{col} H_{col} \rho_S = \frac{p D_{col}}{2 \sigma_S} \pi D_{col} H_{col} \rho_S = p V_{col} \frac{\rho_S}{2 \sigma_S} \quad (9.11)$$

is proportional to the column volume  $V_{col}$  and the operating pressure. The height of the column follows from the number of stages (Fenske equation, Coulson et al., 1985) and the height of a theoretical stage. The height of a theoretical stage is calculated using the mass transfer model of Bravo et al, 1985. The resulting required quantity of steel is shown in figure 9.5. The minimum is found at relatively high temperatures. The white right hand area in the chart represents the flooding condition of the column while the white bottom area represents a three phase system.

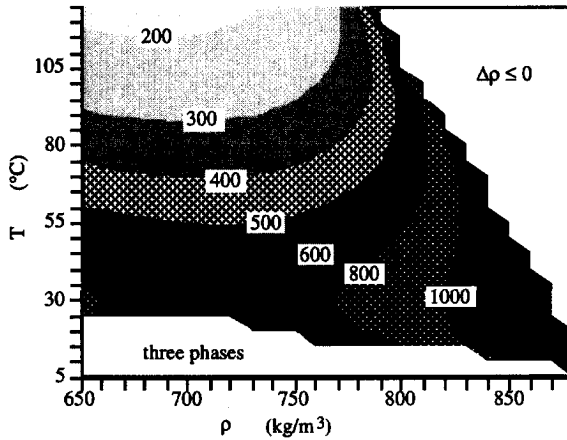


FIGURE 9.5: The quantity of steel contours in (kte) as function of the solvent density and the temperature.

The operating pressure as function of the applied density and temperature is shown in figure 9.6. This graph shows that the lowest required quantities of steel are found at relative large operation pressures. The final extraction conditions are chosen as 110°C and 400 bar, leading to a solvent density of 720 kg/m<sup>3</sup>.

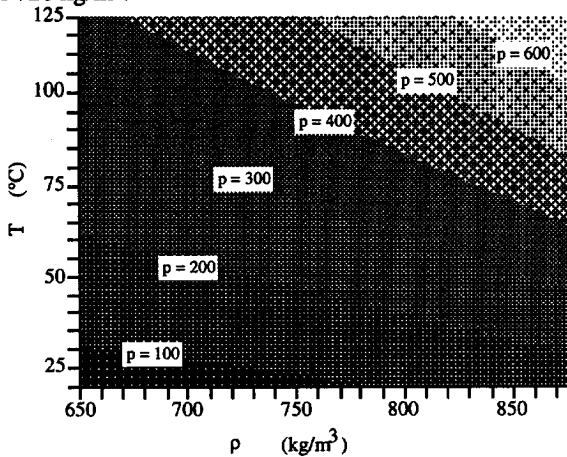


FIGURE 9.6: The operating pressure contours in (bar) as function of the solvent density and the temperature.

*Flash vessels*

The carbon dioxide that is dissolved in the oil needs to be separated and recycled into the column. The dissolved quantity of carbon dioxide in the oil was experimentally determined. The result could be correlated using a relation depending on the solvent density;  $X_{CO_2} = 370 \times 10^{-6} \rho_G$ . The settling velocity  $u_o$  of such a vessel can be calculated as:

$$u_0 = 0.035 \sqrt{\frac{\rho_L - \rho_G}{\rho_G}} \quad (9.12)$$

Given the quantity of dissolved carbon dioxide and the conditions the settling equipment is sized.

*The solvent extract separator.*

Apart from the column the separator is an important item since it specifies the separation condition at the bottom of the column via the recycled carbon dioxide. Following the earlier analysis and the maximum allowed temperature of 120°C, it has been chosen to take as reference operating condition 400bar 110°C which leads to a solvent density of 720 kg/m<sup>3</sup>. The extracted product has now to be condensed from the loaded carbon dioxide phase. The recycled carbon dioxide has to go back into the column so that it determines the bottom condition. The concentration of contaminating compounds in the recycled carbon dioxide  $Y_{i,D}$  is equal to:

$$Y_{i,D} = \alpha_{i,D} \frac{Y_{oil,D}}{X_{oil,D}} X_{i,D} = \alpha_{i,D} Y_{oil,D} X_{i,D} \quad (9.13)$$

Here  $\alpha_{i,D}$  is the selectivity at the condition in separation vessel and  $X_{i,D}$  is the concentration of contaminate of the extract in the separator. The bottom contaminate concentration in the solvent phase  $Y_{i,B}$  is given by:

$$Y_{i,B} = \alpha_{i,B} \frac{Y_{oil,B}}{X_{oil,B}} X_{i,B} = \alpha_{i,B} Y_{oil,B} X_{i,B} \quad (9.14)$$

Here  $\alpha_i$  is the selectivity in the column and  $X_{i,B}$  is the concentration of contaminate at the bottom of the column. The restriction of the separation via the recycling of the carbon dioxide is given by the relation between top and bottom stream of:

$$Y_{i,D} \leq Y_{i,B} \quad (9.15)$$

The bottom concentration is specified on 5ppb while the feed contains at maximum a concentration of 200 ppb. It therefore follows that the top concentration can be expressed via:

$$\begin{aligned} FX_{i,F} &= DX_{i,D} + BX_{i,B} \Rightarrow X_{i,F} = \frac{D}{F} X_{i,D} + \left(1 - \frac{D}{F}\right) X_{i,B} \\ 200 &= \frac{D}{F} X_{i,D} + \left(1 - \frac{D}{F}\right) 5 \approx \frac{D}{F} X_{i,D} \Rightarrow X_{i,D} = 200 \frac{F}{D} \end{aligned} \quad (9.16)$$

where the equation

$$F = D + B \quad (9.17)$$

was used. The concentration can now be expressed in terms of feed F and bottom stream B. Using the equations (9.13) to (9.15) it follows that a relation can be deduced that expresses the percentage of bottom stream as function of the solubilities and selectivities as:

$$\begin{aligned} \frac{Y_{i,D}}{Y_{i,B}} &= \frac{\alpha_{i,D} Y_{oil,D} X_{i,D}}{\alpha_i Y_{oil,B} X_{i,B}} = 1 \Rightarrow \frac{X_{i,B}}{X_{i,D}} = \frac{5}{200} \frac{D}{F} = \frac{\alpha_{i,D} Y_{oil,D}}{\alpha_i Y_{oil,B}} \\ \frac{D}{F} &= \frac{1}{40} \frac{\alpha_{i,D} Y_{oil,D}}{\alpha_i Y_{oil,B}} \end{aligned} \quad (9.18)$$

Figure 9.7 shows the relative bottom product stream as function of the temperature and density. Given the extraction condition of  $720 \text{ kg/m}^3$  and  $110^\circ\text{C}$ , the graph shows the relative possible bottom stream towards this condition. However, it can be scaled back by multiplying with the extraction conditions and dividing through any other condition. It is therefore interesting to see that for a process with a commercially interesting yield, the operation step always is found in the left hand down corner with relatively low densities and temperatures.

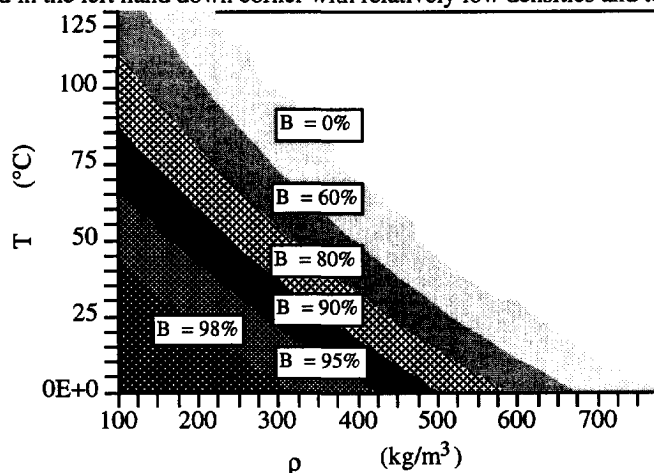


FIGURE 9.7: The bottom flow relative to feed as function of the density and temperature.

#### OVERALL PROCESS COSTS

Using the above information and other design rules the total process is designed as shown in appendix 9.A. The equipment is specified in appendix 9.B. The total running costs are shown below. The main part of these costs is caused by compressor P3. The total capital investments have been estimated by Fluor Daniel B.V. (December, 1993) using an equipment factored estimate, which has a  $-20/+25\%$  accuracy. The important items are specified in table IX.II indicated in thousands of Dutch florins. The total capital costs per ton intake is then calculated as:  $0.17 \times 32.793 \times 10^6/10^5 = f 55.75/te$ , leading to a total price per ton of  $f97.60$ .

TABLE IX.II: The total investment costs in  $kf$  and the operating costs expressed in  $f/te$ .

CAPITAL COSTS			RUNNING COSTS	
Item	Equipment Cost	unit price $kf$ Installed	Item	Units Costs
P1, P2, P4, P5, P6	1 035	2 921	Electrical P3	2.4 MW 23.04
P3	4 800	11 040	Electrical other	0.6 MW 7.20
V1	1 900	7 125	Cooling Water	134 te/h 1.61
V2, V3, V4, V5, V6	1 115	4 182	Manning	5 x f150 000 /A 7.50
E1, E2, E3	706	2 259 +	Carbon dioxide	5 kg/te 2.50
Sub TOTAL		27 527	TOTAL	41.85
Instrumentation		966		
Utilities & Contingency		4 300 +		
TOTAL		32 793		

## CONCLUDING REMARKS

The purification of edible oils using SFE is technically feasible. Both running and investment costs are largely influenced by the solvent recycle and the detailed design should therefore focus on this item. The costs per ton edible oil are considerably larger than that of the currently used technology of vacuum steam stripping (40f/te). However, the final economical evaluation also contains marketing consideration, which are beyond the scope of this research.

The optimization of the process showed that the extraction conditions are a trade-off between selectivity and solubility, which in this case is dominated by the solubility and leads to an at first sight none obvious process condition. Successful use was made of the simple thermodynamic solubility relation, which connects the density of the solvent to the solubility of a component.

## ACKNOWLEDGEMENT

The authors would like to express there gratitude to Unilever for their suggestions and technical support and to Fluor Daniel BV for the calculation of the capital investments.

## NOTATION

Symbol	Description	Unit
A	Constant .....	
a	Vapour pressure depending constant.....	K
B	Bottom flow .....	kg/s
$B_0$	Solvent density depending constant .....	$m^3/kg$
b	Solvent density depending constant.....	$Km^3/kg$
$C_G^{crit}$	Critical capacity factor: .....	m/s
D	Extract flow .....	kg/s
$D_{col}$	Column diameter .....	m
F	Feed flow.....	kg/s
G	Gas flow.....	kg/s
$G_0$	Solvent flow .....	kg/s
$G_{oil}$	Oil flow.....	kg/s
$G_{ex}$	Extract flow .....	kg/s
$H_{col}$	Column height .....	m
$K_i$	distribution factor.....	
L	Liquid flow.....	kg/s
$m_{col}$	Column mass .....	kg
M	Molar weight.....	kg/mol

---

p	Pressure .....	Pa
R	Reflux ratio.....	
R <sub>min</sub>	Minimum reflux ratio .....	
T	Temperature.....	K
T <sub>r</sub>	Reduced temperature of carbon dioxide .....	
t <sub>col</sub>	Column wall thickness.....	m
u <sub>o</sub>	Settling velocity.....	m/s
u <sub>SG</sub>	Superficial solvent velocity.....	m/s
V <sub>col</sub>	Column volume.....	m <sup>3</sup>
X <sub>i</sub>	Mass fraction in the liquid phase .....	kg/kg
Y <sub>i</sub>	Mass fraction in the liquid phase .....	kg/kg
z	Axial co-ordinate .....	m
α <sub>ij</sub>	Selectivity .....	
Δp	Static pressure differences.....	Pa
ρ	Solvent density .....	kg/m <sup>3</sup>
ρ <sub>G</sub>	Gas density.....	kg/m <sup>3</sup>
ρ <sub>L</sub>	Liquid density.....	kg/m <sup>3</sup>
ρ <sub>S</sub>	Steel density.....	kg/m <sup>3</sup>
σ <sub>s</sub>	Normal design stress of the steel .....	N/m <sup>2</sup>

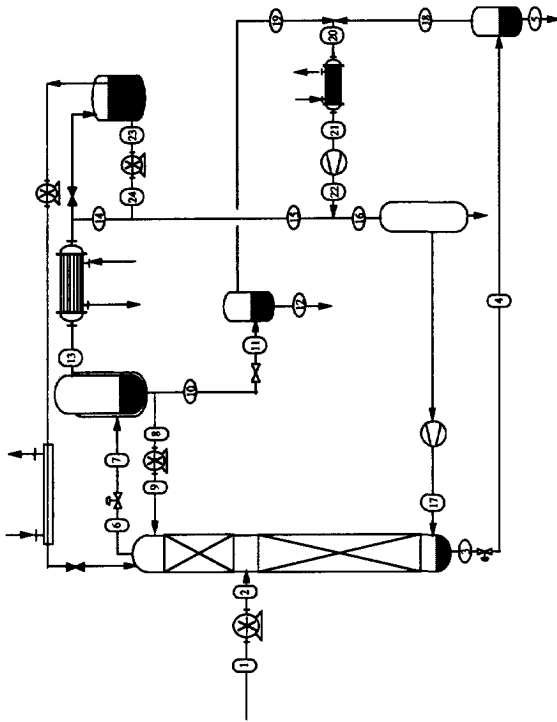
---

## REFERENCES

- [1] Bartle, K., Clifford, A., Jaffar, S., Shilstone, G. *J.Phys.Ref. Data*, **20**, 1991, p713
  - [2] Bravo, J.L., Rocha, J.A., and Fair, J.R., (1985), *Mass Transfer in Gauze Packings, Hydrocarbon Processing*, 91-95.
  - [3] Brunner, G., *Fette Seifen Anstrichm.*, **88**, 1986, p464-474.
  - [4] Coulson, J.M. Richardson, J.F. & Sinnott, R.K., (1983). *Chemical Engineering Vol. 6: Design*, Pergamon Press, Oxford.
  - [5] Haan, de A.B. (1991). *Supercritical fluid extraction of liquid hydrocarbon mixtures*. PhD Thesis, Delft: Delft University Press.
  - [6] Johnston. K.P., Peck, D.G., Kim, S. *Ind. Eng Chem. Res.*, **28**, 1989, p1115.
  - [7] Prausnitz, J.M., Lichtenthaler, R.N., de Azevedo, G.E. 2<sup>nd</sup> ed. 1986, New York.
  - [8] Quirin, K.W., Brunner, G., *Fette Seifen Anstrichm.*, **84**, 1982, p460-468.
  - [9] Sulzer Brother Ltd., 1989, *Information Bulletin*.
  - [10] Schmitt, W.J., and Reid, R.C., (1985), *The influence of the solvent gas on solubility and selectivity in supercritical extraction*, Elsevier Science Publishers B.V., Amsterdam, *Supercritical Fluid Technology*, ed. by Penninger, Radosz, McHugh and Krukonic.
  - [11] Yu, Z-R., Sizvi, S.S.H., and Zollweg, J.A., (1992), *Phase equilibria of Oleic Acid, Methyl Oleate and Anhydrous Milk Fat in Supercritical Carbon Dioxide*, *J. Supercrit. Fluids*, **5** pp. 114-122.
-



### APPENDIX 9.A Flowsheet for the purification of edible oils using carbon dioxide.



	1	2	3	4	5	6	7	8	9	10	11	12	13	14	15	16	17	18	19	20	21	22	23	24	UNITS
CO <sub>2</sub>					0.064	0.045	0.045	0.045	0.045	0.045	0.045	0.045	0.045	0.045	0.045	0.045	0.045	0.045	0.045	0.045	0.045	0.045	0.045	0.09	kg/hr
OIL	12.5	12.5	12	12	2.88	2.88	2.88	2.88	2.88	2.88	2.88	2.88	2.88	2.88	2.88	2.88	2.88	2.88	2.88	2.88	2.88	2.88	2.88	2.88	kg/hr
Chrysene	2.5	2.5	0.06	0.06	0.06	13.09	13.09	10.57	10.57	2.44	2.44	2.44	0.08	0.08	0.08	0.08	0.08	0.08	0.08	0.08	0.08	0.08	0.08	0.08	μg/hr
TEMP.	400	400	12	12	400	75	75	400	75	12	12	12	75	75	75	400	12	12	12	12	12	12	12	75	°C
PRESSURE	110	100	110	53	35	110	35	35	35	20	20	20	35	32	32	110	53	20	53	25	170	16	29	260	bar
DENSITY	814	814	790	V/L	835	720	V/L	823	866	823	V/L	880	270	480	480	460	720	19.5	21.7	19.5	21.3	91	833	250	kg/m <sup>3</sup>

ALTERATIONS

REV DATE 14 October 1993 REV 1.3

Prepared By: P.D. SFR.TUDUHPW.202B

Approved Drawing: SFR.TUDUHPW.202C

**TU Delft**  
Technische Universiteit Delft

Laboratory for Process Equipment

Address: Legationweg 44  
2615 PS Delft  
The Netherlands

PROJ. NO. 91-24/ML/EVER

DATE OF FIRST ISSUE 24 May 1993

CALC. NO.

MADE BY: Gerrit E. Wessche

PLANT SECTION: SFR.TUDUHPW.202  
Drawing Number: SFR.TUDUHPW.202A

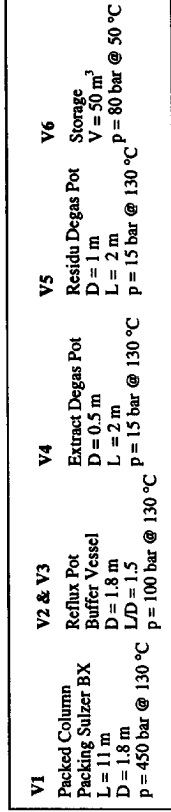
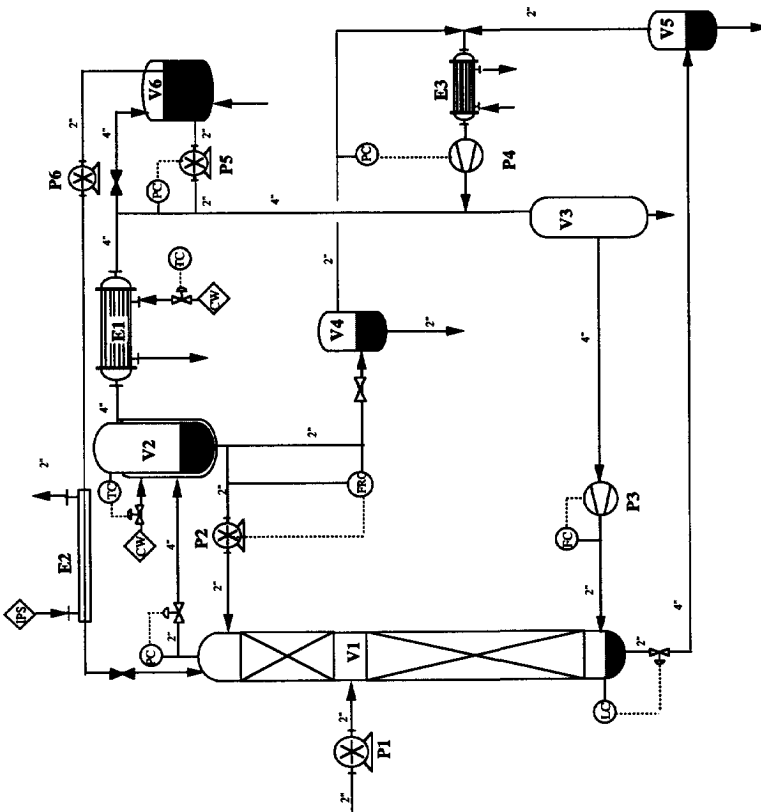
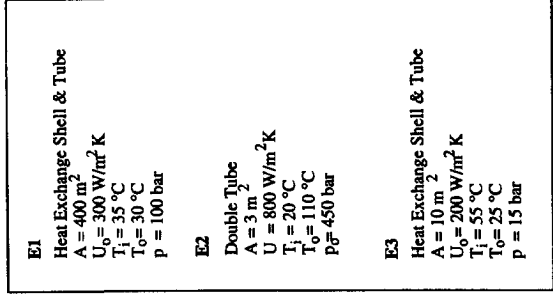
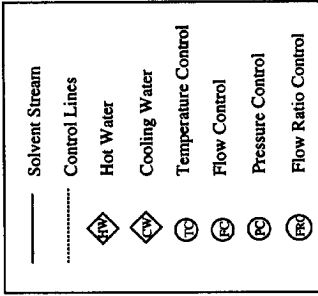
PLANT: Vegetable Oil Production

NOMINAL PLANT CAPACITY 100 tde / A

INSTANTANEOUS THROUGHPUT OF THIS SECTION 12.5 tde / h

NOTES:

APPENDIX 9.B: Equipment list with the design parameters.



- P1**  
Liquid Pump  
P = 150 kW  
L = 12.5 te/h @ 1 - 400 bar
- P2**  
Reflux Pump  
P = 40 kW  
L = 4 te/h @ 75 - 400 bar
- P3**  
Single Stage Pump/Compressor  
P = 2.0 MW  
V = 120 te/h @ 75 - 400 bar
- P4**  
Single Stage Compressor  
P = 150 kW  
V = 4 te/h @ 12 - 75 bar
- P6**  
Start-Up Carbon dioxide Pump  
P = 100 kW  
L = 4.0 te/h @ 40 - 400 bar
- P5**  
Carbon dioxide Pump  
P = 10 kW  
L = 200 kg/h @ 40 - 75 bar

## Process for the Removal of Aromatic Compounds from Off-Shore Production Water using Supercritical Methane

Off-shore produced natural gas is originally saturated with water when directly collected from the well. To enable transportation, the gas is dried to a dew point below the gas hydrate formation temperature. At North Sea platforms this is often accomplished through air cooling and an absorption step using a tri-ethylene glycol (TEG) absorber. During this process not only water but also hydrocarbons are absorbed. When the TEG is subsequently regenerated these hydrocarbons, which turned out to consist mostly of aromatic compounds, end up in the production water stream, which is a waste stream. The level of aromatic compounds in the produced water depends on the specific reservoir, but is often over 100 ppm wt, being far above the by regulations accepted level. On average the production water of gas platforms contains 140ppm wt benzene, 30ppm wt toluene, and 3ppm wt naphthalene. The contamination therefore is such that considerable reduction is required and therefore an attempt has been undertaken to evaluate the potential of using supercritical methane for this purpose.

Experiments were carried out with supercritical methane to clean the water stream of its aromatic compounds. Based on this data a process is designed, that not only reduces the contamination down to 5 ppm, but also should meet the typical platform requirements: robust, save, compact and flexible.

### EXPERIMENTAL SET-UP AND PROCEDURE

To evaluate the possibility of a process that cleans production water with natural gas, experiments were carried out with supercritical methane. Therefore an experimental set-up was used in which a pure methane (purity 99.5%) was contacted with contaminated water. The gaseous methane was fed continuously from a gas cylinder into a bubble stripping vessel using an adjustable valve. The gas flow was measured using the a coriolis mass flow meter. The temperature of the process was regulated with a thermo-static bath. The diameter of the stripping vessel was 36mm and it was filled typically with contaminated water to a 700mm level. This contaminated water was made by adding benzene, toluene and naphthalene to normal tap water. The concentrations of the aromatic compounds were measured using a high pressure liquid chromatograph. The "production" water was pumped into the stripping vessel using a membrane pump, with a capacity of 2 l/h. At the bottom of the column the stripped water was flashed to ambient conditions. The bottom flow was regulated using a needle valve. The amount

of dissolved methane at high pressure was measured by trapping it under a glass cylinder and measuring the volume and temperature. The experiments were carried out by first filling the stripping vessel with contaminated water, after which it was pressurised using supercritical methane from a cylinder and then the stripping was started. The stripping pressure was varied between 50 and 150 bar and was controlled by an automatic valve.

Both batch and continuous experiments were carried out. During the batch experiments no "fresh" contaminated water was pumped into the stripping vessel and no "clean" water was tapped off during the experiments. The continuous experiments were carried out by pumping contaminated water into the stripping vessel, while maintaining the liquid level in the vessel by adjusting the bottom flow of the column. A flowsheet of which is given in figure 10.1.

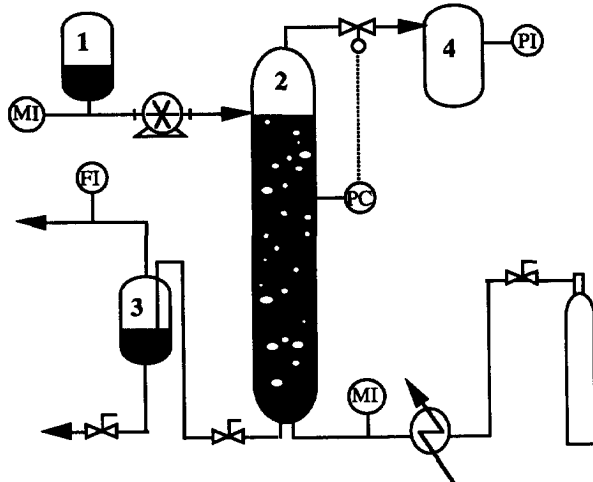


FIGURE 10.1: Experimental set-up fused in this study; 1 feed tank, 2 bubble contactor, 3 flash vessel, 4 extract buffer.

As can be seen from figure 10.1 the cleaning is performed in two related steps. The first step consists of a stripping action in a bubble contactor at elevated pressure, while the second step involves a flash of the pressurised water to atmospheric conditions. This last step causes an additional cleaning by the degassing of the dissolved methane.

*Thermodynamic Description*

The thermodynamic modelling of the process has been performed using the cubical Peng Robinson equation of state (Peng and Robinson, 1976). It describes the pressure (p) as function of the molar volume ( $v_m$ ) and the temperature (T) as:

$$p = \frac{RT}{v_m - b} - \frac{a^T}{v_m^2 + 2bv_m - b^2}, \tag{10.1}$$

where R is the gas constant. In equation (10.1)  $a^T$  represents the attractive molecular forces, while b represents the excluded volume. These parameters can be expressed in terms of the critical temperature ( $T_c$ ) and pressure ( $p_c$ ) of pure components as:

$$a^T = 5.877 b RT_c \left[ 1 + (0.37464 + 1.54226\omega - 0.26992\omega^2) \left( 1 - \sqrt{\frac{T}{T_c}} \right) \right]^2$$

and,

$$b = 0.07780 \frac{RT_c}{P_c},$$

where  $\omega$  is the acentric factor. When the system consists of a mixture of  $n$  components, these parameters are calculated using the van der Waals mixing rules as:

$$a^T = \sum_{i=1}^n \sum_{j=1}^n x_i x_j (1 - k_{ij}) \sqrt{a_i^T a_j^T}$$

and,

$$b = \sum_{i=1}^n \sum_{j=1}^n x_i x_j \frac{b_i + b_j}{2},$$

where  $x_i$  represents the mole fraction of a component. The term  $k_{ij}$  represents the non ideal binary attractive interaction parameter. This parameter needs to be determined from experimental data. When the binary interaction parameter is established the distribution factor of a component ( $K_i$ ) over the phases can be calculated:

$$K_i = \frac{y_i}{x_i}, \quad (10.2)$$

where  $y_i$  represents the mole fraction in the gas phase. The distribution factor will be used as process design parameter.

### Process Models

Since the experiments are carried out at non equilibrium conditions, the result will depend on the mass transfer rate. To be able to determine the distribution factor from these experiments it is required to describe the mass transfer. Figure 10.2 shows the process as carried out during the experiments. It consists of a stripping step and a flash action in series. To analyse the experimental results, it is necessary to develop process models for the evaluation.

### Flash Vessel

The feed of the flash vessel consists of a high pressure liquid stream (L) with an quantity of dissolved methane ( $V^o = x_{CH_4}L$ ). Using the mass balance of each component and the equilibrium condition ( $y_i^{end} = K_i^{flash} x_i^{end}$ ), the concentration of the flash vessel feed stream is calculated:

$$x_i^{out}(L + V^o) = x_i^{end}L + y_i^{end}V^o$$

$$x_i^{out} \approx x_i^{end} + K_i^{flash} x_i^{end} \frac{V^o}{L} = x_i^{end} \left( 1 + K_i^{flash} x_{CH_4}^{out} \right) \quad (10.3)$$

This equation determines the bottom flow of the stripping vessel.

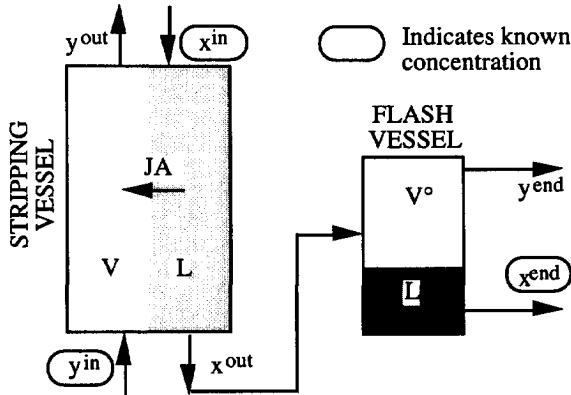


FIGURE 10.2: Schematic drawing of the operation in which the known concentrations are indicated.

*Stripping Vessel*

The gas stream (V) that is contacted with the water in the stripping vessel, will extract an quantity of the contaminants. The concentrations in the gas stream leaving the stripping vessel can also be expressed using a mass balance:

$$\begin{aligned}
 V(y_i^{out} - y_i^{in}) &= L(x_i^{in} - x_i^{out}) \\
 y_i^{out} &= \frac{L}{V}(x_i^{in} - x_i^{out}) \quad , \quad (10.4)
 \end{aligned}$$

where the condition of a contaminated free gas stream is used ( $y_i^{in} = 0$ ). With equations (10.3) and (10.4) the compositions in the process can be determined.

*Continuous Stripping*

For the modelling of the mass transfer in the stripping vessel, the gas flow is considered as a plug flow, moving up in the liquid that is considered as ideally mixed. A standard differential equation is found (see e.g., Colburn, 1941; Taylor and Krishna, 1993), which is integrated over the contacted height (H);

$$- \ln \left( \frac{x^{out} - \frac{y^{out}}{K}}{x^{out}} \right) = \frac{k^{OV} a}{u_{SV}} H \quad , \quad (10.5)$$

Here  $k^{OV}$  represents the overall mass transfer coefficient based on the gas phase,  $a$  is the interface area per unit volume and  $u_{SV}$  represents the superficial gas velocity. Replacing the overall gas transfer coefficient by the overall liquid transfer coefficient and using the mass balance of equation (10.4) the overall liquid mass transfer coefficient can be isolated as:

$$k^{OL} = \frac{c_t^V}{c_t^L} \frac{K u_{SV}}{aH} \ln \left( \frac{S}{S + 1 - \frac{x^{in}}{x^{out}}} \right) \quad , \quad (10.6)$$

where  $S$  represents the stripping factor ( $S = KV/L$ ) and  $c_t^L$  and  $c_t^V$  are the molar concentrations in the gas and liquid phase. Since the mass transfer resistance is expected to be located in the liquid, the overall mass transfer coefficient based on the liquid phase should be constant. This

in contrary with the overall mass transfer coefficient based on the gaseous phase  $k^{OV}$ , which is a function of the distribution factor (K).

### Batch Stripping

The batch experiment can be described by considering the operation as a liquid batch ( $L_0$ ) with uniform concentration, being contacted with a limited amount of the gas over a contact time. This contact time is equal to the quotient of the column height and the rise velocity of the bubbles ( $u_t$ ). The concentration in the liquid that leaves the stripping vessel after a batch time  $t_0$  can be expressed as (see Appendix 10.A):

$$x^{out} = x^{in} \left[ \frac{KV H}{L_0 u_t} \exp\left(-\frac{c_t^L k^{OL} aH}{c_t^V K u_{SV}}\right) - \frac{KV H}{L_0 u_t} + 1 \right] \frac{u_t t_0}{H} \quad (10.7)$$

The overall liquid mass transfer coefficient can be isolated as:

$$k^{OL} = \frac{c_t^V K u_{SV}}{c_t^L aH} \ln \left( \frac{\frac{KV H}{L_0 u_t}}{\frac{KV H}{L_0 u_t} - 1 + \left(\frac{x^{out}}{x^{in}}\right) \frac{H}{t_0 u_t}} \right) \quad (10.8)$$

In the above derived equations the specific area per unit of volume ( $a$ ) is a non specified parameter. However it can be calculated from the gas hold-up ( $\phi_V$ ) and the bubble diameter ( $d_b$ ) as:

$$a = \frac{6\phi_V}{d_b} = \frac{6}{d_b} \frac{\pi r^2 u_{SV} \frac{H}{u_t}}{\pi r^2 H} = \frac{6}{d_b} \frac{u_{SV}}{u_t} \quad (10.9)$$

In the experiments intermediate flow rates were used, such that various estimation methods can be used to calculate the bubble diameter (Treybal, 1980). However, it was observed visually that the bubbles possess a uniform size distribution. It is therefore decided to use for all experiments an identical method to estimate the bubble diameter (van Krevelen and Hoftijzer, 1950):

$$d_b = \left( \frac{6d_i \sigma}{g \Delta \rho} \right)^{\frac{1}{3}} \quad (10.10)$$

Here  $d_i$  represents the inner tube diameter of the gas distributor ( $d_i = 3.85\text{mm}$ ),  $\sigma$  represents the surface tension,  $g$  is the gravitational acceleration and  $\Delta \rho$  represents the density difference between the gas and liquid. Given the low gas hold-up, less than 3%, the terminal rising velocity is estimated using an expression for single bubbles as given by Maneri and Mendelson (1967);

$$u_t = \sqrt{\frac{2\sigma}{d_b \rho_L} + \frac{g d_b}{2}} \quad (10.11)$$

This relation completes the set of equations needed for the description of the mass transfer.

## EXPERIMENTAL RESULTS

*The Solubility of Methane in Water*

The solubility of methane in water was measured several times. From these results the Henry coefficient ( $H_{\text{CH}_4, \text{H}_2\text{O}}$ ) of methane in water was determined to be  $10^{4.75}\text{bar}$ , so that the concentration methane in the water can be calculated by:

$$x_{\text{CH}_4} = \frac{P_{\text{CH}_4}}{H_{\text{CH}_4, \text{H}_2\text{O}}} \quad (10.12)$$

This concentration is required to quantify the effect of the flash as well as the stripping experiments.

*Distribution Factors*

The distribution factors were established by carrying out batch experiments. As is shown in Appendix 10.A the data can at first order be correlated with an exponential function. The use of this approach is demonstrated in figure 10.3. In this figure the exponential decrease of the toluene concentration as function of the total quantity of methane is shown.

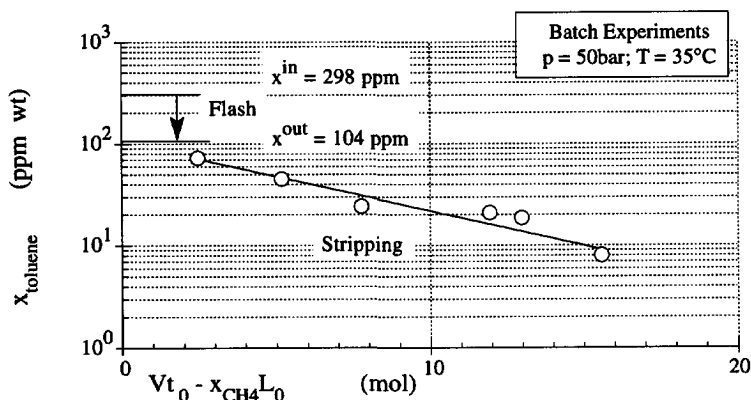


FIGURE 10.3: Series of batch experiments varying the amount of methane using water that was contaminated with 298 ppm toluene.

Extrapolation to zero ( $V_{t0} - x_{\text{CH}_4}L_0 = 0$ ), leads to a concentration of 104 ppm, which is the concentration after the flash in case no stripping gas is used. The distribution coefficient at atmospheric conditions can now be determined from the mass balance and can be obtained using equation (10.3) and (10.12);

$$K_{\text{tol}}^{\text{flash}} = \left( \frac{x^{\text{in}}}{x^{\text{out}}} - 1 \right) \frac{1}{x_{\text{CH}_4}} = 2098$$

This result can be used to determine the binary interaction parameter between, water and toluene for the Peng-Robinson equation of state. The interaction parameters between water-benzene and water-naphthalene are found to be similar.



The binary interaction parameters between methane and the aromatic compounds were established using VLE data from literature (Darwish et al., 1994, Legret et al., 1982) and verified with cited values (Knapp et al., 1982, Ohe, 1990) which were obtained at higher temperatures. Since the aromatic compound concentrations were small in both liquid and gas phase, the binary interaction parameters between the aromatic compounds were neglected. All used interaction parameters are shown in table I.

TABLE I: The binary interaction parameters (Sang-Do and Akgerman, 1990) for the given components at 35°C. All coefficients are near infinite water dilution. The bold values are fitted parameters using the experimental results.

k <sub>ij</sub>	Water	Water	Methane	Toluene	Benzene
	Experiment	Literature	Literature		
Methane	<b>-0.19</b>	-0.22			
Toluene	<b>-0.146</b>	-0.106	0.088		
Benzene	<b>-0.089</b>	-0.024	0.073	0.0	
Naphthalene	<b>-0.11</b>	-0.11	0.116	0.0	0.0

Since the binary interaction parameters of the aromatic compounds with water are the most important for the flash step, these have been determined by fitting the model to the experimental data. Most values obtained in this study are in reasonable agreement with the values found in literature. Only a significant difference between the binary interaction parameter of benzene and water with the value reported in literature (Sang-Do and Akgerman, 1990) is found. It should be noted that values determined in this study, all have a safe effect on the process design. The fitted binary interaction parameter of methane and water (-0.19) predicts a smaller solubility of the methane, so that it reduces the flash effect after the stripping. In addition, the fitted interaction parameters for the aromatic compounds all predict a smaller or equal distribution coefficient than predicted from literature data.

The slope of figure 10.3 holds the information on the mass transfer coefficients within the sparge column. This information will be used to evaluate the reliability of the experimental results.

#### Mass Transfer Coefficients

With known distribution factors equation (10.6) or (10.8) can be used to calculate the mass transfer coefficients from the experimental results. The experimental mass transfer coefficients can be compared with the theoretical values obtained from the penetration theory and with empirical correlations. The comparison is done using the Sherwood number ( $Sh = k^L d_p / D^L$ ). The diffusion coefficients for benzene, toluene and naphthalene at 35°C are estimated as: 1.34, 1.15, and 0.97  $\text{m}^2/\text{s}$ . The results of the calculated Sherwood numbers are shown in figure 10.4.

The penetration theory for circulating bubbles (see Appendix 10.B) predicts a Sherwood number of approximately 1200 and the empirical relation of Calderbank and Moo-Young (see Appendix 10.B) predicts a Sherwood number of approximately 1500. An average Sherwood number of 1287 was found for the batch experiments, while an average Sherwood number of 1457 was found for the continuous experiments. Both results are in close agreement with either the theoretical and the empirical relation.

It can therefore be concluded that although the vessel had a length over diameter ratio of 20, the liquid in the vessel can still be considered as nearly ideal mixed.

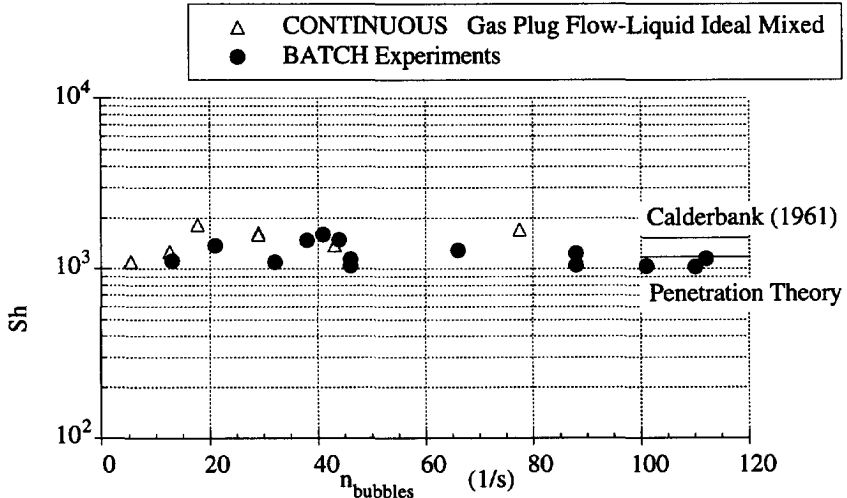


FIGURE 10.4: The Sherwood number for batch and continuous experiments as function of the number of bubbles generated per second.

### PROCESS DESIGN

Using the obtained information several options are open for the design of a separation process. Figure 10.5 shows the estimated distribution factors using the Peng-Robinson equation of state with the determined binary interaction parameters. A minimum in the distribution factor is found at intermediate pressures of 50 bars, which is a typical pressure for maximum retrograde condensation. The graph suggests that the cleaning of the production water should either be carried out at low or at high pressures. It is interesting to notice that the larger molecules are stripped better at high pressures and that a high pressure stripping process can be carried out in more compact equipment. The effect which one intends to obtain when applying a supercritical extraction therefore is located at the right hand part of the graph, showing the exponential increase of the distribution factor with increasing pressure. The distribution factors at 300bar reduce to values that are of the same order of magnitude when applying a 4 bar operation. Both processes therefore require an equal quantity of natural gas.

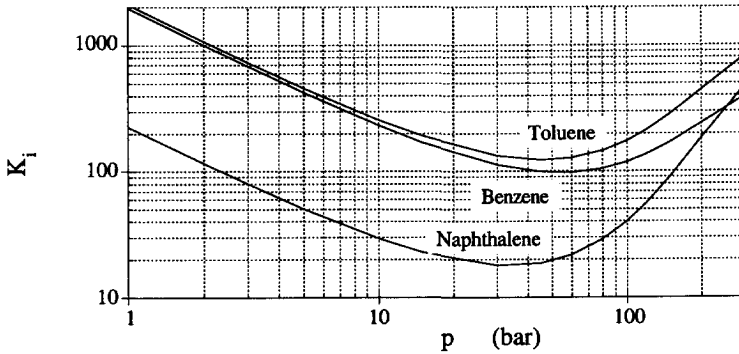


FIGURE 10.5: Calculated distribution factors at a temperature of 35°C, given a two phase methane-water system containing traces of the given poly-aromatic components.

Given an initial concentration  $x^{in}$  and a required concentration  $x^{out}$  the required number of equilibrium stages for a stripping process can be calculated using Kremser relation:

$$N = \ln \left[ \frac{x^{in} - \frac{y^{in}}{K}}{x^{out} - \frac{y^{in}}{K}} \left( 1 - \frac{1}{S} \right) + \frac{1}{S} \right] \frac{1}{\ln S} \quad (S \neq 1), \text{ and} \quad N = \frac{x^{in} - x^{out}}{x^{out} - \frac{y^{in}}{K}} \quad (S = 1) \quad (10.13)$$

The characteristics of the equation are shown in figures 10.6A and 10.6B. Using the figures 10.5 and 10.6 the relevant concentrations in the process can be calculated.

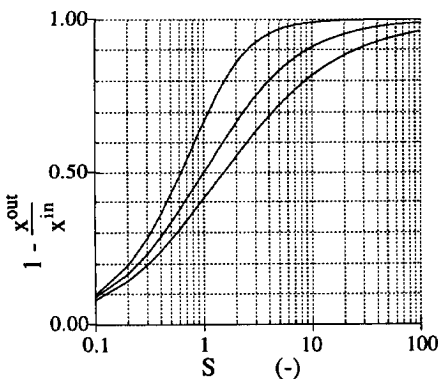


FIGURE 10.6A: Fraction removed as function of the stripping factor and the number of equilibrium steps

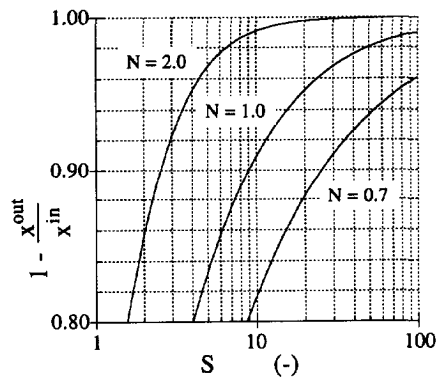


FIGURE 10.6B: Enlargement, showing the relevant part of figure 10.6A.

The objective of this process is to reduce the aromatic compounds to a 5ppm wt% concentration. This means that approximately 98% needs to be removed. For the stripper a bubble column could be used. When designed well, by dimensioning an optimum height over diameter ratio of the column given a certain in-going gas and liquid stream, two equilibrium steps can be achieved. This would require a stripping factor of only 7, to remove 98% of the contaminants. As already can be seen from our experiments, this only is attainable in a bubble column with a large height over diameter ratio. Such a column will have a very limited operation range. However, a high pressure stripping process will always require a depressurisation of the waste water. This implies that the process always will have a flash step, with an additional cleaning effect on the water stream. It is for these two reasons that a more flexible and simpler process is explored, which uses a single stage stripping process. In this process the natural gas and the waste water are contacted co-currently using a static mixer and a gas liquid separator. When using a stripping factor of 12, approximately 92% of the contaminants will be removed in this single stage contactor, while in the flash stage the reduction to 98% is achieved. The process is illustrated in figure 10.7.

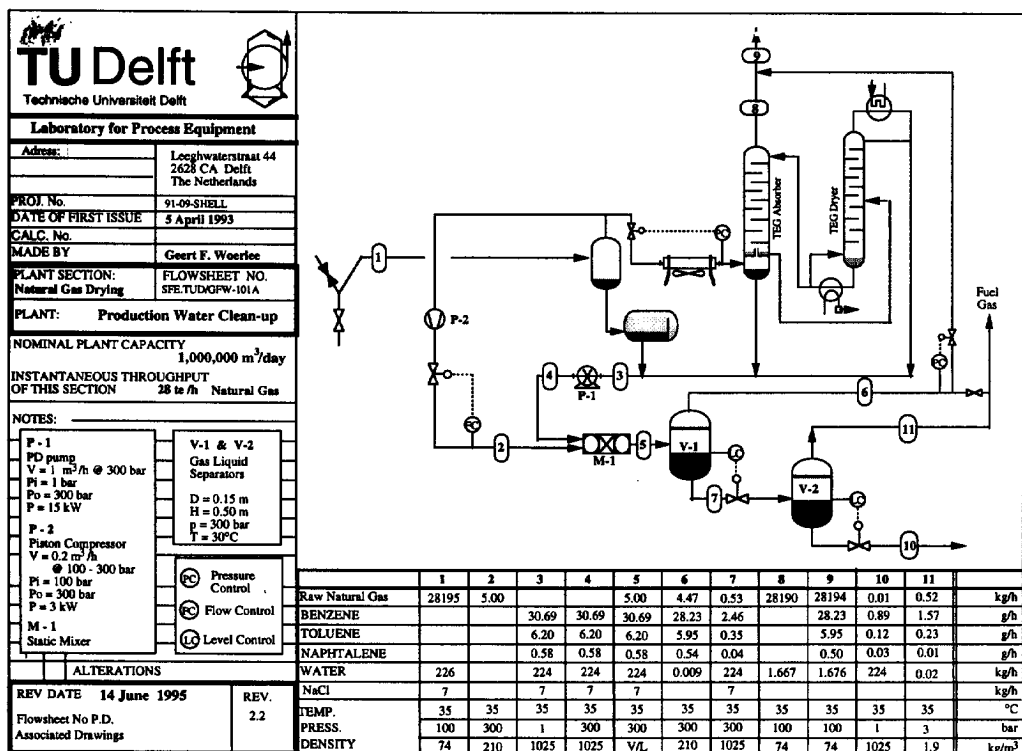


FIGURE 10.7: Process flowsheet.

The upper half of the flowsheet shows the usual gas drying process. The produced water (flow 3) is fed with a piston pump to the additional cleaning process. The required stripping gas is taken directly after the well separator and pressurised using a small compressor. Both streams are contacted in a pipe with a static mixer. The residence time in the pipe is designed such that one equilibrium step is approached. The gas from the high pressure gas-liquid separator can be recycled to the main product stream. The water stream is depressurised to 3 bar in a flash-vessel. This pressure is chosen so that the escaping natural gas can be used as fuel gas. The overall flowsheet shows that the required natural gas for cleaning the waste water stream is 0.17% of the produced natural gas.

The applied diameters for the separation vessels are taken 10 times the for gravitational settling required size (Coulson et al., 1983). In this design they should therefore be considered as buffer vessels. The pump and the compressor are taken 4 times the necessary size to increase flexibility. Next to the fact that the designed process is robust it can also be considered as save, since at no point the streams are contacted with air. The process needs no additional maintenance other than which is normally required for pumps, compressors and control systems. Finally it should be noticed that all equipment is small, so that the total area for the process would hardly exceed two square meters. The total height of the equipment is determined by the vessels and will therefore not be more than three meters.

#### *Process Costs*

The installed capital costs for a gas platform, producing 1 million m<sup>3</sup> natural gas per day, are estimated on \$350 000. This estimation is based on the required main plant items.

The cleaning of the water required 7m<sup>3</sup>/h of natural gas . The total quantity of electrical power for the production water cleaning is established as: 0.7 + 3.7 = 4.4kW. This results in a estimated total operating costs per hour as: 4.4 x 0.08 + 7 x 0.10 = \$1.05.

#### CONCLUDING REMARKS

In this study it has been shown that aromatic hydro-carbons dissolved in water produced from natural gas reservoirs, can be removed in a simple stripping process by using the natural gas at high pressures. For off-shore gas production the proposed system meets all the common technical requirements; compact, simple, robust and save.

#### APPENDIX 10.A (*Batch Stripping*)

A batch experiment can be described by considering the operation as a liquid batch ( $L_0$ ) with uniform concentration, being contacted with a limited quantity of the gas ( $\Delta V$ ) over a time ( $dt$ ). A differential equation based on the concentration changes in the gas phase is made over the vessel,

$$\frac{dy}{(y^* - y)} = - \frac{k^{OV} c_t^y a \pi r^2 H}{\Delta V} dt, \quad (10.A1)$$

where  $\pi r^2$  is the cross-section area of the vessel and  $y^*$  is the hypothetical concentration in equilibrium with the bulk of the liquid phase ( $y^* = Kx$ ). Integrating equation (10.A1) over a time  $\Delta t$  at which the quantity  $\Delta V$  is contacted with the liquid one obtains:

$$\ln \left( \frac{x^0 - \frac{y^{\Delta t}}{K}}{x^0} \right) = \left( -c_t^L \frac{k^{OL_a} \pi r^2 H \Delta t}{K \Delta V} \right)$$

$$\ln \left( 1 - \frac{L_0}{K \Delta V} \left( 1 - \frac{x^{\Delta t}}{x^0} \right) \right) = \left( -\frac{c_t^L}{c_t^V} \frac{k^{OL_a} H}{K u_{SV}} \right), \quad (10.A2)$$

where  $x^0$  is the initial liquid concentration and  $x^{\Delta t}$  is the concentration after the contact time. The time step  $\Delta t$  has been eliminated by use of the simple relation  $V = \pi r^2 c_t^V u_{SV} = \Delta V / \Delta t$ . Continuing the derivation one obtains:

$$\frac{x^{\Delta t}}{x^0} = \frac{K \Delta V}{L_0} \exp \left( -\frac{c_t^L}{c_t^V} \frac{k^{OL_a} H}{K u_{SV}} \right) - \frac{K \Delta V}{L_0} + 1 \quad (10.A3)$$

Therefore, the concentration after time  $\Delta t$  can be expressed explicitly in terms of the concentration before the time step. The number of time steps is dependent on the contact time within the vessel. This contact time can be related to the rise velocity of the bubbles and the height of the column. Given a batch time  $t_0$  the number of steps should be equal to:  $t_0 u_t / H$  The final expression for the batch experiments can therefore be written as:

$$x^{out} = x^{in} \left[ \frac{K V H}{L_0 u_t} \exp \left( -\frac{c_t^L}{c_t^V} \frac{k^{OL_a} H}{K u_{SV}} \right) - \frac{K V H}{L_0 u_t} + 1 \right]^{\frac{u_t t_0}{H}} \quad (10.A4)$$

By changing the amount of methane used in batch experiments, while keeping the other variables constant, information about the stripping and the flash step is obtained. To have a simple first interpretation of the results a relation between the total amount of gas used and the decrease of the concentrations can be derived from equation (10.A4). When the exponential term in equation (10.A4) is small it can be expanded in a Taylor series as:

$$\frac{x^{out}}{x^{in}} \approx \left[ \frac{K V H}{L_0 u_t} \left( 1 - \frac{c_t^L}{c_t^V} \frac{k^{OL_a} H}{K u_{SV}} \right) - \frac{K V H}{L_0 u_t} + 1 \right]^{\frac{t_0 u_t}{H}}$$

$$= \left[ 1 - \frac{c_t^L}{c_t^V} \frac{k^{OL_a} H}{K u_{SV}} \frac{K V H}{L_0 u_t} \right]^{\frac{t_0 u_t}{H}}$$

and continue by taking the logarithm, with the result:

$$\ln \left( \frac{x^{out}}{x^{in}} \right) = \ln \left[ 1 - \frac{c_t^L}{c_t^V} \frac{k^{OL_a} H^2}{u_{SV} u_t} \frac{V}{L_0} \right]^{\frac{t_0 u_t}{H}}$$

$$\approx -\frac{t_0 u_t}{H} \frac{c_t^L}{c_t^V} \frac{k^{OL_a} H^2}{u_{SV} u_t} \frac{V}{L_0}$$

$$= -\frac{c_t^L}{c_t^V} \frac{k^{OL_a} H}{u_{SV}} \frac{V t_0}{L_0} = -\frac{c_t^L}{c_t^V} \frac{k^{OL_a} H}{d_b u_t} \frac{V t_0}{L_0} \quad (10.A5)$$

Equation (10.9) has been used in the last step to eliminate the specific surface.

## APPENDIX 10.B (mass transfer relations)

*Penetration Theory*

The mass transfer relation that is best applicable for the results found is the one based on the penetration theory for short contact times, which can be derived from the elementary consideration and leads to the expression:

$$Sh = \frac{d_b}{D^L} k^L = \frac{d_b}{D^L} \sqrt{\frac{4 D^L}{\pi t}} = \frac{d_b}{D^L} \sqrt{\frac{4 D^L}{\pi d_b}} u_t \quad (10.B1)$$

The contact time in this equation is calculated as the time for the bubble to rise one particle diameter.

*Empirical relation*

The results can also be interpreted using the empirical correlation given by Calderbank and Moo-Young (1961) for large clean bubbles;

$$Sh^L = 0.0042 \frac{d_b}{D^L} \left( \frac{\Delta \rho \eta_L g}{\rho_L^2} \right)^{\frac{1}{3}} \left( \frac{D^L \rho_L}{\eta_L} \right)^{\frac{1}{2}} = 0.0042 d_b \left( \frac{\Delta \rho^2 g^2}{\rho_L \eta_L D^L} \right)^{\frac{1}{6}} \quad (10.B2)$$

## NOTATION:

a	Interfacial area .....	$m^2 m^3$
$a^T$	Attraction parameter.....	$J/mol m^6 mol^{-2}$
b	vd Waals co-volume .....	$m^3 mol^{-1}$
$c_t^L$	Liquid concentration .....	$kmol m^{-3}$
$c_t^V$	Gas concentration .....	$kmol m^{-3}$
$d_b$	Bubble diameter .....	m
$d_i$	Inner tube diameter.....	m
$D^L$	Liquid diffusion coefficient .....	$m^2 s^{-1}$
g	Gravitational acceleration.....	$9.81 m s^{-1}$
H	Level in stripping vessel.....	m
$k_{ij}$	Binary attraction parameter.....	
$k^L$	Liquid mass transfer coefficient .....	$m s^{-1}$
$k^{OL}$	Overall liquid mass transfer coefficient .....	$m s^{-1}$
$k^{OV}$	Overall gas mass transfer coefficient.....	$m s^{-1}$
K	Distribution factor.....	$mol mol^{-1}$
L	Molar liquid flow.....	$mol s^{-1}$
$L_0$	Liquid batch size .....	mol
n	Number of components .....	
N	Number of equilibrium stages .....	
M	Molar mass.....	$kg mol^{-1}$
p	Pressure .....	Pa
$p_c$	Critical pressure .....	Pa
r	Radius of the stripping vessel .....	m
R	Gas constant .....	$8.31441 J mol^{-1} K^{-1}$
S	Stripping factor.....	$mol mol^{-1} mol s^{-1} mol^{-1} s$
Sh	Sherwood number .....	
$t_0$	Batch time .....	s
T	Temperature.....	K
$T_c$	Critical temperature .....	K
$u_{SV}$	Superficial gas velocity.....	$m s^{-1}$
$u_t$	Bubble rise velocity.....	$m s^{-1}$

$v_m$	Molar volume.....	$m^3 \text{ mol}^{-1}$
$V$	Molar gas flow .....	$\text{mol s}^{-1}$
$V^p$	Molar gas flow dissolved in the liquid.....	$\text{mol s}^{-1}$
$\Delta V$	limited amount of gas.....	$\text{mol}$
$x$	Liquid mol fraction.....	$\text{mol mol}^{-1}$
$x^{\text{in}}$	Liquid mol fraction entering the stripping.....	$\text{mol mol}^{-1}$
$x^{\text{out}}$	Liquid mol fraction leaving the stripping.....	$\text{mol mol}^{-1}$
$x^{\text{end}}$	Liquid mol fraction after flash vessel .....	$\text{mol mol}^{-1}$
$y$	Gas mol fraction.....	$\text{mol mol}^{-1}$
$y^{\text{in}}$	Gas mol fraction entering the stripping.....	$\text{mol mol}^{-1}$
$y^{\text{out}}$	Gas mol fraction leaving the stripping.....	$\text{mol mol}^{-1}$
$y^{\text{end}}$	Gas mol fraction after flash vessel .....	$\text{mol mol}^{-1}$
$y^*$	Apparent gas concentration $y^*=Kx$ .....	$\text{mol mol}^{-1}$
$\Delta\rho$	Density difference .....	$\text{kg m}^{-3}$
$\rho_L$	Liquid density .....	$\text{kg m}^{-3}$
$\phi_V$	Gas hold up.....	$\text{m}^3 \text{ m}^{-3}$
$\sigma$	Interfacial tension .....	$\text{N m}^{-1}$
$\omega$	Acentric factor .....	

## REFERENCES:

- [1] Calderbank, P.H., and Moo-Young, M.B., The continuous phase heat and mass transfer properties of dispersions, *Chem. Eng. Sci.* **16** 39-51 (1961).
- [2] Colburn, A.P., Simplified Calculation of Diffusional Processes, *Ind. Eng. Chem.*, **33** 459 (1941).
- [4] Coulson, J.M. Richardson, J.F. & Sinnott, R.K., *Chemical Engineering Vol. 6: Design*, Pergamon Press, Oxford, (1983).
- [4] Darwish, N.A., Gasem, A.M., and Robinson, R.L., Solubility of Methane in Benzene, Naphthalene, Phenanthrene, and Pyrene at Temperatures from 323 to 433 K and Pressures to 11.3 MPa., *J. Chem. Eng. Data*, **39** 781-784 (1994)
- [5] Knapp, H., Döring, R., Oellrich, L., Plöcker, U., and Prausnitz, J.M., Vapour-Liquid Equilibria for Mixtures of Low Boiling Substances, *DECHEMA Chemistry Data Series, Vol VI, Frankfurt/Main* (1982)
- [6] Legret, D., Richon, D., and Renon, H., Vapour-Liquid Equilibria of Methane-Benzene, Methane-Methylbenzene (Toluene), Methane-1,3-Dimethylbenzene (m-Xylene), and Methane-1,3,5-Trimethylbenzene (Mesitylene) at 313.2K up to the Critical Point., *J. Chem. Eng. Data*, **27** 165-169 (1982).
- [7] Maneri, C.C., and Mendelson, H.D., *AIChE J.*, **14**, 295 (1968).
- [8] Ohe, S., Vapour-Liquid Equilibrium data at high Pressure, Kodansha, Tokyo and Elsevier, Amsterdam, *Physical Sciences Data* **42**, (1990).
- [9] Peng, D.-Y., Robinson D.B., *Ind. Eng. Chem. Fundam.* **15** 59-64 (1976).
- [10] Sang-Do, Y., and Akgerman, A., Supercritical Extraction of Organic mixtures from aqueous solutions', *AIChE J.* **36** 1743-1747 (1990).
- [11] Taylor, R., and Krishna, R., *Multicomponent Mass Transfer*, Wiley Series in Chemical Engineering, New York (1993).
- [12] Treybal, R.E., *Mass Transfer Operations*, 3<sup>rd</sup> ed, Wiley Series in Chemical Engineering, New York (1980).
- [13] Van Krevelen, W., and Hoftijzer, P.J., *Chem. Eng. Prog.*, **46** 29 (1950).



## Process for the Fractionation of Citrus Oils using Supercritical Carbon Dioxide

Citrus peel oils are widely used as flavour ingredients. With the exception of lime oil, which is recovered by distillation, the citrus oils are recovered directly from the peels of fresh fruits. Citrus oils are characterised by having a high percentage of terpenoid hydrocarbons and a relatively low content of terpenoid oxygenated compounds, which are mainly responsible for the aroma properties. The terpene hydrocarbons are poorly water soluble and have a high tendency to polymerize and oxidize with an associated deterioration of the flavour. Therefore, these oils are often further processed using distillation or extraction to remove the major part of the hydrocarbons. Due to the high sensitivity to thermal stress, off-flavours are sometimes introduced during distillation and solvent removal. As a result there is a need for separation processes that allow efficient separation under mild thermal conditions. Fractionation of citrus oils using supercritical carbon dioxide might be such a mild separation method.

The following research should lead to a preliminary design of a supercritical separation process for citrus oils using carbon dioxide. The design will be based on a capacity of 40te/A of product intake, which is a bulk production for flavour industry. To make a comparison with conventional processes possible, the process will be designed on a 5-fold increase basis. Given the thermal sensitivity of the material the temperature of the process should not exceed 60°C.

### EXPERIMENTAL PROCEDURE AND RESULTS

To evaluate the possibility of citrus oils separation using carbon dioxide, a closer examination of the raw material is necessary. Table XI.I show the composition of a typical "Italian lemon oil". As can be seen in this table more than 90% of the non oxygen containing compounds have a boiling point lower than the oxygenated compounds and because carbon dioxide separates normally on basis of volatility, they can be removed from the extract. Clearly the raw product is a complex blend of exotic components. When the fractionation of the total raw material would be evaluated this would create an analytical bottle-neck. It is for this reason that the problem is reduced to a key component study of two close boiling compounds. Given the availability of such compounds and the composition as shown in table XI.I, limonene is selected as bulk component (light key) and linalool is chosen as least volatile (heavy key) component.

TABLE XII: Composition of Italian lemon oil, showing the component's name, gross formula, retention index, molecular concentration, and boiling point.

Component	Formula	Ret. Index	Concentration mol/mol %	Boiling Point (°C)
$\alpha$ -thujene	C <sub>10</sub> H <sub>18</sub>	670	0.42	152
$\alpha$ -pinene	C <sub>10</sub> H <sub>18</sub>	678	1.81	156
camphene	C <sub>10</sub> H <sub>18</sub>	692	0.05	
methyl heptenon	C <sub>7</sub> H <sub>12</sub> O	709	0.01	
sabinene	C <sub>10</sub> H <sub>18</sub>	714	1.73	164
$\beta$ -pinene	C <sub>10</sub> H <sub>18</sub>	718	11.37	165
2,3-dehydrocineole	C <sub>10</sub> H <sub>18</sub> O	727	0.06	
$\beta$ -mycrene	C <sub>10</sub> H <sub>16</sub>	730	1.38	
$\alpha$ -terpinene	C <sub>10</sub> H <sub>16</sub>	758	0.58	174
1,8-cineole	C <sub>10</sub> H <sub>16</sub> O	766	0.57	176
<b>limonene</b>	<b>C<sub>10</sub>H<sub>16</sub></b>	<b>769</b>	<b>67.16</b>	<b>177</b>
$\gamma$ -terpinene	C <sub>10</sub> H <sub>16</sub>	796	9.02	183
di-hydro linalool	C <sub>10</sub> H <sub>16</sub> O	800	0.03	
terpinolene	C <sub>10</sub> H <sub>16</sub>	823	0.36	186
<b>linalool</b>	<b>C<sub>10</sub>H<sub>18</sub>O</b>	<b>831</b>	<b>0.09</b>	<b>196</b>
fenchol	C <sub>10</sub> H <sub>18</sub> O	843	0.00	201
$\beta$ -terpineol	C <sub>10</sub> H <sub>18</sub> O	873	0.00	
cironellal	C <sub>10</sub> H <sub>18</sub> O	878	0.09	210
p-methadien-8-ol	C <sub>10</sub> H <sub>18</sub> O	890	0.00	
bomeol	C <sub>10</sub> H <sub>18</sub> O	895	0.01	207
p-cymen-8-ol	C <sub>10</sub> H <sub>14</sub> O	905	0.01	
terpinen-4-ol	C <sub>10</sub> H <sub>18</sub> O	908	0.02	211
p-methadien-8-ol	C <sub>10</sub> H <sub>16</sub> O	915	0.00	
$\alpha$ -terpineol	C <sub>10</sub> H <sub>18</sub> O	918	0.12	219
decanal	C <sub>10</sub> H <sub>20</sub> O	927	0.00	208
nerol	C <sub>10</sub> H <sub>18</sub> O	955	0.02	224
citronellol	C <sub>10</sub> H <sub>20</sub> O	955	0.02	
neral	C <sub>10</sub> H <sub>16</sub> O	960	0.71	227
geraniol	C <sub>10</sub> H <sub>18</sub> O	979	0.02	229
geranial	C <sub>10</sub> H <sub>16</sub> O	988	1.22	229
linalyl acetate	C <sub>12</sub> H <sub>20</sub> O <sub>2</sub>	990	0.02	220
isom. of p-methadien-8-ol	C <sub>10</sub> H <sub>16</sub> O	997	0.00	
isom. of p-methadien-8-ol	C <sub>10</sub> H <sub>16</sub> O	1016	0.00	
terpin hydrate	C <sub>10</sub> H <sub>20</sub> O <sub>2</sub>	1047	0.00	
isom. of terpin hydrate	C <sub>10</sub> H <sub>20</sub> O <sub>2</sub>	1065	0.00	
p-1-methene-3,8-diol	C <sub>10</sub> H <sub>18</sub> O <sub>2</sub>	1067	0.00	
isom. of terpin hydrate	C <sub>10</sub> H <sub>20</sub> O <sub>2</sub>	1069	0.00	
neryl acetate	C <sub>12</sub> H <sub>20</sub> O <sub>2</sub>	1080	0.33	231
geranyl acetate	C <sub>12</sub> H <sub>20</sub> O <sub>2</sub>	1105	0.40	245
caryophyllene	C <sub>15</sub> H <sub>24</sub>	1163	0.47	256
$\alpha$ -bergamotene		1178	0.78	
$\beta$ -bisabolene	C <sub>15</sub> H <sub>24</sub>	1245	1.15	262
7-methoxycoumarine		1407	0.00	

All experiments were carried out on experimental set-up using a counter-current extraction column of one meter (de Haan, 1991). Because of the high volatility of the components involved all experiments were conducted using fresh carbon dioxide only. The extracted stream was flashed continuously to atmospheric conditions, so that an amount of the extracted components remained in the gas stream. This stream was compensated, to avoid systematic deviations in the measured solubilities. To overcome this problem the flash temperature (T) was monitored constantly and using the vapour pressure of the products the amount in the flash gas was calculated and added to the measured liquid extract. The vapour pressures (p) were calculated using the Peng-Robinson equation of state (Peng and Robinson, 1974);

$$p = \frac{RT}{v_m - b} - \frac{a}{v_m^2 + 2bv_m - b^2} \tag{11.1}$$

which equation was used also for the interpretation of the experimental data and for the process design. Here ( $v_m$ ) is the molar volume and (a) represents a temperature dependent attraction term, which is expressed as function of the critical temperature ( $T_c$ ), the excluded volume (b) and the acentric factor ( $\omega$ );

$$a = 5.877 b RT_c \left[ 1 + (0.37464 + 1.54226\omega - 0.26992\omega^2) \left( 1 - \sqrt{\frac{T}{T_c}} \right) \right]^2 \tag{11.2}$$

For a mixture of n components the attractive term is calculated using the van der Waals mixing rules as:

$$a = \sum_{i=1}^n \sum_{j=1}^n x_i x_j (1 - k_{ij}) \sqrt{a_i a_j} \tag{11.3}$$

Here  $k_{ij}$  describes the non-ideal mixing behaviour of the attraction term. This binary interaction parameter is normally determined using vapour liquid equilibrium data. The excluded volume term of a mixture is calculated as:

$$b = \sum_{i=1}^n \sum_{j=1}^n x_i x_j (1 - l_{ij}) \frac{b_i + b_j}{2} \tag{11.4}$$

where  $l_{ij}$  is the binary co-volume parameter. Since the volumetric change when mixing liquids is small the binary co-volume parameter is expected to be small as well. The necessary parameters of the pure components are shown in table XI.II.

TABLE XI.II: Physical properties of the used components. Indicated are the molar weight, the critical temperature and pressure, the acentric factor and the established viscosity parameters.

Component No.	M	$T_c$	$P_c$	$\omega$	
#	(kg/mol)	(K)	(bar)	(-)	
Carbon Dioxide	1	0.04401	304.2	73.8	0.239
Limonene	2	0.13624	654.4	27.5	0.327
Linalool	3	0.15424	661.4 <sup>†</sup>	26.2 <sup>†</sup>	0.502 <sup>‡</sup>

<sup>†</sup>Estimated by Temelli et al., (1990).

<sup>‡</sup>Estimated using Ambrose method (Reid et al., 1980).

Counter current extractions at low solvent to feed rates were carried out, using the binary mixtures: limonene-carbon dioxide and linalool-carbon dioxide to measure the solubility of the selected components. By measuring the raffinate and extraction streams at various conditions the binary interaction parameters of the Peng-Robinson equation of state as function of the temperature was determined. The data of ternary extraction experiments were used to verify the obtained information and to establish the binary interaction parameter between limonene and linalool for which no direct method was at our disposal. The experimental procedure is shown in figure 11.1. The measured interaction parameters for limonene-carbon dioxide and linalool-carbon dioxide are shown in figures 11.2A and 11.2B.

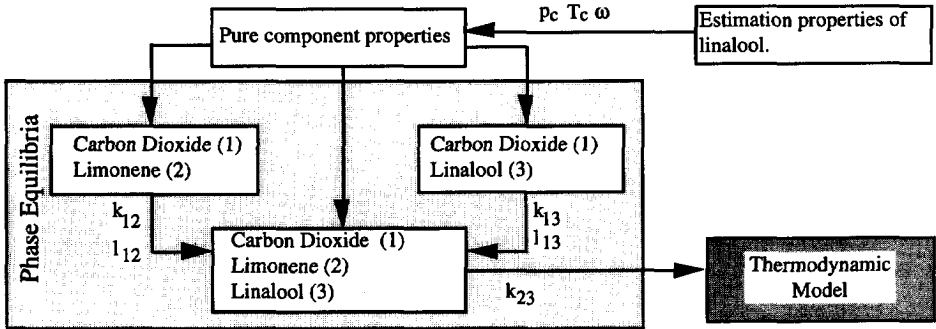


FIGURE 11.1: Experimental procedure to model the thermodynamics of the key components for a citrus oils extraction with carbon dioxide.

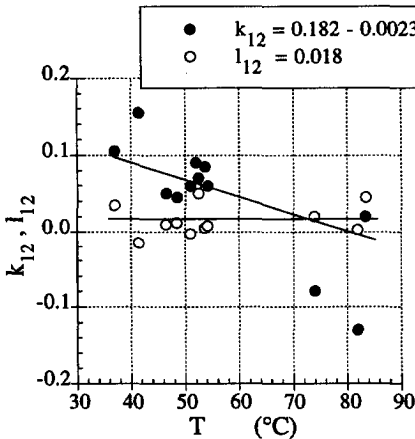


FIGURE 11.2A: Measured and modelled binary interaction and co-volume parameters between carbon dioxide and limonene.

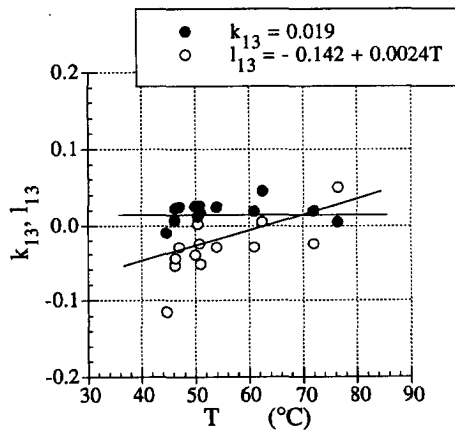


FIGURE 11.2B: Measured and modelled binary interaction and co-volume parameters between carbon dioxide and linalool.

As indicated in figure 11.1, the binary interaction parameters between limonene and linalool ( $k_{23}$ ) were determined on basis of ternary data assuming  $l_{23}$  to be zero. This has been done by fitting this parameter on the experimentally found selectivities at low solvent to feed stripping

experiments. The established binary interaction parameter as function of the temperature is shown in figure 11.3.

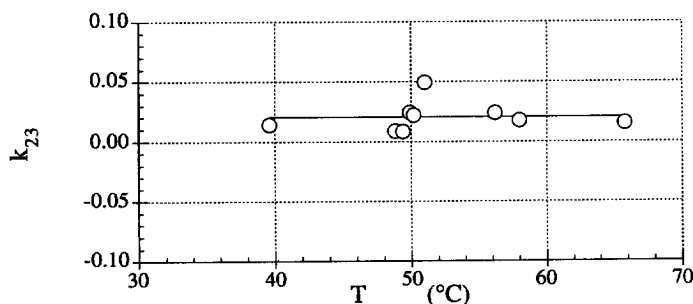


FIGURE 11.3: The determined binary interaction parameter by fitting the solvent free selectivity between limonene and linalool with the measured values obtained by carbon dioxide extraction.

Because of the applied procedure all errors made at an earlier stage will be condensed in the binary interaction parameter between limonene and linalool. This will be reflected in  $k_{23}$ . Figure 11.3 shows that the fitted parameter is constant with temperature and that its average value equals:  $k_{23} = 0.0202 \pm 0.0096$ , where the error indicates a 95% accuracy interval. The fitted binary interaction parameter is small and independent of the temperature. Considering the similar size and molecular structure of the compounds this was to be expected. When the binary interaction parameter is estimated using the UNIFAC method (Sandler, 1987) a value of  $k_{23} = 0.04$  is found. Table XI.III shows the experimental data for the ternary experiments and the deviations with the thermodynamic model. The selectivity has been calculated based on limonene, being the more volatile component.

TABLE XI.III: Measured solubilities and selectivities for ternary system and the model deviations<sup>‡</sup>. The linalool feed fraction was 0.125 for all experiments.

T °C	p bar	$\alpha_{23}$ -	$\Delta\alpha_{23}$ %	$x_1$ mol/mol	$\Delta x$ %	$y_2 + y_3$ mol/mol	$\Delta y$ %
39.6	76	1.792	12	0.964	11	0.00246	6
48.8	81	1.834	9	0.899	12	0.00284	1
49.4	74	1.970	11	0.870	16	0.00329	37
49.9	82	1.601	-4	0.898	12	0.00343	13
50.2	80	1.663	-1	0.858	10	0.00321	17
51.0	78	1.317	-30	0.860	13	0.00280	12
56.2	82	1.688	-3	0.776	3	0.00353	32
58.0	74	1.902	3	0.749	8	0.00183	-32
65.8	90	1.851	4	0.861	12	0.00411	-6

<sup>‡</sup> All deviations are calculated as:  $(x_{\text{meas}} - x_{\text{cal}}) / x_{\text{meas}} \times 100\%$ .

The table shows a fair agreement of the measurements with the model. However, on average the model under predicts the solubilities. It is often observed that the cubic equation predicts the calculated two phase region to be larger than that found by experiments (Prausnitz et al., 1986), especially in the near critical region. Because in this example the experiments are carried out close to the lower critical solution temperature, it is not unusual that the deviations are between 10 and 30%. From an engineering point of view this is not alarming for the solvent phase, but attention should be paid to the liquid phase were the large carbon dioxide solubility can cause a very low surface tension.

The model and the measured data were compared with systems reported in literature. Di Giacomo and Calvarano (1970) measured gas compositions in the ternary system carbon dioxide-limonene-citral (citral is a general name for a mixture of neral and gerenial), while liquid compositions were measured by Pavlicek and Richter (1993) for three binary systems. Data for the system carbon dioxide-linalool is also given by Iwai et al., (1994). The developed thermodynamic model for CO<sub>2</sub>-limonene-linalool show deviations, which are smaller than 20% with the reported solubilities.

### PROCESS DESIGN

Given the composition of the raw material the process is designed for increasing the linalool content in the raffinate with a factor of five, leading to a 5-fold cold press. The feed is taken as 5kg/h and is modelled as: 5%wt linalool and 95%wt limonene. The process is designed so that 99% of the linalool intake is concentrated in the raffinate stream. Knowing the sensitivity of the supercritical separation process concerning the solvent to feed ratio this parameter is established first by optimising the separation conditions.

#### *Separation Conditions*

Normally when establishing the optimum process conditions the selectivity and the solubility of the components in the solvent are the first parameters that need to be considered. Due to the large solubility of carbon dioxide in the liquid phase, the range of process conditions is restricted. This solubility will cause a decrease in surface tension, which will result in the instability of the liquid film flow on a packing (Hiller et al., 1993). Figure 11.4 shows the solubility of the carbon dioxide in the mixture limonene-linalool for various temperatures as function of the pressure. The graph shows the sharp increase of the solubility of carbon dioxide in the liquid phase with increasing pressure.

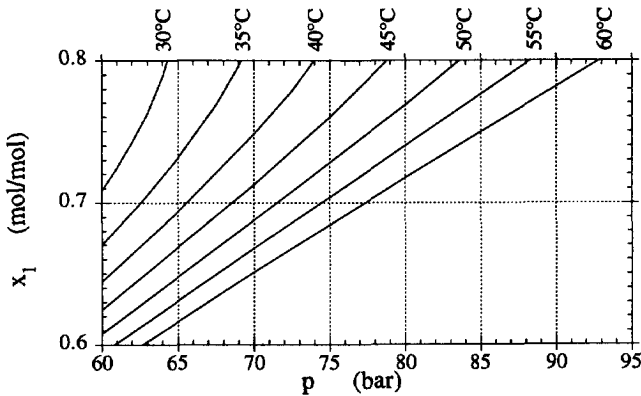


FIGURE 11.4: Solubility of the carbon dioxide in the mixture limonene (95%wt) linalool (5%wt) for various temperatures as function of the pressure.

For each temperature, a pressure can be found where the two phase region of the mixture ends. To avoid reaching this single phase region prematurely and to avoid an unstable film flow, the design will be restricted to a carbon dioxide concentration in the liquid phase that is smaller than 80%. Since the model predicts the two phase region too wide, this can be considered as a conservative choice. Although an extra boundary condition is introduced, the main design parameters for the actual fractionation still are the solubility and selectivity. Figures 11.5 and 11.6 show these parameters as function of the pressure, for various temperatures.

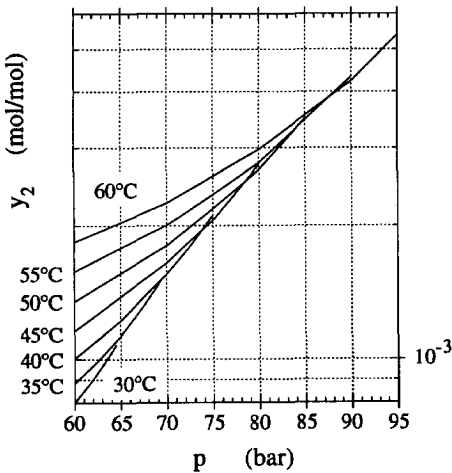


FIGURE 11.5: Calculated solubility of limonene as function of the pressure for various temperatures.

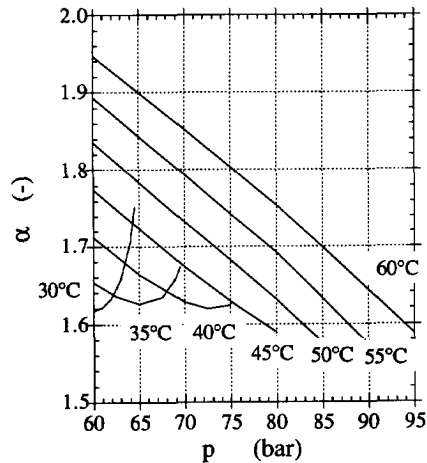


FIGURE 11.6: Calculated solvent free selectivities of limonene as function of the pressure for various temperatures.

It is often found that with increasing solubility the selectivity decreases. However, this is an example where the reverse occurs. The increase of the solubility with temperature is caused by the fact that in this region the positive effect of temperature on the vapour pressure is stronger than the negative effect of temperature on solvent density, resulting in a net increase of the solubility. The origin of the increase in selectivity stems from the fact that the decrease in density with temperature affects the solubility of limonene more than that of linalool. The separation temperature therefore is taken on the maximum allowed temperature of 60°C. Using the by the model established solubilities and selectivities the number of equilibrium stages required at various operating pressures can be determined using the Smoker equation (see, e.g., Coulson et al, 1983). Table XI.IV shows the results of these calculations, in which a reflux ratio (R) of 1.4 times the minimum reflux is applied.

TABLE XI.IV: Calculated concentrations, streams and number of stages for a process fractionating citrus oils at a temperature of 60°C for various pressures.

p bar	$\alpha_{23}$ -	$x_1$ mol/mol	$y_2$ mol/mol	R -	G kg/s	L + E kg/s	$N_s$ -	$N_r$ -
60	1.95	0.582	0.0018	1.52	0.504	0.0028	5.0	19.1
70	1.85	0.651	0.0023	1.70	0.423	0.0030	5.3	20.6
80	1.75	0.718	0.0030	1.93	0.351	0.0033	5.7	22.4
90	1.64	0.782	0.0042	2.27	0.280	0.0036	6.4	25.1
100	1.50	0.846	0.0068	2.90	0.206	0.0043	7.6	30.3

In this table  $N_s$  represents the number of equilibrium stages in bottom or stripping section of the column, while  $N_r$  represents the number of stages in the top or rectifying section of the column. The reflux (L) and extract (E) streams are on solvent free basis, to accomplish these streams a large solvent stream (G) is required. The flow symbols are indicated in figure 11.7.

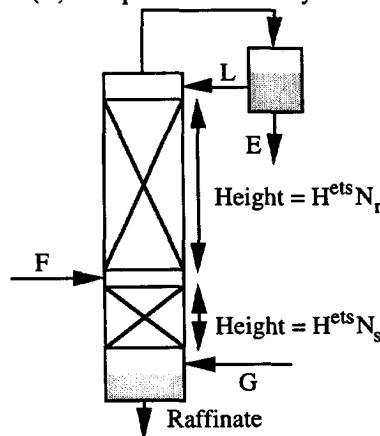


FIGURE 11.7: The flows and sizes over the column.



The costs of the column are estimated by calculating the mass of column ( $m_{col}$ ). To calculate the mass the height ( $H_{col}$ ), the diameter ( $D_{col}$ ) and the wall thickness ( $t$ ) of the column are required. The height of the column is calculated by multiplying the height of an equivalent stage (see, e.g. Treybal, 1980) with the required number of stages;

$$H_i^{ets} = \frac{\ln S_i}{S_i - 1} \frac{u_{SG}}{a_p} \left( \frac{1}{k^G} + \frac{m_i}{k^L} \right) \approx \frac{\ln S_i}{S_i - 1} \frac{u_{SG}}{a_p} \frac{1}{k^G} \quad (11.5)$$

In this equation  $u_{SG}$  represents the superficial gas velocity,  $a_p$  the specific surface area of the packing, and  $k^G$  and  $k^L$  represent the mass transfer coefficients in the solvent and liquid phase respectively. Although both mass transfer coefficients are of similar magnitude, due to the low solubility of limonene and linalool in the solvent phase, the distribution coefficient ( $m_i$ ) becomes small, so that the resistance in the liquid phase can be neglected. The mass transfer coefficient in the solvent phase is calculated using the model of Bravo et al., (1985) for structured packing, which correlates the gas Sherwood ( $Sh$ ) number as function of the Reynolds ( $Re$ ) number and the gas Schmidt number ( $Sc$ ) as:

$$Sh = 0.0338 Re^{0.8} Sc^{0.33} \quad (11.6)$$

Equations (11.5) and (11.6) require estimations for the physical properties of the system. The densities of the streams are calculated using the Peng-Robinson equation of state. The viscosity of the solvent phase  $\eta_G$  is estimated by considering it as pure carbon dioxide using the relation of Ulebin and Makarushkin (1976). The viscosity of the liquid phase  $\eta_L$  is determined applying a mixing rule based on mass fraction ( $X_i$ ) of the pure component viscosities  $\eta_i$ ;

$$\eta_L = \prod_{i=1}^n \eta_i^{X_i} \quad (11.7)$$

The Sulzer 500BX packing is selected as internal for the column. The maximum solvent flow is established using the capacity diagram of the packing supplier (Sulzer, 1989). For the calculation of the diameter of the column  $D_{col}$ , a design gas velocity of 80% of the flooding capacity is taken. For simplicity the height of of an equivalent stage of the rectifying section is taken equal to the stripping section. After determination of the streams and physical data the height of the column can be determined. The design pressure  $p_d$  determines the wall thickness of the column and is taken as 1.2 times the operating pressure, so that the mass of the column can be approximated as:

$$\frac{m_{col}}{\rho_{steel}} = 1.2t H_{col} \pi D_{col} = 1.2 \frac{p_d D_{col}}{2\sigma} (N_s + N_r) H_i^{ets} \pi D_{col} = 2.26 \frac{p_d D_{col}^2}{\sigma} (N_s + N_r) H_i^{ets} \quad (11.8)$$

where  $\sigma$  represents the design stress of the steel, for which a value of  $\sigma = 120 \text{N/mm}^2$  is chosen. The results of the calculations and estimations are shown in table XI.V.

TABLE XI.V: Estimated physical properties and the calculated design solvent load for a process fractionating citrus oils at a temperature of 60°C for various pressures. Indicated are the column dimensions when using a Sulzer 500BX packing and the quantity of steel for construction.

p bar	$\rho_L$ kg/m <sup>3</sup>	$\rho_G$ kg/m <sup>3</sup>	$\eta_L$ mPa s	$\eta_G$ mPa s	$D^G$ n m <sup>2</sup> /s	$S_i$ -	$u_{SG}$ m/s	$D_{col}$ m	$H^{ets}$ m	$m_{col}$ kg
60	769	129	0.214	0.0182	47.0	1.00	0.312	0.126	0.602	210
70	772	162	0.170	0.0187	37.7	1.05	0.258	0.113	0.579	204
80	771	201	0.133	0.0195	30.5	1.09	0.209	0.103	0.553	200
90	766	250	0.101	0.0205	24.8	1.12	0.156	0.094	0.503	192
100†	747	318	0.077	0.0232	20.1	1.11	0.105	0.089	0.414	186

† Because of the large solvent solubility (>80%) in the liquid phase, a 100 bar operation is excluded from the analysis.

Regarding the results shown in table XI.V the column dimensions are approximately equal for all pressures. The optimum process is therefore determined only by the solvent to feed ratio. When taking into account all earlier mentioned boundary conditions, one would select 90bar as operating pressure. However, the lowest pressure of 60 bar is considered as an alternative, because at this pressure the process can be operated isobarically.

### Isobaric Separation

For the performance of the process the separator conditions are as important as the extraction column conditions. This application deals with products that show a lower critical solution temperature, which implies that an isobaric separation, i.e. at column pressure, will be difficult. As can be seen in figure 11.5 a maximum decrease in solubility of a factor of two, can be obtained in an isobaric separation at 60bar by *reducing* the temperature from 60 to 35°C. At higher pressures an isobaric separation is nearly impossible due to the cross over behaviour of the solubilities at higher pressures. Because of the boundaries set for the maximum operation temperature and the maximum concentration of carbon dioxide in the liquid, a temperature increase at high pressure cannot be used. Because the concentration of limonene in the raffinate stream is 75%, the factor 2 solubility decrease still allows an isobaric separation to a 10-fold cold press. The price that has to be paid for not reducing the solubility of the extract stream further is an increase of the required solvent stream. Making a solvent free mass balance over the separator, three outgoing streams can be distinguished, which are the solvent free extract E and reflux L streams and the solvent stream G with outgoing dissolved product fraction  $y_1^0$ . Since the composition and volume of the extract stream are fixed, the required in going quantity of dissolved product in the separator is readily calculated,

$$y_1^N G = E + L + y_1^0 G \quad \Rightarrow \quad G = \frac{E + L}{y_1^N - y_1^0}, \quad (11.9)$$

of which the required quantity of solvent is derived. Here  $y_i^N$  represents the molar product fraction in the top of the column. Since  $y_i^N = 2y_i^0$  a double amount of solvent is required in this case. In equation (11.9) the inlet and outlet solvent streams are taken identical, a justified simplification given the small extract and reflux streams in comparison with the total solvent stream.

### Separation by throttling

The other possible process design considers a pressure reduction. When using the optimum conditions the separation process is operated at 90bar and 60°C. When an adiabatic expansion is used the temperature of the carbon dioxide can be found from an enthalpy diagram, so that the mol fraction limonene can be calculated (see figure 11.8).

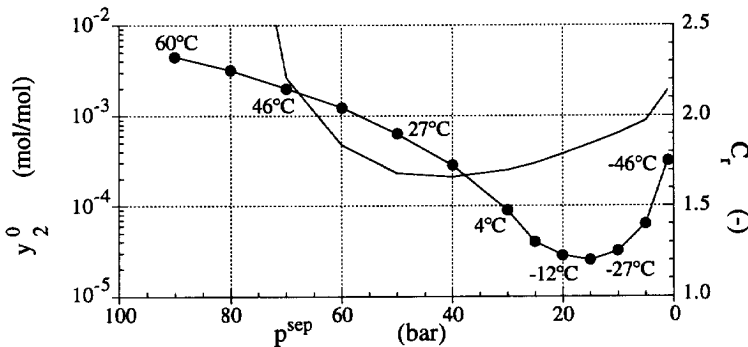


FIGURE 11.8: The limonene concentration in the solvent recycle stream when reducing the pressure by adiabatic expansion and a relative cost curve for the separation pressure. The temperature due to the expansion is indicated.

Only a small pressure drop to 70bar would be required to reduce the limonene concentration in the solvent phase to 50%. However, figure 11.8 shows also a reduced cost parameter  $C_r$ . This parameter contains the operating costs and the capital costs. The operating costs are related to the pressure drop and the solvent flow and the capital costs are represented by the product of the solvent flow and pressure. The total costs ( $C_t$ ) per unit of time can therefore be expressed as:

$$C_t = c_{op}\Delta p \frac{y_i^N}{y_i^N - y_i^0} G_{min} + c_{cap}p \frac{y_i^N}{y_i^N - y_i^0} G_{min} \quad (11.9)$$

Here  $c_{op}$  and  $c_{cap}$  are constants, which indicate the annual operating and capital costs and  $G_{min}$  represents the minimum amount of solvent ( $y_i^0 = 0$ ). The dimensionless reduced cost parameter can be expressed as:

$$C_r = \frac{C_t}{c_{cap}G_{min}p} = \frac{c_{op}}{c_{cap}} \frac{\Delta p}{p} \frac{y_i^N}{y_i^N - y_i^0} + \frac{y_i^N}{y_i^N - y_i^0} \quad (11.10)$$

As first approximation the ratio of the constants  $c_{op}$  and  $c_{cap}$  is assumed equal to unity for supercritical applications. The equation is of course a simplification of the total costs, but it holds the essence of the costs for a supercritical separation process, in which total costs are proportional with the required quantity of solvent. The separation pressure found by applying this rough approach is 40bar. The solubility curve of figure 11.8 shows that only a substantial decrease of limonene in the carbon dioxide can be achieved by reducing both temperature and pressure. The maximum solvent product separation using an adiabatic expansion is achieved at 15bar. A further pressure reduction would increase the vapour volume, causing the vapour pressure of limonene to become dominant.

Both the isobaric process and the pressure reduction process can create enough reduction in the vapour concentration to create the required reflux and bottom concentration.

### PROCESS EVALUATION

As has been concluded from the previous section, both the isobaric and the throttle process are possible. This section will therefore first discuss the technical aspects of both processes, where after an economical comparison will be made. The preliminary process designs of both options are shown in Appendices 11.A and 11.B.

#### *Technical Evaluation*

The most characteristic feature of both options is the large amount of solvent required. A solvent to feed ratio of 609 for the isobaric option and 200 for the throttle process type is required. This is due to the low solubility in the supercritical phase, which cannot be increased given the maximum temperature of 60°C. The factor 3 larger solvent cycle stream is for 50% caused by the limonene solubility in the solvent phase of the separator, causing a continuous recycling of the limonene through the whole process as described through relation (11.8). The other 50% is due to the lower solubility in the extraction column, which is only partly compensated by the larger selectivity at 60bar.

An other important effect of the large solvent to feed ratio is that both processes will potentially suffer from wetting problems. This is caused by the fact that the liquid flow rates in the rectifying and stripping section are 0.196kg/m<sup>2</sup>/s and 0.357kg/m<sup>2</sup>/s for the isobaric process and 0.778kg/m<sup>2</sup>/s and 1.207kg/m<sup>2</sup>/s for the throttle process, which are all under the recommended liquid flow rates mentioned in literature (see, e.g., Coulson, 1987). It is for this reason that a gauze type of packing is used, which due to the capillary structure will increase both the liquid hold-up and the wetting rate.

For both processes the design pressure is taken to be the separation pressure for all main plant items. Given the relative small sizes of the main plant items, this will most likely be a less expensive option, than different safety measures throughout the process.

In the isobaric process a pump is used to assure a sufficient solvent recycle flow. The use of gravity only would require the condensation of the carbon dioxide stream to create a sufficient static pressure difference for the circulation. The condensation of the solvent stream would require an additional 125kW, while a 1kW pump can meet the requirements.

The processes are designed so that the temperature in the solvent and product streams never exceeds a temperature of 60°C. Only the carbon dioxide recovery compressor is allowed to exceed this temperature in theory, to enable a single recompression.

Due to the low demand of carbon dioxide, the most inexpensive supply will be using gas bottles, so that no storage facilities are required. This will be reflected in the price of the carbon dioxide.

*Economical Evaluation*

The capital costs for both processes are shown in table XI.VI. These are estimated based on the main plant items (MPI). The costs of the columns are mainly determined by the supporting construction and hardly by the column itself. The table shows that the investment costs are nearly equal for both process designs. It is in this case difficult to estimate exact price, given the small sizes of the equipment. A substantial difference in costs can only be caused by the price difference of the shell and tube heat exchangers of the isobaric process and the double stage compressor for the throttle process. Clearly, the investment costs for this relatively small process are insensitive for the applied solvent recycle method. The operating costs of both processes are of more interest (see table XI.VII).

TABLE XI.VI: Capital costs for the fractionation of citrus oils as designed isobarically (left) and using a throttle (right). The numbers of the main plant items refer to the flowsheets 11.A and 11.B.

Item	No.	MPI	Inst.	Inst.	MPI	No.	Item
Isobaric process				Throttle process			
				kf	kf		
Column (800kg steel)	C1	40	120	90	30	C1	Column (500kg steel)
Packing		16	32	14	7		Packing
Shell & tube heat ex.	E1&E2	72	216	210	70	P3	2 stage comp (17kW)
Pump (1kW)	P3	10	30	90	30		Interstage cooler
Degas comp (0.5kW)	P2	20	60	60	20	P2	Degas comp (500W)
Separator	V1	20	80	45	15	V1	Separator
Double tube heat ex.	E3	3	9	18	6	E1&E2	Double tube heat ex.
Flash vessels	V2&V3	20	60	60	20	V2&V3	Flash vessels
Feed Pump	P1	9	27	54	18	P1&P4	Feed and reflux pump
Subtotal		210	634	641	216		Subtotal
Allowance 20%			127	128			Allowance 20%
<b>Total</b>			<b>761</b>	<b>769</b>			<b>Total</b>

TABLE XI.VII: Overall cost comparison for the isobaric and pressure controlled process for the fractionation of citrus oils. The top section shows the running costs of the processes, while the bottom part shows the labour and investment costs.

Process		Isobaric	Throttle	Isobaric		Throttle	
		Required	Required	Unit	Unit price	Costs	Costs
		hourly	hourly		f	f/h	f/h
Running Costs:	Electrical	2	15	kWh	0.12	0.24	1.80
	Cooling water 20°C	1.5	0.5	m <sup>3</sup> /h	0.10	0.15	0.05
	Hot Water 70°C	35	1	kWh	0.03	1.05	0.03
	Carbon Dioxide	0.19	0.21	kg	2.00	0.38	0.42
						<b>1.82</b>	<b>2.30</b>
		Costs	Costs				
		kf/A	kf/A				
Capital Costs:	Labour (5 shift)	500	500			62.50	62.50
	17% of Investment	129	131			16.17	16.35
<b>Total</b>						<b>82.31</b>	<b>83.45</b>
Costs per kg citrus oils incl. labour:						16.46	16.69
Costs per kg citrus oils excl. labour:						3.60	3.73

Although the process is an unfavourable example of an isobaric process, a 20% reduction in utility costs is obtained. If for the hot water stream a condensate stream of an other process can be used, even a 66% reduction in utility costs can be achieved. However, due to the size of the plant all utility costs are totally insignificant compared to both the investment costs and the labour costs. Especially the labour costs affect the total price, since by applying a worst case scenario a whole shift needs to be put on the plant. However, the labour costs can be reduced quite simply by operating the process only in 2 shifts. This would increase the investments, but the labour costs are reduced substantially. Although our design criteria were somewhat different from Perre et al., (1994), the reported tendencies are similar, both technically and economically.

The process costs of the traditional processes are approximately f10 per kg intake, so that the carbon dioxide separation method is more expensive. However, advantages like quality improvements are difficult to assess in financial terms.

#### CONCLUDING REMARKS

This paper has demonstrated the technical possibility of separating citrus oils using a supercritical carbon dioxide separation method. The economical evaluation indicates that the costs are comparable with the current methods i.e. distillation and liquid extraction. Two possible process operations are discussed for the recycling of the carbon dioxide, being an isobaric method and a throttle of the recycle stream. The isobaric process shows at least a

reduction in operating costs of 20%, which can increase to 66% when a waste hot water stream is available from another plant. Due to the size of the plant the investment costs are approximately equal for both processes.

Taking in mind the close to non existence of the utility costs compared with labour and investment costs and the advantage of a more flexible operation of the process using a pressure drop recycle method, it can be concluded that for the given plant size and application the throttle process is more appropriate. However, the exercise has shown that for larger applications the isobaric option will be a valuable option even for products having a lower critical solution temperature.

NOTATION:

$a$	Attraction parameter.....	$J/mol\ m^6\ mol^{-2}$
$a_p$	Interfacial area .....	$m^2\ m^3$
$b$	vd Waals co-volume .....	$m^3\ mol^{-1}$
$c_{op}$	Operating costs per unit pressure drop and unit flow .....	$f\ Pa^{-1}kg^{-1}$
$c_{cap}$	Capital costs per unit pressure and unit flow .....	$f\ Pa^{-1}kg^{-1}$
$c_t^L$	Liquid concentration .....	$kmol\ m^{-3}$
$c_t^G$	Gas concentration .....	$kmol\ m^{-3}$
$C_T$	The relative costs parameter.....	(-)
$C_t$	The total costs per unit of time.....	$f\ s^{-1}$
$D_{col}$	Column diameter .....	$m$
$D^G$	Gas diffusion coefficient .....	$m^2\ s^{-1}$
$F$	Feed flow .....	$kg\ s^{-1}$
$g$	Gravitational acceleration.....	$9.81\ m\ s^{-1}$
$G$	Mass solvent flow.....	$kg\ s^{-1}$
$G_{min}$	Minimum required solvent flow .....	$kg\ s^{-1}$
$H_{col}$	Height of the column .....	$m$
$H_{ets}$	Height of an equivalent stage .....	$m$
$k_{ij}$	Binary attraction parameter.....	(-)
$k^L$	Liquid mass transfer coefficient .....	$m\ s^{-1}$
$k^G$	Gas mass transfer coefficient .....	$m\ s^{-1}$
$K_i$	Distribution factor ( $K_i = y_i/x_i$ ).....	$mol\ mol^{-1}$
$l_{ij}$	Binary co-volume parameter.....	(-)
$L$	Solvent free liquid flow .....	$kg\ s^{-1}$
$n$	Number of components .....	(-)
$N_r$	Number of equilibrium stages in rectifying section .....	(-)
$N_s$	Number of equilibrium stages in stripping section.....	(-)
$m_i$	Distribution coefficient ( $c_t^L\ m_i = K_i\ c_t^G$ ).....	(-)

$m_{col}$	Mass of the column .....	(kg)
$M$	Molar mass .....	$\text{kg mol}^{-1}$
$p$	Pressure .....	Pa
$p_c$	Critical pressure .....	Pa
$p_d$	Design pressure .....	Pa
$p_{sep}$	Separator pressure .....	Pa
$R$	Gas constant .....	$8.31441 \text{ J mol}^{-1} \text{ K}^{-1}$
$R$	Reflux ratio .....	(-)
$S_i$	Stripping factor .....	$\text{mol mol}^{-1} \text{ mol s}^{-1} \text{ mol}^{-1} \text{ s}$
$Sh$	Sherwood number .....	(-)
$t$	Column wall thickness .....	m
$T$	Temperature .....	K
$T_c$	Critical temperature .....	K
$u_{SG}$	Superficial gas velocity .....	$\text{m s}^{-1}$
$u_{SG}^{max}$	Maximum superficial gas velocity in the separator .....	$\text{m s}^{-1}$
$x_i$	Liquid mol fraction .....	$\text{mol mol}^{-1}$
$X_i$	Liquid mass fraction .....	$\text{kg kg}^{-1}$
$y_i$	Gas mol fraction .....	$\text{mol mol}^{-1}$
$y_i^N$	Gas mol fraction leaving the column .....	$\text{mol mol}^{-1}$
$y_i^0$	Gas mol fraction entering the column .....	$\text{mol mol}^{-1}$
$\alpha_{ij}$	Selectivity ( $K_j \alpha_{ij} = K_i$ ) .....	(-)
$\Delta\rho$	Density difference .....	$\text{kg m}^{-3}$
$\eta_G$	Gas viscosity .....	Pa s
$\eta_L$	Liquid viscosity .....	Pa s
$\rho_G$	Gas density .....	$\text{kg m}^{-3}$
$\rho_L$	Liquid density .....	$\text{kg m}^{-3}$
$\rho_{steel}$	Steel density .....	$\text{kg m}^{-3}$
$\sigma$	Stress coefficient of the steel .....	$\text{N m}^{-2}$
$\omega$	Acentric factor .....	(-)

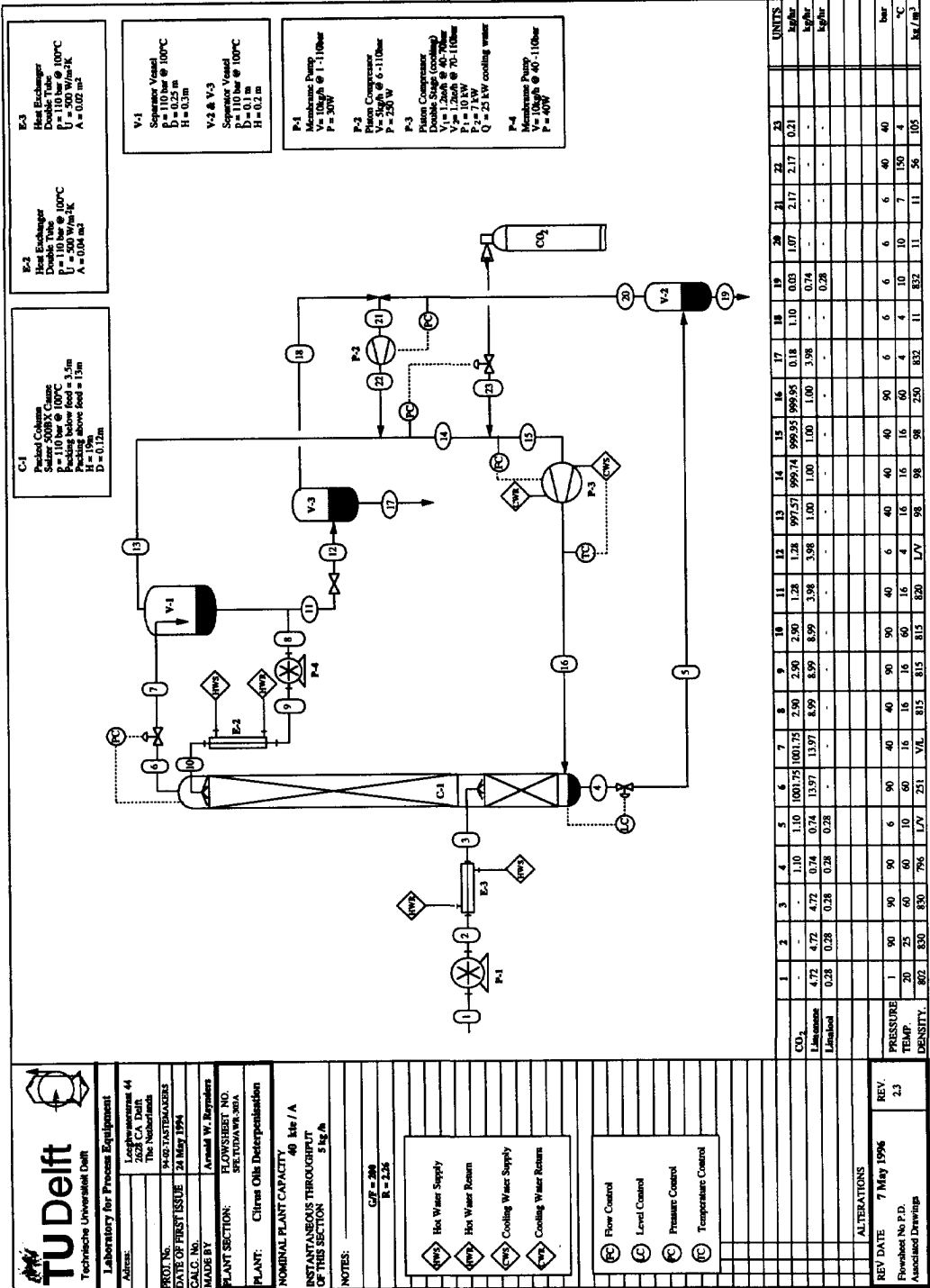
## REFERENCES:

- [1] Bravo, J.L., Rocha, J.A., and Fair, J.R., Mass Transfer in Gauze Packings, Hydrocarbon Processing, 91-95 (1985).
- [2] Coulson, J.M., and Richardson, J.F., Chemical Engineering Volume 2, 3rd ed, Pergamon Press, Oxford (1987).
- [3] Coulson, J.M., and Richardson, J.F., Chemical Engineering Volume 6: Design, Pergamon Press, Oxford (1983).
- [4] Chouchi, D., Barth, D., and Nicoud, R.M., (1994), *Fractionation of citrus cold-pressed oils by supercritical CO<sub>2</sub> desorption*, 3rd Int. Symposium on Supercritical Fluids, TOME 2 pp. 183- 188, Strasbourg, 17-19 October.
- [5] Di Giacomo, A., and Calvarano, Ess. Der. Agrum., 40 340, (1970).
- [6] Haan de, A.B., Supercritical Fluid Extraction of Liquid Hydrocarbon Mixtures, PhD thesis, Delft University Press, Delft (1991).



- 
- [7] Hiller, N., Schiemann, H., Weidner, E., and Peter, S., Interfacial Tension in Systems with a Supercritical Component at High Pressures, *Chem. Eng. Technol.*, **16** 206-212, (1993).
  - [8] Iwai, Y., Hosotani, N., Morotomi, T., Koga, Y., and Arai, Y., High Pressure Vapor-Liquid Equilibria for Carbon Dioxide + Linalool, *J. Chem. Eng. Data*, **39** 900-902 (1994).
  - [9] Pavlicek, J., and Richter, M., *Fluid Phase Equilibria*, **90** 125 (1993).
  - [10] Peng, D.-Y., Robinson D.B., *Ind. Eng. Chem. Fundam.* **15** 59-64 (1976).
  - [11] Perre, C., Delestre, G., Schrive, L., and Carles, M., (1994), Deterpenation process for citrus oils by supercritical CO<sub>2</sub> extraction in a packed column, 3rd Int. Symposium on Supercritical Fluids, TOME 2 pp. 465- 470, Strasbourg, 17-19 October.
  - [12] Prausnitz, J.M., Lichtenthaler, R.N. and Gomez de Azevedo, E., *Molecular Thermodynamics of Fluid-Phase Equilibria*, Prentice-Hall Inc, 2<sup>nd</sup> ed, New York (1986).
  - [13] Reid, C.R., Prausnitz, J.M. and Poling, E.P., *Properties of Gases & Liquids*, McGraw-Hill, 4<sup>th</sup> ed, New York (1988).
  - [14] Sandler, S.I., *Chemical Engineering Thermodynamics*, Wiley Series in Chemical Engineering, New York (1987).
  - [15] Sulzer Brother Ltd., *Seperation Columns for Distillation and Absorption*, Information Bulletin, (1989).
  - [16] Temelli, F., and O'Connel, J.P., Thermodynamic Analysis of Supercritical Carbon Dioxide of Terpenes cold-pressed Orange Oil, *Ind. Eng. Chem. Res.*, **29** 618-624, (1990).
  - [17] Treybal, R.E., *Mass Transfer Operations*, 3<sup>rd</sup> ed, Wiley Series in Chemical Engineering, New York (1980).
  - [18] Ulebin, S.A., Makarushkin, V.I., *Teploenergetika*, **6** 65-69, (1976).

APPENDIX 11.A: Flowsheet for a Throttling SFE Process for citrus oils



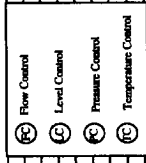
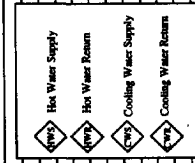
**TU Delft**  
Technische Universiteit Delft

Laboratory for Process Equipment  
Address: Leeghwaarderweg 44  
2628 CA, Delft  
The Netherlands

PROJ. NO.: 94-02-7A5T8D0A2E2S  
DATE OF FIRST ISSUE: 24 May 1994  
CALC. NO.:  
MADE BY: Arnold W. Reijnders  
FLOW-SHEET NO.: SEE TUDAWR-80A  
PLANT SECTION:  
PLANT: Citrus Oils Deterpenisation

NOMINAL PLANT CAPACITY: 40 kgc / A  
INSTANTANEOUS THROUGHPUT OF THIS SECTION: 5 kg/h

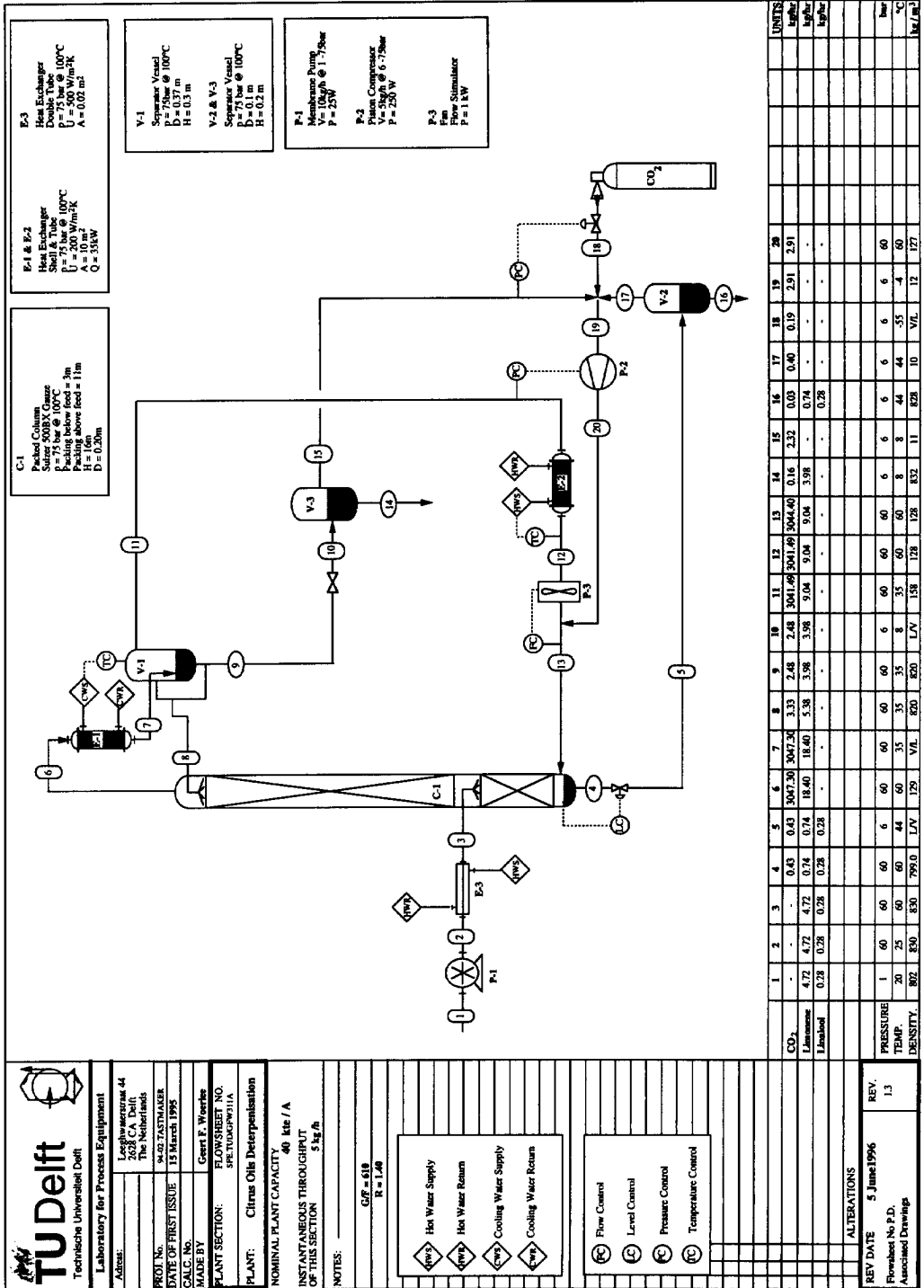
NOTES:  
G/F = 200  
R = 2.25



ALTERATIONS

REV. DATE	7 May 1996	REV.
Flow-sheet No. P.D.	2.3	
Associated Drawings		

APPENDIX 11.B: Flowsheet for an Isobaric SFE Process for citrus oils





## The Future of Supercritical Separations

Although research activities concerning supercritical separations are conducted at many universities, the increase of the number of industrial applications for supercritical separation has been limited since the first extraction of caffeine from coffee. Researchers who try to advocate supercritical techniques often list the advantages of the process (see e.g., Krukoniš et al., 1993);

- *Change in consumer awareness towards green products,*
- *Changes in government regulations,*
- *Increased demands on product performance,*
- *Enhancing competitive advantage of a products.*

However, in industry the engineer is normally not asked about the advantages of a certain product or production method. The business only asked the question indicated in figure 1.4;

What are the production costs? (A)

By answering this question, he will examine several available techniques and during the comparison of the alternatives he will ask himself:

What is the robustness of the process? (B)

Evaluating the results of both questions, will lead him to advice in order of preference: (vacuum) distillation, crystallisation or liquid extraction. Only when these techniques fail he will consider an alternative as supercritical separation. The reason for this is clear, the investment costs for supercritical separations are large and the possibility to check the design on a large enough scale to validate the potential of supercritical separation is limited to batch extractions. If there is an alternative for a supercritical separation it is advisable to use it.

The above leads to the question: should supercritical separations be considered at all? This can be answered by evaluating the history of supercritical fluid technology. The reason to use supercritical extraction for coffee beans, has not been the superior supercritical extraction, but the ban of methylene chloride. It is not difficult to forecast a ban of solvents as methylene chloride and hexane and this would lead a growing use of supercritical separations applying carbon dioxide as solvent. Moreover one should ask, when are they going to be banned? Given the wide use of these solvents in industry, the development will be slower than for coffee beans extraction. However, a strategic research on supercritical separations for certain products is as wise as not using it, when an alternative is available.

Next to the above argument to do research on supercritical technology, it sometimes happens that the questions (A) and (B) can be answered positively for supercritical separation. Since the start of large industrial supercritical batch extraction the technique has evolved and proven to be

economical feasible for the production of light cigarettes and the extraction of hop and various types of herbs and species. The availability of engineering knowledge on the scale-up and operation of these batch operations made this development possible. The lack of large scale pilot plants for supercritical separation of liquids is a large drawback for the technique.

Again a new question evolves from the earlier; In which industry is supercritical separation going to be used? The advantages of the technique could lead to a favourable situation in some markets. Three potential motivations can be distinguished for supercritical separations. Given the advantages of supercritical fluids, products made from natural materials and food products will benefit most by applying supercritical separation. The products can benefit from the "green" process image and therefore have a *market* driven incentive. Known potential processes are:

- flavour extraction (citric oil refining, extraction from seeds),
- edible oil applications (cleaning of edible oils, refining of fish oil),
- bio-technical processes (extraction from aqueous streams, carotene extraction),
- general food processes (extraction of fat from potatoes chips, sucrose ester purification).

A second class of applications is due to *regulations*. The uses of harmful chemicals for which alternatives are available are likely to be restricted in the future. Carcinogenic solvent will be banned in due time. Possible processes where a non toxic supercritical fluid could be used as an alternative solvent are:

- extraction with benzene (caprolactam process),
- extraction with chlorinated hydrocarbons (cleaning of precision instruments).

A third class of applications is where supercritical extraction offers *technological* advantages compared with conventional techniques. Potential processes are:

- off-shore production water cleaning,
- cleaning of polluted soil or harbour sludge,
- purification of thermal sensitive polymers.

Due to the advantages, the growth of applications in the food related industry will be largest, while due to the relative sensitivity products, a growth of the number of applications can also be expected in the fine chemical and pharmaceutical industry. Next to this, restrictive regulation on solvent usage are also likely for pharmaceutical products. The number of applications in the gas and oil industry and bulk chemicals will at first instance increase only due to possible process advantages.

### RECOMMENDATIONS

To stimulate the industrial applications it is important to develop potential processes, both to increase the reliability of design rules and to give examples for industry. Three various processes are presented in this thesis (chapter 9 to 11). Normally one would not expect to find economical feasible applications in a thesis, but the potential of cleaning off-shore production

water using supercritical methane is large. However, this time the introduction will strongly depend on governmental regulations.

The main motivation for this thesis has been to increase the robustness of supercritical separation design rules. This was the reason for the development of the hydrodynamic (chapter 3 and 4) and mass transfer (chapter 5) models. Chapter 7 showed that this has been relatively successful. However, the implications concerning packing design (chapter 6) have probably a larger spin-off for vacuum distillation than for supercritical separations.

Although some design rules have been given a stronger basis, further developments are required concerning heat exchangers and scale-up rules. Larger test facilities for supercritical separation are necessary for two reasons. Firstly, the design rules need to be confirmed on a larger scale. Secondly, it will provide the possibility for industry to conduct production tests. Such a future development can be combined with the in chapter 8 presented isobaric supercritical separation for liquids. In this way a further increase of the robustness of supercritical separations is combined with the development towards a less costly separation technique.

#### REFERENCES

- [1] Krukonis, V., Brunner, G., and Perrut, M., (1994), *Industrial operations with supercritical fluids: current processes and perspectives on the future*, 3rd Int. Symposium on Supercritical Fluids, TOME 1 pp. 1- 22.





# Samenvatting

## Hydrodynamica en massatransport in gepakte kolommen en hun toepassingen voor superkritische scheidingen

Dit proefschrift beschrijft de verdere ontwikkeling van het scheiden van vloeistoffen met behulp van een superkritisch oplosmiddel. Het beoogt een bijdrage te leveren tot het verwerven van meer robuuste ontwerpregels voor superkritische scheidingsprocessen en tot het verkrijgen van een beter inzicht aangaande de kosten welke aan deze processen gekoppeld zijn.

Een superkritische scheiding van een vloeistof wordt meestal uitgevoerd met een in tegenstroom opererende gepakte kolom. Tijdens het scheiden van de vloeistoffen speelt het hydrodynamisch gedrag van de gas- en vloeistoffase een belangrijke rol. Dit beïnvloedt zowel de capaciteit als de stofoverdracht. Onder superkritische omstandigheden is over dit hydrodynamische gedrag nog weinig bekend.

Ten einde het hydrodynamische onderzoek uit te voeren bij superkritische condities is een hoge druk scheidingskolom voor vloeistoffen gebouwd, welke staat beschreven in hoofdstuk 2. Deze heeft een aantal unieke mogelijkheden zoals een thermische reflux en de mogelijkheid om de drukval over de pakking te meten bij werkdrukken van 100 bar en meer.

Om het hydrodynamische gedrag onder superkritische condities te kunnen voorspellen, worden in hoofdstuk 3 en 4 modellen ontwikkeld welke drukval, vloeistofgedrag en capaciteit in de gepakte kolom beschrijven. Hiertoe zijn bestaande theorieën, welke geschikt zijn voor meer conventionele condities, verder ontwikkeld. Voor de ontwikkeling van de modellen wordt de pakkinggeometrie beschreven met drie parameters; het specifiek oppervlak, de porositeit en de effectieve stromingshoek. Gebruikmakend van meetgegevens wordt aangetoond dat de modellen het hydrodynamische gedrag voor veranderende fysische eigenschappen als viscositeit, dichtheid en oppervlaktespanning goed voorspellen.

In hoofdstuk 5 worden de modellen betreffende het hydrodynamische gedrag aangewend om het massatransport te beschrijven. De verbondenheid van de drukval met het massatransport in de gas- en vloeistoffase wordt in dit hoofdstuk aangetoond. De beschrijving van de vloeistoffase toont het bestaan van drie belangrijke invloeden aan; het massatransport in de vloeistoffase wordt met toenemend Reynolds getal gedomineerd door respectievelijk de dikte van de vloeistoffilm, de geometrie van de pakking, en golven op het vloeistof oppervlak. Deze laatste worden in direct verband gebracht met de drukval over de gepakte kolommen.

In hoofdstuk 6 worden de implicaties voor de geometrie van de pakking, welke uit de eerdere hoofdstukken volgen, in kaart gebracht. Dit wordt bewerkstelligd door de kosten voor

een gepakte kolom als functie van de geometrische pakkingparameters te minimaliseren. Het blijkt dat het gebruik van grotere effectieve stromingshoeken economisch voordelig is voor toepassingen waar de drukval geen rol speelt. Het meest kosteffectieve specifiek pakkingoppervlak is afhankelijk van de scheidingstoepassing en doorzet. Tenslotte wordt een voorspelling gedaan met betrekking tot een betere geometrie van de pakking. Door de pakkinghoogte te vergroten kan de drukval verlaagd worden en wordt de capaciteit van de gepakte kolom vergroot.

In hoofdstuk 7 worden de ontwikkelde algemene modellen gebruikt voor het interpreteren van data welke onder superkritische omstandigheden zijn verkregen. Het betreft hier de drukval over de pakking, de verblijftijd van vloeistof, de capaciteit en het massatransport. Hiermee wordt aangetoond dat de ontwikkelde hydrodynamische modellen bruikbaar zijn onder superkritische omstandigheden. Door de grote invloed van de kolomkosten blijkt het gebruik van pakkingen met een groot specifiek oppervlak ( $750\text{m}^2/\text{m}^3$ ) voor superkritische scheidingen voordelig.

De algemene procesinrichting voor het superkritische scheiden van vloeistoffen wordt geëvalueerd in hoofdstuk 8. Hierin wordt aangetoond dat bij isobaar hergebruik van het superkritische oplosmiddel de noodzakelijke energiehoeveelheid voor de scheiding van dezelfde omvang wordt als bij normale distillatie, met dit verschil dat voor de superkritische scheiding laagcalorische warmte kan worden gebruikt. Hierdoor zouden superkritische scheidingen concurrerend kunnen worden met vacuümdistillatie.

In de laatste hoofdstukken worden voorbeelden gegeven van superkritische processen welke mogelijke industrieel interessant zijn. Achtereenvolgens worden besproken: de verwijdering van verontreinigingen uit eetbare oliën met behulp van superkritisch koolzuur, het verwijderen van polycyclische koolwaterstoffen uit produktiewater van gasplatforms en het fractioneren van eterische oliën welke uit citrusvruchten worden verkregen. Doordat met een superkritische scheiding de zuivering van eetbare en etherische oliën bij lage temperaturen wordt uitgevoerd, treedt er geen thermische degradatie van de produkten op zoals bij distillatie. Hierdoor wordt een "groen" produkt verkregen. Deze toepassingen zijn daarom vooral uit marketing-overwegingen interessant. Uit de studie voor het reinigen van produktiewater blijkt dat dit zowel technisch als economisch een aantrekkelijke optie is.

Hoewel superkritische scheidingen voordelen kunnen bieden ten opzichte van conventionele technieken, is het gebrek aan testfaciliteiten op grote schaal een belangrijk nadeel. Voordat superkritische scheidingen daadwerkelijk kunnen worden toegepast in de procesindustrie, moeten dergelijke faciliteiten worden geconstrueerd.

## Summary

This thesis reports on new developments in the field of supercritical separation. It intends to contribute to more robust design rules for supercritical separation processes and to obtain a better understanding of the costs involved.

A supercritical separation of a liquid is usually carried out in a counter-current packed column. During the separation the hydrodynamic behaviour of the gas and liquid phase influences the separation. This behaviour controls both the capacity and the mass transfer of the column. Hydrodynamics at supercritical conditions is an unexplored research field that is covered in this thesis.

To enable the hydrodynamic research at supercritical conditions a high pressure separation column has been constructed, which is described in chapter 2. The column has unique features such as a thermal reflux and the possibility to measure the pressure drop over the packing at operating pressures exceeding 100bar.

The description of the hydrodynamic behaviour in packed columns required the development of general models concerning pressure drop, liquid behaviour and column capacity. These models and theories are also valid at more conventional conditions. The developed models use the specific surface area, the porosity and an effective inclination angle to describe the packing geometry. In chapters 3 and 4 it is shown that these models can predict the influences of physical properties, e.g.: viscosities, densities and surface tension on the hydrodynamic behaviour correctly.

In chapter 5 the hydrodynamic models are used to describe the mass transport. Without any empirical adjustment a direct dependence of the pressure drop on the mass transport in both the gas and liquid phase is disclosed. It is also shown that the liquid phase mass transfer in packed columns shows three important influences. These are subsequently, the liquid film thickness, the packing geometry and the interface waves. The influence of the waves can be connected with the pressure drop over the packing.

In chapter 6 the geometrical influences on the packing performance as predicted by the developed models are shown. These influences are examined by calculating the costs of a packed column as function of the geometrical packing parameters. It is shown that larger inclination angles with respect to the vertical of the column are most economical for applications that are not restricted by the pressure drop. The most cost effective specific surface of a packing is dependent on the application and the column size. In the last paragraph of this chapter a new packing geometry is suggested. By increasing the packing height the pressure drop over the packing can be decreased while the capacity of the packing can be increased.

In chapter 7 the general models are used to analyse data that are collected at supercritical conditions. The data at supercritical conditions concern pressure drop, liquid hold-up, capacity and mass transfer. All data can be clarified using the developed general models. Due to the relative large investment costs for a supercritical separation column, the analysis of the most cost effective column shows an optimum at large specific surface areas ( $750 \text{ m}^2/\text{m}^3$ ).

The total supercritical process for the separation of liquid mixtures is evaluated in chapter 8. This evaluation shows that when applying an isobaric solvent cycle the required quantity of energy for the separation will be approximately identical to the required energy of distillation. However, the energy for the supercritical separation can be recovered from low calorie energy stream of another process. The supercritical separation process therefore can become compatible with vacuum distillation.

The last three chapters show three supercritical separation processes, which could be of interest industrially. The applications are subsequently: the removal of trace components from edible oil using carbon dioxide, the removal of aromatic compounds from production water using supercritical methane, and the fractionation of citrus oils using supercritical carbon dioxide. Because of the mild temperatures that can be applied for supercritical separations, no thermal degradation of the edible or ethereal oils occurs. Besides this the use of carbon dioxide as solvent for the process classifies the process as "green". The two supercritical separations involving food products are therefore interesting from a market perspective.

Although supercritical separations of liquid mixtures can have clear advantages compared with conventional techniques, the lack of large scale test facilities is still a major drawback. Before supercritical separations can flourish in process industry general test facilities need to be constructed.

# Curriculum Vitae

## PERSONAL NOTES:

Name: Geert Feye Woerlee  
Date of birth: January 7th 1962  
Married with Rosalinda Catharina van Hoek

## WORKING EXPERIENCE:

**1992-present** FeyeCon Engineering Consultancy  
Activities: Consultant for process industry  
Specialities: -supercritical separation processes,  
-packed column design,  
-thermodynamics and physical properties.

**1989-1991** Process Engineer at ICI International Polyurethane's Process R&D  
Activities: Research on new processes and assistance on production projects.  
Projects: • Development of in-line mixing system to de-bottleneck blending facilities.  
• Research on CFC replacing blowing agents in foams.  
• Development of supercritical processes for the polyurethane division.

**1985-1988** Student Assistant at the Technical University Delft  
Activities: Guidance of physics and chemistry students during their research projects.

## EDUCATION:

**1991-1995** PhD research at the Technical University Delft  
Objectives: • Design and construction of supercritical liquid separation unit.  
• Examination of the feasibility of supercritical separations.  
• Increase of the reliability of design rules for supercritical separations.

**1981-1988** *Applied Physics* at the Technical University Delft  
4th year project: Characterisation of spectrally selective layers using ellipsometry.  
5th year project: Dynamic ageing of insulating polyurethanes foams.

**1974-1981** *Secondary School* at "de Christelijke Scholengemeenschap Melanchthon", Rotterdam.

## PUBLICATIONS:

- H. Haitjema and G.F. Woerlee, *Analyses of Tindioxide Coatings by Multiple Angle of Incidence Ellipsometry*, thin solid films, 1988.
- G.F. Woerlee and J. de Graauw, *The Removal of Traces from Edible Oils Using SFE*. Proceedings of 3rd Int. Sym. on SCF. Tome 2, 1994.
- J. de Graauw and G.F. Woerlee, *Process for the Removal of Aromatic Compounds from Off-Shore Production Water using Supercritical Methane*, AIChE Summer meeting, 1995.
- G.F. Woerlee, A.W. Reijnders, K.B. de Roos, and J. de Graauw, *Process for the Fractionation of Citrus Oils using Supercritical Carbon Dioxide*, Proceedings of 4th Int. Sym. on SCF, Sendai, 1997.
- G.F. Woerlee, and J. de Graauw, *Mass Transfer in Packed Column Using Supercritical Systems with Either Mainly Gas or Liquid Phase Resistances*, Proceedings of 4th Int. Sym. on SCF, Sendai, 1997.

## PATENTS:

- G.F. Woerlee, *Process and Device for Separating a Mixture or Extracting a Material*, Int. Pub. No. WO 94/13377. Int. App. No. PCT/NL93/00264, priority date 11.12.1992.
- G.F. Woerlee, *Gestructureerde pakking voor stof- en/of warmte-uitwisseling tussen vloeistof en een gas, alsmede houder voorzien van een dergelijke pakking* Dutch application NL 1005990, priority date 6.5.1997.

